GEAP-23773
FEBRUARY 1978

[redacted]

DEMONSTRATION OF FUEL RESISTANT TO PELLET-CLADDING INTERACTION FIRST SEMIANNUAL REPORT JULY — DECEMBER 1977

COMMONWEALTH RESEARCH CORPORATION
SUBCONTRACT 3-20-46
U.S. DEPARTMENT OF ENERGY
PRIME CONTRACT EN-77-C-02-4473

GENERAL ELECTRIC

DISCLAIMER

GEAP-23773
February 1978
DRF No. J11-102

GEAP--23773

DE84 004977

DEMONSTRATION OF FUEL RESISTANT TO PELLET-CLADDING INTERACTION

First Semiannual Report
July — December 1977

Compiled by
H. S. Rosenbaum
Program Manager

Approved: J. S. Armijo, Manager
Core Materials Engineering

Approved: R. A. Proebstle, Manager
Applied Metallurgy and Chemistry

Prepared for the
Commonwealth Research Corporation Under Subcontract 3-20-46
U.S. Department of Energy
Prime Contract EN-77-C-02-4473

Printed in the United States of America
Available from
National Technical Information Service
U.S. Department of Commerce
5285 Port Royal Road
Springfield, VA 22161
Price: Printed Copy $7.75, Microfiche $2.25

NUCLEAR ENERGY ENGINEERING DIVISION • GENERAL ELECTRIC COMPANY
SAN JOSE, CALIFORNIA 95125

GENERAL ELECTRIC

LEGAL NOTICE

This report was prepared by General Electric as an account of work sponsored by the U.S. Department of Energy ("DOE"). Neither DOE, members of DOE, nor GE, nor any person acting on behalf of either, including Commonwealth Edison Company and Commonwealth Research Corporation:

A. *Makes any warranty or representations, express or implied, with respect to the accuracy, completeness, or usefulness of the information contained in this report, or that the use of any information, apparatus, method, or process disclosed in this report may not infringe privately owned rights; or*

B. *Assumes any liabilities with respect to the use of, or for damages resulting from the use of, any information, apparatus, method, or process disclosed in this report.*

TABLE OF CONTENTS

LIST OF ILLUSTRATIONS

LIST OF ILLUSTRATIONS (Continued)

LIST OF ILLUSTRATIONS (Continued)

LIST OF ILLUSTRATIONS (Continued)

LIST OF TABLES

CONTRIBUTORS

R. B. Adamson, Nuclear Technology Department (NTD)

J. A. Baumgartner, Boiling Water Reactor Systems Engineering Department (BWRSED)

R. E. Brown, Nuclear Technology Department (NTD

B. Cheng, Nuclear Technology Department (NTD)

J. H. Davies, Nuclear Technology Department (NTD)

R. E. Donaghy, Wilmington Manufacturing Department (WMD)

R. P. Gangloff, Corporate Research and Development (CRD)

P. C. Kelly, Corporate Research and Development (CRD)

R. S. Moore, Wilmington Manufacturing Department (WMD)

L. D. Noble, Nuclear Technology Department (NTD)

H. S. Rosenbaum, Nuclear Technology Department (NTD)

S. R. Specker, Nuclear Technology Department (NTD)

D. S. Tomalin, Corporate Research and Development (CRD)

C. D. Williams, Wilmington Manufacturing Department (WMD)

S. B. Wisner, Nuclear Technology Department (NTD)

ABSTRACT

This Program has as its ultimate objective the demonstration of advanced fuel concepts that are resistant to the failure mechanism known as fuel pellet-cladding interaction (PCI). Since currently used fuel in the nuclear power industry is subject to the PCI failure mechanism, reactor operators limit the rates of power increases and thus reduce their capacity factors in order to protect the fuel. Two concepts are being prepared for demonstration within this Program: (a) Cu-Barrier fuel and (b) Zr-Liner fuel. These advanced fuels (known collectively as "barrier fuels") have special fuel cladding designed to protect the Zircaloy cladding tube from the harmful effects of localized stress and reactive fission products during reactor service.

Within the present workscope the large-scale demonstration of the PCI-resistant fuel is being designed generically to show feasibility of such a demonstration in a commercial power reactor of type BWR/3 having a steady-state core. The current plans for the Demonstration will involve on the order of 100 bundles (at least 64) of each concept. Using the core of Quad Cities-1 reactor at the beginning of Cycle 6 as an example, the insertion of the demonstration PCI-resistant fuel and the reactor operational plan are being designed so that the PCI-resistance of the Demonstration fuel can be tested without undue risk to the other fuel in the core. The most favorable approach appears now to be the grouping of the test fuel into four symmetrically placed test cells. Each test cell is surrounded by a buffer of high-burnup fuel with low reactivity. The control blade within each test cell would be withdrawn near the end of the reactor cycle to power ramp test the Demonstration fuel.

Support tests to date for the Demonstration have shown that these barrier fuels (both the Cu-Barrier and the Zr-Liner types) are resistant to PCI. These results come from laboratory tests on both unirradiated and irradiated materials where the cladding is subjected to stress corrosion tests in I_2 or in Cd; these tests are believed to simulate the PCI conditions. Furthermore, actual fuel irradiation tests have shown that both of these fuel concepts can withstand very severe power ramps without fuel failure at burnup levels up to ~9 GWd/t-U. The power ramp tests are such that conventional fuel consistently fails under these test conditions.

Four lead test assemblies (LTA) of the advanced PCI-resistant fuel are being fabricated for insertion into the Quad Cities-1 Boiling Water Reactor at the beginning of Cycle 5 (January 1979). These assemblies will include two with Cu-Barrier and two with Zr-Liner fuel cladding. These LTA's are intended to accumulate burnup ahead of the Demonstration fuel to demonstrate fuel performance aspects other than PCI-resistance. The LTA's will be thoroughly examined at various burnup levels to evaluate the fuel performance. The performance data to be obtained from the LTA's support the Demonstration experiment and facilitate licensing of the Demonstration. Design of the LTA's is at an advanced stage. A unique feature of the design is the inclusion within each LTA of two segmented fuel rods. Segments can be removed from the bundles at various burnup levels as desired for evaluation and for further testing. Final runs for production of the Cu-Barrier and of the Zr-Liner fuel cladding for the LTA's have been successful.

HIGHLIGHTS

- Initial nuclear design results indicate that demonstration of a PCI-resistant fuel is feasible in a reactor of type BWR/3 which has a steady-state core. The demonstration fuel can be power ramped to test resistance to PCI with minimum risk to conventional fuel in the core.

- Cu-Barrier and Zr-Liner experimental fuel rods at burnup levels up to ~9 GWd/t have been shown to resist power ramps known to produce PCI failures in conventional fuel at that burnup; similar power ramp experiments are planned to test PCI resistance at higher burnup levels.

- Cu-Barrier fuel made with the new electroless plate method resisted PCI in a power ramp test after burnup of >4 GWd/t-U.

- Simulated PCI tests under laboratory conditions have shown that irradiated Zr-Liner tubing is apparently immune to attack by cadmium, and it tends to resist (but is not entirely immune to) stress corrosion attack by molecular iodine.

- Similar tests have shown that irradiated Cu-Barrier tubing resists the embrittlement due to Cd, but the resistance to embrittlement is degraded if the copper and the Zircaloy have interdiffused to produce a layer of an intermetallic phase.

- Simulated PCI tests with unirradiated Zr-Liner tubing indicate that PCI resistance is not a sensitive function of liner thickness.

- Simulated PCI tests with unirradiated Cu-Barrier tubing showed that good PCI resistance occurred with several different barrier types: (a) electroplated, (b) electroless, and (c) electroless deposited over a zirconia layer.

- Cu-Barrier tubing absorbs hydrogen from a wet hydrogen environment, but a zirconia film between the copper and the Zircaloy tends to retard the absorption of hydrogen.

- Preliminary fabrication runs in preparation for the manufacture of the Lead Test Assemblies have been successfully completed.

1. INTRODUCTION

In commercial water-cooled nuclear reactors used for central station electric power production, the fuel is based on urania which is sheathed or clad with zirconium alloys such as Zircaloy. Experience in the nuclear industry with fuel rods of Zircaloy-clad urania has indicated several causes for fuel rod failure. Most of these causes have been corrected by improvements in fuel design specifications and improvements in the manufacturing processes. There persists one class of fuel rod failures which has yet to be eliminated and which appears to be of a fundamental nature. These failures are caused by the direct interaction between the irradiated urania fuel, including its inventory of fission products, and the Zircaloy fuel sheath, or cladding. This phenomenon has been called "fuel/cladding interaction" or fuel "pellet-cladding interaction" (PCI). The incidence of such failures is closely linked to the power history of the fuel rod and to the severity and duration of power changes. Pellet-cladding interaction fuel rod failures have occurred in both Boiling Water Reactors (BWR) and Pressurized Water Reactors (PWR) as well as in Canadian Deuterium Moderated Reactors (CANDU) and Steam Generating Heavy Water Reactors (SGHWR). To ameliorate this situation, reactor operational procedures have been established which minimize the incidence of fuel rod failures by PCI. While the operational procedures have been successful in reducing the incidence of fuel failures, the procedures are inconvenient to reactor operators and are costly in terms of reduced capacity factor for plant operation and thus in reduced electrical output. There is a strong incentive to provide a remedy that would eliminate the need for these operational procedures.

Building upon the General Electric Company's (GE's) extensive previous efforts (1969-1977) to understand the PCI phenomenon and to develop potential remedies, this Program was designed to demonstrate two remedies which GE had already identified as having good potential for success: (a) Cu-Barrier fuel and (b) Zr-Liner fuel. Cu-Barrier fuel has a Zircaloy sheath with a very thin layer of copper plated on the inner surface. Zr-Liner fuel has a Zircaloy fuel cladding with a metallurgically bonded layer of zirconium on the inner surface.

The ultimate objective of this Program is to realize demonstration of the PCI-resistance of a fuel based on one or both of these potential PCI remedies. The demonstration will be in a commercial Boiling Water Reactor and it is intended to test a sufficient quantity of fuel to form a reliable data base regarding the performance characteristics of the new fuel. While it is not yet known in which reactor or reactors the actual demonstration(s) will occur, it probably will be in a reactor with a steady-state core, where the fuel to be demonstrated will be introduced as part of a reload batch.

Prior to the actual demonstration there will be developed an adequate data base to enable design and licensing; fabrication and quality assurance problems must be addressed; and there must be extensive nuclear physics, fuel management, and power history analyses so that the experimental fuel is properly tested with minimum risk to other fuel in the core. Consequently, the Program has been structured to consider each of these aspects.

This is the first semiannual progress report for this Program, and it represents the work done in the last 6 months of calendar year 1977. Much of this work used information, irradiated specimens (both fueled and unfueled), and some experimental techniques previously developed by GE. These techniques explained herein and some data obtained prior to this time period are presented within this report.

2. BACKGROUND

2.1 THE PCI MECHANISM

Starting in 1966, PCI failures were observed in power ramp tests of Dresden-1 Type 1 fuel segments; the ramp tests were done at the General Electric Test Reactor (GETR). Subsequent ramp tests and analyses of failures from commercial water-cooled reactors lead to the identification of PCI as the cause of failure.

The incidence of PCI failures was found to depend on absolute power, increase in power, duration of the power increase, previous power history, and burnup. Also, there was a power threshold below which failures did not occur. The relation of power threshold as a function of burnup was similar for both GETR tests and field experience. Results from CANDU reactors were qualitatively similar but had a higher sensitivity to PCI due to their thin collapsed cladding design.

Mechanistic tests with irradiated cladding and fresh fuel, unirradiated cladding and irradiated fuel, and irradiated fuel rods annealed prior to testing, indicated that although cladding stress was an important parameter, a chemical embrittling agent was also essential. This reasoning is consistent with the observation that duration of a power increase is an important factor. Furthermore, even after irradiation to high fluence levels, the residual ductility in Zircaloy cladding is too great to allow the low-ductility cracks observed in ramped fuel. However, certain chemical agents were found to reduce ductility to small values.

Convincing evidence of the importance of a chemical agent comes from fractographic studies. In the absence of specific chemical species, and regardless of stress state, strain rate, temperature, or state or irradiation, the Zircaloy tubes always fracture by ductile microvoid coalescence. Even when the Zircaloy is heavily irradiated and is plastically unstable, the fracture mechanism is ductile. However, in the presence of certain chemical agents (I_2 or Cd) the fracture of Zircaloy is brittle as evidenced by intergranular or transgranular cleavage and fluting features on the fracture surfaces. These unmistakable indications of the presence of chemical agents were found in incipient cracks in the cladding of unfailed fuel which had been power ramped to produce PCI.

Although a chemical agent is essential, the stress on the cladding caused by PCI is also essential. A mechanical model has been developed and has demonstrated that the critical parameters are:

1. the stochastic nature in which pellets are located within the fuel tube and the volume occupied by pellet segments (cracked pellets) as a function of burnup.

2. the volume occupied by cracked pellets increases as a function of burnup and of the severity of power changes.

Analytical modeling can explain the occurrence of high stresses at pellet-pellet interfaces, and mid-pellet locations where PCI cracks are most commonly found. The models clearly show that strain concentrations occur in the cladding at radial pellet crack locations; the strain concentration is enhanced where the strain due to pellet cracks has superposed on it the strain at pellet-pellet interfaces. In addition, creep-down of cladding also adds to the mechanical interaction of fuel and cladding when the reactor power is increased. In Figure 2-1, the synergism between a stress/strain concentration and the harmful species is schematically illustrated.

An important part of the GE investigations was the study of the chemistry of the inside of an operating fuel rod and the definition of which fission products, singly or in combinations, are the necessary chemical agent or agents responsible for the PCI failures. Inventories of fission products were computed in detail (see Figure 2-2). Thermodynamic and kinetics calculations were done to define the expected chemical species, including unstable species resulting from radiolytic reactions. Experiments were performed to determine which fission products could produce the low-ductility fractures observed in PCI failures. The experiments defined two important fission product elements, iodine and cadmium, which produce marked embrittlement of stressed zirconium alloys and duplicated the brittle fracture morphologies of PCI defects observed in the cladding of power-ramped fuel. Figures 2-3 and 2-4 illustrate the embrittling

effects of iodine and cadmium, even when the Zircaloy is in its intrinsically ductile, unirradiated condition. With irradiated Zircaloy tested in a plane strain configuration, either iodine or cadmium can produce fractures at strain levels similar to those observed in fuel cladding that had failed by PCI.

The chemistry of fission products in UO_2 fuel is a complex function of stoichiometry. Thermodynamic calculations have shown that the initial excess of oxygen in the UO_2 tends to favor iodine early in life, but with more burnup the oxygen content diminishes, especially near the cladding, and the potential for embrittlement by cadmium tends to increase. The pure elements are not necessary for embrittlement. In several tests, iodine and cadmium as well as their compounds and mixtures with other fission products have been found to be capable of producing brittle fracture of zirconium alloys.

2.2 REMEDIES AND TESTS OF REMEDIES

Based on knowledge of the PCI mechanism, a wide range of possible remedies have been evaluated, and many are still in various stages of elevaluation in fuel irradiation tests. Remedies can be classified roughly: (a) those which reduce the mechanical interaction between fuel and cladding, and (b) those which prevent or ameliorate chemical interaction between the harmful fission products and the cladding. Remedies which fit into either or both of these categories have been evaluated or are presently being irradiated. The kinds of remedy concepts already considered are very broad, but maintain the basic fuel as UO_2 clad with Zircaloy.

Both laboratory and reactor tests have been used in the GE evaluation program. Laboratory tests of unirradiated and irradiated fuel cladding in iodine, cadmium, and other environments have included: (a) localized ductility tensile tests in plane stress and in plane strain configurations, (b) expanding mandrel tests to directly simulate PCI loading conditions, and (c) pressurized-tube tests. Reactor tests have included: (a) power-ramped fueled capsules with PdI_2 added to the fuel to simulate burnup, (b) accelerated irradiation tests of thin-walled fuel rods which were power ramped in the General Electric Test Reactor after low burnup at low powers, and (c) segmented fuel rods irradiated in commercial BWR's and subsequently ramp tested in GETR. In addition, there have been economic studies, licensability studies, fabrication process development, and loss-of-coolant accident (LOCA) simulation tests of some of the more promising concepts.

Among the many different remedy concepts tested, the two which are the subject of this Program are the most promising at this time. These are (a) the Cu-Barrier and (b) the Zr-Liner concepts. In (a) the copper barrier is applied by a plating technique in a thin layer (~5-10 μm) to otherwise finished fuel tubes prior to assembly of fuel rods. In (b) a thicker (~75 μm) pure zirconium liner is metallurgically bonded to conventional cladding material by co-extrusion of tube shells and subsequent tube reduction in a manner that is similar to the current commercial tubing manufacturing process.

The prime PCI remedies (Cu-Barrier and Zr-Liner) were selected after a comprehensive analytical and experimental screening process. Criteria considered in the screening process included: resistance to PCI in fuel rod tests, resistance to embrittlement by I_2 and Cd in laboratory tests, resistance of barrier properties to radiation-induced degradation, reactivity penalty, fabricability, cost, licensability, reprocessing, etc.

This exhaustive evaluation of many concepts and materials has led to these prime candidate remedies. The main advantages and disadvantages of these materials are summarized as follows.

Copper

- Copper is chemically reactive with both iodine and cadmium, and is inherently immune to stress corrosion or liquid metal embrittlement by either of these elements. Thus copper has a chemical effect in preventing access of harmful fission products to the fuel cladding.

- Laboratory testing has shown that pure copper is immune to stress corrosion by iodine or cadmium. Additional testing of Zircaloy tubing protected with copper plating has demonstrated the protective effects of copper.

- Several fuel rods protected with plated copper barriers have been ramped to high powers (~20 kW/ft) without failure. Several unprotected fuel rods, or rods protected with marginally effective PCI remedies, have all failed equivalent tests at substantially lower powers.

- Copper plating has an inherent reactivity penalty. This penalty can be controlled to acceptable levels by using very thin (5 to 10 μm) layers.

- Fabricability of prototype full-length fuel cladding has been demonstrated. Prototype quality control methods for copper layer thickness measurements have also been developed.

- Copper can form a molten eutectic mixture with Zircaloy cladding during postulated LOCA transients. Tests, however, have shown that this eutectic formation does not affect the cladding deformation and rupture properties during simulated LOCA transients. Additional margin is anticipated with copper plated on autoclaved Zircaloy surfaces, because the two metals will be kept from direct contact by a ceramic phase (ZrO_2) during the LOCA transient.

- Copper properties may be degraded by slow, solid-state reaction with the Zircaloy cladding during fuel operation. This reaction can lead to the formation of an intermetallic phase which may degrade the protective character of the copper. Limited tests to date with fuel rods containing this intermetallic layer have shown very high resistance to PCI. Should the intermetallic phase prove to limit the useful life of Cu-Barrier fuel, it is believed that the use of copper plating on autoclaved surfaces will prevent the formation of the intermetallic layer.

- In a defected fuel rod copper might promote hydriding and further degradation of the failed cladding. Additional tests are required to assess this possibility. Again, the use of copper plated on autoclaved Zircaloy could have a beneficial effect in reducing any copper-induced hydriding of defected fuel rods.

Zirconium

- In its pure form, zirconium is softer than Zircaloy when compared at the same fluence. Highly irradiated pure zirconium has approximately the same yield strength as unirradiated Zircaloy-2. Pure zirconium acts to inhibit stress and strain localization due to pellet-cladding interaction, and keeps stresses below the threshold level necessary to produce brittle cracks.

- Pure zirconium tends to resist embrittlement by cadmium, but it is not immune to embrittlement by iodine. However, resistance to embrittlement by both species has been demonstrated in mandrel tests performed on unirradiated and irradiated cladding specimens containing metallurgically bonded (75-μm-thick) pure zirconium barriers.

- Fuel rods protected with 75-μm-thick pure zirconium liners (metallurgically bonded to the cladding) have been ramped to high powers (~20 kW/ft) without failure. Several unprotected fuel rods, or rods protected with marginally effective PCI remedies, have all failed equivalent tests at substantially lower powers.

- Pure zirconium has no reactivity penalty. For this reason, it can be used as a relatively thick liner, thus making it more resistant to mechanical damage during fuel loading or operation.

- Fabricability of prototype full-length fuel cladding has been demonstrated with high-purity (crystal bar) zirconium and moderate-purity (low-oxygen sponge) zirconium liners. Because pure zirconium is very soft, it is susceptible to manufacturing-induced surface defects. Additional work must be done to qualify fabrication processes to reduce these defects to commercially acceptable levels.

- Zirconium has no potential for molten eutectic formation during LOCA transients. Tests have shown that pure zirconium liners do not affect cladding deformation and rupture properties during simulated LOCA transients.

- Most of the physical and chemical properties of zirconium are very similar to those of Zircaloy-2. For example, equivalent coefficients of thermal expansion enhance fabricability and minimize the potential for in-service delamination of the liner. Equivalent chemical properties mean that the hydride degradation of defected fuel rods containing zirconium liner cladding should be the same as that of conventional cladding. In addition, no impact on fuel reprocessing is anticipated.

- Pure crystal bar zirconium is an expensive material that is not currently available in amounts necessary for manufacture of large numbers of fuel bundles. Lower-purity sponge zirconium is cheaper, is available, and may have the same level of resistance to PCI. If tests indicate that sponge zirconium has adequate resistance to PCI, the major cost disadvantage of this concept will be significantly reduced.

In-reactor accelerated tests of these remedy designs have been performed with thin-walled cladding to enhance compressive creep under the action of the coolant pressure and thus increase the severity of pellet-cladding interaction at low burnup. In such experiments fuel is incubated at lower power ($\leq$10 kW/ft) to burnups of approximately 4 GWd/t-U, and it is then power ramped to powers as high as 21 kW/ft. In such tests reference fuel without PCI remedies and fuel containing marginal remedies consistently failed during the power ramp. By comparison, fuel rods with the Cu-Barrier and Zr-Liner remedies survived the test without failure; subsequent examinations revealed that incipient defects had not initiated in the cladding. Evaluations at higher burnups are in progress. Segmented ($\sim$3 ft-long) fuel rods containing reference cladding, and Cu and Zr barrier cladding (in addition to other remedy concepts) are being incubated at lower power in three commercial BWR's in preparation for subsequent power ramp tests. Some of these rods have reached exposures of 12 GWd/t.

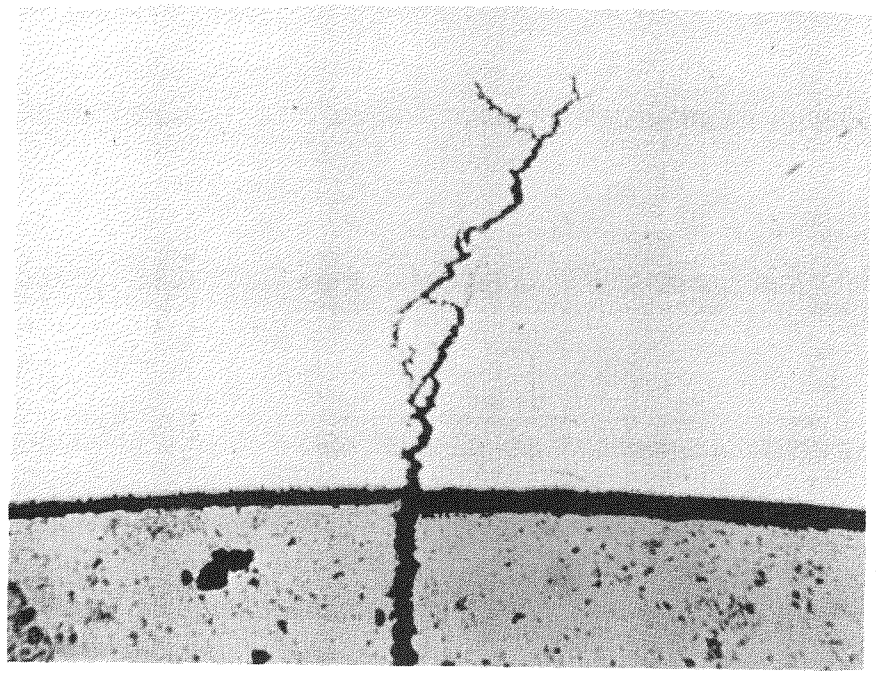

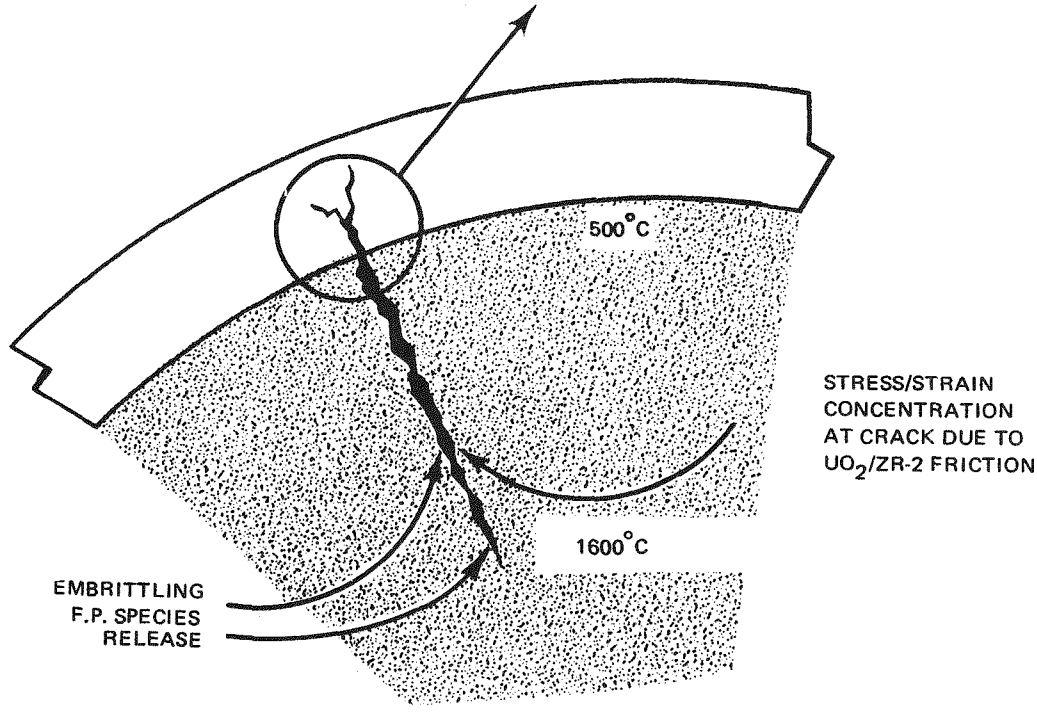

Figure 2-1. PCI Failure Mechanism

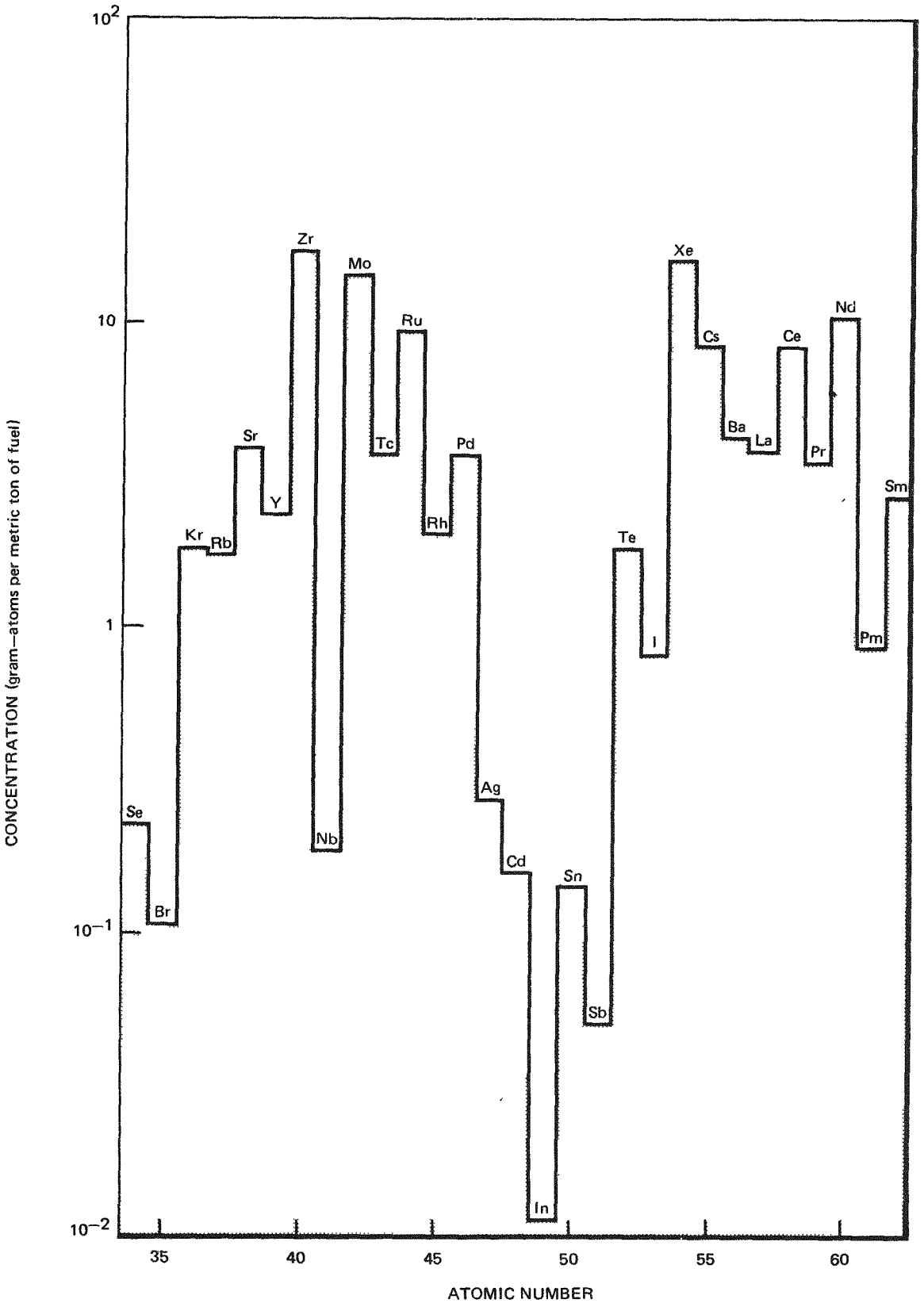

Figure 2-2. Concentration of Fission Product Elements in Fuel at 13,800 MWd/Te Burnup

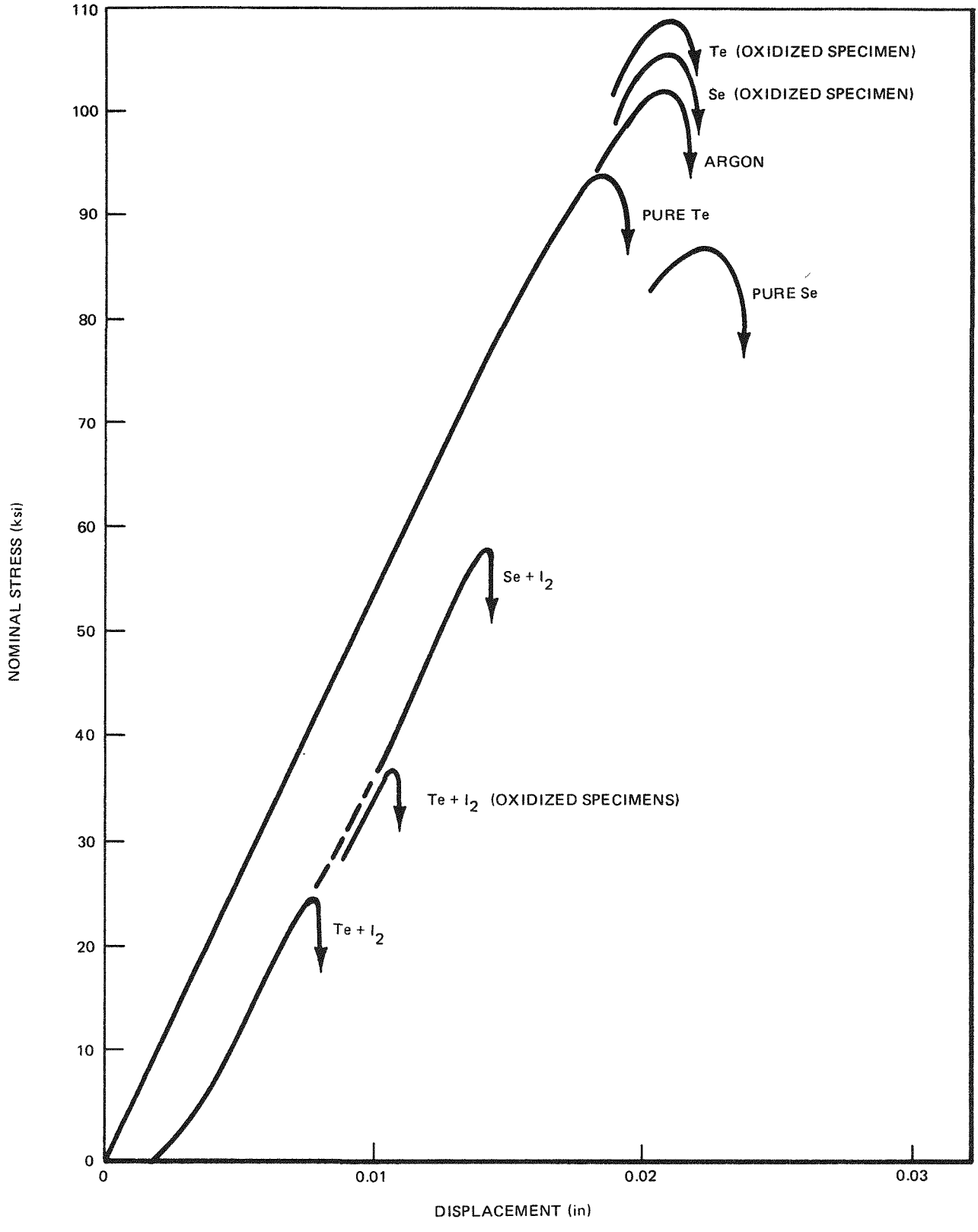

Figure 2-3. Influence of Iodine on Engineering Stress and Elongation Properties of Notched Zircaloy-2

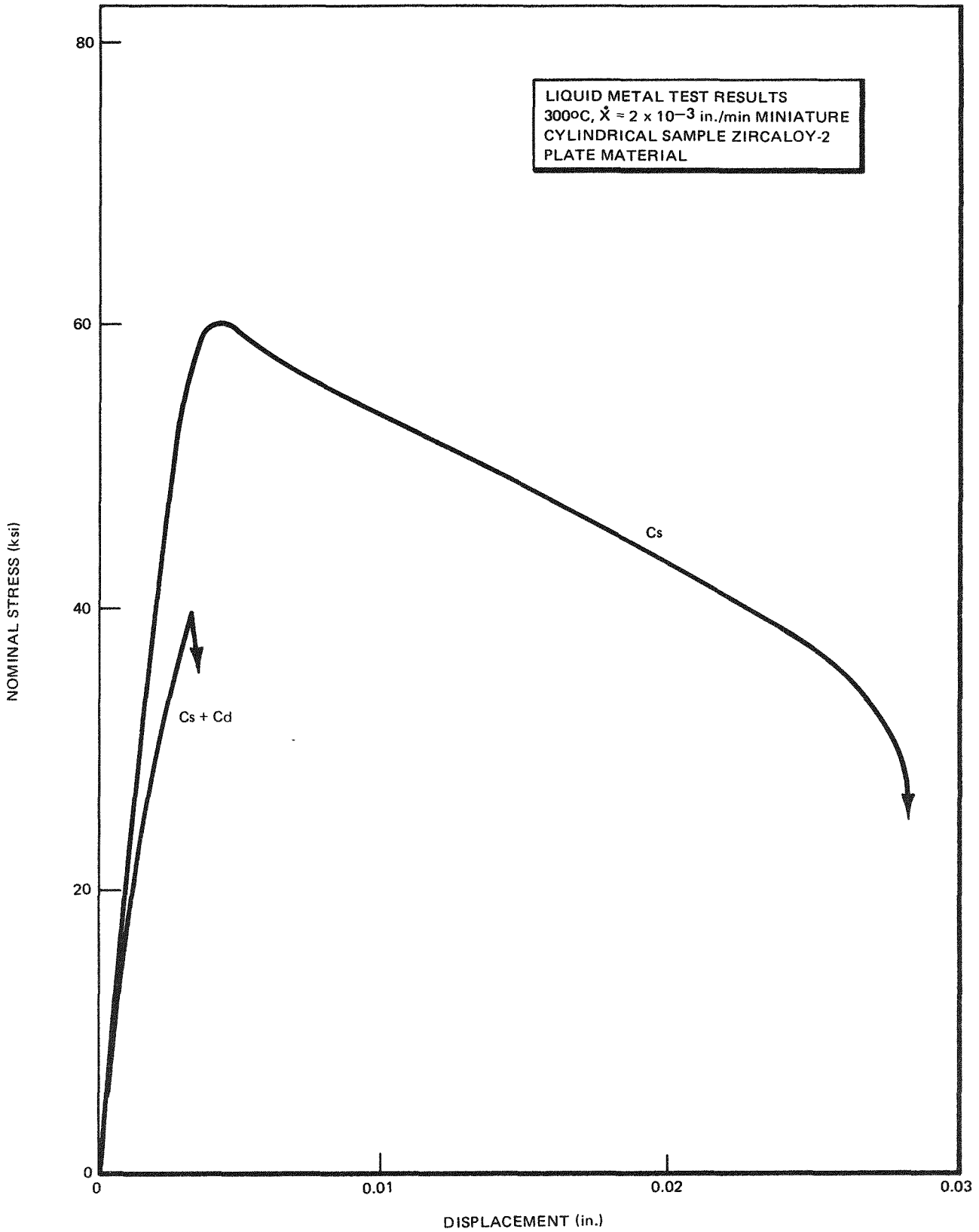

Figure 2-4. Effect of Cadmium (Diluted in Cesium) on the Ductility of Zircaloy Plate When Tested in Tension, Engineering Stress versus Elongation

3. PROGRAM SCOPE

As presently structured, this Program leads ultimately to the large-scale demonstration of the two remedy concepts discussed here: Cu-Barrier and Zr-Liner. The Program has been divided into two phases:

PHASE 1. Design and Supporting Tests

PHASE 2. Large-Scale Demonstrations

PHASE 1 contains the detailed planning and all of the initial work required to support the large-scale demonstration of the two remedy concepts. Thus, PHASE 1 includes:

1. Planning and nuclear engineering necessary to design the irradiation aspects of the demonstrations.

2. Laboratory and reactor tests of resistance to failure by PCI.

3. Laboratory tests and calculations relevant to loss-of-coolant accidents (LOCA) and to reactivity-initiated accident (RIA) conditions to assure an adequate licensing data base for new fuel configurations.

4. Design, fabrication, irradiation, and evaluation of lead test assemblies (LTA's) which are intended as prototypes and will accumulate reactor exposure and burnup in advance of the large-scale demonstration. The lead test assemblies will serve as a primary licensing vehicle for the large-scale demonstration.

PHASE 2 will continue the work of PHASE 1 to completion and will also include:

1. Manufacturing of the fuel for the large-scale demonstration.

2. The demonstration *per se*; that is, the irradiation (including specially designed power ramps to test PCI resistance) and the evaluations.

This report is the first Semiannual Progress Report for this Program and is concerned solely with the initial stages of PHASE 1 activities.

4. PHASE 1 PROGRAM DESCRIPTION

4.1 Part 1. DESIGN OF LARGE-SCALE DEMONSTRATION

4.1.1 Objectives

1. Design the Demonstration experiment such that the resistance of the barrier fuel to PCI is unambiguously tested, while minimizing the risk to the other fuel in the core.

2. Select reactor for the Demonstration and obtain concurrence from the reactor owner.

3. Design the nuclear aspects of the Demonstration fuel bundles, including: fuel rod enrichments, rod locations, and distribution of gadolinia.

4. Establish the patterns for loading, discharge, and repositioning of fuel assemblies.

5. Specify reactor operational variables as required to satisfy the needs of both the Demonstration and the reactor owner/operator.

4.1.2 Technical Approach

The feasibility of the Demonstration will be determined using the Quad Cities-1 plant at the beginning of Cycle 6 as an example of an operating BWR/3 with a steady-state core. The general approach to the problem is to insert the advanced PCI-resistant fuel as part of the normal reload batch. The Demonstration must then be designed such that: (a) the PCI resistance of the advanced fuel is demonstrated, (b) the conventional fuel is operated under standard procedures, and (c) the procedural operational requirements imposed on the reactor owner/operator by this Demonstration do not inhibit the reactor performance unduly, and are acceptable to the utility. In Part 1 it is intended that the following work be done within the present work scope:

1. Develop generic refueling strategies and operational guidelines for an unambiguous large-scale demonstration of the PCI-resistant fuel.

2. Define the number of demonstration fuel bundles required, along with their approximate enrichments and gadolinia contents.

3. Verify the feasibility of the design relative to the experimental and operational constraints imposed by those needs of the Demonstration and by the reactor owner/operator. Verification will consist of a 3-dimensional coupled nuclear-thermal hydraulic simulation of the Demonstration in Quad Cities Unit 1, beginning in Cycle 6.

4. Perform detailed lattice analyses to evaluate generic changes to the standard reload designs required to meet the Demonstration criteria. (Actual bundle design will be done after the selection of the host reactor and a realistic target insertion date. Therefore, actual bundle design is outside the PHASE 1 work scope.)

4.2 Part 2. SUPPORT TESTS FOR LARGE-SCALE DEMONSTRATION

Objectives:

1. Evaluate the barrier fuel and select preliminary designs and specifications for the PHASE 2 demonstration.

2. Perform analyses and simulation experiments to verify that the barrier fuel performs equivalent to standard fuel during loss-of-coolant accidents (LOCA) and reactivity-initiated accidents (RIA).

3. Extend the present data base, and test the barrier fuels' resistance to PCI at higher burnups.

4. Develop process and quality assurance procedures in advance of a commitment to manufacture the fuel for the PHASE 2 demonstration.

4.2.2 Technical Approach

4.2.2.1 Task 1.0 Laboratory Tests

In this task the Cu-barrier itself and its ability to resist the PCI failure mechanism will be evaluated by use of certain laboratory tests on both unirradiated and on irradiated Cu-plated Zircaloy tubing samples. In addition to this preliminary evaluation of PCI resistance, there are some potential problems with Cu-Barrier fuel which will be explored:

1. Possible formation of brittle intermetallic phases due to interdiffusion of copper with Zircaloy.

2. Effects of the Cu-barrier on hydrogen pickup and degradation of defected fuel rods.

Because Zr-liners of various purity levels are being considered, this task will compare the stress-corrosion-cracking behavior of irradiated zirconium of various purity levels. The corrosive environment will consist of liquid cesium saturated with Cd.

Tubing with Zr-liners of two purity levels (crystal bar zirconium and low-oxygen sponge zirconium) will be inserted into the GETR for irradiation at ~300°C to fluence levels of ~1.5×10^{21} n/cm^2 (E>1 MeV). These specimens are to be tested with an expanding mandrel in I_2 vapor and in Cd to roughly simulate PCI at high burnup.

4.2.2.2 Task 2.0 Licensing Tasks

Data to assure the Zircaloy fuel cladding with a Cu-barrier or with a Zr-liner is equivalent to conventional fuel cladding under LOCA and RIA conditions will be obtained. The LOCA experiments will be done with unirradiated cladding loaded with dummy fuel pellets and subjected to a temperature-pressure transient that simulated LOCA conditions. The RIA experiments will be done at the Nuclear Safety Research Reactor (NSRR) in Japan (simulation of a sudden control rod drop with fuel initially at room temperature).

4.2.2.3 Task 3.0 Fuel Irradiation Tests

Subtask 3.1 Accelerated PCI Tests. Short fuel pins will be irradiated in the GE Test Reactor (GETR) and then power ramped to test PCI resistance at burnup of ~4 GWd/t.* In these tests the PCI phenomena are accelerated by use of thin cladding (to enhance mechanical interaction) and by enriched fuel (to rapidly accumulate burnup and fission product inventory). Tests will be done to evaluate an improved plating method with two Cu-barrier configurations: (a) Cu plated directly onto the Zircaloy, and (b) Cu plated onto an oxidized Zircaloy surface.

Fuel pins with cladding having metallurgically bonded Zr-liners have been prepared for irradiation and testing in the GETR as described for Cu-barriers. These represent Zr-liners of two purity levels: crystal bar zirconium and low-oxygen sponge zirconium. Irradiation will be continued until burnup of ~4 GWd/t is achieved, and the Zr-liner fuel pins will be tested by power ramping.

Subtask 3.2 Segmented Rod Irradiation Experiments. Here fuel has been manufactured in segmented rods and assembled into special (SRP)** fuel bundles for irradiation in some commercial BWR's: Quad Cities-1, Monticello, and Millstone. The fuel with various developmental configurations but with standard BWR enrichments is irradiated in the BWR's to accumulate burnup. The fuel is then power-ramp tested in the GETR. Unlike the accelerated irradiations, these experiments use actual BWR exposure to accumulate burnup; there is no acceleration. The only deviation from normal service conditions is that power levels are kept low during the burnup accumulation to accentuate the PCI effect during the subsequent power ramp tests.

---

*Burnups are for short tons of uranium
**Segmented Rod Program

Irradiated fuel segments with Cu-barrier (electroplated) will be tested for PCI resistance, and new Cu-Barrier fuel (new electroless technique) will be manufactured for insertion in the appropriate BWR's with a segmented rod (SRP) bundle. The new segments will represent both of the Cu-barrier modifications: (a) copper plated directly on Zircaloy, and (b) copper plated on oxidized Zircaloy. Irradiated fuel segments with Zr-liners of crystal bar zirconium will be tested for PCI resistance with power ramp tests in GETR, while additional segments representing both the crystal bar zirconium and the sponge zirconium liner will be manufactured for future irradiation in the appropriate BWR's.

4.3 Part 3. LEAD TEST ASSEMBLIES

4.3.1 Objectives

The objectives of this task are to:

1. Fabricate and irradiate lead test assemblies of barrier fuel prototypical of that in the PHASE 2 demonstration.
2. Irradiate in a manner to accumulate burnup at high powers ahead of the fuel in the demonstration.
3. Evaluate the performance of the barrier fuel by non-destructive examinations.

4.3.2 Technical Approach

The actual demonstration of the Cu-Barrier and the Zr-Liner fuel concepts will start with the fabrication, irradiation, and evaluation of lead test assemblies.

Each LTA will be a full-size fuel bundle with an 8 x 8 array of fuel rods, prototypical of the materials and dimensions of the PHASE 2 demonstration bundles. The purpose of lead test assemblies is to accumulate burnup ahead of the PHASE 2 demonstration to detect any unforeseen problems that are unique to barrier fuel, and manifested only in full-size, high-power bundles. Thus, the evaluation of the lead test assemblies contributes to the effort to license the PHASE 2 demonstration. By its very nature, a lead test assembly requires careful characterization and documentation prior to irradiation, extensive power history measurement and documentation, and thorough evaluation of fuel performance at various burnup levels.

Four lead test assemblies, two with Cu-Barrier fuel and two with Zr-Liner fuel will be fabricated and tested. The four lead assemblies will be as follows:

1. Cu-barrier directly on Zircaloy
2. Cu-barrier applied to oxidized Zircaloy
3. Zr-liner of crystal bar zirconium
4. Zr-liner of low-oxygen sponge zirconium

As a contingency, two fuel rods in each of the four lead test assemblies will be segmented (four segments in each segmented rod). These segments are readily removable and will be available for examinations and possibly additional experiments (perhaps power ramp testing) if desired.

The target for insertion of the LTA is the Quad Cities-1, beginning of Cycle 5 (currently scheduled for mid-January 1979).

The task structure within Part 3 is as follows:

Task 1.0	Design and Licensing
Task 2.0	Fabrication
Task 3.0	Characterization
Task 4.0	Irradiation and Evaluation

5. PROGRESS IN CURRENT REPORT PERIOD – PART 1. DESIGN OF LARGE-SCALE DEMONSTRATION (R.E. Brown and S.R. Specker, NTD)

5.1 INTRODUCTION

The initial phase of the design effort is directed at verifying the feasibility of the demonstration in a reactor of type BWR/3. This will be accomplished by performing a 3-dimensional simulation of the demonstration in Quad Cities Unit 1 (QC-1) beginning in Cycle 6. The objective of the study is to develop generic loading strategies and operational procedures which will yield a calculated core performance which meets normal design constraints as well as the goals of the demonstration. The final phase of the nuclear design will be directed at a detailed design of the demonstration in the host reactor, which has yet to be selected.

The major emphasis during the current period has been on evaluation of various fuel loading strategies to be used for the demonstration. This section of the report contains the design criteria and goals used as a design basis and the results of the nuclear evaluations performed. The scope of work to be performed in the nuclear area during the next report period is outlined.

5.2 DESIGN PROCEDURE

The design criteria employed are given in Table 5.2-1. The initial phase of the design is a generic simulation being performed in QC-1. The first batch of PCI-resistant fuel is loaded into Cycle 6. The fuel cycle criteria are that each cycle be an 18-month cycle at a capacity factor of 61±1%. This is equivalent to a cycle energy requirement of 825 to 852 GWd.

The PCI-resistant fuel will be simulated during the generic design effort by using the standard 8x8D lattice (retrofit) bundle designs. The final design will use actual PCI-resistant fuel bundle designs which will be based upon the current retrofit designs with changes in selected rod enrichments and/or gadolinia content which may be required to meet the demonstration goals. However, the standard hardware design will be retained.

Table 5.2-1
DESIGN CRITERIA

Quad Cities Unit 1 — Start demonstration in Cycle 6.

Energy – 18-month cycles with energy generation of 838.5 GWd.

Nominal reload fuel subject to standard thermal and mechanical design limits.

Standard Operation Regarding Power Changes – Apply to nonbarrier fuel only.

Standard Design Methods — Benchmarking against more detailed methods where required.

Barrier fuel to be incubated at a LHGR <8 kW/ft at all times prior to ramping. LHGR during ramping ≤13.4 kW/ft.

Barrier fuel will use standard 8x8D lattice (retrofit) hardware design.

All current reload design limits are applicable.

Standard methods will be employed throughout the design with the use of benchmarking analyses to define the range of uncertainty caused by the nonstandard core loading required.

The primary design constraint is that the demonstration should not restrict normal plant operation or energy capability. Operational restrictions and risk to the nonbarrier fuel must be held to a minimum.

5.3 DESIGN CONCEPT

5.3.1 Fuel Loading

The goal of the demonstration is to test the resistance of the barrier concepts to PCI failure during the operational lifetime of the fuel. To this end, PCI-resistant fuel will be loaded into a BWR/3 and incubated at low power (below 8 kW/ft) to various exposures. The fuel will then be ramped to a high power to demonstrate PCI resistance. A total of four ramps are currently projected. A different group of fuel will be ramped at each of the four exposure increments.

The current refueling concept for the test fuel is to load all of the barrier fuel of a given type in one cycle. The fuel is divided into four equal groups, one group to be ramped per cycle. The group of fuel to be ramped during the current cycle will be loaded into four-bundle control-blade-centered cells, termed test cells. The test cells are partially isolated from the remainder of the core by a ring of exposed nominal bundles. These bundles act as a buffer to minimize the power response changes in the fuel adjacent to the test fuel during ramping. The bundles loaded into this buffer ring will be of sufficiently high exposure to assure that the power in these bundles remains at low values during the ramping. The remaining barrier fuel that has not been ramped is located in low-power regions of the core. These regions are near, but not on, the periphery of the core. The fuel that has been ramp tested is treated like nonbarrier fuel in subsequent cycles (see Figure 5.3-1).

The number of test cells required depends upon the number of test fuel bundles to be ramped per cycle. Two cases have been evaluated in parallel. The first case involved a demonstration in which 64 bundles would be ramp tested over a span of four cycles. Towards the end of each cycle 16 bundles would be tested, and these would be arranged in four test cells placed symmetrically in the core (see Figure 5.3-1).

The second case involved ramp tests of 128 bundles which would be ramp tested over a span of five cycles. During three of these cycles, eight test cells would be required (see Figure 5.3-2). At present the four-cell configuration (first case) appears most promising, and that is the concept that is being developed further.

The test fuel loaded during Cycle 6 or 7 represents about 40% of the reload batch size. The remainder of the fuel loaded is standard 8x8D reload fuel.

5.3.2 Operation

The ramping process takes place near the end of each cycle during the demonstration. The fuel in the test cell is held at or below 8 kW/ft by inserting the associated control blade to ~75%. These blades are not moved during the cycle. The ramping process starts at the point in the cycle when all the control blades except those in the test cells are fully withdrawn. The test cell blades are then notched out, causing the fuel segments* in the test fuel to increase in power. The goal of the demonstration is to ramp as many axial fuel segments as possible to the operating linear heat generation rate (LHGR) limit of 13.4 kW/ft (see Figure 5.3-4).

The power distribution in a test fuel bundle during a control blade withdrawal is shown in Figure 5.3-5. Figure 5.3-5a shows the average LHGR in the fuel bundle before and after the blade is withdrawn (6-notch withdrawal). Figure 5.3-5b shows the LHGR of the peak power rod. The peak power rod will be the corner rod adjacent to the control blade. This is due to the control blade history effect. The control blades are notched to the fully withdrawn position at which point the ramping and cycle end.

* In the present context and throughout Section 5 the term "fuel segment" refers to the fuel located between two axial nodes. The nodes form a 3-dimensional array used to define location within the core. Later in this report (Sections 6 and 7) the term "fuel segment" will refer to a portion of a fuel rod which is physically segmented. Such "segmented fuel rods" are so constructed that individual segments can be readily removed for testing.

- FUEL OF GIVEN TYPE LOADED IN ONE CYCLE
- FOUR GROUPS - ONE GROUP RAMPED PER CYCLE
- FUEL TO BE RAMPED IS LOADED IN TEST CELL

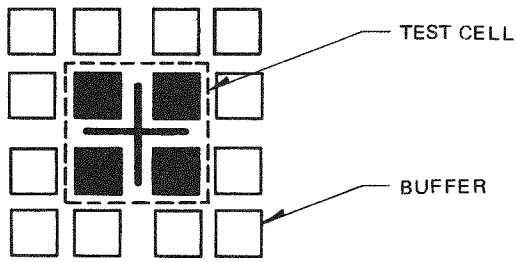

- TEST CELL SURROUNDED BY A BUFFER RING
- REMAINING NON-RAMPED FUEL IS LOADED NEAR CORE EDGE
- 4 OR 8 TEST CELLS PER CORE

Figure 5.3-1. Loading Strategy — Test Fuel

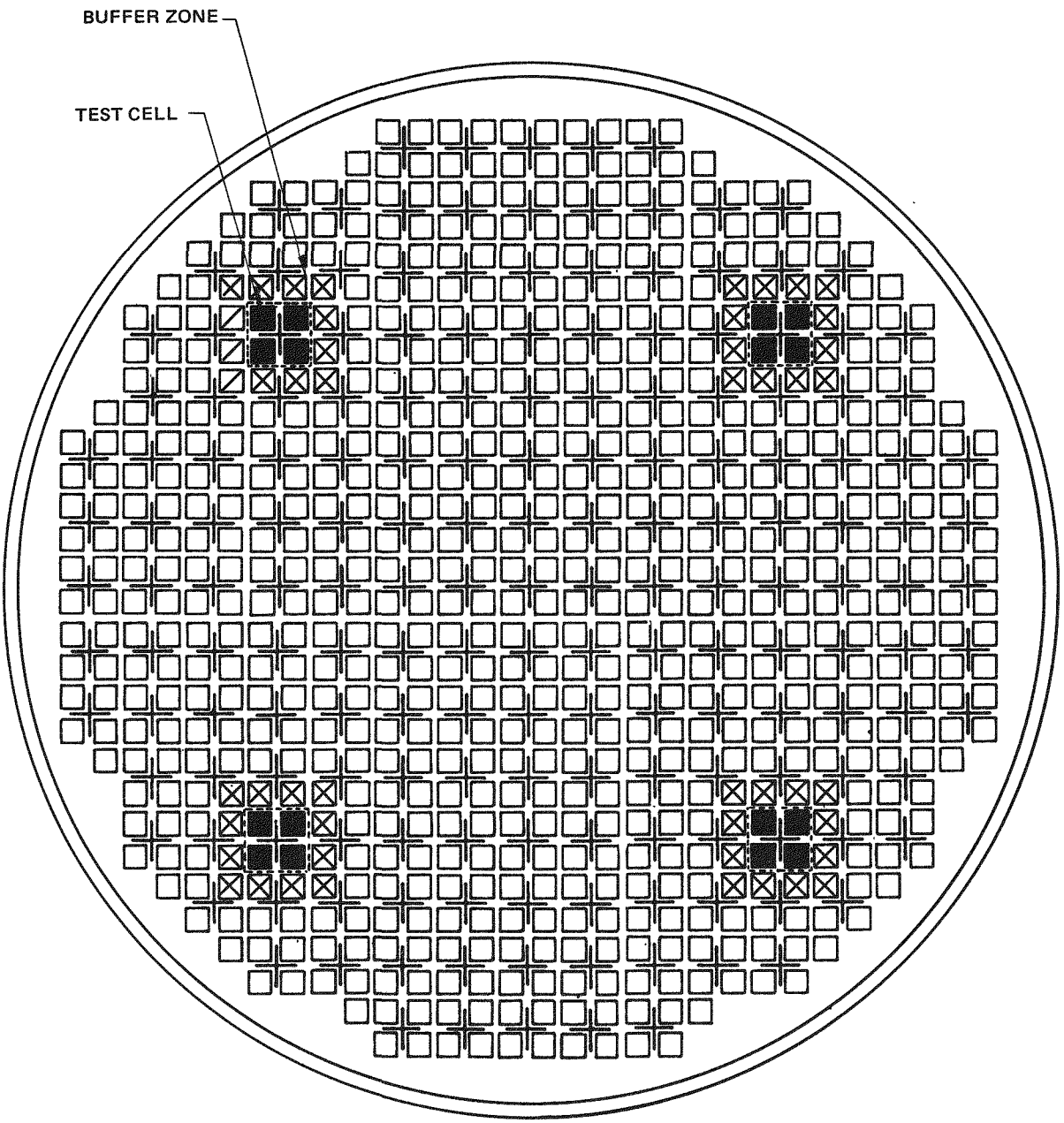

Figure 5.3-2. Test Cell Locations

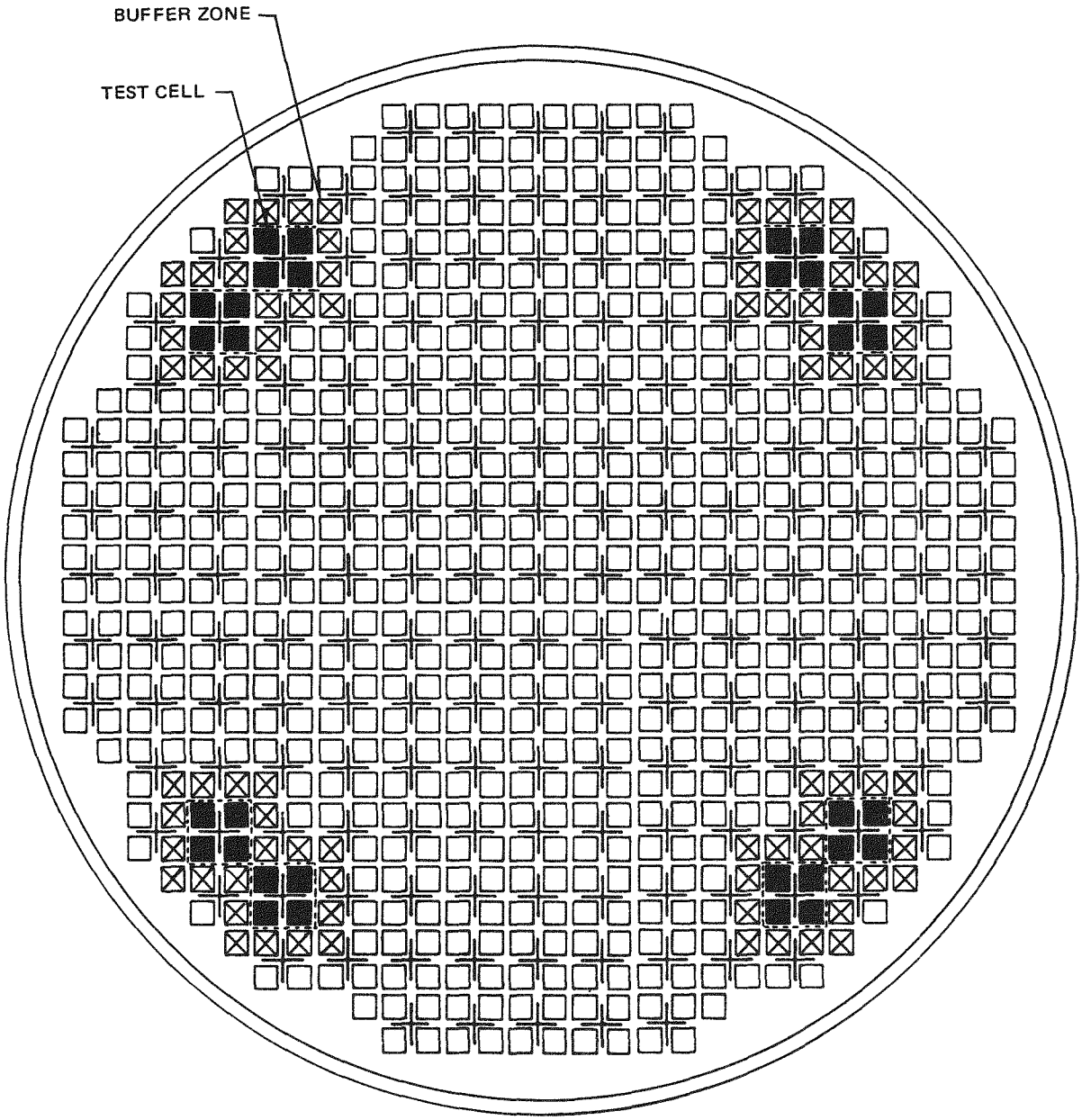

Figure 5.3-3. Test Cell Locations

- TEST CELL CONTROL BLADES INSERTED 75% THROUGH CYCLE
- RAMPING STARTS APPROXIMATELY 15 - 20 FULL POWER DAYS BEFORE END OF CYCLE. RAMPING PRODUCED BY NOTCHING BLADE OUT.

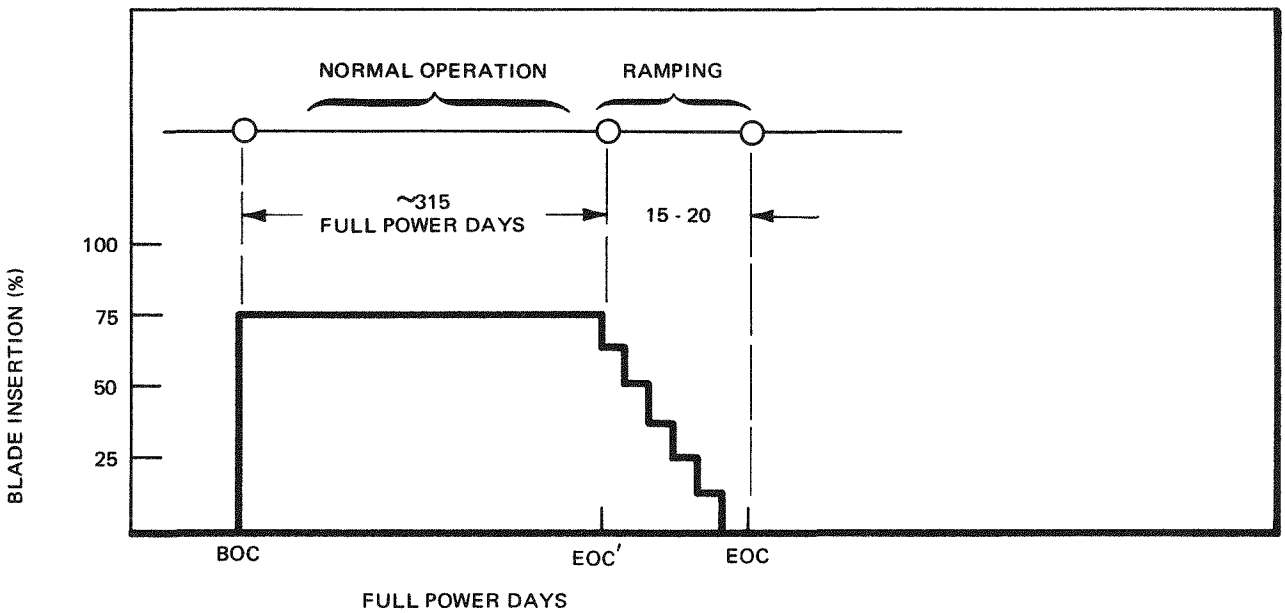

Figure 5.3-4. Operational Strategy

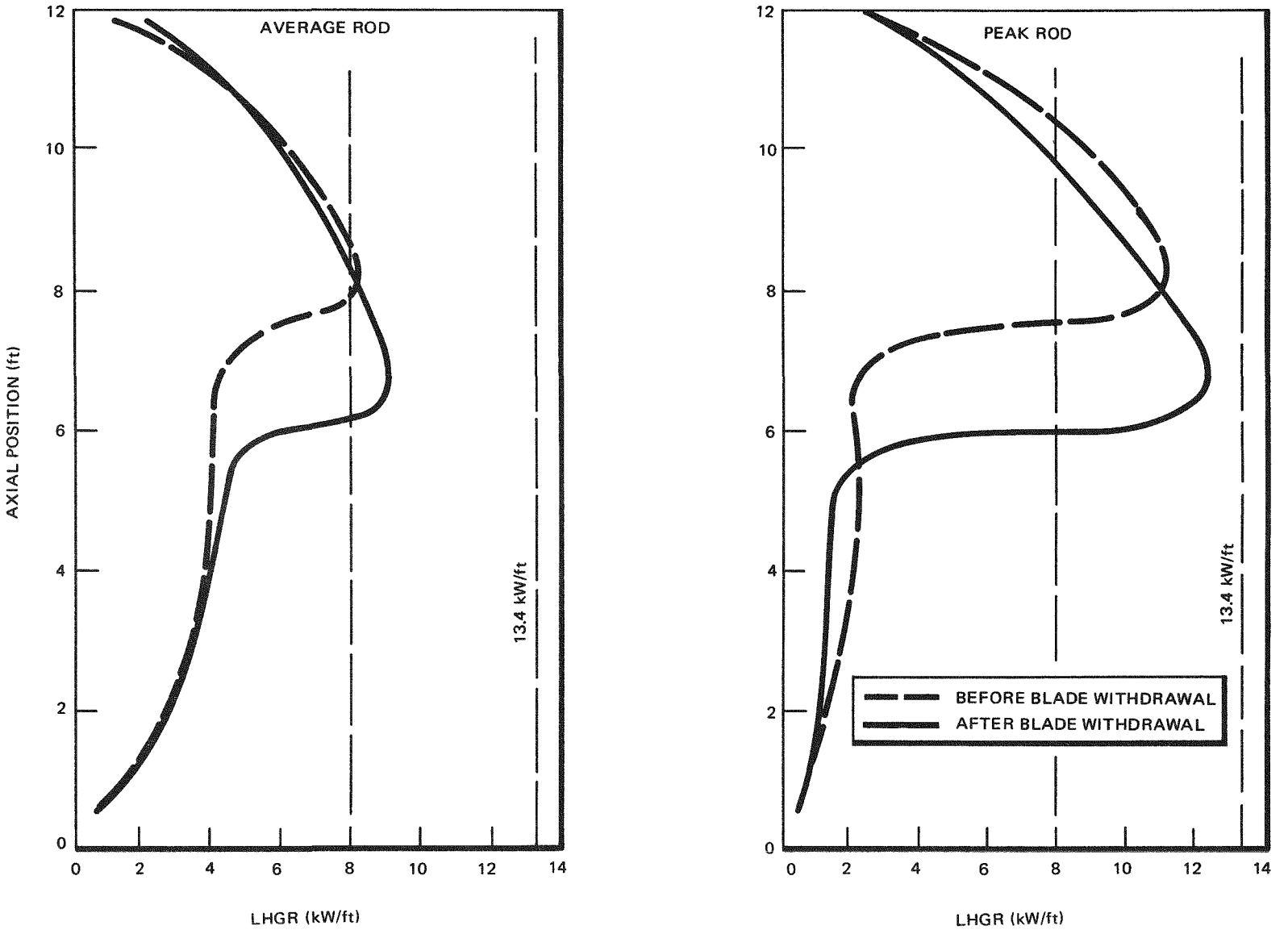

Figure 5.3-5. Axial Power Distributions for Blade Pull of 6 Notches (1.5 feet)

5.4 RESULTS

Two demonstration simulations have been performed and analyzed. The first simulation assumed only one barrier concept will be demonstrated, the second case assumed both concepts are demonstrated in a single core. The core loading and cycle energy performance calculated for the two simulations are given in Tables 5.4-1 through 5.4-4.

Table 5.4-1 gives the cycle performance for the case which assumes only one type of barrier fuel is to be demonstrated in a given core. The test fuel batch of 64 bundles is loaded in Cycle 6. Three bundle enrichments are used, the low-enrichment bundles being ramped during Cycle 6 and the high-enrichment bundles during Cycle 9. The energy calculated for each cycle is given in the third column and the 18-month cycle capacity factor is given in the last column. The discharge exposure summary for this case is given in Table 5.4-2. The desired average discharge exposure is 25,800 MWd/t-U. Note, the test fuel remains in the core for one cycle beyond the last cycle of the demonstration.

Tables 5.4-3 and 5.4-4 give similar results for the second case, which demonstrates both barrier concepts. The first type of test fuel is loaded in Cycle 6 and the second type in Cycle 7. The type 1 test fuel is ramped in Cycles 6 through 9 and the type 2 in Cycles 7 through 10. Table 5.4-5 gives the discharge exposure summary of the two batches loaded in Cycles 6 and 7.

Table 5.4-1
SINGLE TEST FUEL TYPE – CYCLE PERFORMANCE

Cycle	Bundles Loaded Number	Enrichment (% U-235)	Cycle Energy (GWd)	Capacity Factor (%)
6	16 [a]	2.39	838.2	61.0
	32 [a]	2.65		
	16 [a]	2.82		
	104	2.65		
7	16	2.39	848.9	61.7
	144	2.65		
8	16	2.39	840.6	61.1
	152	2.65		
9	16	2.39	853.0	62.0
	148	2.65		
10	16	2.39	848.1	61.7
	140	2.65		

[a] Test Fuel — 2.39e bundles are ramped in Cycle 6,
2.65e bundles in Cycles 7 and 8,
2.82e bundles in Cycle 9.

Table 5.4-2
DISCHARGE EXPOSURE SUMMARY – CASE 1

Bundle Enrichment (% U-235)	Number Discharged	Cycle Discharged	Discharge Exposure (MWd/t)
2.65	92	9	27669
2.65	12	10	25529
2.39[a]	16	10	25583
2.65[a]	32	10	24331
2.82[a]	16	10	25583

Average Discharge Exposure = 26539 MWd/t

[a] Test Fuel

Table 5.4-3
CYCLE PERFORMANCE
BOTH PCI BARRIER FUEL TYPES DEMONSTRATED

Cycle	Bundles Loaded Number	Enrichment (% U-235)	Cycle Energy (GWd)	Capacity Factor (%)
6	16[a]	2.39	838.1	61.0
	16[a]	2.65		
	32[a]	2.82		
	104	2.65		
7	32[b]	2.65	825.1	60.4
	32[b]	2.82		
	16	2.39		
	84	2.65		
8	16	2.39	850.8	61.9
	150	2.65		
9	16	2.39	844.4	61.4
	144	2.65		
10	16	2.39	828.8	60.3
	156	2.65		
11	16	2.39	838.5	61.0
	148	2.65		

[a] Test Fuel — Type 1
[b] Test Fuel — Type 2

Table 5.4-4
DISCHARGE EXPOSURE SUMMARY – CASE 2

Bundle Enrichment (% U-235)	Type	Number Discharged	Cycle Loaded	Cycle Discharged	Discharge Exposure (MWd/t)
2.65	N	92	6	9	28351
2.65	N	8	6	10	27545
2.39	1	16	6	10	22994
2.65	1	16	6	10	23450
2.82	1	32	6	10	21337
2.39	N	16	7	10	26436
2.65	N	60	7	10	27478
2.65	N	24	7	11	26353
2.65	2	16	7	10	25901
2.65	2	16	7	11	24248
2.82	2	32	7	11	22307

Average for fuel loaded in Cycle 6 = 25942 MWd/t

Average for fuel loaded in Cycle 7 = 25724 MWd/t

N = Nominal nonbarrier fuel
1 = Type 1 barrier
2 = Type 2 barrier

Table 5.4-5
TRANSIENT XENON STUDIES

Control Rod Position (Notches Withdrawn)		Peak Average Linear Heat Generation Rate (kW/ft)			
Before	After	Before	After (1)	After (2)	(2) – (1)
12	24	3.94	9.32	9.93	0.61
12	18	3.98	8.36	8.78	0.42
18	24	4.47	9.21	9.60	0.39
24	30	4.75	9.64	10.00	0.36
30	36	4.69	9.77	10.23	0.46
36	42	4.10	9.46	10.22	0.76
24	28	5.99	9.49	9.72	0.23

(1) ≡ Peak LHGR immediately following control blade movement
(2) ≡ Peak LHGR during xenon transient

The LHGR's obtained during ramping for each cycle were estimated based upon available lattice performance results and generic transient xenon studies coupled with steady-state blade pull analyses. The blade pull analyses were performed in the following manner. First, the reactor state was calculated at the point in the cycle for which the reactor is critical with only the test cell blades inserted (EOC). The power distribution was then calculated with the test cell blades at various positions. The results of these analyses are the average LHGR's for the fuel segments not including the transient xenon effect or the local peaking in the fuel segments. These two effects are estimated based upon available data.

The power in the test fuel nodes that become energized following a control blade withdrawal will increase essentially instantaneously to a power greater than the equilibrium value calculated by the above studies due to the lower-than-equilibrium xenon concentration. Immediately following the blade pull the xenon concentration will be reduced by the higher flux level, causing the power to increase further. Table 5.4-5 summarizes the results of several blade-withdrawal-induced xenon transient studies performed for the case 1 Cycle 6. The results indicate that for a 6-notch withdrawal (>0.5 foot blade move) the average LHGR will increase 0.4 to 0.76 kW/ft. The results show that the increase (indicated in the last column) is a strong function of the number of notches the blade is withdrawn and a function of the axial location. These studies are continuing to determine the effect of other variables, such as bundle exposure, on the power level changes caused by the xenon transients.

The relative power distribution in the fuel segments becoming uncontrolled during the blade withdrawal must be known in order to calculate the actual LHGR's. To determine the relative power distributions the effect of exposure accumulation with the control blade inserted must be accounted for. This is known as the control blade history (CBH) effect. The power in a controlled fuel segment will be significantly depressed (to 0.4 or 0.5 relative power) in the corner adjacent to the inserted blade. The fuel rods in this corner deplete more slowly relative to the bundle average during the controlled period. This can result in the corner fuel rods becoming the limiting rods in the segment after the blade is withdrawn. The increase in the uncontrolled corner rod power following long periods of controlled exposure accumulation is a function of the exposure when the segment becomes controlled, the exposure accumulated and the segment void fraction while controlled, and the general lattice design (i.e., C-lattice versus D-lattice). Table 5.4-6 contains the estimated local peaking factors for typical fuel segments being ramped in Cycles 6 through 9. (Note, these are estimates based upon prior lattice analyses of a reload lattice design which is similar to the retrofit designs used in this study. The analysis of the retrofit bundles is in progress.) These values can be used with the transient xenon study results and the blade pull analyses to estimate the LHGR's obtained during ramping of the test fuel. These results are contained in Tables 5.4-7 and 5.4-8.

Tables 5.4-7 and 5.4-8 contain the estimated peak LHGR obtained during the ramping of the test fuel for both refueling strategies. The LHGR's contained in this table range from a low value, which assumes no added peaking due to xenon transients, to a high value, which assumes a maximum increase in LHGR due to xenon transients. The estimated local peakings given in Table 5.4-6 were used. The average exposure of the bundle in which the peak value occurred is also given.

Table 5.4-6
EXPECTED LOCAL PEAKING IN RETROFIT
LATTICE DESIGNS – WITH CONTROL BLADE HISTORY (CBH) EFFECT

Bundle Enrichment (% U-235)	Exposure,[a] E (MWd/t)	Relative Power,[b] P	ΔExposure[c] (CBH)	ΔP[d]	Corner Rod Relative Power at Exposure E + ΔE
2.54	0	1.08	5000	0.16	1.24
2.82	5000	1.05	5000	0.25	1.30
2.82	12000	1.01	4500	0.30	1.31
3.01	18000	1.00	4500	0.35	1.35

[a] Exposure, E, in fuel segment when blade inserted.
[b] Corner rod (W-W corner) relative power at exposure, E.
[c] Exposure interval, ΔE, while controlled (MWd/t).
[d] Power increase due to CBH effect.

Table 5.4-7
PEAK LHGR'S OBTAINED DURING RAMPING OF TEST FUEL – CASE 1

Cycle	Bundle Enrichment (% U-235)	Bundle Average Exposure (MWd/t)	Peak LHGR (kW/ft)
6	2.39	4842.0	12.0 — 13.4
7	2.65	8249.0	11.0 — 12.1
8	2.65	14921.0	9.6 — 10.7
9	2.82	20336.0	9.2 — 10.3

Table 5.4-8
PEAK LHGR'S OBTAINED DURING RAMPING OF TEST FUEL — CASE 2

Cycle	Bundle Average Barrier Type[a]	Exposure (MWd/t)	Peak LHGR (kW/ft)
6	1	4839	12.0 — 13.4
7	1	9632	10.9 — 11.9
7	2	3562	11.0 — 12.0
8	1	15719	9.8 — 10.8
8	2	8312	10.4 — 11.5
9	1	18661	8.4 — 9.5
9	2	16171	8.1 — 9.1
10	2	20056	8.6 — 9.7

[a] Type 1 loaded in Cycle 6, Type 2 loaded in Cycle 7.

5.5 DISCUSSION

The estimated peak LHGR's given in Tables 5.4-7 and 5.4-8 indicate that the resistance of the barrier fuel to PCI failure is not being severely tested for fuel of high exposure (last two ramps). The peak LHGR's obtained are in the range of those expected for fuel of the given exposure in the lower-power-density BWR/3's. However, in BWR/4 – BWR/6 plants a higher LHGR during normal operation can be expected. The purpose of the experiment is to demonstrate the intrinsic resistance of the barrier fuel to PCI failure. Thus, changes in the design of the demonstration are being made to increase the expected LHGR's obtained during the final two ramps.

The design changes being investigated are:

1. Lattice design changes to increase corner pin peaking. The current lattice designs (retrofit) being used to simulate the barrier fuel have been designed to minimize the corner pin peaking due to CBH. The designs have the corner fuel rods derated (lower enrichment) relative to the average enrichment. The result is lower corner pin peaking by virtue of a lower initial rod power prior to blade insertion. Studies are in progress to determine changes which will increase both the corner rod and adjacent rods peaking after periods of controlled exposure accumulation. This will result in more fuel rods reaching the operating LHGR limit and a better demonstration of the barrier concepts.

2. Refueling strategy changes to increase average LHGR during ramping. A method to increase the LHGR to which the test fuel can be ramped is the use of fresh PCI-resistant fuel to drive the higher exposure test fuel. This fuel would be loaded into two locations of a test cell and the higher exposure fuel in the remaining two.

Several other changes which result in smaller increaes in the peak LHGR are under study. The major emphasis in the near term will be directed toward increasing the severity of the test while maintaining the progress made to date.

6. PROGRESS TO DATE – PART 2. SUPPORT TESTS FOR LARGE-SCALE DEMONSTRATION

6.1 Task 1.0. LABORATORY SUPPORT

6.1.1 Subtask 1.1 Expanding Mandrel Tests (R. P. Gangloff and D. S. Tomalin, CRD, and R. B. Adamson and S. B. Wisner, NTD)

The environmental aspect of the PCI failure mechanism has been studied in both unirradiated[1] and irradiated[2] Zircaloy-2 tubing using the experimental technique called Localized Ductility Testing and in irradiated sheet using plane strain tensile specimens.[3] However, these tests do not adequately treat the mechanical aspects of PCI. Thus Coffin and Gangloff[1] adapted the expanding mandrel test technique[4] to consider both the environmental and mechanical aspects of PCI under controlled laboratory conditions.

The key elements of the test are illustrated in a cutaway view of the experimental apparatus, Figure 6.1-1. An Al_2O_3 sleeve was used to simulate the frictional conditions produced by oxide fuel. This sleeve was cracked and radially pressed into the tube wall by hardened segments which were themselves displaced by radial expansion of a central zirconium slug. The piston for axially compressing the slug was coupled to the tube sample via Viton O-ring seals which isolated the test environment from ambient. The entire assembly was surrounded by a radio frequency coil for elevated temperature testing.

Both gaseous iodine and cadmium environments were studied with unirradiated Zircaloy-2 and barrier-modified Zircaloy-2 specimens. Figure 6.1-2 presents a schematic illustration of a cross section through the midplane of the apparatus to show how the components were configured for testing in I_2. For tests in cadmium the hardened segments were of Alloy 17-7PH and the cadmium was plated directly onto the outer surface of the Al_2O_3 sleeve opposite the segment radial interfaces. Tests in cadmium can be done below or above the cadmium melting temperature (321°C).

Additional work[5] was conducted to further adapt the test technique to the task of evaluating irradiated barrier-modified Zircaloy-2 cladding under simulated PCI conditions. Although many of the testing procedures were unique to the testing of irradiated material, the basic technique followed very closely the earlier work of Coffin and Gangloff.[1] Mandrel tests on irradiated material were conducted to determine the influence of neutron irradiation on the barrier and cladding properties and on the PCI mechanisms. Of particular interest is the effect of irradiation on the strength of high-purity crystal bar zirconium. Since zirconium was chosen primarily to prevent strain localization stress concentration, it is important to ascertain the influence of the expected increase in flow stress with high-fluence exposure. Although the copper barrier is not expected to undergo significant irradiation strengthening, it is of interest to determine the effects of any irradiation-enhanced interdiffusion of copper and zirconium on the failure strain. The materials listed below were irradiated in the General Electric Test Reactor to a fluence near 2×10^{21} n/cm^2 ($E > 1$ MeV):

1. Product line 8x8 recrystallized Zircaloy-2.

2. As above, with inside surface electroplated with 0.0004 inch copper, diffusion bonded prior to irradiation [heat treatment nominally at 1070°F (577°C)].

3. Zircaloy-4 tubing coextruded with a crystal bar zirconium (80 ppm oxygen) liner, 0.0027 inch thick.

Results are illustrated by comparing the total diametral strain at maximum load (i.e., through-wall rupture) for each barrier system. Figure 6.1-3 offers such a comparison for both unirradiated and irradiated specimens tested in an iodine environment. Where embrittlement has occurred, irradiation significantly lowers the observed strain to failure. Electroplated copper improves the behavior of reference Zircaloy-2 but the degree of improvement could not be determined since the copper plating was chemically removed by the iodine, exposing bare Zircaloy. Crystal bar zirconium provides significant improvement to iodine stress corrosion cracking to at least 4% average diametral strain in both the unirradiated and irradiated conditions. However, the presence of significant incipient cracks in the crystal bar liner indicates that chemical immunity is not obtained in that system.

Test results for a liquid cadmium environment are illustrated in Figure 6.1-4. The crystal bar zirconium liner (unirradiated or irradiated) appears to impart immunity to cadmium embrittlement, as does copper in the unirradiated condition. However, severe embrittlement was experienced for the irradiated copper barrier case. This effect is suspected to be associated with a Cu-Zr intermetallic layer produced by diffusion bonding, a process which is not used for the present generation of copper barrier tubes.

During this reporting period, additional barrier specimens have been prepared for future irradiation in the GE Test Reactor. These specimens include barriers made of crystal bar zirconium, low-oxygen sponge zirconium, electroless plated (EP) copper directly on Zircaloy, and EP copper on oxidized Zircaloy. In addition, crystal bar zirconium and electroplated copper barrier tubes have been retrieved from plenum sections of segmented fuel rods (see Subtask 3.2) which have been irridated in a power reactor and then power ramp tested. Tests were done also on unfueled test specimens irradiated at the Big Rock Point reactor. Mandrel evaluations of these specimens will be conducted in 1978.

A substantial effort to evaluate barrier parameters using unirradiated material has been put forth during this reporting period. Studies of five parameters are reported here.

1. Establish the barrier effectiveness of zirconium of varying degrees of purity by expanding mandrel testing of unirradiated tubing exposed to argon, iodine, or cadmium.

   High-purity iodide Zr-lined Zircaloy-2; intermediate purity low-oxygen sponge Zr-lined Zircaloy-2; and commercial-purity sponge Zr-lined Zircaloy-2 composite tube lots were coextruded at CRD and tube reduced according to standard rocking procedures at WMD. The performance of each type of tubing was evaluated for simulated PCI conditions, and the results were compared to data for iodide Zr-lined Zircaloy-2 fabricated by Armijo, et al., and for product line Zircaloy-2.

   The results of 35 expanding mandrel experiments established that each purity of unirradiated Zr-lined Zircaloy-2 outperformed standard Zircaloy-2 tubing for both gaseous iodine and solid cadmium based test conditions. Each purity of Zr-lined Zircaloy fractured at equivalent average diametral strain levels for potentially embrittling liquid and solid cadmium and for inert argon test environments. Fractographic analyses indicated that the zirconium liner ruptured by ductile microvoid nucleation, growth, and coalescence in the presence of solid cadmium, and independent of liner purity and hardness. Zirconium-lined Zircaloy was embrittled by gaseous iodine for each liner purity; however, the average strain at failure was two to four times larger than values for unlined Zircaloy-2 tested under comparable conditions. The average diametral failure strain decreased moderately with increasing liner hardness. Iodine-assisted brittle cleavage-type cracking was observed for all zirconium liners independent of purity and hardness. Specific data are presented in Figures 6.1-5 to 6.1-7, and are tabulated in Table 6.1-1. The fractographic observations are summarized according to the mode of fracture of the Zr-liner (i.e., B = brittle, D = ductile).

   Sixty-mil-thick cold rolled sheet materials were fabricated from zirconium cylinders employed in the production of coextruded Zr-lined Zircaloy-2 tube shells. Plane strain tensile samples were machined from a sheet of each of the three zirconium purities. Tensile tests were conducted at 300°C and at a slow strain rate in vacuum. The results of these experiments (Figure 6.1-8) indicated that, for cold worked materials (57% reduction), the impurities associated with the intermediate-purity sponge zirconium increased the yield strength by 13% compared to high-purity iodide zirconium. Commercial-purity sponge zirconium exhibited a yield strength that was 21% higher than iodide zirconium and only 8% higher than select sponge zirconium. Similar strength differentials were observed for fully recrystallized samples heat treated at 580°C. These strength differentials are probably related to the increased carbon levels typical of sponge zirconium; dissolved oxygen is not a potent strengthener of zirconium at 300°C.

   The results of these experiments indicate that sponge Zr-lined Zircaloy-2 qualifies for consideration as an alternative for high-purity iodide zirconium, and should be irradiated for additional laboratory evaluations.

2. Establish the barrier effectiveness of zirconium as a function of barrier thickness by expanding mandrel testing of unirradiated tubing exposed to argon, iodine, or cadmium.

Table 6.1-1
EXPANDING MANDREL TEST RESULTS (DIAMETRAL FAILURE STRAIN, %)

	Zircaloy-2	Iodide Zr, 80 ppm O_2	Sponge Zr, 500 ppm O_2	Sponge Zr, 1000 ppm O_2
Argon, 300°C	5.2	5.6		
		6.2	6.1 D	5.2
		5.3		
		6.9	5.6	
		6.2		
$4x10^{-5}$ atm, I_2, 350°C	1.9	5.3 B		
	2.0	3.8 B	6.2 B	4.0
		4.4 B	>8.0 N	
		>6.0 B	5.8 B	
		6.1 B		
$4x10^{-5}$ atm I_2, 350°C (No Al_2O_3)	1.7	>4.8 I		3.0
		>8.0 N	3.8 B	
Cadmium, 300°C	2.6	7.2 D		
	2.7	7.5 D	7.0 D	5.2
	2.7	7.3 D	7.5 D	5.0
	2.8			>8.0 N
Cadmium, 335°C	2.2	>8.0 N	7.7	>8.0 N
			>8.0 N	>8.0 N

D – Ductile Fracture
B – Brittle Fracture
I – Incipient Cracks
N – No Through Cracking

Variable zirconium liner thicknesses were produced by continuously pumping an $HF-HNO_3-H_2O$ solution through commercial-purity sponge Zr-lined Zircaloy-2 tubing for various exposure times. The original liner thickness was reduced to as low as 0.6 mil by the chemical polishing procedure. The performance of Zr-lined Zircaloy-2 was established as a function of liner thickness by expanding mandrel simulation testing with both gaseous iodine and solid cadmium environments. Chemically polished, unlined Zircaloy-2 samples were fractured at average diametral strains that were equivalent to data for as-rocked tubing, indicating that a chemically polished tube inside surface *per se* could be embrittled.

The results of 13 expanding mandrel experiments indicated that all zirconium liner thicknesses between 0.6 and 3.0 mils were protective for both I_2 and Cd test conditions. Specifically, average diametral strains at fracture for lined tubing exceeded the values for production Zircaloy-2 tested under comparable conditions. For iodine test conditions the average diametral strain at failure was independent of liner thickness, and was 80% higher for Zr-lined Zircaloy-2 compared to unlined Zircaloy tubing (see Figure 6.1-9). Results were obtained for solid cadmium test conditions, as shown in Figure 6.1-10. The majority of data indicated that liner thicknesses greater than 2 mils provided a three-fold increase in the diametral failure strain compared to Zircaloy-2; thinner liners provided a 60% improvement margin. Additional experiments and associated materials characterizations are in progress to resolve this inconsistency. Liner thicknesses will be metallographically measured, liner fracture surfaces will be fractographically characterized, and duplicate expanding mandrel experiments will be conducted.

3. Establish the barrier effectiveness of electroless copper compared to electroplated copper by expanding mandrel testing of unirradiated tubing exposed to argon, iodine, or cadmium.

   Zircaloy-2 tubing from lots that were evaluated by extensive mandrel testing was copper plated by an electro-deposition process at Vallecitos Nuclear Center and by the optimal electroless plating process at Wilmington. Five expanding mandrel tests with iodine and cadmium environments established that the electroless copper plate provided equally good resistance to simulated PCI fracture compared to electroplated tubing. Even defective (blistered) electroless copper plated Zircaloy-2 exhibited a diametral strain at fracture that was three times higher than the value for unplated Zircaloy-2 tested with 0.03 torr gaseous iodine. The blisters and associated poor copper plate adherence had no observable influence on the good performance of Cu-barrier Zircaloy-2 for this form of the expanding mandrel simulation. Specific data are shown in Table 6.1-2.

4. Establish the barrier effectiveness of copper as a function of copper-zirconium intermetallic compound formation by expanding mandrel testing of unirradiated tubing exposed to argon, iodine, or cadmium.

   Eight cadmium and five gaseous iodine containing expanding mandrel tests were conducted as summarized in Table 6.1-3. In general it was concluded that the performance of unirradiated copper plated Zircaloy-2 tubing was degraded by the presence of copper-zirconium intermetallic phases which result from interdiffusion of copper with Zircaloy. While as-plated Cu-lined Zircaloy-2 exhibited a three-fold increase in failure strain compared to standard Zircaloy-2 for iodine test conditions, strains to failure for samples with 50% of the copper converted to intermetallic phases (580°C heat treatment) were reduced to about the level of unplated Zircaloy-2. Samples, heat treated to convert all the copper layer to Cu_xZr_y intermetallics (625°C heat treatment) were fractured at slightly lower diametral strains than comparable unplated Zircaloy-2 control samples. Metallographic observations revealed that the intermetallic layers were cracked extensively. Apparently, intermetallic cracking accentuated simulated PCI crack initiation.

   For solid and liquid cadmium test conditions (tests at 300 and 335°C, respectively), as plated and heat treated Cu-lined Zircaloy-2 tube samples exhibited equivalent good performance independent of the amount of copper converted to intermetallic and compared to standard unplated Zircaloy-2 control results. Metallographic observations indicated that the intermetallic layers were cracked, and the remaining copper was often breached adjacent to areas of simulated PCI. In spite of the apparently deleterious influence of Cu_xZr_y phases, composite tube performance was good. This anomaly is ascribed to the fact that copper reduces the embrittling tendencies of Cd, apparently through influences on the kinetics of cadmium transport during straining. In addition, intermetallic phases have little influence on expanding mandrel tube performance with Cd because the heat treatments required to produce Cu-Zr interdiffusion recrystallize rocked Zircaloy-2. The resultant soft material is inherently more immune to cadmium embrittlement in the unirradiated condition.

   In spite of the difficulties associated with evaluation of Cu-plated Zircaloy-2 tubing with Cu_xZr_y, it was concluded that copper-Zircaloy interdiffusion could be deleterious to copper plated fuel rod performance.

5. Establish the barrier effectiveness of copper applied over oxidized (autoclaved or anodized) Zircaloy by expanding mandrel testing of unirradiated tubing exposed to argon, iodine, or cadmium.

   Three iodine-containing expanding mandrel tests provided a preliminary indication that electroless copper plated directly on Zircaloy-2, oxygen gas oxidized (at 400°C) Zircaloy-2, and autoclaved (at 400°C) Zircaloy exhibited equivalently good performance compared to unplated Zircaloy-2. A factor-of-three improvement in the average diametral fracture strain was observed as indicated in Table 6.1-4. The sample of Cu-Barrier on an autoclaved Zircaloy surface was blistered. However, the resistance to simulated PCI in the expanding mandrel test in I_2 was apparently unaffected by the blisters.

Table 6.1-2
COMPARISON OF ELECTROLESS Cu-BARRIER AND ELECTROPLATE Cu-BARRIER

	Expanding Mandrel Data	
	$4x10^{-5}$ atm I_2, 350°C	Cadmium, 300°C
Zircaloy-2	1.9 to 3.2% (5) Av = 2.6%	2.4 to 3.0% (5) Av = 2.6%
Zircaloy-2 + 0.0004 in. Cu Electroplated	6.7%	6.4%
Zircaloy-2 + 0.0004 in. Cu Electroless	6.9%	
Zircaloy-2 + 0.0003 in. Cu Electroless		6.0 to 6.8% (2) Av = 6.4%

Table 6.1-3
EFFECT OF COPPER-ZIRCALOY INTERDIFFUSION ON BARRIER PERFORMANCE
(Strain to Fracture)

		Test Conditions		
Material	Heat Treatment	Cd at 300°C	Cd at 335°C	I_2 vapor ($4x10^{-5}$ atm, 350°C)
As-rocked Zircaloy-2	None	2.7%	2.1%	2.0%
	450°C, 92h	2.0		
	625°C, 100h	6.0		4.1
As rocked Zircaloy-2 with 0.4 mil Cu-Barrier	None	6.4%	>8.0%	6.7%
	450°C, 92h	5.1	>6.0	
	580°C, 2½h	>8.0	>6.0	4.8
	625°C, 100h		>6.2	1.4

Table 6.1-4
COPPER BARRIER ON OXIDE COMPARED WITH
COPPER BARRIER PLATED DIRECTLY ON ZIRCALOY
(Strain to Fracture)

Zircaloy-2	**1.9 to 3.2% (5 Tests)** **Av = 2.6%**
Zircaloy-2 with 0.4 mil Cu-Barrier	6.9%
Zircaloy-2 autoclaved with 0.4 mil Cu-Barrier on oxide	6.9%
Zircaloy-2 oxidized in O_2 with 0.4 mil Cu-Barrier on oxide	4.7%

Expanding Mandrel Tests, $4x10^{-5}$ atm I_2, 350°C

6.1.2 Subtask 1.2 Barrier Characterization and Stability (B. Cheng and R. B. Adamson, NTD)

6.1.2.1 Introduction

Questions have arisen as to the effect of the copper barrier on cladding hydriding characteristics in the event of fuel rod defection.

It is thought that in defected rods, reaction of ingressing steam with UO_2 fuel would result in a wet hydrogen atmosphere in the fuel rods. Laboratory tests by Shannon[6] indicate that in hydrogen-containing environments, hydriding of Zircaloys, either pickled or autoclaved, will occur when the steam or oxygen arrival rate falls below that value required to maintain the protective oxide film. This value was found to be as low as ~0.002 psig (0.1 mm Hg) partial pressure. Copper plating on Zircaloy tubing can be expected to restrict the arrival of oxygen to the Zircaloy surface, and thus the Zircaloy tubing could become vulnerable to hydriding if hydrogen can preferentially diffuse across the copper plating to reach the cladding surface. Comparison of existing diffusion coefficients for hydrogen and oxygen in copper, i.e., $D_H^{Cu} = 1.5 \times 10^{-5}$ versus $D_O^{Cu} = 2.95 \times 10^{-10}$ cm^2/s at 400°C, indicate that the possibility of accelerated hydriding of copper-plated cladding should not be overlooked.

The aim of the present test is to evaluate performance of copper-plated tubing in hydrogen-containing environments.

6.1.2.2 Experimental Procedures

The specimens tested were ~1 inch long, half rings of Zircaloy-2 tube manufactured in Wilmington (WMD). Surface conditions include the following:

Standard autoclaved Zircaloy-2
Standard pickled Zircaloy-2
Oxidized in 1 atm dry O_2 at 400°C, Zircaloy-2
Copper plated on inside surface of pickled Zircaloy-2
Copper plated on inside surface of autoclaved Zircaloy-2
Copper plated on inside surface of oxidized (1 atm dry O_2 at 400°C) Zircaloy-2
Copper plated on inside surface of pickled Zircaloy-2, then autoclaved (10 psig steam at 400°C for 24h)

Some samples were prepared with a 200Å Ni or 50Å Pt film vapor deposited on the inner surface. These films were used to enhance the surface dissociation of hydrogen gas.[7]

The test setup is shown schematically in Figure 6.1-11. The tubing samples were placed in a horizontal Pyrex glass tube installed within a tubular furnace. The temperature of the furnace was measured with a chromel-alumel thermocouple, and was recorded with a strip chart recorder. The wet hydrogen gas mixture was produced by passing 1 atmosphere hydrogen gas through a bubbler containing distilled water at room temperature (22°C). The hydrogen flow rate was controlled at ~330 cm^3/min by the flowmeter. The H_2/H_2O ratio was calculated from the electrochemical potential outputs of the oxygen meter. The hydrogen gas was finally burnt at a torch at the line outlet. Before testing was started, the test line was continuously flushed with nitrogen gas for 2 hours to remove any residual oxygen.

Two series of tests have been carried out. In the first test, tubing samples were exposed to a wet hydrogen environment having a pressure ratio $H_2/H_2O \sim 33 \pm 5$ at 355 ± 8°C for 72 hours. In the second test, the H_2/H_2O ratio was ~18 ±5, temperature 400°C, and test duration 360 hours.

Post-test evaluation included metallography and neutron radiography.

6.1.2.3 Results and Discussion

355°C – 72 Hour Test. The tubing samples tested in this experiment are shown in Figure 6.1-12. The wet hydrogen environment contained water vapor at ~0.45 psig partial pressure ($H_2/H_2O \sim 33$), which significantly

exceeded the reported minimum value for inhibiting Zircaloy-2 hydriding, 0.002 psig. This was confirmed from the metallographic examination of the unplated autoclaved sample, showing no accelerated hydriding, Figure 6.1-13(I). The vapor-deposited nickel film on autoclaved sample, which presumably would accelerate surface hydrogen dissociation, was shown to have no significant effect on hydrogen pickup of the Zircaloy-2 sample, Figure 6.1-13(II).

All three samples with copper plated on a pickled surface were found to form hydride platelets, as shown in Figure 6.1-14. The hydrided samples all have a thin massive hydride layer of up to ~10 μm at the interface between the Zircaloy and the copper barrier. The equivalent hydrogen content estimated from the density of uniform hydride platelets is ~300 ppm for all three samples. The interface oxide in the sample with copper plated on autoclaved tubing was found to effectively prevent hydrogen from entering the cladding, Figure 6.1-14(II). The protection by this interface oxide is believed to be temporary, as will be discussed later.

The autoclave treatment of a sample with copper plated on pickled tubing resulted in some interesting features. It can be seen from Figure 6.1-12 that the copper surface is shiny and free of any tarnish. Figure 6.1-15(I) shows that a continuous interface layer, presumably an oxide,* was formed by the autoclave treatment and the copper barrier was still visually intact. Hydrogen pickup tests of this sample showed that it also resisted hydriding attack similar to the sample with copper plated on autoclaved tubing.

400°C – 360 Hour Test. The post-test surface appearance of the ten samples tested are shown in Figure 6.1-16. In this test, the partial pressure of water vapor, ~0.8 psig (H_2/H_2O ~ 18), is slightly higher than the value used in the 355°C – 72 hour test. The difference in H_2/H_2O ratio is not expected to result in any significant influence in the hydriding of Zircaloy-2. Micrographic examination has again shown that in this passive environment all Zircaloy samples without a copper plating, i.e., autoclaved, pickled, oxidized, and pickled plus a 50A Pt film, were resistant to hydriding attack, Figure 6.1-17.

Samples of copper plating on either pickled, oxidized, or autoclaved tubing were heavily hydrided, Figures 6.1-18 and 6.1-19. It can be seen that some of the hydrides, Figures 6.1-18(Ib) and 6.1-19(IIb), exhibit a cellular structure. On the sample of copper on pickled tubing, an oxide-like layer was found beneath the copper barrier, Figure 6.1-18(Ia), suggesting that oxidant has probably diffused across the copper barrier or from specimen edges to form a zirconium oxide film. Presence of the interface oxide during testing, however, did not prevent hydrogen from entering the Zircaloy. In fact, the preformed autoclaved or oxidized oxide films beneath the copper barrier all remain visually intact while hydriding of the Zircaloy beneath the oxide films occurred. The interface oxide, however, seems to retard hydrogen entry to the Zircaloy, as can be seen in Figures 6.1-18(II) and 6.1-19, where the density of hydrides decreases with increasing oxide thickness.

The difference in the results of the copper-on-autoclaved samples tested at 355 and 400°C suggests that the interface oxide provided transient hydriding protection to the Zircaloy. Lacking an oxygen supply from external sources, the ZrO_2 will gradually become sub-stoichiometric due to diffusion of oxygen into the Zircaloy. The sub-stoichiometric zirconia has been proposed to be permeable to hydrogen,[7] leading to hydriding of Zircaloy. The incubation time for Zircaloy hydriding to occur would therefore decrease with increasing temperature and with decreasing interface oxide thickness.

6.1.3 Subtask 1.3 Effects of Irradiation on Zirconium of Various Purity Levels (D. S. Tomalin and P. C. Kelly, CRD, R. B. Adamson, NTD)

6.1.3.1 Introduction

One of the potential PCI remedies is a Zircaloy fuel cladding with a metallurgically bonded liner of unalloyed zirconium. Expanding mandrel tests of such tubing in the unirradiated and irradiated conditions and in-pile ramp tests of experimental fuel have shown this concept to be very promising (see Subsection 6.1.1 and 6.3). However, there have been few opportunities to examine the effects of neutron irradiation on possible liner embrittlement, and those tests which have been performed have been on composite tubing with a liner of high-purity crystal bar zirconium. Lower

*This layer is resistant to the standard pickling solution: 5 vol % HF (48% aq)/45 HNO_3 (70% aq)/50 H_2O.

purity commercial grades of zirconium are more economically attractive as liner materials, but the effect of the increased yield strength due to higher oxygen contents and/or irradiation hardening have an unknown effect on their performance in simulated fission product environments. The work described here examined some of these effects under controlled laboratory conditions.

The techniques which are being applied were established by considerable testing of unirradiated materials. However, the use of irradiated specimens has required some significant modifications and development work. The modified test techniques and the results of preliminary tests which have been performed on irradiated specimens in Cs/Cd environments at 350°C are reported.

6.1.3.2 Materials

Specimens have been, or will be, fabricated from three sources of irradiated material. The first group comes from a segment of Zircaloy-4 sheet irradiated in the Oyster Creek power reactor at 288°C (550°F) to a fluence of about 2×10^{21} n/cm^2 ($E > 1$ MeV). The sheet segments have the tensile axis of the specimens coincident with the rolling direction.

The second group of specimens were originally fabricated and irradiated for another program.[8] Of the eleven available specimens, seven are uniaxial tensile and four are plane strain specimens. Table 6.1-5 itemizes pertinent information about these specimens. One remaining uniaxial and three unirradiated controls should be available in the first quarter of 1978.

The final group of specimens were prepared by R. B. Adamson and irradiated in the Big Rock Point Reactor. They were irradiated at approximately 327°C (620°F) to a fluence estimated at 0.6×10^{21} n/cm^2 and returned to Vallecitos in the fourth quarter of 1977. The carrier rods are being disassembled and the flux wires analyzed. The specimens are itemized in Table 6.1-6 and should be available for testing in the first quarter of 1978.

Table 6.1-5
IRRADIATED CRYSTAL BAR ZIRCONIUM SPECIMENS[9]

Specimen Designation	Fluence, 10^{21} n/cm^2 ($E > 1$ MeV)	Previously Tested
L-2	1.67	Yes
L-5	3.10	No
L-6	3.10	No
L-8	1.67	No
L-9	1.67	Yes
L-11	1.53	No
L-12	3.09	Yes
L-14	1.67	Yes
L-15	1.38	Yes
L-16	1.53	Yes

Table 6.1-6
ZIRCONIUM SPECIMENS IRRADIATED IN BIG ROCK POINT

Material	Estimated Fluence 10^{21} n/cm^2 ($E > 1$ MeV)	Previously Tested
Crystal Bar Zirconium		
Recrystallized	0.6	No
Cold Worked	0.6	No
Beta Quenched	0.6	No
Sponge Zirconium		
Recrystallized	0.6	No
Cold Worked	0.6	No
Beta Quenched	0.6	No

6.1.3.3 Specimen Preparation

Most of the tests to be conducted will be performed on one of the specimen configurations illustrated in Figures 6.1-20 and 6.1-21. The small specimen was designed to test the limited supply of available irradiated material. Figure 6.1-22 illustrates that one "standard" uniaxial tensile specimen will yield four miniature uniaxial tensile specimens if it has been previously tested and five if it has not. Figure 6.1-23 illustrates that one standard plane strain specimen will yield two reduced plane strain specimens of the same notch geometry after the standard specimen has been tested.

Specimen blanks were transformed into their respective configurations using standard electrical discharge machining (EDM) techniques. Figure 6.1-24 shows a specimen in the EDM tank before it is immersed in kerosene. The electrode illustrated here is a "cookie cutter" type used to introduce a gage section and alignment pin holes simultaneously in a miniature uniaxial tensile specimen.

6.1.3.4 Tensile Testing Procedures

Cesium Loading. A stainless steel capsule configuration has been adapted to accomplish elevated temperature testing in argon, cesium or cesium/cadmium environments. A miniature specimen is loaded into serrated friction grips using alignment pins for proper orientation. These grips are then screwed into the stainless steel chamber and the bellows attached. To ensure that an uncontaminated environment is maintained inside the capsule, the bellows seat on a polished copper gasket, which is nickel plated for chemical compatibility with cesium. Figure 6.1-25 offers an exploded view of the system components. If a cesium/cadmium test is to be conducted, a piece of cadmium wire that has been cleaned in a solution of 50% HCl (37 wt % aq) + 50% H_2O is placed in the proximity of the specimen before securing the grips in the capsule. Subsequently, the capsule is bolted closed and mounted on the cesium loading station as illustrated in Figure 6.1-26. The system is then baked out under vacuum (280°C/3 hours/$<10^{-4}$ torr) to remove any condensable vapors. When an adequate partial pressure has been attained ($>10^{-4}$ torr) the cesium (99.9% pure) is loaded into the capsule by breaking the tip of the cesium ampule with a plunger magnetically driven from outside the capsule. The capsule is then isolated from the system with a Pyrex pinch-off seal and removed.

After a test has been conducted, the capsule is remounted on the station and the cesium removed by vapor distillation into a cold trap. After approximately 3 hours of baking, an estimated 95% of the cesium will have been distilled into the trap and it is then isolated from the system and removed. The trap is stored so that the cesium can be chemically analyzed at a later date if desired. The capsule is removed from the cesium station and cleaned with isopropyl alcohol, brite dip [250 ml H_2O, 150 ml HF (50 wt % aq), 100 ml HNO_3 (70 wt % aq)], water, and acetone prior to any subsequent tests.

Tensile Loading. Constant extension rate tests are performed on the specimens by loading them in a standard Instron tensile testing machine. Figure 6-1-27 shows the capsule attached to pull rods which couple with the Instron load train. Elevated temperatures are maintained by a resistance furnace and auxiliary heaters for the appendages on the capsules. Control thermocouples are spot-welded to the outside of the capsule at the approximate level of the specimen gage section and connected to a closed loop Electromax IV controller which drives an silicon controlled rectifier power supply. During a test, a thermal gradient is imposed on the capsule so that the maximum temperature occurs at the top of the capsule. Such a gradient keeps the cesium condensed in the bottom, submersing the specimen gage section.

The system is allowed to reach thermal equilibrium prior to starting a test. The most sensitive indication of thermal equilibrium is the load-time output; the criterion used is that the load must remain constant for a period of 10 minutes before equilibrium is considered to be achieved. This usually occurs within approximately 90 minutes of heat up.

The test output is a record of load-time and an x-y plot of load-extension where the extension signal is taken from a linear variable differential transformer (LVDT) and signal conditioner. The LVDT senses the relative motion between the bottom and top of the capsule via extension arms to remove it from the region of elevated temperature.

6.1.3.5 Results

Considerable testing of irradiated Zircaloy-4 miniature uniaxial tensile specimens has been conducted to qualify this new specimen geometry. The results of these tests are summarized in Figure 6.1-28 where the loading curves of the miniature specimens are compared to that of a more conventional sized specimen (0.1 x 0.25 x 0.09 inch gage section). Ultimate strengths in the range of 65-76 ksi were observed for the miniature specimen as compared to 73-77 ksi for the larger tensile specimens prepared from the same material. All of these tests were conducted at 350°C at a nominal strain rate of 10^{-3} min^{-1}. In addition to the agreement in ultimate strength and uniform strain, a further indication of the quality of these loading curves is the observed modulus of 3-5 x 10^6 psi which is within a factor of 2 or 3 of the known modulus. The apparent disagreement in total strain and flow stress after instability is a gage length effect which is emphasized by the inhomogeneity of plastic flow in irradiated zirconium alloys. The general quality of these loading curves leads to the conclusion that the properties of the miniature specimens adequately represent the bulk material properties of irradiated zirconium; considerable material conservation is achieved by their use.

In addition to the argon tests, an irradiated Zircaloy-4 specimen has also been tested in a cesium/cadmium environment. After the cesium loading procedure and during isolation of the capsule from the system, the glass pinch off seal cracked, allowing the capsule to come up to atmospheric pressure at approximately 150°C. The cracked Pyrex glass was immediately repaired and the capsule re-evacuated. The test was conducted at 350°C at a nominal strain rate of 10^{-3} min^{-1} with the results illustrated in Figure 6.1-29. The loading curve for a similar specimen tested in argon is also included for comparison. Embrittlement of the specimen by cesium/cadmium is evidenced by the large decrease in strain to failure from that observed in an argon test. Preliminary scanning electron microscopy (SEM) confirmed the embrittlement as illustrated in Figures 6.1-30 and 6.1-31. The specimen tested in argon (Figure 6.1-30) exhibited considerable necking prior to the ductile rupture, and the fracture morphology was characterized by the dimpled topography evident at higher magnification. The specimen tested in cesium/cadmium was characterized by a flat fracture surface with essentially zero reduction in area (Figure 6.1-31). At higher magnifications it was characterized by a faceted morphology with extensive secondary cracking.

Preliminary tests have also been performed on crystal bar zirconium specimens in argon and cesium/cadmium environments. The miniature tensile specimens were machined from specimen L-2 (Table 6.1-5) which received a fluence of 1.67 x 10^{21} n/cm^2. Figure 6.1-32 presents the loading curves from these tests which were also conducted at 350°C at a nominal strain rate of 10^{-3} min^{-1}. The argon test produced results in good agreement with those reported by Rieger and Lee[8] for the parent specimen and is further evidence of the legitimacy of the miniature specimen geometry. SEM fractography (Figure 6.1-33) indicates a dimpled ductile rupture with significant reduction in area.

Testing a similar irradiated crystal bar zirconium specimen in an uncompromised cesium environment with approximately 2% cadmium did not produce any detectable change in the loading curve, in contrast to the results for irradiated Zircaloy-4. As would be suggested by the loading curve, SEM fractography shows the specimen fractured in a ductile manner with appreciable necking (Figure 6.1-34).

These preliminary tests suggest irradiated crystal bar zirconium is not susceptible to cesium/cadmium embrittlement under at least one condition where irradiated Zircaloy-4 specimens are susceptible.

6.1.3.6 Future Work

Work will continue on characterizing the mechanical properties of the irradiated crystal bar zirconium specimens in cesium/cadmium environments. Test variables to be examined include strain rate, test temperature, and stress state. In addition, the irradiated sponge zirconium specimens will become available for tests on the effect of composition. Tests in an iodine environment will also be started.

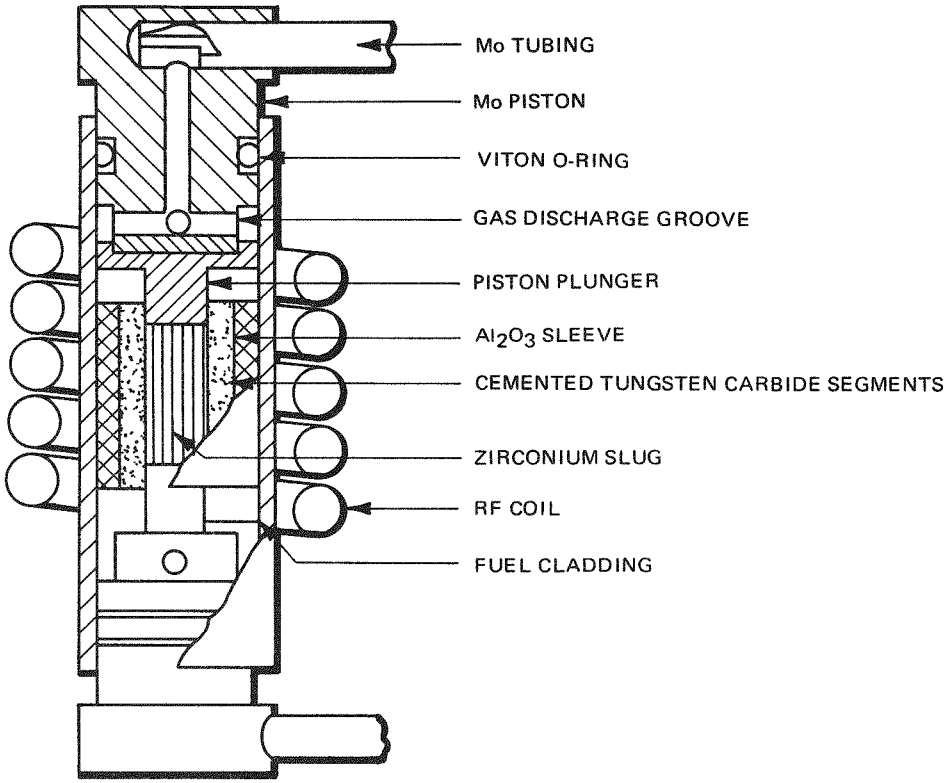

Figure 6.1-1. Schematic Illustration of the Expanding Mandrel Test Configuration

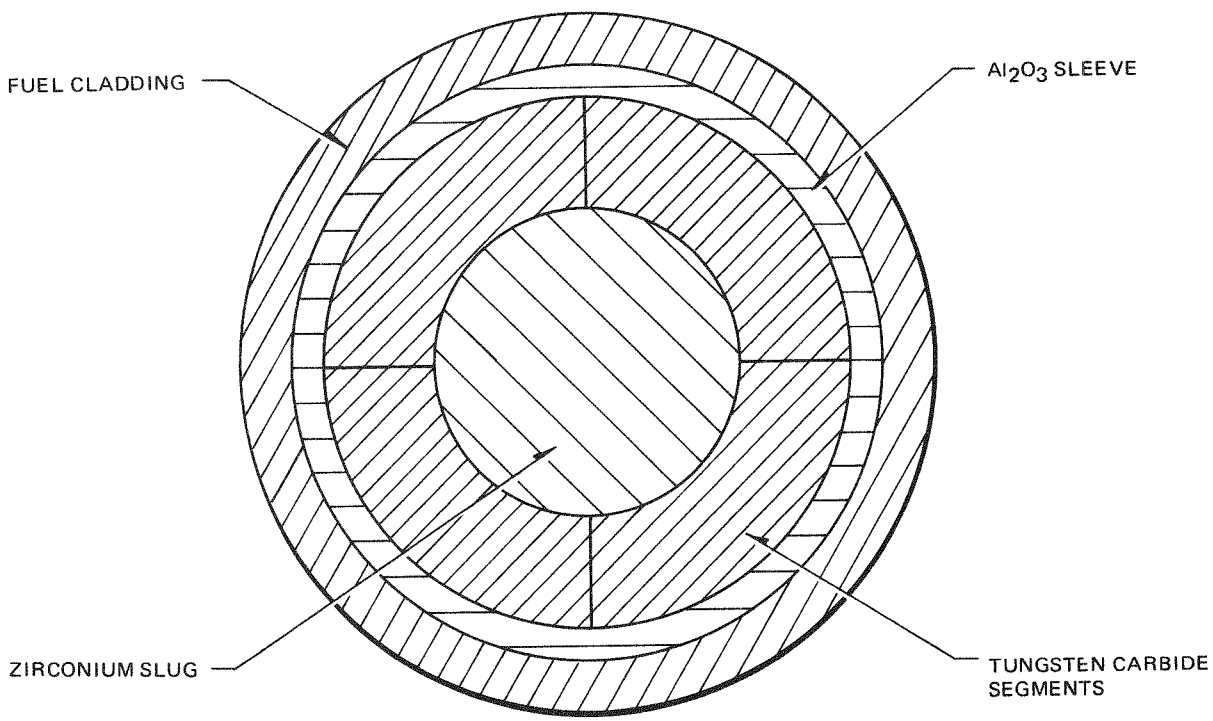

Figure 6.1-2. Schematic Illustration of a Cross Section Through the Segmented Expanding Mandrel Configuration

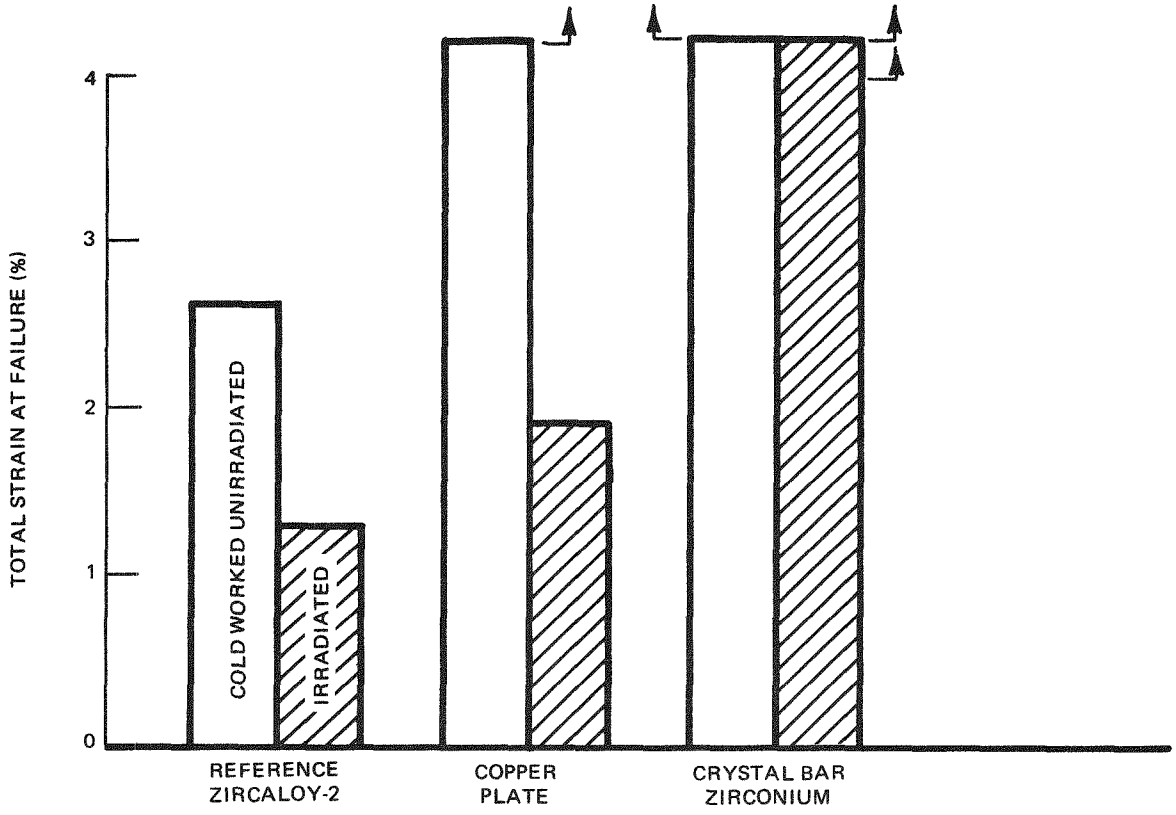

Figure 6.1-3. Comparison of Barrier Performance in Iodine Environment at 335°C. Upward arrow indicates test interrupted without specimen fracture.

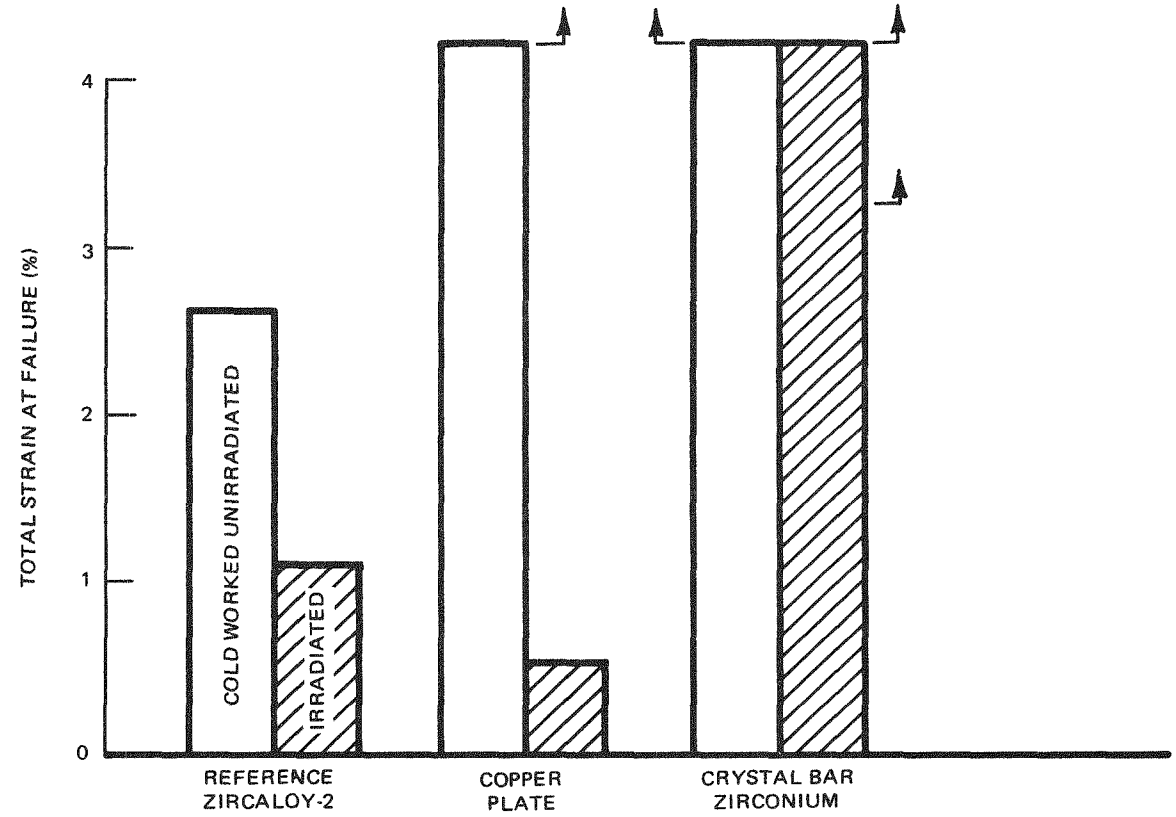

Figure 6.1-4. Comparison of Barrier Performance in Liquid Cadmium Environment at 335°C. Arrow indicates test interrupted without specimen fracture.

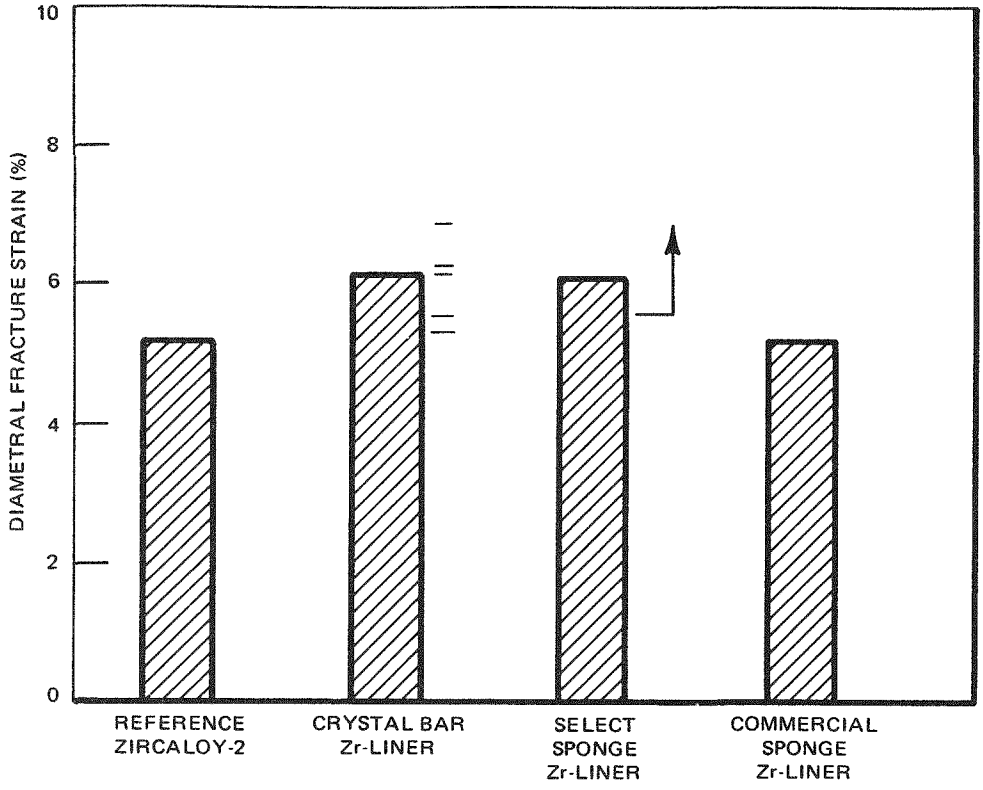

Figure 6.1-5. Expanding Mandrel Test Data for Cold-Worked (As-Rocked) Zr-Liner Zircaloy-2 Tubing, Inert Environment. Each horizontal dash indicates an individual datum with the bar drawn to the mean. Vertical arrow means the test was interrupted without specimen fracture.

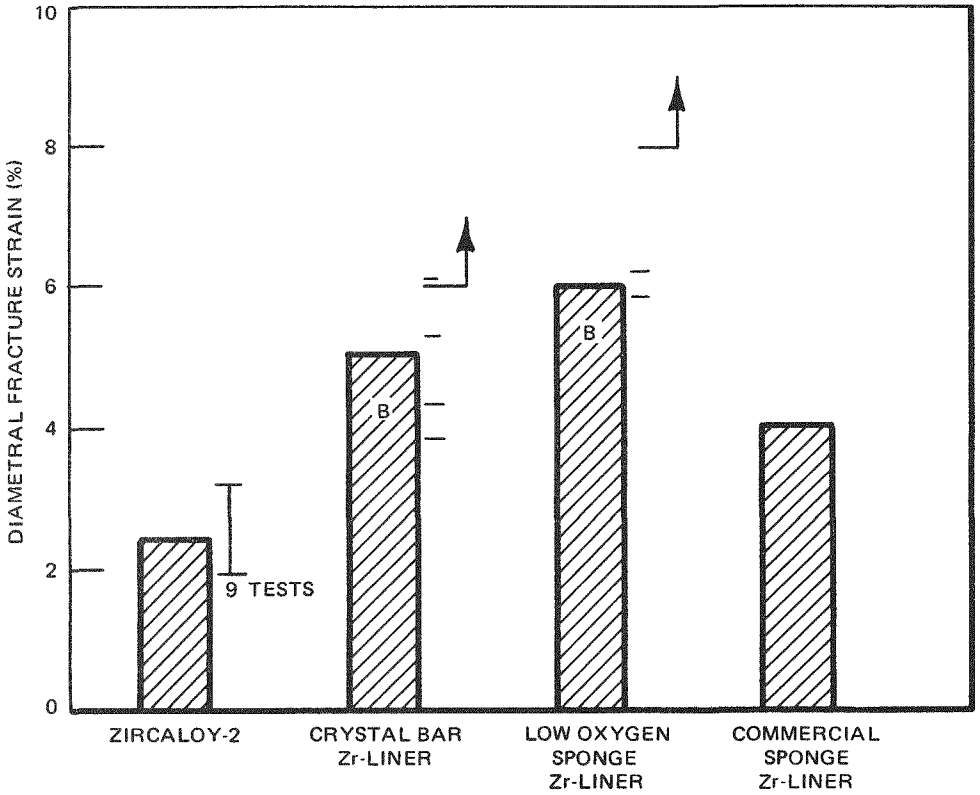

Figure 6.1-6. Cold-Worked Zr-Liner Zircaloy-2 Tubing Tested in I_2 Atmosphere. Individual data are indicated as in Figure 6.1-5. The reference tubing (Zircaloy-2) has 9 data with the range as shown and the bar drawn to the mean.

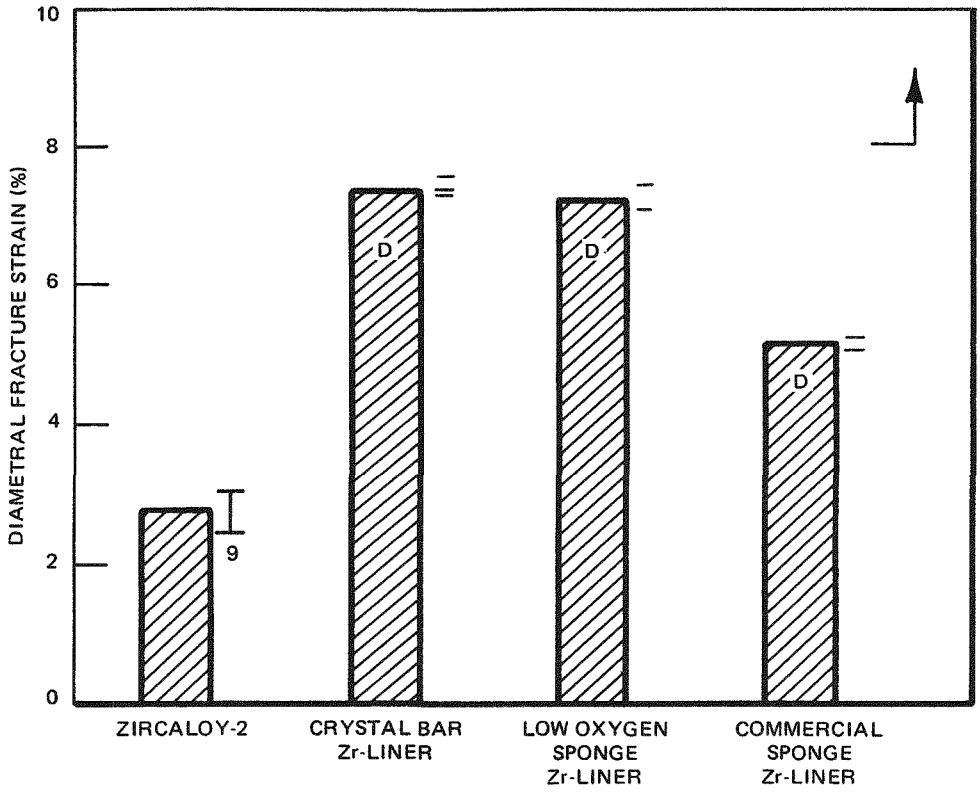

Figure 6.1-7. Cold-Worked Zr-Liner Zircaloy-2 Tubing Tested in the Presence of Cd

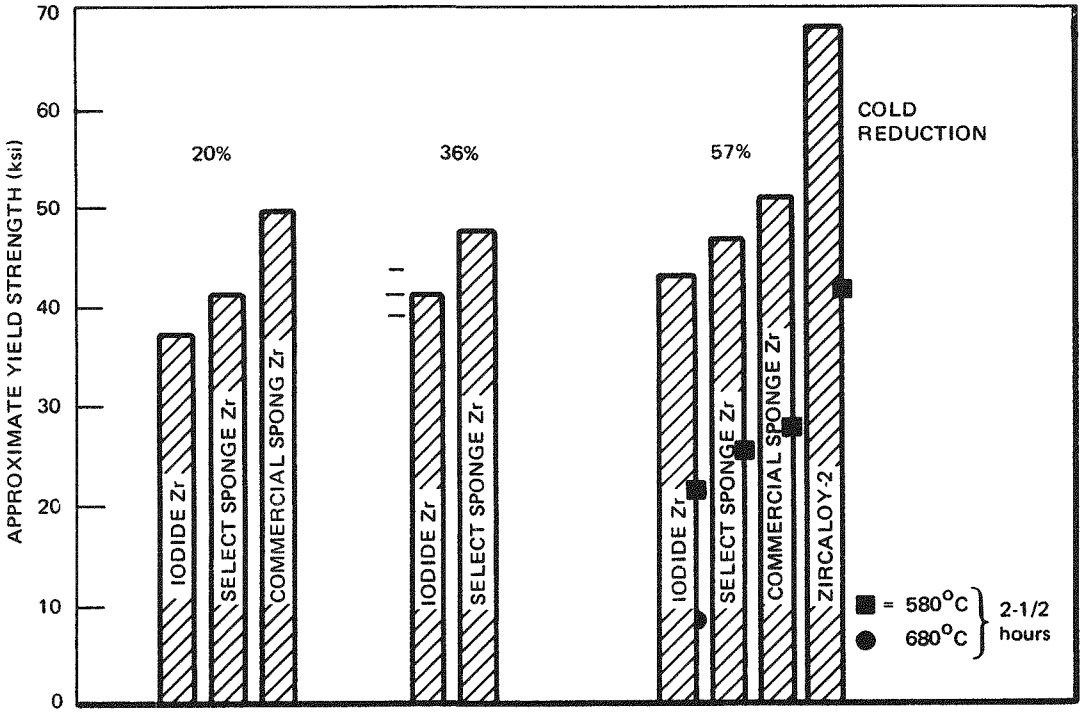

Figure 6.1-8. Effect of Purity of Zr-Liner on Strength as Tested in Plane Strain at 300°C after Various Amounts of Cold Work (Indicated as % Cold Reduction) and Anneal. ("Select" sponge is synonymous with "low oxygen" sponge.)

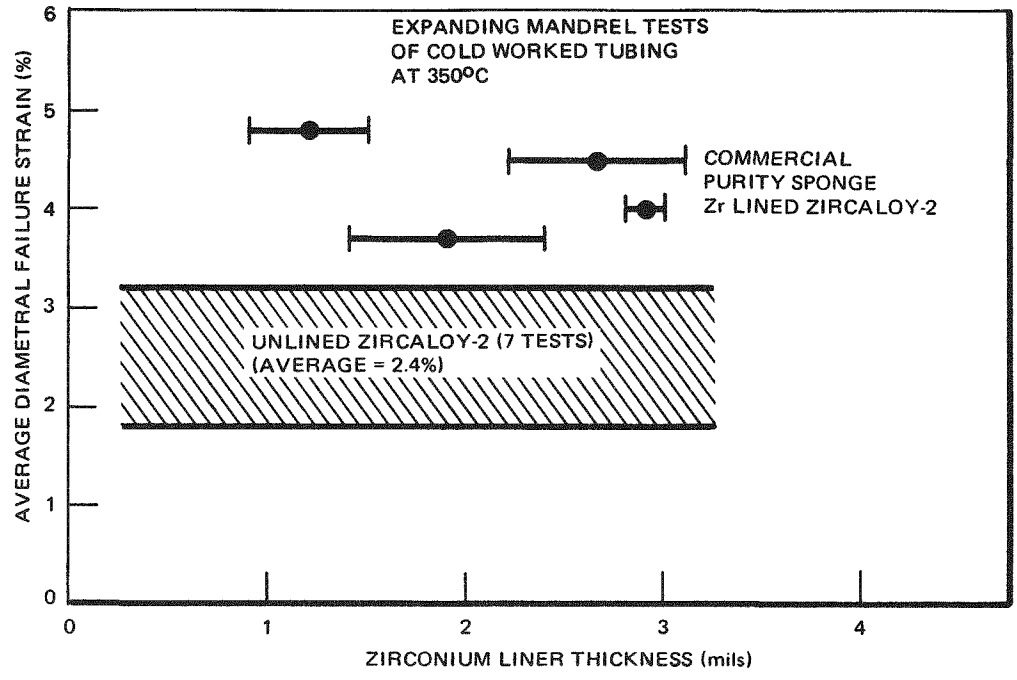

Figure 6.1-9. Effect of Zr-Liner Thickness on Resistance to Stress Corrosion Cracking in I_2 (4×10^{-5} atm)

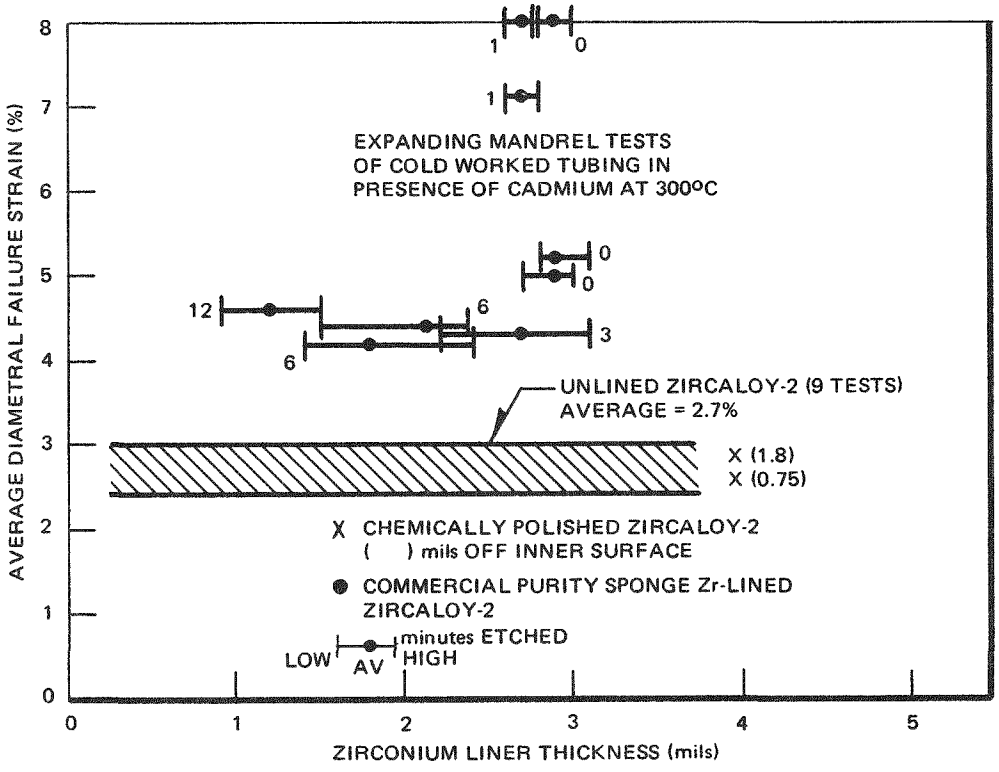

Figure 6.1-10. Effect of Zr-Liner Thickness on Resistance to Cracking in the Presence of Cd

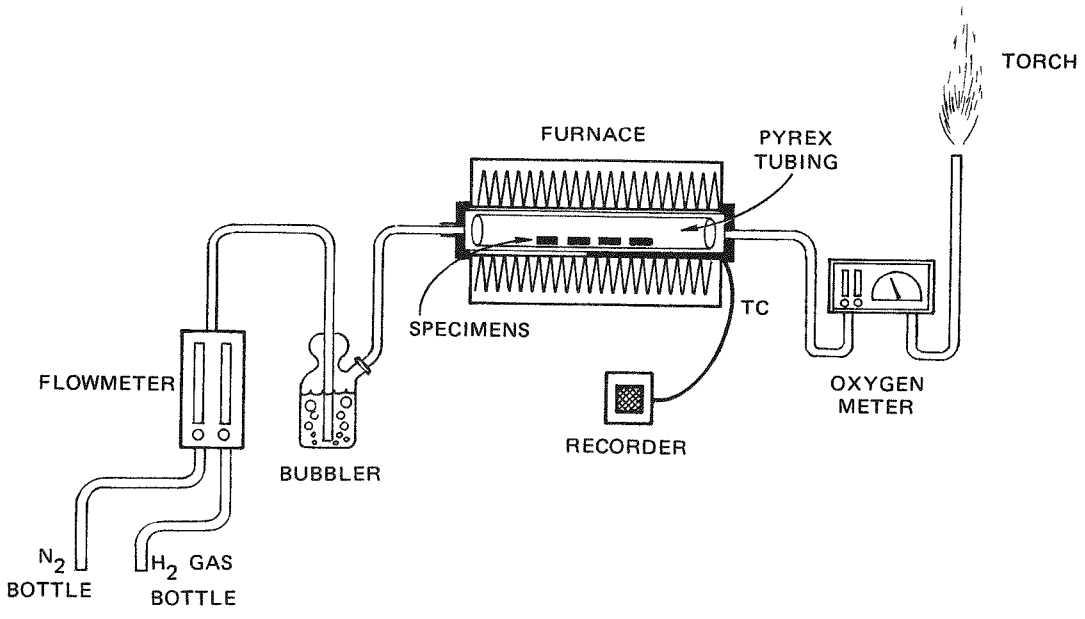

Figure 6.1-11. Schematic of the Setup for Hydrogen Pickup Test

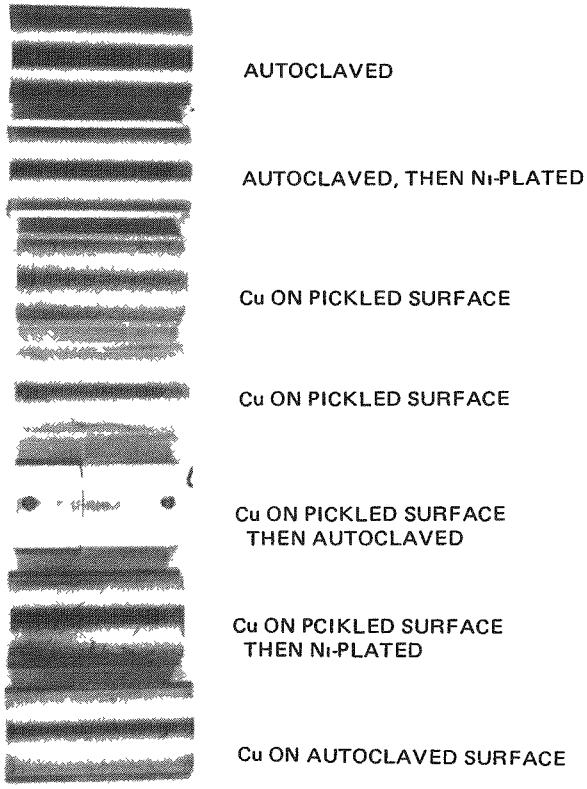

Figure 6.1-12. Pre-Test Surface Appearance of the Specimens Tested in a Wet Hydrogen Atmosphere with H_2/H_2O ~33 at 355°C for 72 Hours

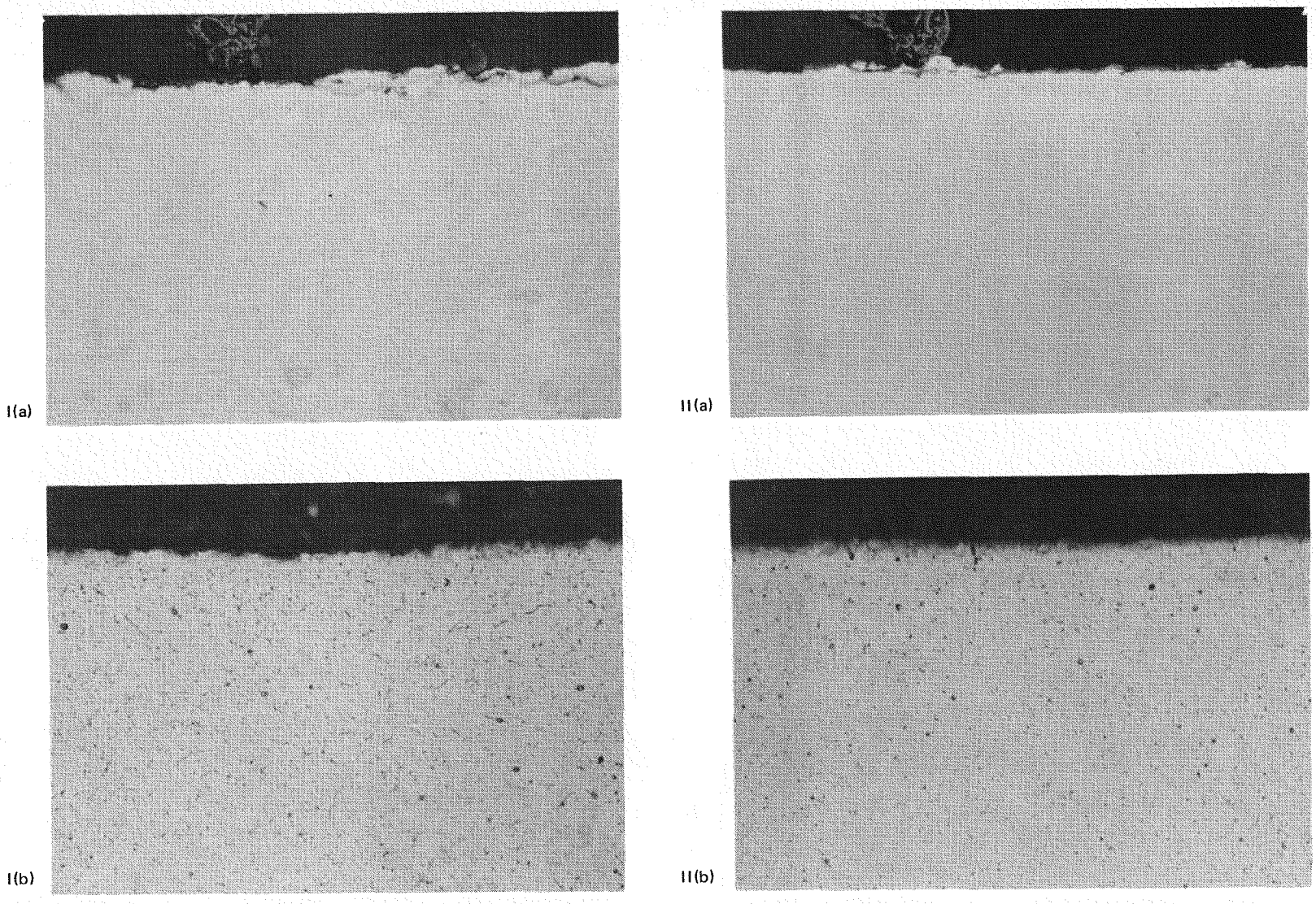

Figure 6.1-13. Micrographs of the Transverse Sections of the Specimens Tested at 355°C for 72 Hours; (a) as polished, (b) etched for hydrides, 500X. Surface Pre-Treatments are (I) autoclaved, (II) autoclaved plus a 200 A vapor-deposited nickel film.

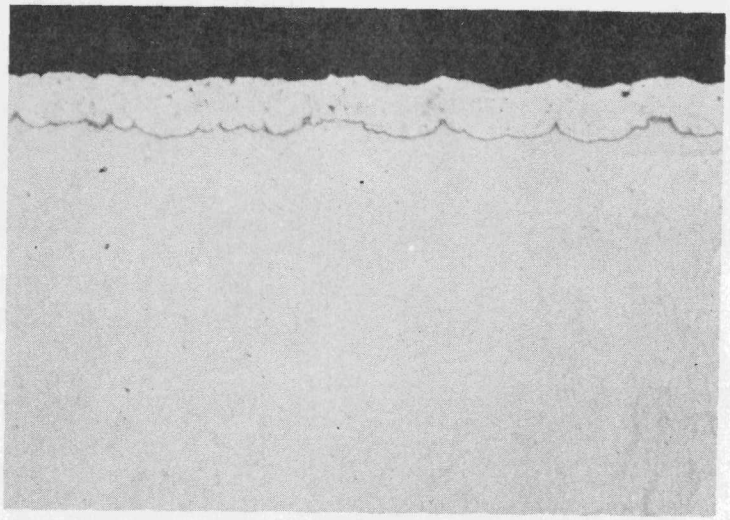

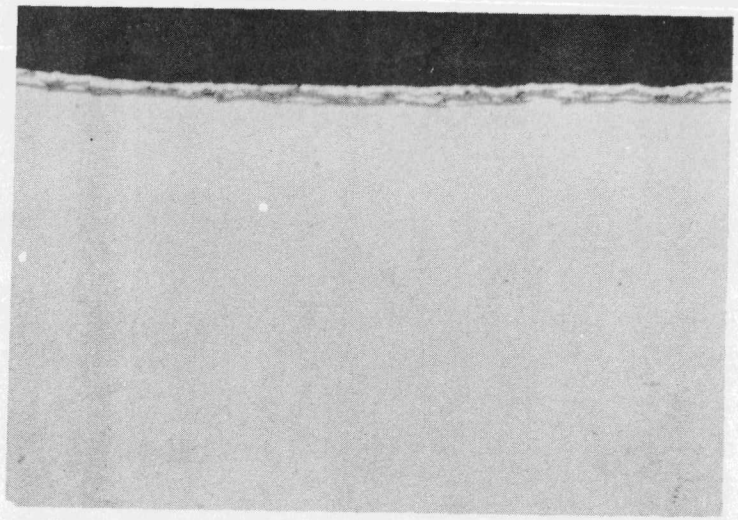

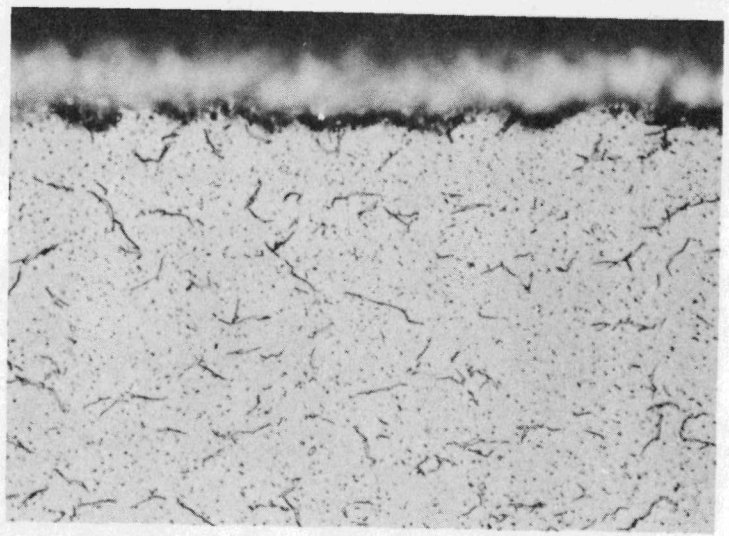

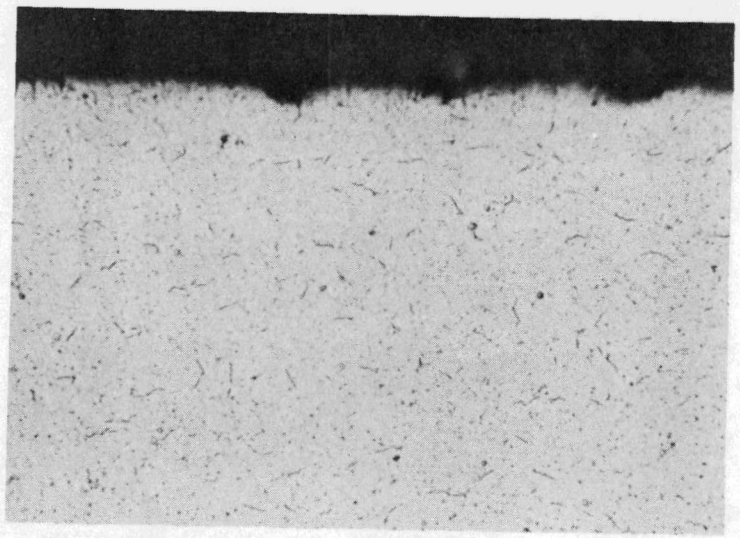

Figure 6.1-14. Micrographs of the Transverse Sections of the Specimens Tested at 355°C for 72 Hours; (a) as polished, (b) etched for hydrides, 500X. Surface Pre-Treatments are (I) copper plated on pickled tubing, (II) copper plated on autoclaved tubing.

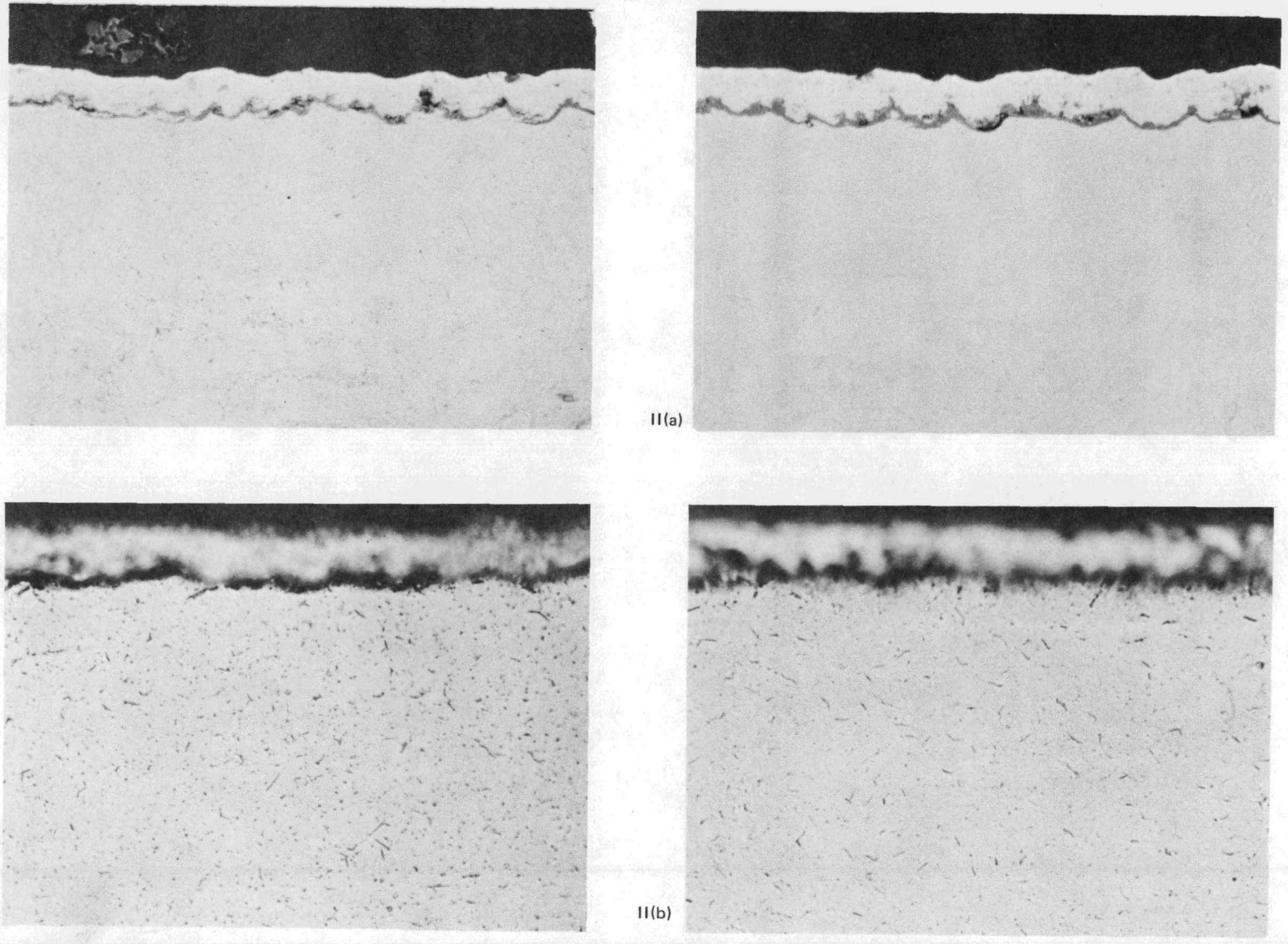

Figure 6.1-15. Micrographs of the Transverse Sections of the Copper Plated on Pickled Tubing Followed by Standard Autoclave Treatment; (I) before, and (II) after being tested in a wet hydrogen atmosphere at 355°C for 72 hours. Specimens (a) are as polished, and (b) etched for hydrides.

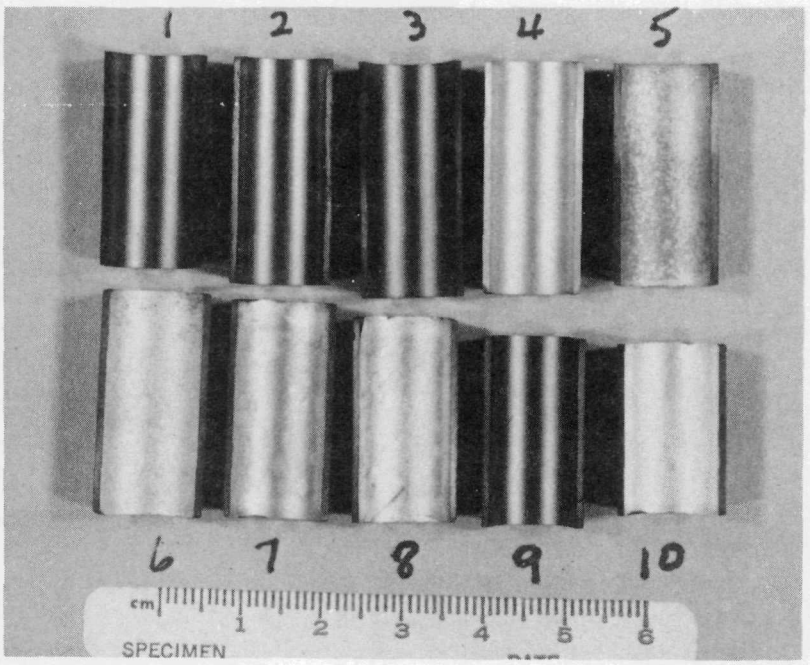

Figure 6.1-16. *Post-Test Surface Appearances of the Specimens Tested in a Wet Hydrogen Atmosphere with H_2/H_2O ~ 13-20 at 400 ± 3°C for 360 Hours.*

(1) Autoclaved Surface
(2) Autoclaved Surface + 50A Platinum Film
(3) Pickled Surface
(4) Pickled Surface + 50A Platinum Film
(5) Copper on Pickled Surface
(6) Copper on Pickled Surface + 50A Platinum Film
(7) Copper on Autoclaved Surface
(8) Copper on Autoclaved Surface + 50A Platinum Film
(9) Oxidized in Dry Oxygen
(10) Copper on Oxidized Surface

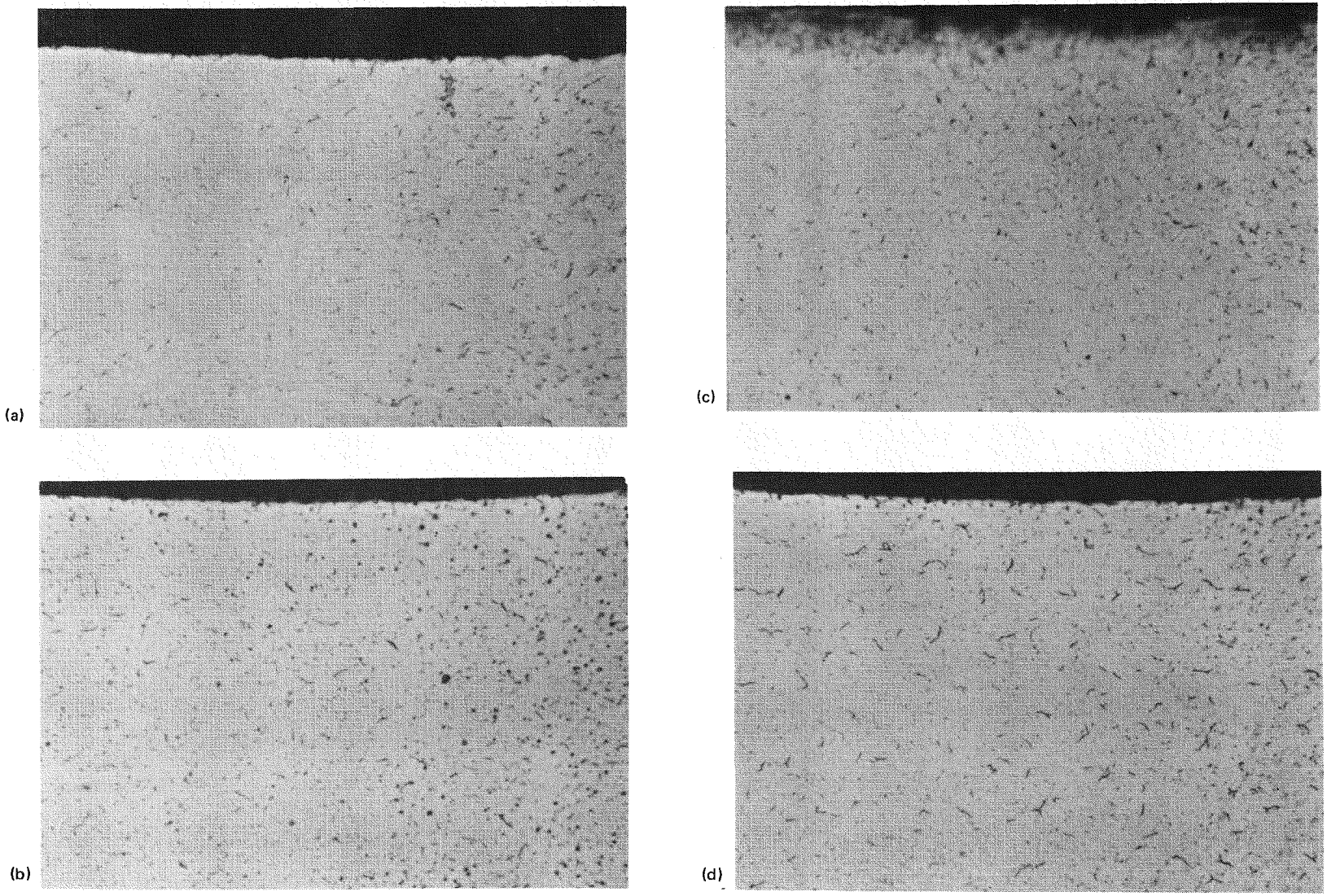

Figure 6.1-17. Micrographs of the Transverse Sections of the Specimens Tested in a Wet Hydrogen Environment at 400°C for 360 Hours; (a) pickled, (b) pickled + 50A platinum film, (c) autoclaved surface, (d) oxidized surface. Specimens are etched for hydrides, 500X.

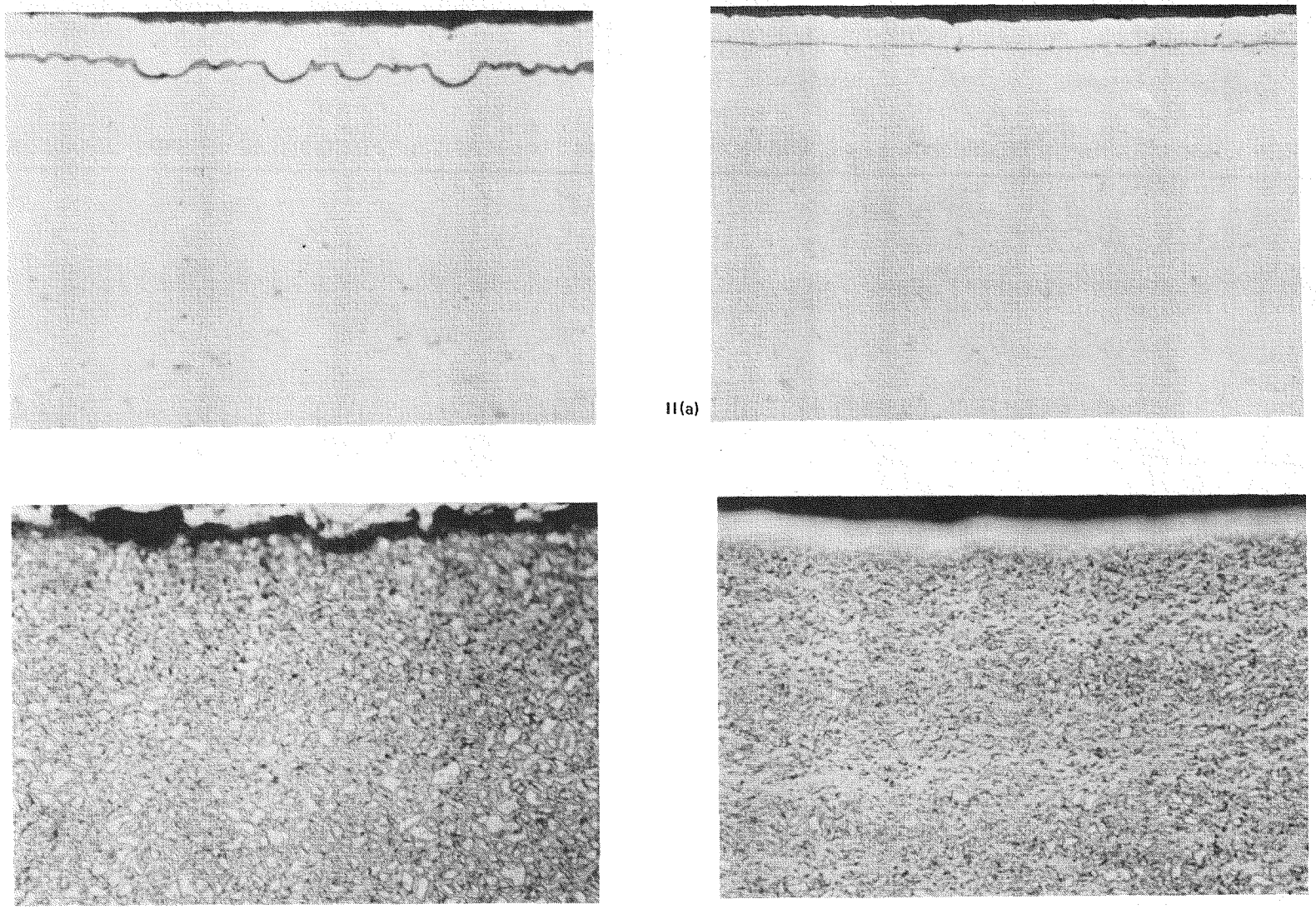

Figure 6.1-18. *Micrographs of the Transverse Sections of the Specimens Tested at 400°C for 360 Hours; (a) as polished, (b) etched for hydrides, 500X. Surface Pre-Treatments are (I) copper plated on pickled tubing, (II) copper plated on oxidized tubing.*

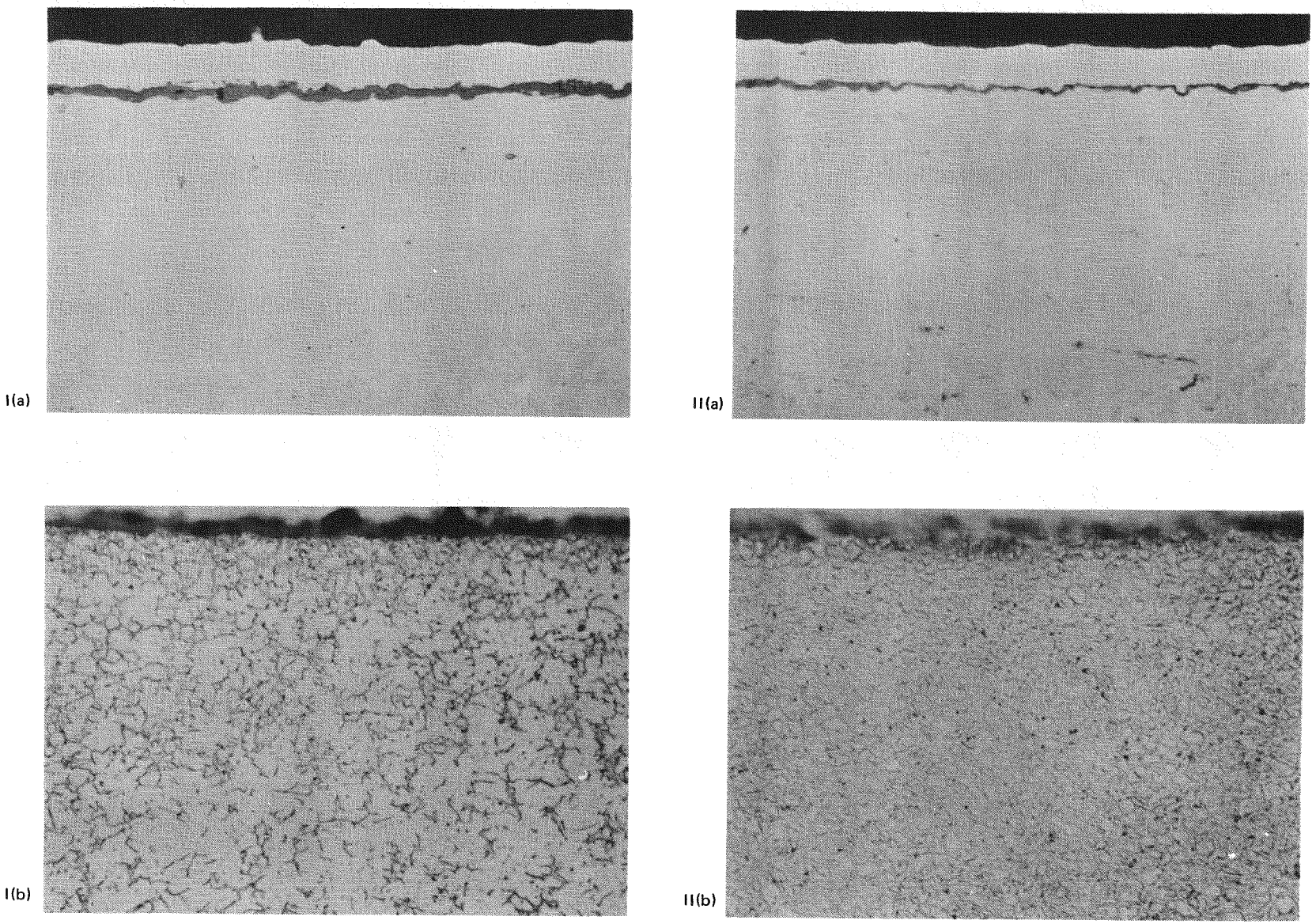

Figure 6.1-19. Micrographs of the Transverse Sections of the Specimens Tested at 400°C for 360 Hours; (a) as polished, (b) etched for hydrides, 500X. Surface Pre-Treatments are (I) copper plated on autoclaved tubing, (b) copper plated on autoclaved tubing + 50A platinum film.

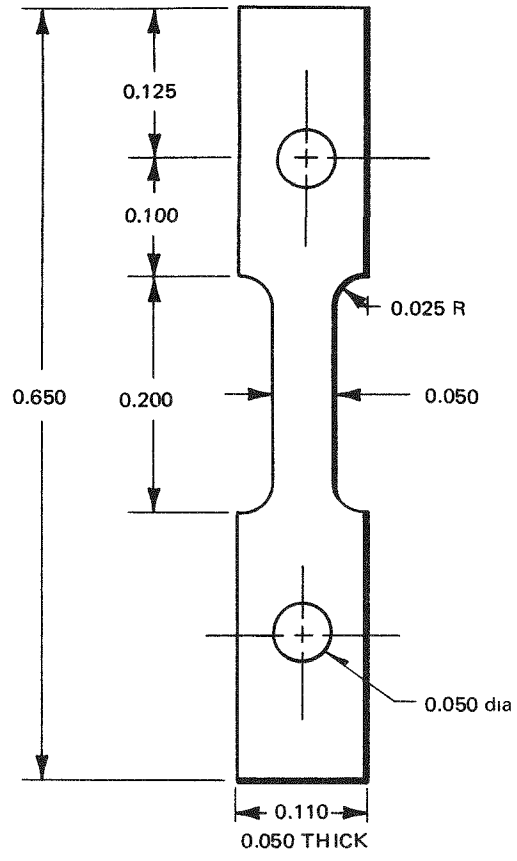

ALL DIMENSIONS IN INCHES

Figure 6.1-20. Miniature Uniaxial Tensile Specimen

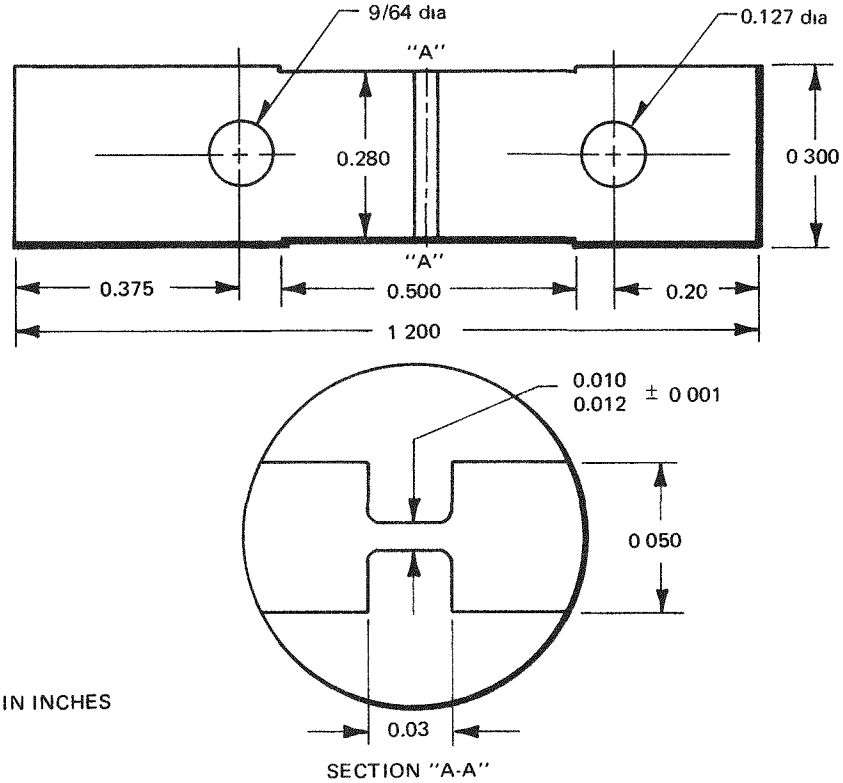

ALL DIMENSIONS IN INCHES

Figure 6.1-21. Reduced Plane Strain Tensile Specimen

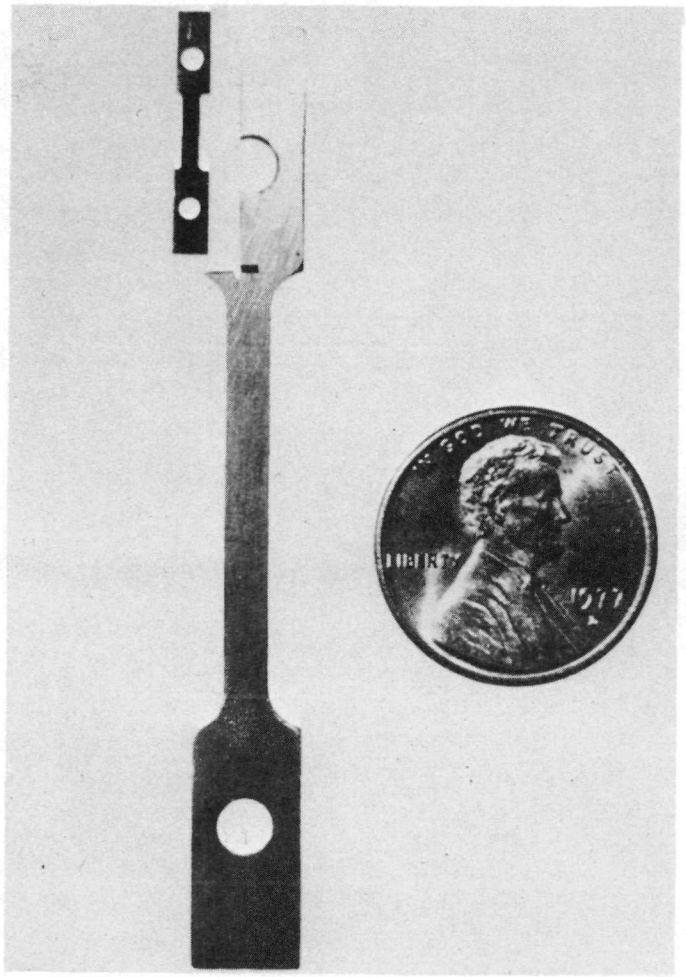

Figure 6.1-22. Miniature Uniaxial Tensile Specimen Compared with the Standard Uniaxial Specimen from which it is Machined

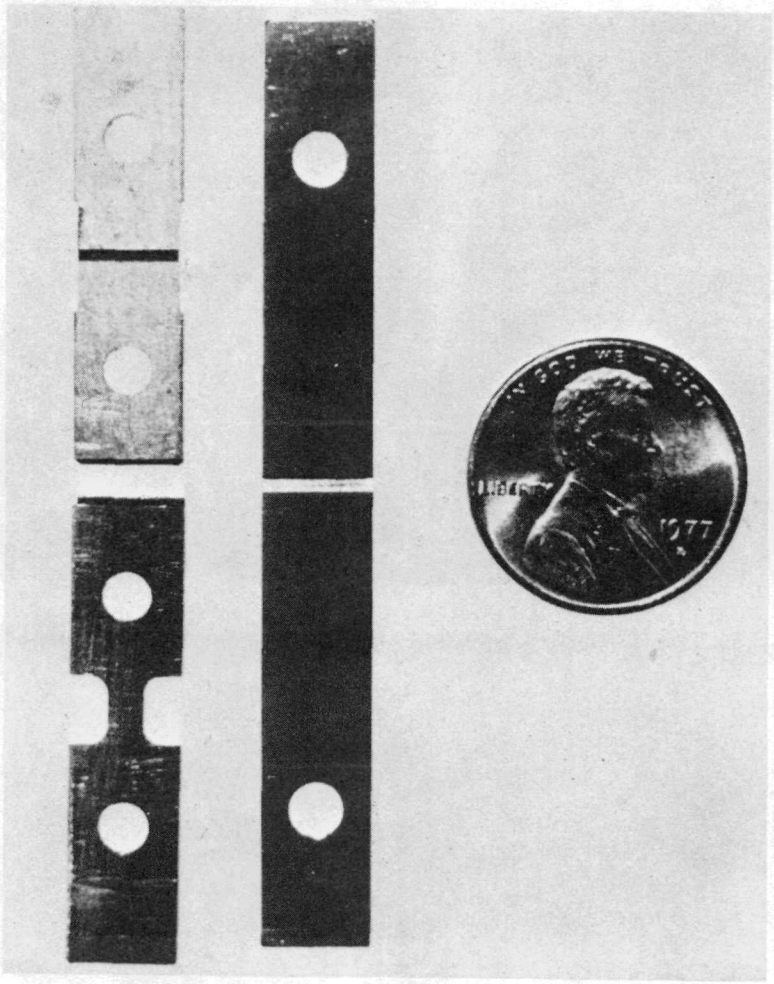

Figure 6.1-23. Reduced Plane Strain (Top) and Uniaxial (Bottom) Tensile Specimens Compared with the Standard Plane Strain Specimen from which they are Machined

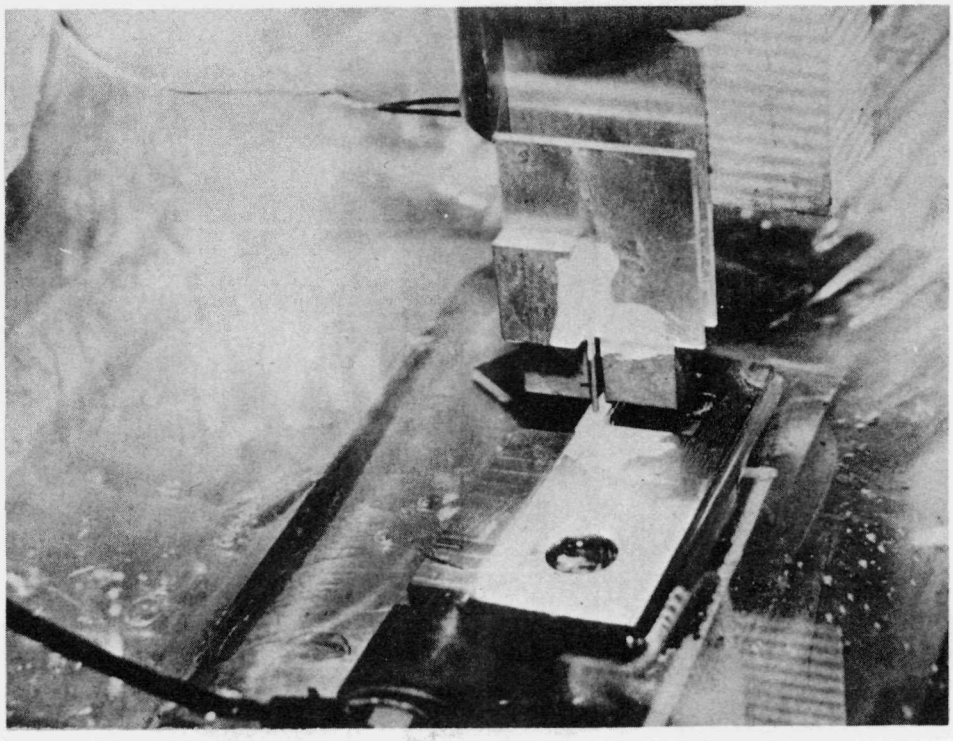

Figure 6.1-24. View of EDM Setup Used to Fabricate Tensile Specimens

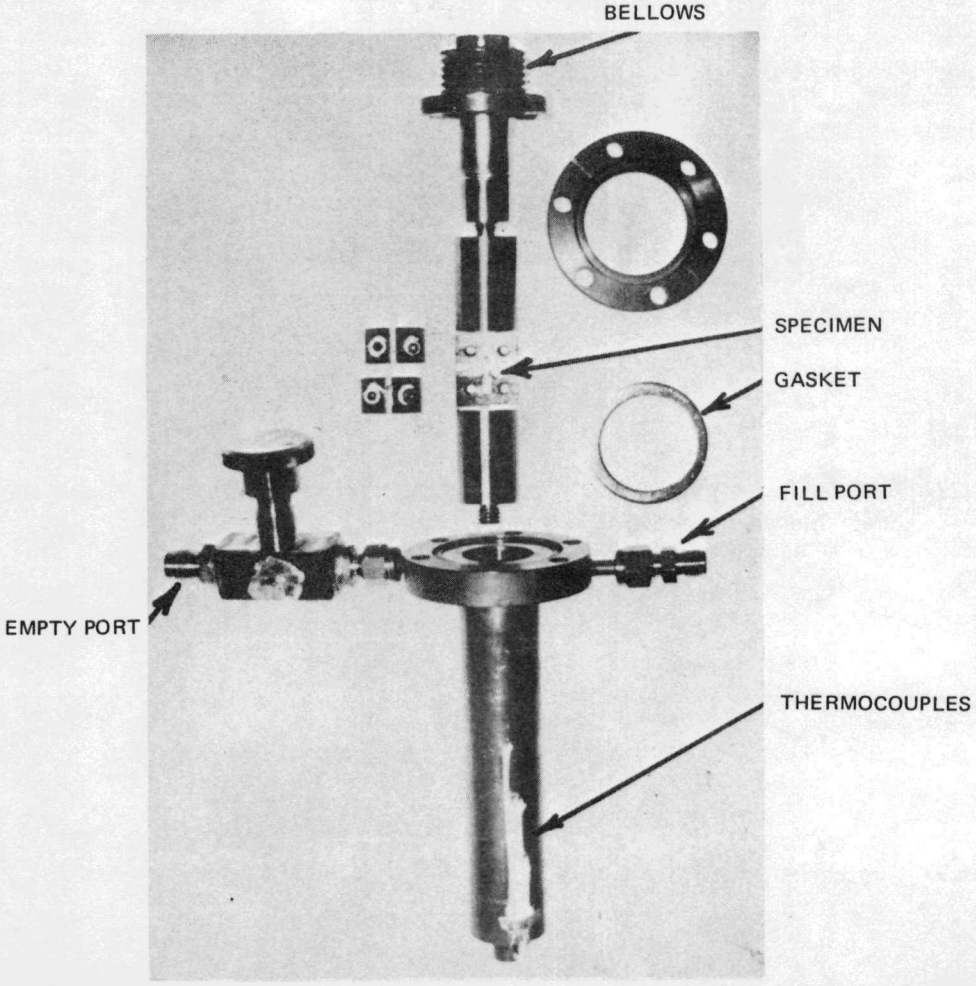

Figure 6.1-25. Exploded View of Capsule System Used to Tensile Test in a Cesium Environment

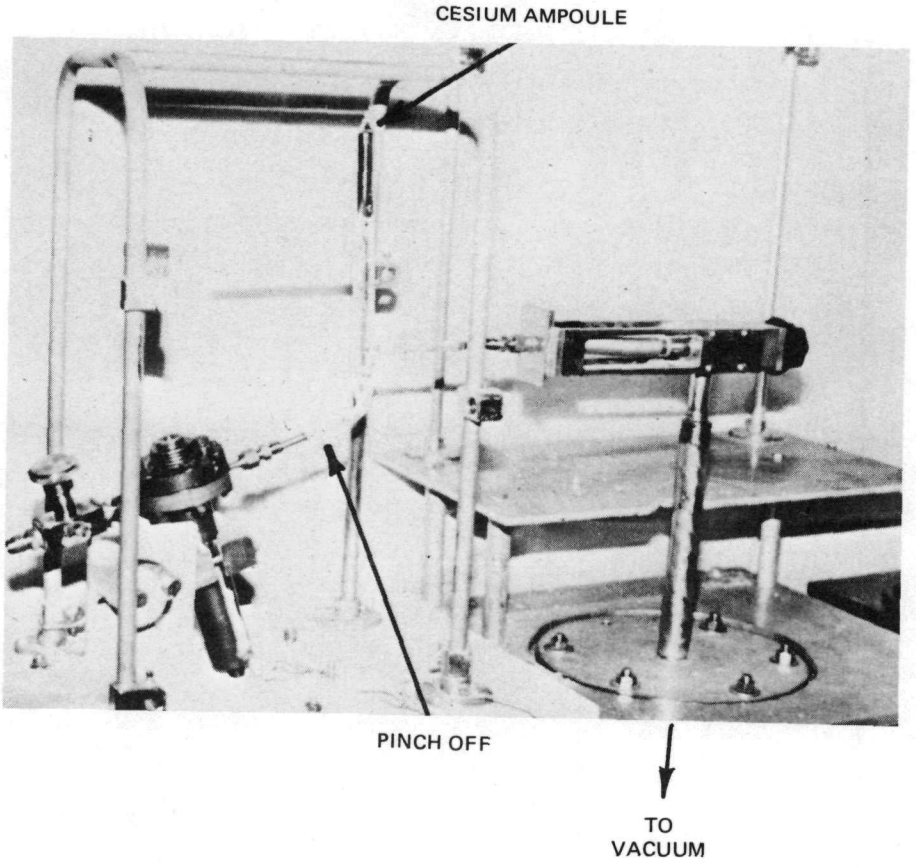

Figure 6.1-26. Cesium Loading/Emptying Station Setup for Loading Capsule with a 10 Gram Cesium Charge

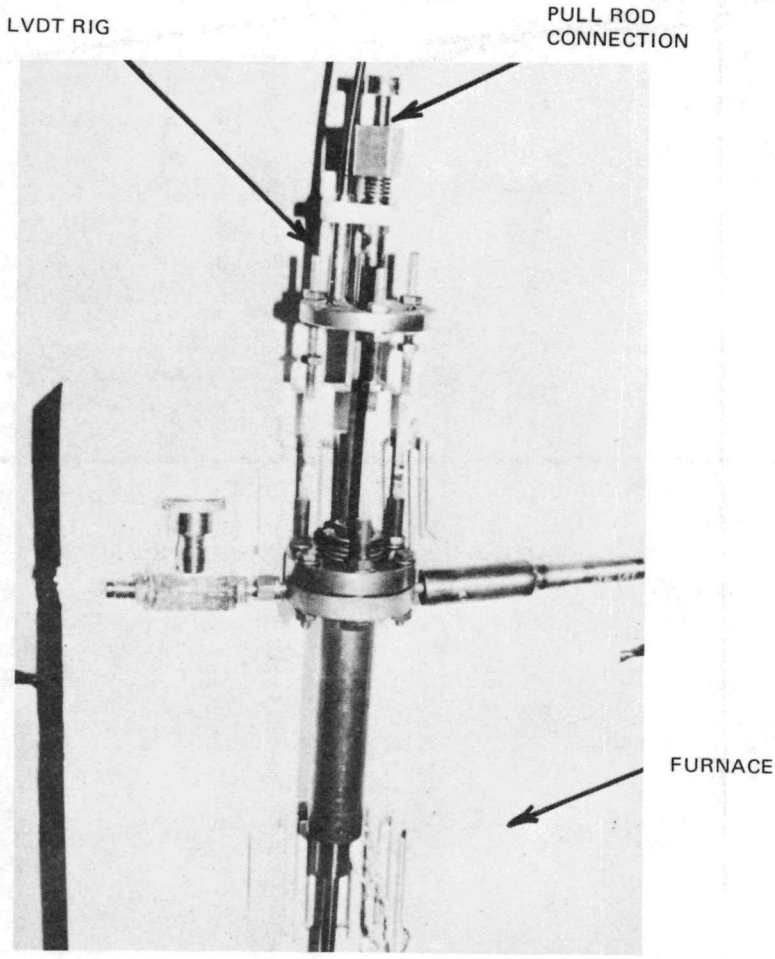

Figure 6.1-27. Capsule Load Train and Resistance Furnace

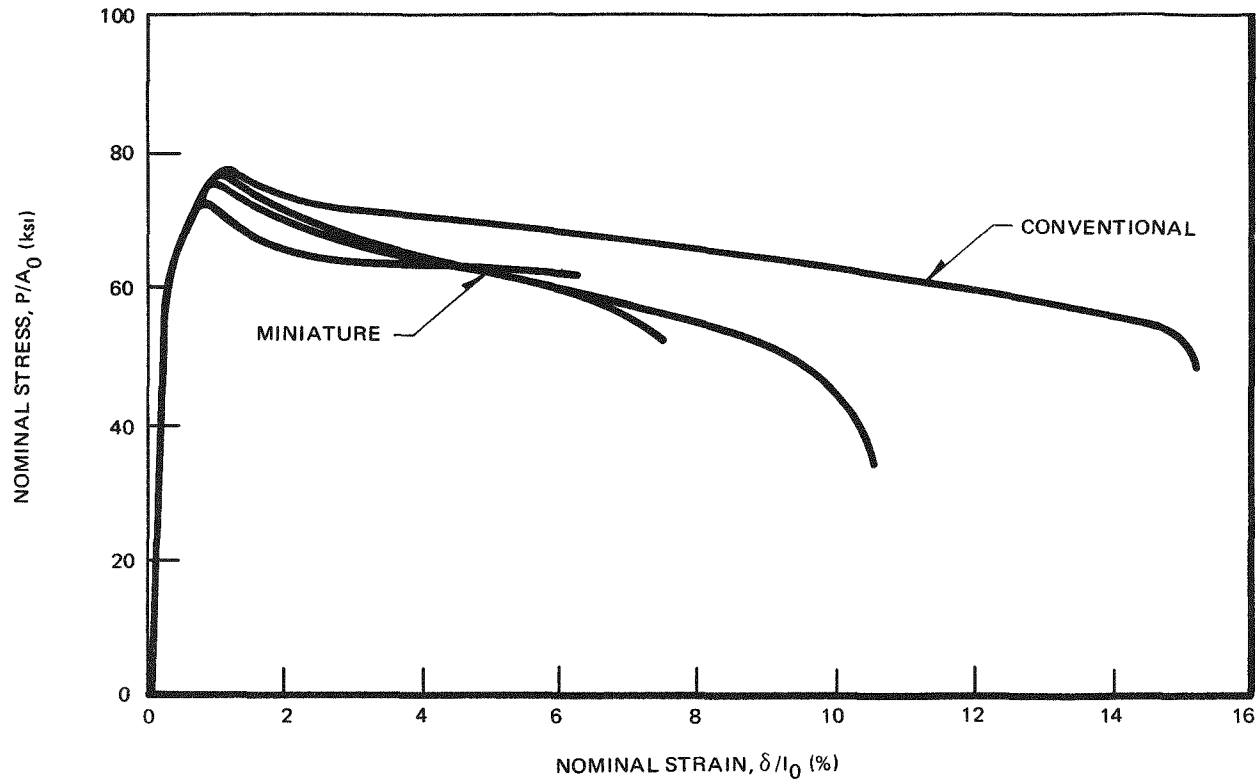

Figure 6.1-28. Comparison of Loading Curves for Miniature Tensile Specimen and Larger Cross Section Uniaxial Tensile Specimens of Irradiated Zircaloy-4 Sheet Material Tested at 350°C

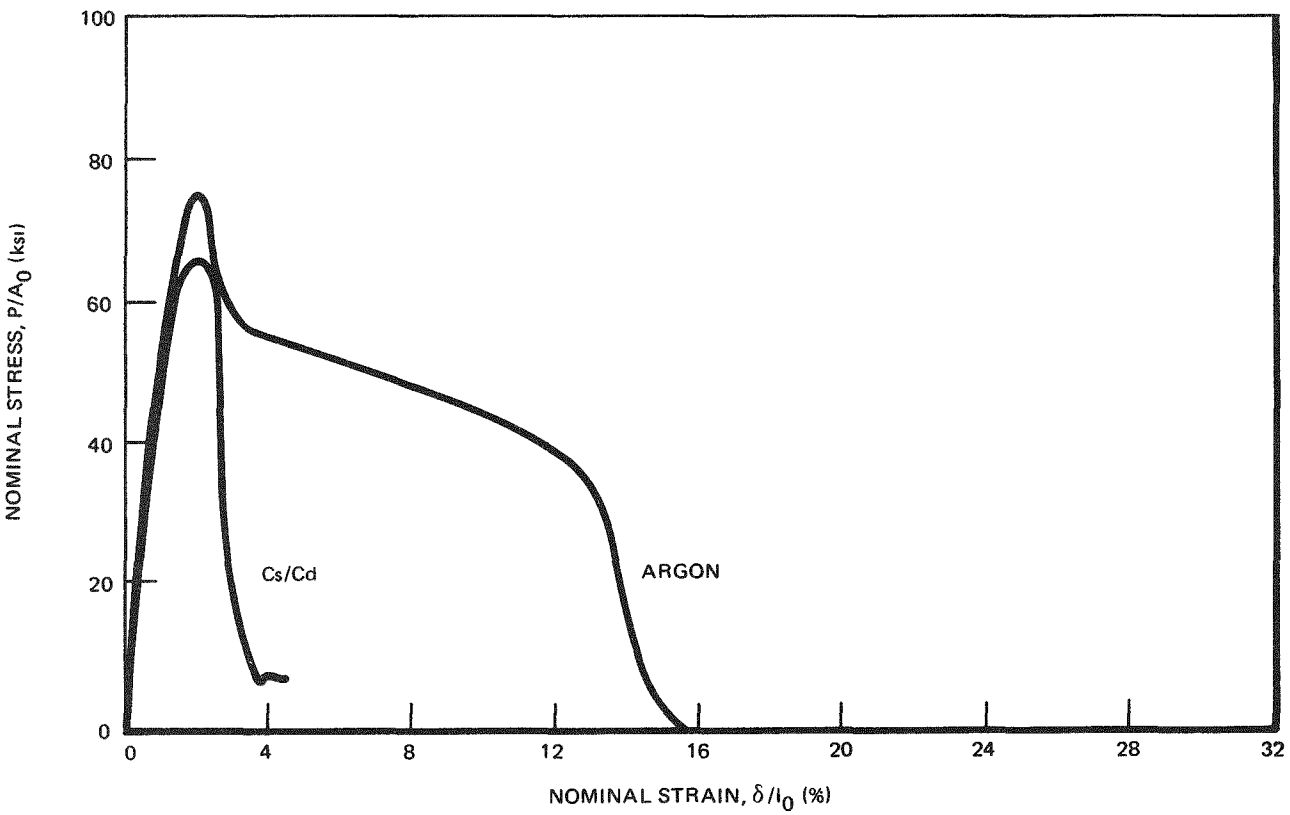

Figure 6.1-29. Comparison of Loading Curves for Miniature Tensile Specimens of Irradiated Zircaloy-4 Sheet Tested in Argon and Cesium/Cadmium Environments at 350°C

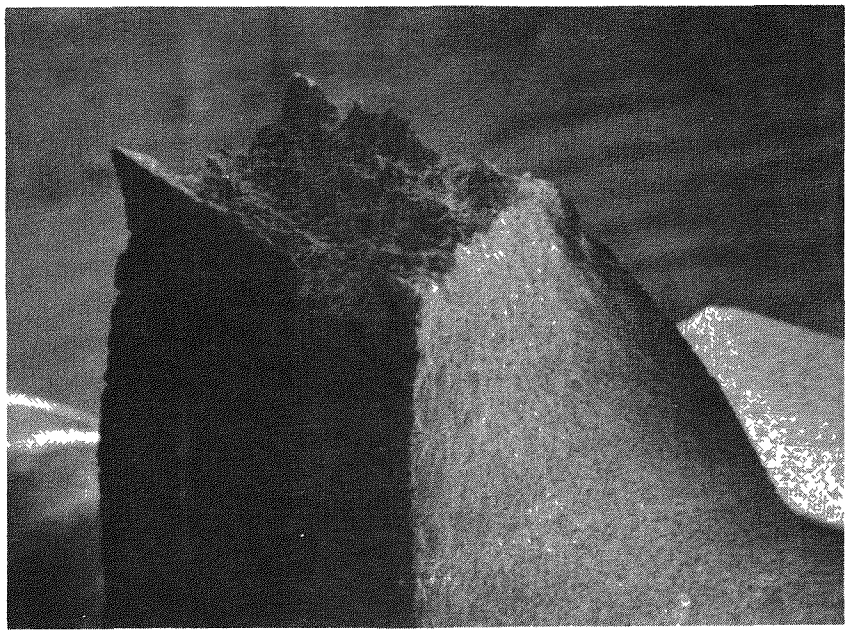

(a)

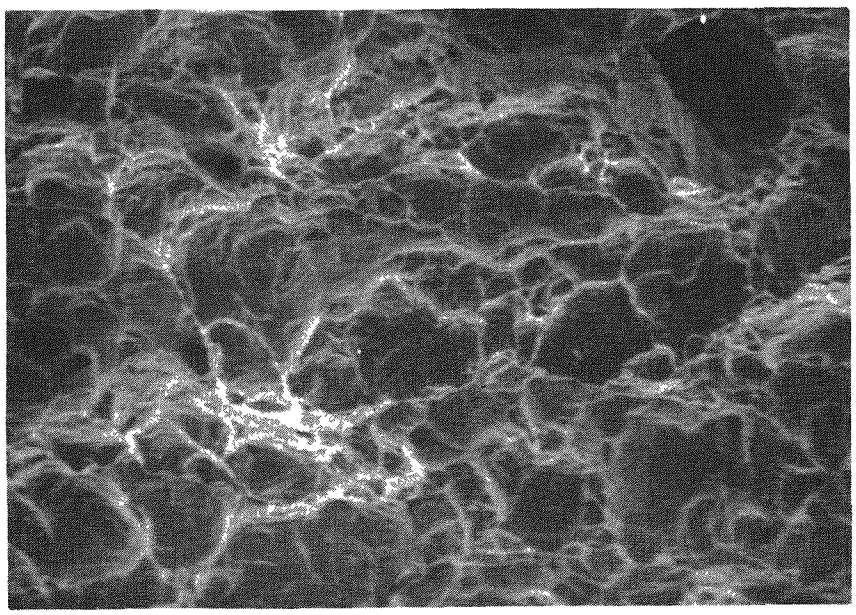

(b)

Figure 6.1-30. Scanning Electron Micrographs of Irradiated Zircaloy-4 Specimen Tested in Argon at 350°C; (a) ~50X, (b) ~500X

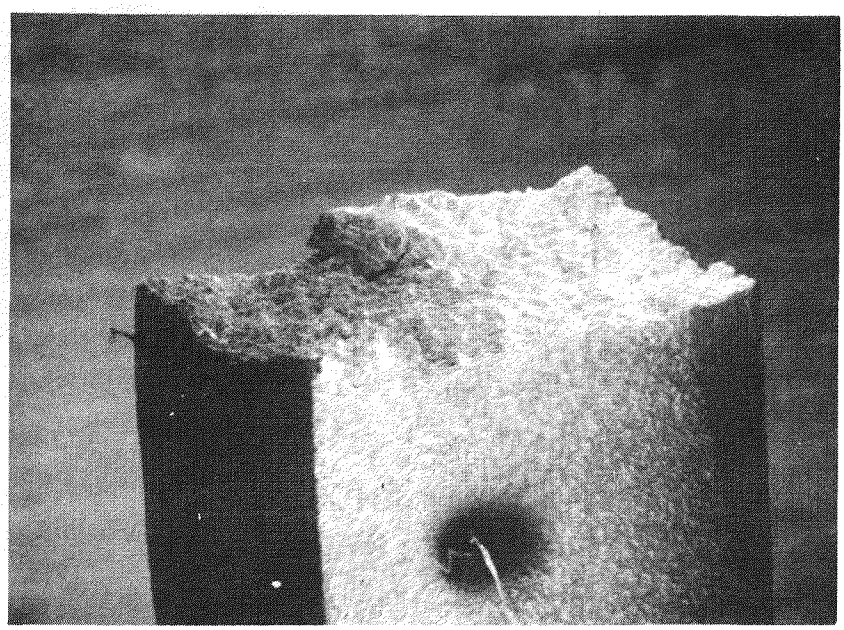

(a)

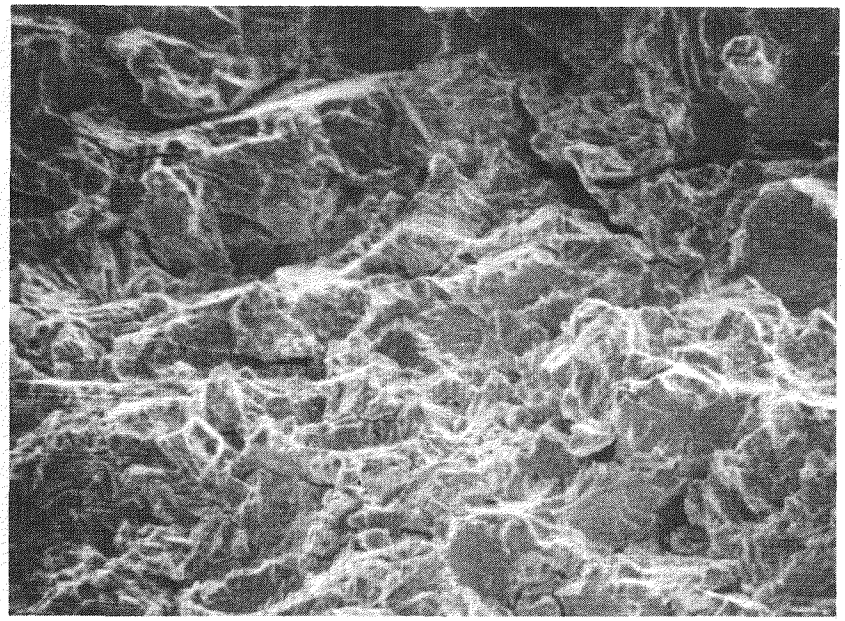

(b)

Figure 6.1-31. Scanning Electron Micrographs of Irradiated Zircaloy-4 Specimen Tested in Cesium/Cadmium Environment at 350°C; (a) ~50X, (b) ~500X

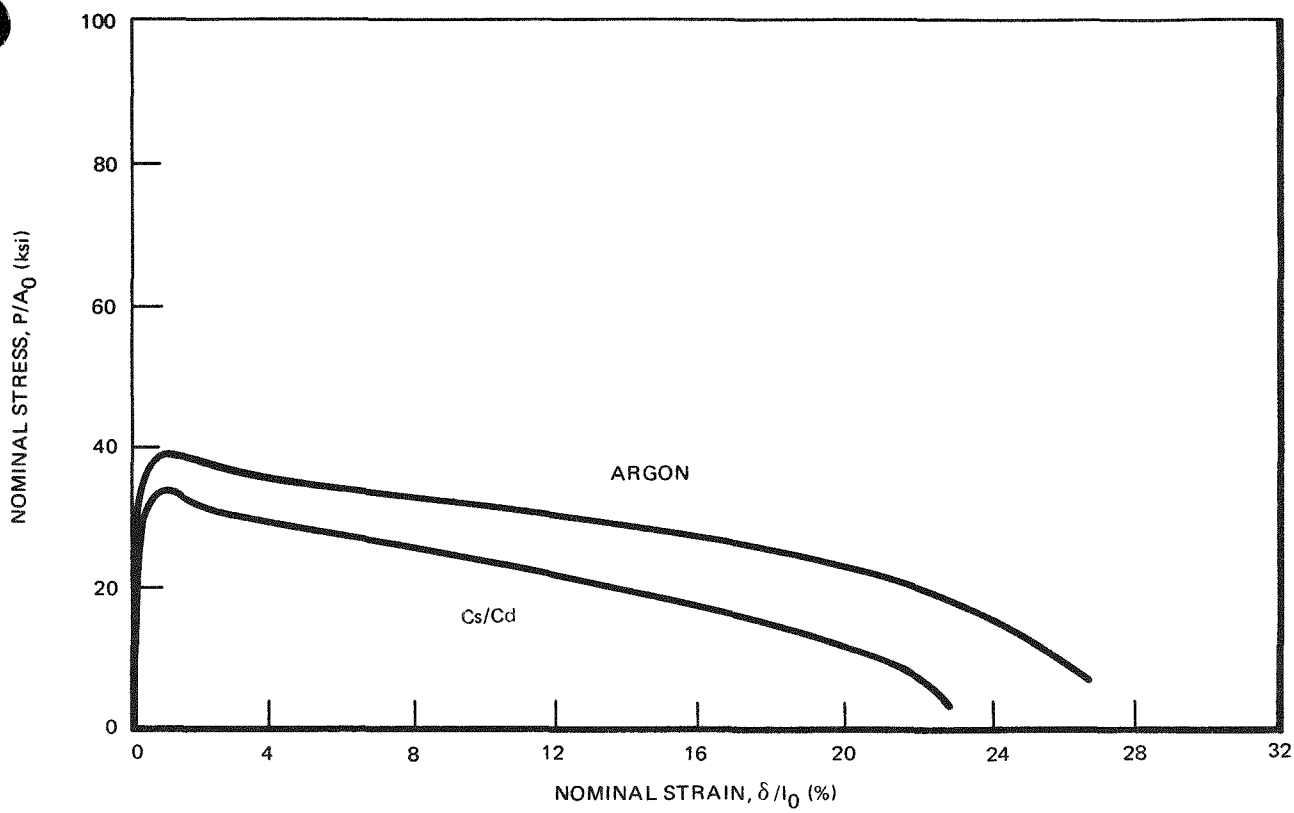

Figure 6.1-32. Comparison of Loading Curves for Irradiated Crystal Bar Zirconium Tensile Specimens Tested in Argon and Cesium/Cadmium Environments at 350°C

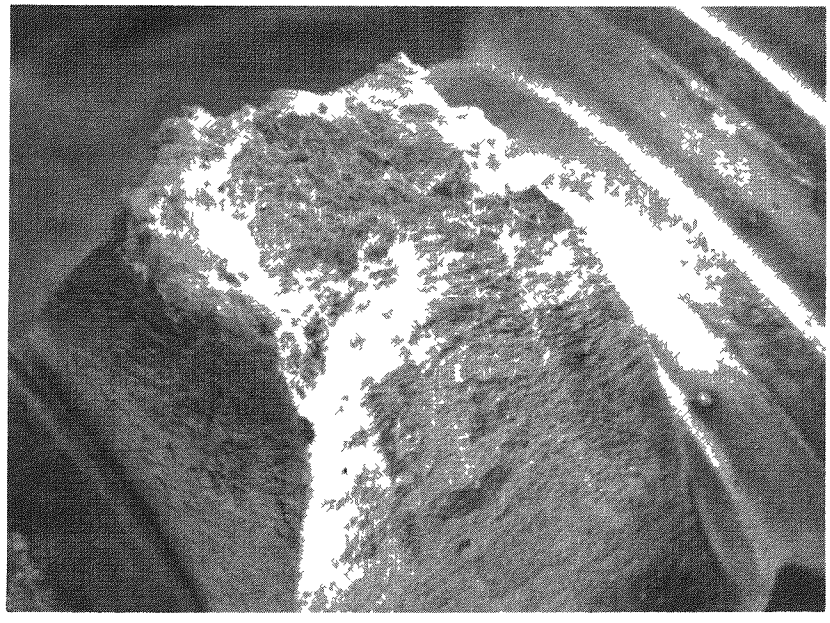

(a)

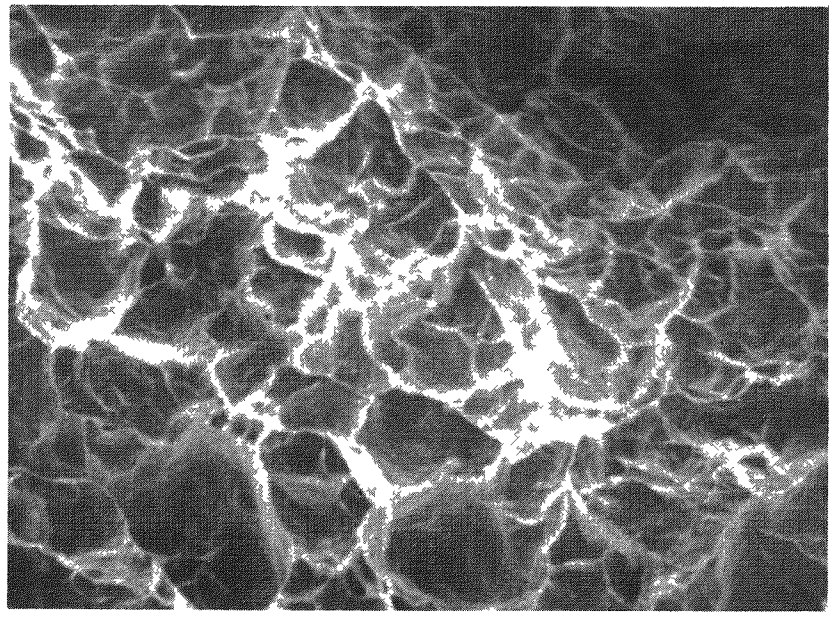

(b)

Figure 6 1 33 *Scanning Electron Micrographs of Irradiated Crystal Bar Zirconium Specimen Tested in Argon at 350°C, (a) ~50X (b) ~500X*

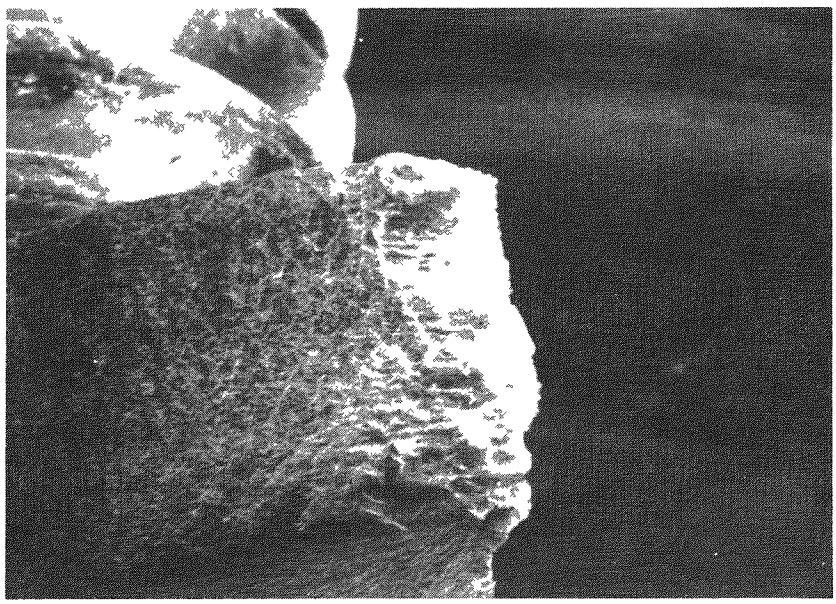

(a)

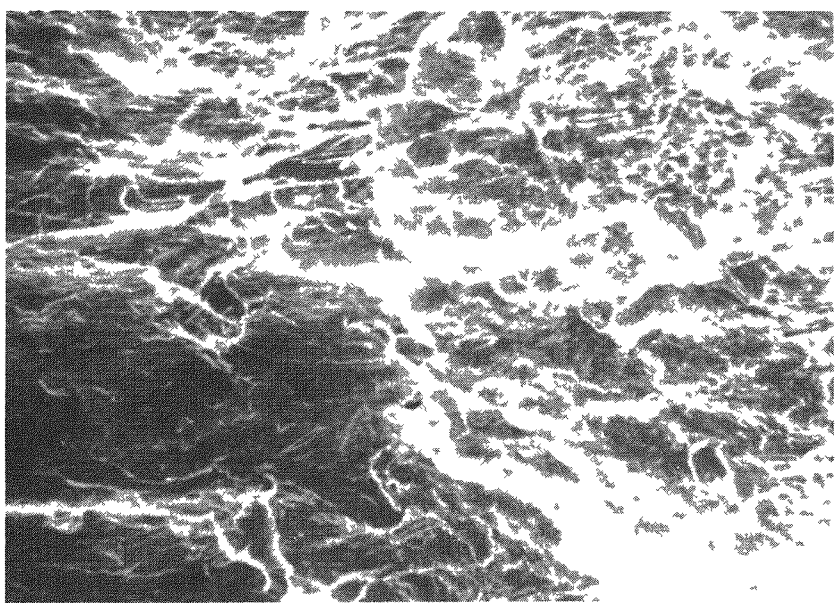

(b)

Figure 6.1-34. Scanning Electron Micrographs of Irradiated Crystal Bar Zirconium Specimen Tested in Cesium/ Cadmium Environment at 350°C, (a) ~50X, (b) ~500X

6.2 Task 2.0 LICENSING TESTS

6.2.1 Subtask 2.1 Loss of Coolant Accident (LOCA) (R. B. Adamson, NTD)

6.2.1.1 Objective

During a postulated LOCA, fuel rods are subject to transient pressure and temperature conditions. The objective of the present tests is to compare the behavior of cladding having Cu-barrier or Zr-liner with the behavior of reference Zircaloy-2 cladding under those conditions. It is planned to conduct tests using the following tubing material:

1. Zircaloy-2
2. Zircaloy-2 with electroless Cu-barrier
3. Zircaloy-2 with electroless Cu-barrier plated onto an oxidized Zircaloy surface
4. Zircaloy-2 with crystal bar zirconium liner

6.2.1.2 Background Information

Several tests were conducted on Cu-barrier rods previous to the start of the present program. Empty cladding tubes were resistively heated along either of two temperature-time paths:

a. 1°F/sec to 2200°F (0.56°C/sec to 1204°C)

b. 40°F/sec to 1600°F (22.2°C/sec to 871°C), hold for 50 seconds, 2.5°F/sec to 2200°F (1.4°C/sec to 1204°C)

These tests were performed with the interior of the tube pressurized with argon to simulate fission gas pressure and the exterior exposed to circulating steam. Perforation temperature was measured and correlated with the applied hoop stress. Little difference between reference and Cu-barrier or Zr-liner tubing was apparent. Circumferential elongation at fracture appeared to be decreased in the Cu-barrier tube subjected to the 1600°F hold period.

6.2.1.3 Progress in Current Report Period

1. Preliminary temperature-pressure-time profiles appropriate for the postulated LOCA conditions have been obtained.

2. Experimental apparatus has been assembled and is currently being calibrated and checked out. Figure 6.2-1 is a schematic diagram of the testing apparatus. Tubing will be loaded with depleted urania pellets and will be resistively heated. Internal pressure will be supplied by argon gas and external pressure by steam, argon, or air. Temperature will be measured by internal thermocouples and an external infra-red pyrometer. The temperature-time profile will be automatically programmed.

3. Copper-barrier tubing is currently on hand, and Zr-liner tubing will be available in February 1978.

4. Testing will be started during the first quarter of calendar year 1978.

6.2.2 Subtask 2.2 Reactivity Initiated Accident (L. D. Noble, NTD)

The objective of this task is to obtain experimental evidence that the performance of fuel with a copper or zirconium barrier is comparable to that of standard fuel during Reactivity Initiated Accidents (RIA).

For a BWR, the design basis RIA is a hypothetical case in which the control rod (blade) becomes decoupled from the control drive while in the inserted position. It is then postulated that the control drive is withdrawn, but the control rod remains in the reactor, to drop out, suddenly, at some later time. Analysis indicates that the most severe transients occur during ambient or hot standby conditions. The barrier tubing will be tested under both of these conditions.

The ambient and heated tests will be conducted in 1978 and 1979 at the Nuclear Safety Research Reactor (NSRR) in Japan through arrangements with Battelle, the Nuclear Regulatory Commission (NRC), and the Japan Atomic Energy Research Institute (JAERI). Hot standby tests would be performed later at the Power Burst Facility (PBF) in Idaho, possibly with irradiated fuel.

Currently, 31 tests with GE barrier tubing are planned for NSRR. Eighteen of the tests are to be at room temperature and atmospheric pressure. Included will be 8 reference rods with standard tubing, and 5 rods, each of copper and zirconium barrier tubing. Thirteen tests will be performed at high temperature (286°C) and pressure (73 kg/cm^2); 8 with reference tubing, and 5 with either copper or zirconium barrier tubing. This test matrix may be modified as a result of initial test results.

The RIA tests deposit energy into the fuel very rapidly by pulsing the reactor (such as NSRR) with a large power burst of short duration. For NSRR, the power burst may typically have a half width of 4 to 5 ms, and the energy deposition may be as high as 500 cal/g of UO_2, depending on the fuel enrichment. At very high energy depositions, the fuel becomes fragmented, while at low magnitude depositions no visible change occurs. At intermediate energies, external cladding oxidation, cladding deformation, and small cracks may develop.

The tests planned for NSRR would include energy depositions up to approximately 350 cal/g as indicated in the test matrix of Table 6.2-1. As indicated, these will span the expected range of test conditions from clad oxidation through complete fragmentation.

The fuel rods are being manufactured at Battelle Northwest Laboratories. Tubing has been provided by General Electric. The fuel and fabrication are being provided by the NRC.

A licensed shipping container was provided to Battelle by GE. It is now at the Battelle site for shipping of the rods to Japan as soon as they are fabricated. Shipment is expected in 1978.

Table 6.2-1
PLANNED NUCLEAR SAFETY RESEARCH REACTOR TESTS

Fuel Type/Test Condition	Energy Deposition (cal/g UO_2) 120	150	215 to 240	250	350	Total Number
Reference/Ambient	1	1	4	1	1	8
Copper/Ambient	0	1	2	1	1	5
Zirconium/Ambient	0	1	2	1	1	5
Reference/High Temperature and Pressure	1	1	4	1	1	8
Copper or Zirconium/High Temperature and Pressure	0	1	2	1	1	5
						31

EXPECTED RESULTS
(Based on Previous NSRR Tests)

Oxidation	~ 120 cal/g
Deformation	~ 150 cal/g
Crack	~ 230 cal/g
Break	~ 250 cal/g
Fragmentation	~ 350 cal/g

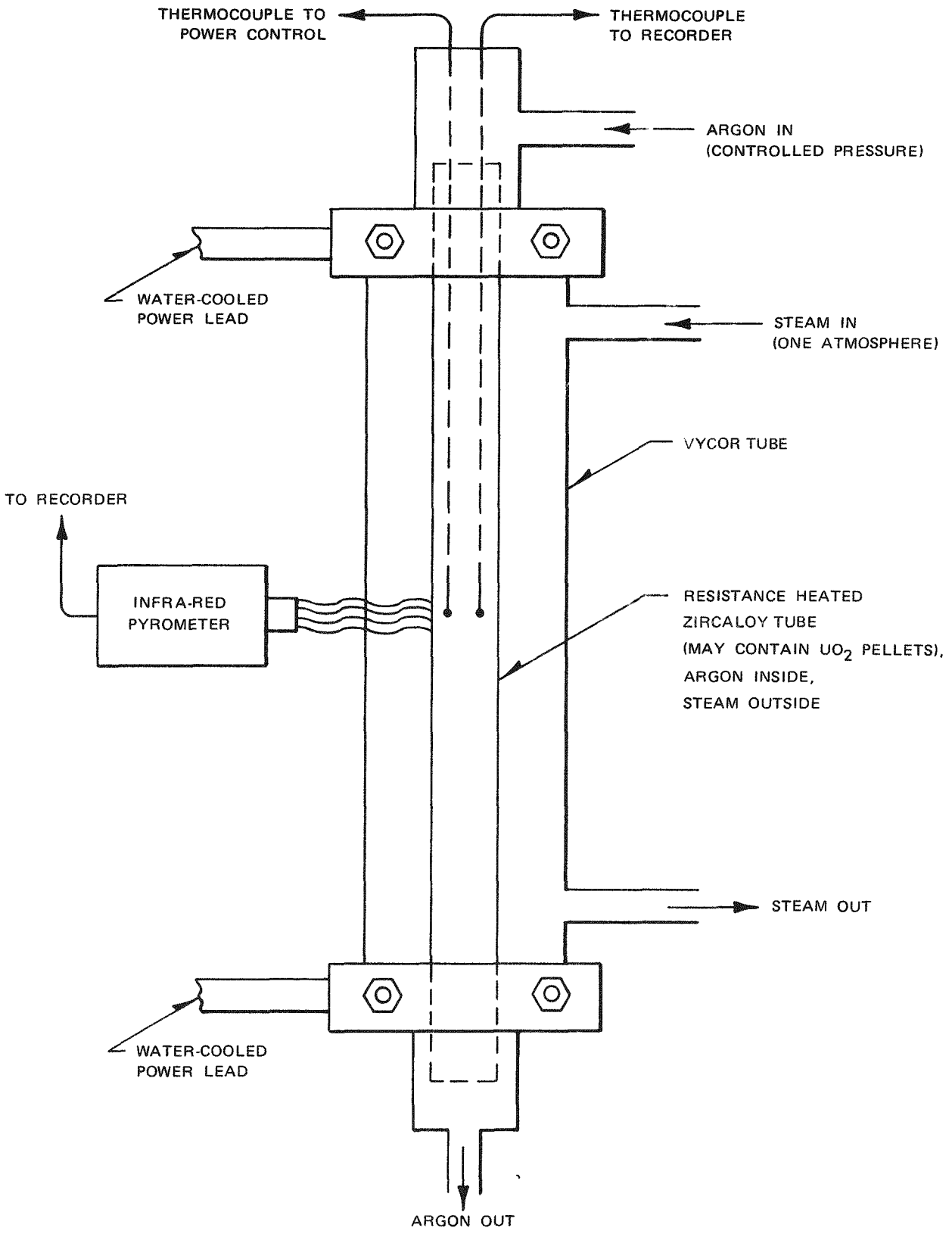

Figure 6.2-1. LOCA Setup Schematic

6.3 Task 3.0 FUEL IRRADIATION TESTS

6.3.1 Subtask 3.1. Accelerated PCI Tests (Collapsed Cladding) (J. H. Davies, NTD)

6.3.1.1 Introduction

Major obstacles to the development of a useful in-reactor test of PCI remedies are the long lead times required to sensitize BWR fuel to potential PCI failure and the statistical spread in test results, especially at low exposures. The long lead times reflect the exposure dependence of the PCI phenomenon, which includes both chemical and mechanical components. The main chemical component is the generation of a sufficient inventory of embrittling fission products in the fuel, which is a function of burnup and is largely independent of fuel design. The mechanical components include several effects which combine to reduce the effective pellet-cladding gap, leading to strains imposed on the cladding by thermal expansion of the fuel pellets during ramping. For BWR fuel with free-standing cladding and generous as-fabricated gaps, hard pellet-cladding mechanical interaction depends on statistical effects related to pellet geometry, fabrication procedures, and power history, as well as exposure.

It was believed that a severe, accelerated test of PCI remedies, with reduced statistical spread in the data, might be developed by eliminating the exposure dependence of the mechanical component of PCI; for example, by using a non-free standing cladding design with tight, as-fabricated pellet-cladding gap. Here the effective gap is essentially zero from the start of the irradiation and power ramping imposes reproducible high stresses and strains on the cladding. Support for this approach was provided by the reported results[9] on CANDU test fuel, which employs a cladding design wherein the cladding is not free standing. Unmodified CANDU test rods failed at a a burnup of ~2.5 GWd/t following power ramps from ~10 to ~19 kW/ft. The mode of failure, brittle cladding cracks, was characteristically similar to PCI failure in BWR fuel.

If these results could be reproduced in the General Electric Test Reactor, the tests could be performed in an elapsed time of ~120 days. That is, an accelerated test for screening potential PCI remedies could be developed.

A test matrix was designed with the initial objective of demonstrating that reference fuel rods (unmodified Zircaloy-2 cladding and UO_2 fuel pellets) would fail reproducibly by PCI when ramped to high powers at modest burnups and secondly to test potential remedy designs under the same conditions. The test matrix included several types of barriers and coatings as well as fuel chemistry modifications. This report describes the experience with reference rods and with Cu-barrier and Zr-liner rods, two PCI remedy designs, which successfully survived the test.

6.3.1.2 Experimental

Design. As described elsewhere, (Subsection 6.3.2) fuel rod testing in GETR is performed in individual test capsules simulating BWR conditions.

A cladding wall thickness of 16.5 mils was selected for these collapsed cladding (CC) tests after fuel modeling studies indicated that the power to reach mechanical failure criteria was relatively insensitive to cladding thickness in this range. The thin-wall Zircaloy-2 cladding was fabricated from tubing with an initial wall thickness of 28 mils by machining the outer surface with a specially designed tool, leaving the unsupported plenum region at full wall thickness. The fuel was loaded with a nominal diametral gap of 2.5 mils.

Each CC rod assembly consisted of two individual segments or fuel rods as shown in Figure 6.3-1. The enriched fuel column in each rod was 12 inches long with a natural UO_2 pellet and a flux depressor pellet (hafnia-10% yttria) at each end. Analyses indicated that with this design each fuel rod could be power ramped above the projected failure threshold independently of the other, following an incubation period where both rods accumulated roughly equivalent exposures. This is achieved by taking advantage of the shape of the axial flux profile as a function of control rod bank during a GETR power run. By adjusting the axial position of the irradiation capsule and selecting the time when the ramp test is performed, the power peak can be on one rod or the other with little or no power change (ΔP) applied to the second rod, depending on the maximum peak power achieved. Typical power profiles during the incubation and ramping phases of the test are shown in Figure 6.3-2. A burnup profile is shown in Figure 6.3-3. The incentive to irradiate two fuel rods per capsule was to fully utilize the limited number of available GETR pool positions and to save time and expense.

The CC Test Matrix is shown in Table 6.3-1 and additional design details are summarized in Table 6.3-2.

Table 6.3-1
COLLAPSED CLADDING TEST MATRIX

Rod Identification	Test Variable[a]
CC-2A,B	Reference
CC-4A,B	Reference
CC-6A,B	Reference
CC-8A,B	Reference
CC-37A,B	Reference (28 mil wall)
CC-38A,B	Reference (28 mil wall)
CC-14A,B	0 2 mil Cu-Barrier (electroplated)
CC-43A,B	0 4 mil Cu-Barrier (electroplated, shot-peened)
CC-44A,B	0 4 mil Cu-Barrier (electroplated, shot-peened)
CC-53A,B	0 2 mil Cu-Barrier (electroless)
CC-54A,B	0 4 mil Cu-Barrier (electroless)
CC-60,A,B	0 2 mil Cu-Barrier (electroless on autoclaved oxide surface)
CC-61A,B	0 4 mil Cu-Barrier (electroless on autoclaved oxide surface)
CC-22A,B	3 mil Zr-Liner (crystal bar)
CC-55A,B	3 mil Zr-Liner (low oxygen sponge)
CC-56A,B	3 mil Zr-Liner (low oxygen sponge)

[a] Cladding wall thickness 16 5 mils except where noted

Table 6.3-2
COLLAPSED CLADDING ROD DESIGN DETAILS

Cladding	
Heat Treatment	980°F/2-1/4 hours
Surface Treatment	Autoclaved (Reference, Cu on oxide) Chemically polished ("pickled") (Cu-Barrier, Zr Liner)
Dimensions	
I d	0 437 inch[a]
Wall Thickness	0 0165 inch[b]
Fuel Pellets	
Enrichment	4 6% U-235
Density	96% T D
Geometry	Dished one end
Dimensions	
Length	0 75 inch
Diameter	0 4345 inch[a]
Fuel Rod	
See sketch (Figure 7 3-1)	
No of enriched pellets	16
Fuel-cladding diametral gap	0 0025 inch
Fill gas	95 Ar/5 He at 1 atmosphere
Plenum getter	2 grams Hipalloy®

[a] Four fuel rods (low oxygen sponge Zr-Liner) were fabricated from tubing with an i d of 0 425 inch Fuel pellet diameter was tailored to maintain a nominal as-fabricated gap of 2 5 mils (CC-55A B and CC-56A,B)

[b] Four reference rods (CC-37A,B and CC-38A B) were fabricated from standard tubing, 28-mil wall without reducing the wall thickness

The reference rods in two capsules (CC-37 and -38) did not have the standard reduced wall thickness, but the fuel pellets were loaded with the tight gap. These reference rods were added to the test matrix to explore wall thickness as a variable.

The Cu-barrier cladding reflects the evolution of the process for plating copper onto the inner surface of a Zircaloy tube. As noted in Table 6.3-1, some tubes are electroplated and some are plated by an electroless process. Some of the former were shot-peened after plating in an attempt to mechanically cover possible plating defects. Some of the electroless copper barriers are plated onto a pre-autoclaved oxide surface, which is a design aimed at inhibiting in-service diffusion bonding of the copper layer to the cladding. None of the Cu-barrier designs tested here were metallurgically bonded in fabrication.

The zirconium liner tubing was fabricated by coextrusion. The thickness of the Zr-liner was about 3 mils and it was metallurgically bonded to the Zircaloy-2 in the course of the coextrusion process. The purity of the zirconium liner is a test parameter; the test matrix includes two types of tubing, employing crystal bar and low-oxygen sponge zirconium liners, respectively.

Irradiation. Testing was performed in the General Electric Test Reactor. The GETR facilities and irradiation hardware are described elsewhere (Subsection 6.3.2).

Prior to ramp testing a given rod, it is irradiated at 10.0 kW/ft, peak, to accumulate burnup. During this "incubation" period, the power is adjusted once per day to maintain the required tolerance. In general, approximately 15 GETR power cycles, each lasting 2 or 3 weeks, are required to reach the desired rod average burnup of ~4000 MWd/t. When a rod is first inserted in the GETR for incubation, the power is raised to 10 kW/ft, peak, in 2 kW/ft peak power steps with 15-minute hold times between steps. In subsequent power runs, the rod is positioned to receive the desired neutron flux, and brought to power with the reactor. Once the reactor has reached full power (50 MW), the test rod power is adjusted to the specified limits by a radial adjustment to the Radially Adjustable Facility Tube (RAFT) position. In case of a reactor scram, the capsule is left in position and brought back to power with the reactor.

The requirements for the flux peak location during incubation and later testing necessitate special procedures for the capsule positioning in the facility tube. For the incubation period (10.0 kW/ft, peak) the capsules are positioned to approximately center the two fuel rods about the time-averaged flux peak. The axial position of the capsule relative to the reactor core in the incubating mode is shown in Figure 6.3-4a.

Once the fuel rods have reached the target burnup (~4000 MWd/t), the capsule is transferred to one of two special pool positions which elevate the capsule an additional 5.1 inches without moving the capsule clamp. This positioning, along with a limitation on the GETR control rod bank "window" (21.0 to 21.9 inches) for performing the test (Mode A), allows the lower segment (Rod A) to be ramp tested to the desired power while minimizing the ΔP on the upper segment (Rod B). The capsule positioning is shown in Figure 6.3-4b. A typical power profile is plotted in Figure 6.3-2. Failure of the bottom rod during "Mode A" ramp testing necessitates removal of the capsule from the reactor during the following refueling outage, i.e., before the top rod has been tested. If it is still desired to ramp test the top rod, it must be re-encapsulated and ramped during a subsequent cycle. However, if the bottom rod survives the test, the top rod is ramped simply by lowering the capsule in the facility tube (Figure 6.3-4c) and waiting for a high rod bank (30.0 inches or greater preferred) near the end of a cycle before commencing the ramp (Test Mode B). Single (re-encapsulated) rods are ramped according to Test Mode C (Figure 6.3-4d). The GETR flux profile as a function of rod bank position is shown in Figure 6.3-5.

The basic ramp test sequence is illustrated in Figure 6.3-6. Early ramp tests were programmed to approach peak power in 2 kW/ft steps with 15-minute holds between each step. This hold time was based on the time for the Rod Power Monitoring System (RPMS) to reach equilibrium following the step. The hold times were extended to 1 hour when it became evident that the Failure Detection System (FDS) was taking several minutes to reach the pre-set failure level and some rods underwent an additional ramp step after having failed. The longer hold times also recognize the time dependence parameter $(1 - e^{-\lambda t})$ in the Canadian failure correlation reported in the literature.[10] Using the reported value of 2.3 hours^{-1} for the time constant, λ, the failure probability after 1 hour at a particular peak power is 0.9 times that at infinity, whereas after 15 minutes it is only 0.44 times that at infinity.

Although the FDS can take several minutes to reach the pre-set activity level at which the capsules are taken off test, a more precise failure time can usually be estimated by back extrapolation of the FDS recorder chart output. Following a failure, the capsules are taken off test as quickly as possible. That is, the RAFT's are moved rapidly to the full-out position.

The severe power exercise shown in Figure 6.3-6, following the long hold at the peak test power is intended to ventilate any tight PCI cracks that may have formed, but which have not released enough radioactivity to trigger the FDS. In practice, no failures have occurred at this stage of the test.

Post-Irradiation Examination. After an appropriate cooling period, the capsules are shipped to the hot cells for examination and disposal. A capsule water analysis is made in every case to verify the reported conditions of the rods.

Following decapsulation the fuel rods are gamma scanned before disassembly. The gamma scan provides a record of the burnup profile along a rod and can be used to determine relative burnups at selected nodes. A detailed visual examination follows and the axial and circumferential locations of cladding defects are recorded. Photographs are taken. Rod length measurements are taken and the rods are profiled, if not too badly damaged. Helical profilometry traces and linear traces at 0 and 90 degrees azimuthal rod orientations are taken. Unfailed rods, and some with small defects, are subjected to a pulsed eddy current (PEC) examination to search for undetected defects and incipient cracks. All rods are neutron radiographed. In addition to indicating the condition of the fuel, the neutron radiographs provide confirmation of the condition of the rods, i.e., the plenum getters are invariably hydrided in failed rods and without detectable hydrogen in sound rods.

Selected rods are examined destructively, including a fission gas analysis on sound rods.

6.3.1.3 Results

Ramp Tests. Ramp test results to date are summarized in Table 6.3-3. Seven out of seven reference rods failed this severe test and six of the seven rods failed in a narrow peak power range around 18.5 kW/ft. The peak powers achieved at the high burnup ends of the non-ramped segments help define the failure threshold.

Seven out of seven copper barrier rods and two out of two zirconium liner rods survived the test. The range of maximum peak powers achieved by the surviving rods, 20.2 to 24.2 kW/ft, reflects updated neutron detector calibration factors applied retroactively to the RPMS powers.

The irradiation status of fuel rods still on test is shown in Table 6.3-4.

Nondestructive Post-Irradiation Examination. Nondestructive post-irradiation examination (PIE) has been completed on all the tested rods except CC-6B (none is planned), -38A and B, and -43A and B, and -54A.

Visible defects were observed in each of the three failed reference rods (CC-2B, -4A, and -6A) ramped early in the program. The defects in CC-8A and -37A were not discernible with the standard 4X optical fixture. Some of the defects observed are shown in Figures 6.3-7 and 6.3-8. These "X" mark failures indicate a degree of ductility in the final cladding penetration and have been reported by others as superficial evidence of PCI cracks. Although PCI failures are predominantly non-ductile stress corrosion cracks,[11] the final part of the penetration may fracture by ductile shearing as the stress levels on the last filaments of material exceed the criterion for plastic instability. The absence of "X" marks on CC-8A and -37A is believed to be a consequence of the longer hold times between ramp steps, which favors the stress corrosion crack propagation mechanism.

Through-wall cladding defects, not discernible visually, as well as defects on the inner surface were recorded on PEC traces. These data plus a light and dark print of the neutron radiograph and other PIE information were combined with the helical trace of the rod profile, providing a pictorial summary of the nondestructive PIE results. Pre-irradiation profilometry has also been transcribed onto these charts as a guide to estimating cladding strain. Selected examples of these data summaries are shown in Figures 6.3-9 through 6.3-16. Ridging at pellet interfaces is the most striking feature and in the case of CC-14 this "bambooing" was visible with the naked eye. The high diametral strains (~2%) in the unfailed copper barrier and zirconium liner rods testify to the severity of the test and to the effectiveness of these remedies. The strain rate at ridge locations during ramping is estimated to be $\sim 2.5 \times 10^{-3}$ min^{-1} based on a ramp rate of 2 kW/ft/min.

Table 6.3-3
COLLAPSED CLADDING RAMP TEST RESULTS

Rod No.	Description[a]	Average Burnup (MWd/t)	Maximum Peak Power (kW/ft)	Rod Condition
CC-2A[b]	Reference	4300	15.0[c]	Sound[d]
CC-2B[b]	↓	4500	18.1	Failed
CC-4A[b]		3400	18.4	Failed
CC-4B[b]		3400	14.6[c]	Sound
CC-6A[b]		4800	22.1	Failed
CC-6B		4000	18.8	Failed[e]
CC-8A		5400	18.0	Failed
CC-8B		4800	11.5[c]	Sound
CC-37A	Reference,	5600	19.5	Failed
CC-37B	(28 mil wall)	4700	11.6[c]	Sound
CC-38A	↓	5100	19.7	Failed
CC-38B		4400	13.0[c]	Sound
CC-14A[b]	Cu-Barrier	4500	24.2	Sound
CC-14B[b]	↓	4400	21.2	Sound
CC-43A		4400	21.6	Sound[f]
CC-43B		4000	21.2	Sound[f]
CC-44A		4800	22.0	Sound
CC-44B		4100	21.5	Sound
CC-54A		4400	20.2	Sound
CC-54B		3900	13.8[c]	Sound
CC-22A	Zr-Liner	4800	22.6	Sound
CC-22B	Zr-Liner	4300	22.1	Sound

[a] See text and Table 6.3-1 for details
[b] Fifteen minute hold times between ramp steps (see Figure 6.3-6)
[c] Achieved at high burnup end of rod during ramp test of mating rod. Not intentionally ramped (see Figure 6.3-2)
[d] Incipient PCI cracks located by destructive examination
[e] CC-6B re-encapsulated and ramp tested as a single rod following failure of CC-6A
[f] CC-43 returned to incubation at 10 kW/ft following successful ramp test of A and B rods

Table 6.3-4
STATUS OF COLLAPSED CLADDING RODS ON TEST

Rod No.	Description[a]	Current Average Burnup (MWd/t) A	B	Target Burnup (MWd/t)
CC-43A,B[b]	Cu-Barrier	9975	8675	10000
CC-53A,B	Cu-Barrier	4250	3750	4000
CC-54A,B[c]	Cu-Barrier	4475	3900	4000
CC-55A,B	Zr-Liner	850	625	4000
CC-56A,B	Zr-Liner	2050	1750	4000
CC-60A,B	Cu-Barrier	2500	2100	4000
CC-61A,B	Cu-Barrier	1950	1650	4000

[a] See text and Table 6.3-1 for details.
[b] Ramp tested previously at —4000 MWd/t. See Table 6.3-3.
[c] CC-54A survived ramp (see Table 6.3-3); CC-54B to be ramped following capsule axial adjustment.

Other notable features of the data are multiple cracking in the failed reference rods and the correspondence of defects to ridge locations or pellet interfaces. Also note on the neutron radiographs the hydriding (darkening) of the plenum getters in failed rods; the getters in the sound rods are quite clean. There have been no exceptions to this observation, so the neutron radiographs provide good confirmation of the condition of the rod.

Destructive PIE — Reference Rods. Destructive PIE work, mostly metallography, has been performed on the following rods: CC-2A, -2B, -4A, -8A, -14A, -14B, -22A, -22B, -37A, -44A, and -44B. Results on the latter three have not yet been reported. There was substantial secondary hydriding at the cladding inner surface of the failed reference rods (Figure 6.3-17). Standard BWR fuel cladding is much more resistant to post-failure hydriding damage and the rapid hydriding here is believed to be a consequence of the tight fuel-cladding gap. It is also important to remember that the rods are not completely off-test when the RAFT is in the full-out position, e.g., CC-4A was at 1.2 — 1.8 kW/ft for 314 hours following failure. However, characteristic PCI cracks were located and examined in both failed and unfailed rods. A branching crack extending partially through the wall of CC-8A is shown in detail in Figure 6.3-18 and small incipient cracks are shown in Figure 6.3-19. Crack opening, as in Figure 6.3-18, is a consequence of residual cladding ductility at the crack tip.

Rod CC-2A was not intentionally ramp tested, but experienced a peak power of 15 kW/ft at the high burnup end (see Table 6.3-3 and Figure 6.3-2). The rod did not fail; but four incipient PCI cracks were located at two pellet interfaces which had experienced a power increase. Three of these are illustrated in cross section in Figure 6.3-20. Subsequently, the fracture surfaces of these cracks were examined by scanning electron microscopy (SEM). The transgranular cleavage and fluting features, characteristic of PCI, were noted.

Copper Barrier. A total of ten metallographic sections from CC-14A and -14B have been examined plus a clam shell examination of each rod. Here the cladding of a 5-inch section is slit longitudinally on each side, then opened carefully to allow examination of the cladding inner surface with minimum disturbance of the fuel. Color photographs were taken to document the appearance of the copper barrier, which was bright and copper-colored, except for surface markings imaging fuel cracks and pellet interfaces. Barrier coverage appeared uniform and adherence good with no evidence at up to 10X magnification of barrier defects. There were traces of copper on the fuel surface, however.

The metallographic sections were all taken at cladding ridges (see e.g., Figure 6.3-12) or PEC signal locations. Each transverse specimen was examined at five planes separated by 0.020 — 0.025 inch with the middle plane coinciding with the feature of interest (ridge or PEC signal). No incipient PCI cracks were found, corroborating ramp test evidence (Table 6.3-3) of the effectiveness of the copper barrier design as a PCI remedy.

Generally, the copper barrier was a continuous, fairly uniform layer in all ten sections examined. Filar eyepiece measurements showed an average copper thickness of 0.21 mil with maximum and minimum values of 0.24 mil and 0.17 mil, respectively. There were isolated observations of barrier delamination (Figure 6.3-21), barrier flaws (Figure 6.3-22) and fuel-copper interaction. There were two distinct forms of fuel-copper interaction. In one (Figure 6.3-23) the fuel was mechanically bonded to the copper layer, which was apparently soft enough to flow into surface roughnesses in the fuel. Occasionally some copper had been pulled away from the barrier by contracting fuel. In other areas, fuel had apparently displaced copper in the barrier (Figure 6.3-24); where this fuel penetrated the barrier to contact the cladding, a fairly thick patch of ZrO_2 had formed (Figure 6.3-24b). This interpretation was supported by detailed SEM and microprobe examination of each of these areas. The ZrO_2 patches can be identified on both the backscattered electron image and the x-ray map. These examinations also showed evidence of a cesium-rich second phase in the bonded fuel and some association of iodine with the copper barrier. A line scan across the Zr-Cu interface showed no evidence of interdiffusion within the spatial resolution of the instrument (~1 μm).

Evidence of fuel center melting was observed in both CC-14A and -14B.

Zirconium Liner. Five metallographic sections from CC-22A and three from CC-22B have been examined. Each transverse section was examined at five planes separated by ~0.020 inch.

Generally, the inner surface was continuous and uniform in all sections examined. There was no evidence of delamination, or separation, of the Zr-liner from the Zircaloy tube. Although PEC traces did not record any significant defect signals, some small cladding flaws were noted during the examination. Some of the flaws were deeper than reported in the original fabrication documentation; the deepest (Figure 6.3-25) extended about 1 mil into the 3-mil-thick liner. These flaws had the appearance of gouges or scratches, perhaps inflicted in the soft crystal bar liner material during fuel loading. Other flaws were small, tight defects (Figure 6.3-26). The depth (~0.5 mil) and distribution of these flaws did not appear to be a function of nodal burnup, peak power, or cladding strain, arguing against incipient PCI cracks. In fact, similar flaws were observed in the pre-irradiation characterization of this tubing. Whatever their origin, the flaws showed no tendency for propagating through the zirconium liner material during the power ramp.

Diamond pyramid hardness (DPH) measurements were made on one section from each rod plus an archive cladding section. A remotely operated Tukon hardness tester was employed with a 50-gm load. All specimens had been polished through 0.5μ diamond prior to measurement. The results indicated that the pure Zr-liner had not hardened during irradiation, while the Zircaloy-2 had hardened by 30 to 40%. Additional measurements will be made to verify this observation.

6.3.1.4 Discussion

Seven out of seven reference rods failed this test and six of the seven failed in a narrow peak power range around 18.5 kW/ft. Thus the first objective of the test series – to demonstrate reproducible PCI failure of reference rods – has been met, and test conditions were established for screening potential PCI remedies. Two of the seven failed reference rods had 28-mil-wall cladding; the others had 16.5 mil wall, confirming prior GE experience[11] that susceptibility to PCI is not a sensitive function of wall thickness.

Seven out of seven Cu-barrier rods and two out of two Zr-liner rods survived this severe test. These results, which are consistent with ex-reactor test results,[5] indicate that both of these PCI remedy designs have a substantial performance advantage over standard designs employing unmodified Zircaloy cladding. This experience is supported by early ramp test results (Subsection 6.3.2) on segments incubated in power reactors. As shown in Table 6.3-4, additional tests on both concepts are in place in GETR.

6.3.2 Subtask 3.2. Segmented Rod Irradiation Tests (J. H. Davies, NTD)

6.3.2.1 Introduction

To study the effects of design variables on PCI susceptibility and to develop fuel that is immune to PCI, it is necessary to design and fabricate fuel rods, irradiate them to an appreciable exposure at a relatively low power, and then to power ramp test them.

The vehicle selected for the incubation phase of the experiment (i.e., irradiation to high burnups at moderate powers) was the Segmented Test Rod (STR) assembly. Here many of the full-length rods in a standard BWR fuel bundle are replaced by segmented rods (4 segments per rod). An 8x8 STR is represented in Figure 6.3-27; sketches of a typical segment and a segmented rod assembly are shown in Figures 6.3-28 and 6.3-29, respectively. Hafnium metal sleeves in the segment plenums correct power peaking effects in adjacent full-length rods and hafnia-yttria pellets are included to correct fuel column end effects. The most important feature of the segmented rod design is that the segments are demountable, and replacing segments during site refueling outages is a straightforward procedure. Selected segments can be retrieved at incremental burnups and returned to Vallecitos Nuclear Center for hot cell characterization and ramp testing in GETR.

Three STR assemblies were inserted in different power reactors in 1974. They are designated SRP-1, SRP-2, and SRP-3; they are incubating in Quad Cities-1, Monticello, and Millstone-1, respectively. Because of the experimental nature of the fuel designs, the bundles are located near the edge of the reactor cores to assure that lower peak LHGR's (linear heat generation rate) and higher MCPR's (minimum critical power ratio) will be maintained than are seen or are applied as operating limits in the core center. This licensing restriction is fully compatible with experimental objectives. A summary description of the three STR's is provided in Table 6.3-5. Detailed physics and licensing assessments are performed to support bundle reconstitutions when segments are retrieved for testing and replaced with fresh fuel segments. These reconstitutions are listed in Table 6.3-6, which also shows the projected outage schedule. Table 6.3-7 summarizes bundle burnup data.

Table 6.3-5
SEGMENTED ROD PROGRAM

Reactor	Bundle Design	Insertion Date	Number of Segments
Quad Cities-1 (SRP-1)	7x7 R	July 1974	92
Monticello (SRP-2)	8x8	May 1974	136
Millstone-1 (SRP-3)	8x8	November 1974	136

Table 6.3-6
BUNDLE RECONSTITUTIONS

STR Bundle	Bundle Reconstitution Number	Date
SRP-1	R_1[a]	February 1976
	R_2	April 1977
	R_3	Fall 1978
SRP-2	R_1	September 1975
	R_2	October 1977
	R_3	Fall 1978
SRP-3	R_1	October 1975
	R_2	October 1976
	R_3	Spring 1978
	R_4	Spring 1979

[a] R_1 indicates first reconstitution, R_2 indicates second reconstitution, etc.

Table 6.3-7
SRP STATUS, 4th QUARTER 1977

STR Bundle	Segment Tier	Average Exposure (MWd/t)	Highest SRP Segment Average Exposure (MWd/t)
SRP-1	Top	6021	7554
	Mid Top	9059	11336
	Mid Bottom	8946	12108
	Bottom	8117	11149
	Bundle Average	8036	
SRP-2	Top	7988	10325
	Mid Top	11329	15267
	Mid Bottom	12452	16716
	Bottom	11373	14553
	Bundle Average	10786	
SRP-3	Top	7550	9459
	Mid Top	10203	14263
	Mid Bottom	11379	15747
	Bottom	10869	13560
	Bundle Average	10000	

The key numbers in Table 6.3-7 are the lead segment exposures in the various tiers of the three bundles. The lead segments in the two 8x8 bundles are averaging about 5 GWd/t per year and in the 7x7 bundle (SRP-1) about 4 GWd/t per year. The top tier segments in each case are accumulating burnup at a reduced rate.

The information in Tables 6.3-6 and 6.3-7 can be used to estimate the exposures of replacement segments inserted in the bundles during outages. It can also be used to project segment exposures to some future outage. Detailed physics calculations performed during the current period indicated that the nuclear lifetimes of the bundles can be extended through 1983 without major bundle rejuvenation (i.e., without replacing full-length peripheral fuel rods). A surveillance program was outlined to address thermal-mechanical and material concerns about extending bundle lifetimes.

6.3.2.2 Design Variables

The main objective of this program is to determine the ramp test performance of reference fuel and of Zr-Liner and Cu-Barrier fuel. During the course of the program the material specifications of these cladding designs have changed and, for the copper barrier, new fabrication processes have been developed. Segments incorporating these design changes and process improvements have been introduced into the bundles as the new cladding became available. In this section the development of the designs is briefly traced and the number of segments of each and their status is indicated.

6.3.2.3 Copper Barriers

The reference thickness of the copper barrier was chosen to be 0.4 mil based on the range of fission fragments in copper (0.4 mil exceeds the maximum range of fission fragments in copper). However, good results have been obtained with 0.2-mil-thick barriers in ex-reactor tests and collapsed cladding tests, and both thicknesses are under test in the Segmented Rod Irradiation Tests. There is a small neutron economy incentive to reduce barrier thickness. Also for

neutron economy reasons (applying mainly to other barrier concepts) the segments in the original SRP-3 bundle were fabricated with 28-mil-wall tubing instead of the standard 34-mil-wall thickness. These segments were also pre-pressurized to 17 atmospheres with helium. Replacement segments employ standard cladding (34 mils) and are pre-pressurized with 3 atmospheres of helium. Early in the program the Cu-barrier cladding was made in the laboratory by electroplating copper onto the Zircaloy tube inner surface using a central anode. This process was superseded by an electroless plating process, which was more amenable to scale up. The latter process is also applicable to plating onto a non-conducting surface, e.g., autoclaved tubing. Yet another variable in the Cu-barrier matrix is diffusion bonding of the copper to the Zircaloy. It was felt in the beginning that this would be required to ensure good adherence. Subsequently it has been shown that bonding is not a prerequisite to good adherence, and test results indicate good performance of the non-bonded material. All these variables are represented in the segmented rod test matrix. The number of segments of each design and their irradiation status is summarized in Table 6.3-8.

6.3.2.4 Zirconium Liners

This tubing is fabricated by coextrusion and coreduction. The pure Zr-liner on the cladding inner surface is about 3 mils thick; the balance of the cladding wall thickness is Zircaloy-2. The liners are bonded to the cladding during fabrication.

This tubing has been fabricated to dimensions which are consistent with 8x8 bundle design. The first lot of material employed crystal bar zirconium and was reduced to a total wall thickness of 28 mils (i.e., 3 mils zirconium plus 25 mils Zircaloy-2). Segments fabricated from this tubing are pre-pressurized to 17 atmospheres with helium. Subsequent lots of tubing were fabricated with a 34-mil wall thickness; segments made from this material are pre-pressurized to 3 atmospheres with helium. Three different kinds of tubing were made to this dimension, employing crystal bar, low oxygen sponge, and reactor grade sponge zirconium liners. The number of segments of each design and their irradiation status are summarized in Table 6.3-9.

Table 6.3-8
STATUS OF COPPER BARRIER SEGMENTS

STR Bundle	SRP-3							SRP-2				SRP-1	
	Number Inserted				Number Removed			Number Inserted			Number Removed	Number Inserted	Number Removed
Bundle Reconstitution Number	R_0	R_1	R_2	R_3	R_1	R_2	R_3	R_0	R_1	R_2	R_2	R_1	
Electroplated													
0.2 mil bonded	8				2	2							
0.4 mil bonded	8					4	(4)	4			4		
0.2 mil non-bonded	8					4	(2)						
0.4 mil non-bonded									8		2		
Electroless													
0.4 mils			12				(2)					4	
0.2 mils			14				(2)					4	
Electroless on Autoclaved Tube													
0.2 mils				(12)									
0.4 mils										10			

Notes: 1. Electroplated SRP-3 — 28 mil wall cladding, 17 atm He
Electropolated SRP-2 — 34 mil wall cladding, 1 atm He
2. Electroless SRP-3, SRP-2 — 34 mil wall cladding, 3 atm He
3. Electroless SRP-1 — 37 mil wall, 0.489-in.-i.d., 3 atm He
4. Numbers in parentheses are planned changes
5. R_0 refers to original bundle; R_1 indicates first reconstitution, ...

Table 6.3-9
STATUS OF ZIRCONIUM LINER SEGMENTS

STR Bundle	SRP-3				SRP-2		
Bundle	Number Inserted				Number Removed		Number Inserted
Reconstitution	R_0	R_1	R_2	R_3	R_2	R_3	R_2
Crystal Bar							
28-mil wall	8				4	(2)	
		4					
			12			(4)	
34-mil wall				(7)			4
Sponge							
Low Oxygen				(13)			8
Reactor Grade							

Notes: 1. R_0 refers to original bundle, R_1 indicates first reconstitution, ...
2. Numbers in parentheses are planned changes
3. All sponge material in 34 mil wall thickness only

6.3.2.5 Reference Segments

The design and irradiation status of reference segments in the test matrix are summarized in Table 6.3-10. These segments are, for the most part, identical in design to the appropriate batch of Cu-barrier and Zr-liner segments, except for the PCI remedy feature.

Table 6.3-10
REFERENCE SEGMENTS – STATUS

STR Bundle	SRP-3							SRP-2					SRP-1				
Bundle	Inserted				Removed			Inserted			Removed		Inserted			Removed	
Reconsitution	R_0	R_1	R_2	R_3	R_1	R_2	R_3	R_0	R_1	R_2	R_1	R_2	R_0	R_1	R_2	R_1	R_2
28-mil wall																	
1 atm He								16				2					
17 atm He	8				2	2	(2)										
17 atm He		2															
22 atm He								8				2					
34-mil wall																	
1 atm He	6					2	(2)	24				10					
3 atm He			8														
3 atm He				(4)													
37-mil wall (7x7)																	
1 atm He													16			2	6
1 atm He														2			
3 atm He															4		

Notes: 1. R_0 refers to original bundle, R_1 indicates first reconstitution, ...
2. Numbers in parentheses are planned changes

6.3.2.6 Fabrication

The original bundles were fabricated in San Jose, in the Fuel Development Shop. All replacement segments have been fabricated by the Wilmington Manufacturing Department. During the current program, fabrication of SRP-2 replacement segments was completed and the bundle was reconstituted in October 1977 (R_2). Replacement segments for the Spring 1978 reconstitution (R_3) of the SRP-3 bundle were fabricated and shipped to the site. A description of these segments can be read from Tables 6.3-8 through 6.3-10. Pre-irradiation characterization of the segments included: barrier integrity, uniformity, and adherence; segment diametral profilometry; and precise segment length measurements.

6.3.2.7 Experiment

Pre-GETR Characterization. In the course of reconstituting the bundles, the bundles are sipped for soundness and/or individual rods are nondestructively tested, including a visual examination. Selected segments are shipped to Vallecitos for detailed characterization and ramp testing in GETR. A summary description of the segments shipped from SRP-3 is provided in Table 6.3-11. The first shipment of segments from Monticello (SRP-2) is scheduled shortly. This will include all of the R_2 segments identified in Table 6.3-8 and 6.3-10, i.e., 6 copper barrier segments and 14 reference segments.

Table 6.3-11
SRP-3 SEGMENTS SHIPPED TO GE-VALLECITOS NUCLEAR CENTER

Bundle Reconstitution	Vallecitos Segment Identification Number	Design Feature[a]	Estimated Burnup (MWd/t)[b]
R_1	SRP-3/1	0.2 mil Cu Barrier (bonded)	4200
	SRP-3/2	0.2 mil Cu Barrier (bonded)	4200
	SRP-3/7	Reference (28-mil wall, 17 atm)	3500
	SRP-3/8	Reference (28-mil wall, 17 atm)	3600
R_2	SRP-3/11	Reference (28-mil wall, 17 atm)	8900
	SRP-3/12	Reference (28-mil wall, 17 atm)	8100
	SRP-3/13	0.2 mil Cu-Barrier (non-bonded)	7400
	SRP-3/14	0.2 mil Cu-Barrier (non-bonded)	9100
	SRP-3/15	0.2 mil Cu-Barrier (non-bonded)	8300
	SRP-3/16	0.2 mil Cu-Barrier (non-bonded)	5200
	SRP-3/17	Zr-Liner (crystal bar)	7200
	SRP-3/18	Zr-Liner (crystal bar)	9200
	SRP-3/19	Zr-Liner (crystal bar)	8000
	SRP-3/20	Zr-Liner (crystal bar)	5200
	SRP-3/23	0.4 mil Cu-Barrier (bonded)	7100
	SRP-3/24	0.4 mil Cu-Barrier (bonded)	9100
	SRP-3/25	0.4 mil Cu-Barrier (bonded)	8900
	SRP-3/26	0.4 mil Cu-Barrier (bonded)	5700
	SRP-3/27	Reference (34-mil wall, 1 atm)	7900
	SRP-3/28	Reference (34-mil wall, 1 atm)	7300
	SRP-3/31	0.2 mil Cu-Barrier (bonded)	11000
	SRP-3/32	0.2 mil Cu-Barrier (bonded)	10000

[a] Nominal fuel-cladding gap 9 mils (diametral)
[b] Segment burnups estimated from Cs-137 gamma scans by comparison to calibrated standard. Calculated peak power does not exceed 7 kW/ft on any segment.

The pre-ramp characterization comprises ten measurements or observations:

1. Hot Water Leak Check
   May be waived if other failure indicators are negative

2. Gross Gamma Scan

3. Cs-137 Gamma Scan
   Used to estimate segment burnups by comparison to calibrated standard

4. Exact Length

5. Crud Characteristics

6. Visual Examination
   Visible defects, corrosion, spacer markings

7. Profilometry
   Ridging, creepdown, ovality

8. Neutron Radiography

9. Pulsed Eddy Current

10. Rod Bow
    This measurement was added after a rod bow problem was encountered in preliminary ramp tests

Based on these tests and observations, a judgment is made as to whether the segment is suitable for ramp testing. All of the segments examined so far (Table 6.3-11) have been in excellent condition and suitable for testing.

Ramp Testing. Ramp testing to date has been performed in the General Electric Test Reactor (GETR). The test method has been described in the literature by Lyons.[12] Briefly, to provide an environment similar to that experienced in actual BWR service, especially regarding cladding temperatures, the fuel rods are irradiated in individual capsules in the GETR pool. The capsule (Figure 6.3-30) incorporates features which facilitate the natural circulation of the internal pressurized capsule water, thus providing for cooling of the fuel rod. The capsules are housed in Radially Adjustable Facility Tubes (RAFT's) which are located around the reactor core. A RAFT is depicted schematically in Figure 6.3-31, and an overall picture of the GETR ramp test facility is presented in Figure 6.3-32. Controls on the reactor floor allow movement of the RAFT toward or away from the reactor core, thus permitting the required variation in fuel rod peak power levels. Typically, power can be varied continuously from about 1 kW/ft to about 22 kW/ft, depending on the residual reactivity of the fuel rod and the circumferential location of the particular RAFT. Maximum unperturbed thermal flux is $\sim 2 \times 10^{14}$ nv. Continuous on-line test fuel rod peak power measurement is provided by a Rod Power Monitoring System (RPMS), which incorporates neutron detectors for flux measurement, associated hardware, and a minicomputer for flux-to-power conversion calculations. In addition, each capsule is equipped with a Failure Detection System (FDS). A small amount of capsule water is continuously pumped through bypass leads past a radiation detector. In case of rod failure, the increased water activity triggers an alarm as an indication to wind the RAFT to its full-out position. Back-extrapolation of recorder chart output from the FDS provides a fairly precise indication of the actual failure time.

The ramp test sequence depicted in Figure 6.3-33 was selected to subject the test segment to a severe PCI condition, since the principal objective of the test is to demonstrate the PCI immunity of the new designs under conditions where the reference designs are severely at risk. The advantage of the "staircase" ramp is that it provides a measure of the margin of improvement in PCI resistance with a limited number of tests.

Post-Irradiation Examination (following ramp test). The nondestructive phase of the Post-Irradiation Examination (PIE) includes the following:

1. Capsule Water Analysis
   Failure confirmation
2. Gross Gamma Scan
3. Exact Length Measurement
4. Visual Examination
   Visible defects, etc.
5. Profilometry
6. Neutron Radiography
7. Pulsed Eddy Current
8. Rod Bow Measurement

A decision on whether to proceed with a destructive examination of a particular segment depends to some extent on the results of the above. Destructive examination includes gas analysis (on a sound rod), burnup, metallography, cladding inside surface examination (clam shell exam), possibly scanning electron microscopy, and microhardness measurements (Zr-liner). Plenum sections of sound segments are taken for possible expanding mandrel tests.

6.3.2.8 Results

Ramp Testing. The first STR segments to be ramp tested were three which were removed from SRP-3 during the first bundle reconstitution (R_1). They included one reference and two Cu-barrier segments (see Table 6.3-11). Although the burnups were modest, it was felt that the experience would be valuable prior to ramping higher-burnup segments which were following. The apparent ramp test results from these prototype tests are shown in Table 6.3-12. During post-irradiation examination it became clear that there had been something wrong with the test. The failure mechanism of SRP-3/8 was not PCI, but massive localized corrosion from the outside. Both Cu-barrier segments (one failed, one sound) exhibited substantial fuel center melting at nominal peak powers well below that required to cause melting. A testing moratorium was instituted while the cause of these problems was investigated, but not before an additional segment, SRP-3/11, had been ramped.

Table 6.3-12
INITIAL RAMP TEST SERIES RESULTS

Segment Identification Number[a]	Burnup (MWd/t)	Peak Power (kW/ft)	Remarks[b]
SRP-3/1	4300	18.8	Failed, fuel melting
SRP-3/2	4550	18.9	Sound, fuel melting
SRP-3/8	3660	15.3	Failed, accelerated corrosion
SRP-3/11	9000	18.0	Sound, rod bow

[a] See Table 6.3-11 for design features
[b] Fuel melting and accelerated corrosion failure caused by rod bowing problem — see text.

It was quickly established that the external corrosion failure was caused by an inadequacy in the capsule design (see Figure 6.3-30). It was shown that due to tolerance stackups, insufficient allowance had been left to accommodate fuel rod thermal expansion on going to power. As a result of the axial constraint imposed, the fuel rod bowed and probably touched the capsule chimney. Under these conditions (local coolant flow starvation) local overheating of the cladding and accelerated corrosion ensued, leading to failure. The rod bow also had a significant effect on predicted peak powers. The RPMS power prediction assumes concentricity of the fuel rod in the capsule. It was shown that rod bow can produce significant errors in predicted rod power, because of the steep radial flux gradient in the GETR pool.

A rod bow measurement was added to both the pre-and post-ramp characterization requirements. It was shown immediately that SRP-3/11, which had been ramped in an original-design capsule, had a residual bow of 100 mils. A rod bow at power of 300 mils would put it into contact with the capsule chimney. Although SRP-3/11 did not fail, the result is discounted, along with the others in Table 6.3-12, because of the inherent uncertainties.

The capsule design was corrected and a calibration program was established for the RPMS flux detectors. Testing was resumed. Test results are presented in Table 6.3-13. A typical ramp history is shown in Figure 6.3-34 and a power profile (at peak power) is shown in Figure 6.3-35. The hold time at maximum power for rods which survived the ramping sequence was arbitrarily selected to be 24 hours. This was later reduced to 6 hours. In numerous similar ramp tests no fuel rod has failed later than 2 hours after the final ramping step. This is consistent with the rapid stress relaxation which occurs at constant power and with the Canadian Fuelogram correlation,[10] where a 2-to-3 hour hold is equivalent to an infinitely long hold time.

Table 6.3-13
SRP RAMP TESTS – RESULTS SUMMARY

Segment Identification Number	Design Feature	Burnup[a] (MWd/t)	Peak Power (kW/ft)	Results
SRP-3/27	Reference, 34-mil wall, 1 atm He	7900	18.2	Failed after ~1 hour
SRP-3/28	Reference, 34-mil wall, 17 atm He	7300	18.1	Failed after 25 minutes
SRP-3/12	Reference,[b] 28-mil wall, 1 atm He	8100	16.1	Failed after ~50 minutes
SRP-3/15	0.2 mil Cu-Barrier (non-bonded)	8300	18.2	Survived 24 hours
SRP-3/13	0.2 mil Cu-Barrier (non-bonded)	7400	18.0	Survived 24 hours
SRP-3/18	3 mil Zr-Liner	9200	18.0	Survived 24 hours
SRP-3/14	0.2 mil Cu-Barrier (non-bonded)	9100	18.0	Survived 6 hours[c]
SRP-3/17	3-mil Zr-Liner	7200	18.0	Survived 6 hours[c]
SRP-3/19	3-mil Zr-Liner	8000	18.1	Survived 6 hours[c]

[a] Burnups estimated from Cs-137 gamma scans prior to GETR testing
[b] Cladding wall thickness and He pressure in SRP-3/12 same as Cu-barrier and Zr-liner segments
[c] Hold time at maximum power truncated because of imminent GETR shutdown — see text

It is noteworthy that six out of six PCI remedy rods survived the severe ramp test, whereas three out of three reference segments failed.

Post-Irradiation Examination. Although the ramp test results shown in Table 6.3-12 have been discounted because of the rod bow problem, the PIE is of interest. In particular, examination of the state of the copper barrier in both the failed and the sound rods provided useful information.

The results of the nondestructive phase of the PIE of SRP-3/1, -3/2, and -3/8 are summarized in Figures 6.3-36, 6.3-37, and 6.3-38, respectively. These figures also show the locations of samples taken for metallography, burnup, etc. Where profilometry traces have been taken, the pre-ramp (helical) profile envelope has been transcribed onto the chart to show up diameter changes. Both a light and a dark print of the neutron radiographs are also attached, although reproduction quality is poor. Note the darkened getters in the plenum of the failed rods, indicating post-failure hydrogen pickup. Other features of the neutron radiographs that are not easily discerned in the figures are listed below.

SRP-3/1

- Extensive UO_2 central voiding at 15.5 – 23.5 inches, with maximum width (~0.2 inch) at cladding split location
- End plugs hydrided (or trapped H_2O)
- Getter hydrided

SRP-3/2

- Possible light UO_2 central voiding at 11.5 – 20.0 inches
- Moderate UO_2 central voiding at 20.0 – 23.5 inches, with maximum width (~0.1 inch) at 22.5 inches
- No hydriding of cladding, end plugs, or getter

SRP-3/8

- No obvious central voiding
- Localized cladding hydriding at 7.3 – 8.0 inches, 20.3 – 21.0 inches and 24.9 – 25.2 inches
- Possible hydriding of both end plugs
- Getter hydrided

Also shown in the PIE summary figures are comments on the visual examinations, noting important or unusual observations, and the locations and interpretations of PEC signals. The latter are somewhat subjective and of mixed value. Very large signals, which indicate through-wall PCI cracks, have usually been confirmed by metallography, but signals indicating inside cracks, especially small ones (signal index <20), reflect all types of inside flaws and sundry effects without individual signatures; these are rarely confirmed as indications of incipient PCI cracks.

Metallography. The locations of metallographic specimens are shown in Figures 6.3-36 through 6.3-38. In the case of transverse specimens the arrows indicate the plane examined, usually after removal of an additional 0.2-in. slice using a precision diamond wheel in the metallography cell. Longitudinal metallography samples are identified. The metallographic section numbers assigned to these samples, numbering from the bottom (left) of the rods to the top (right) are as follows:

SRP-3/1: C153, C154, C155, C156, C157, C158
SRP-3/2: C161, C162, C163
SRP-3/8: C166, C167, C169

SRP-3/1. The appearance of the cladding split is shown in Figure 6 3 39 Clearly this high-strain failure was not a PCI crack Figures 6 3 39b and 6 3 39c show evidence of substantial center melting which strained the cladding beyond its yield point The high strain, failed region is shown in detail in Figure 6 3 40 The shear type failure is accompanied by appreciable thinning of the cladding wall Note also the corrosion crater extending ~6 mils into the cladding wall Pre ramp tests did not indicate any such defects in the cladding and this feature is believed to be similar to the accel erated outside surface corrosion features noted on SRP 3/8 and caused by the rod bowing problem (see Figure 6 3 41)

No characteristics of a PCI type failure were found in the sections inspected, but post failure hydriding was extensive Figure 6 3 42 shows typical hydride appearance in the cladding for sections from both ends of the rod Both sections showed a pronounced hydride case around the inside surface The hydrogen contents in the cladding, excluding the hydride case on the inside, are given in Table 6 3 14 General hydriding in the region of the plenum (section C158) gave an estimated hydrogen content of approximately 100 ppm (Figure 6 3 43) However, a hydride layer was observed around the inside in the plenum region which was heavier than in other sections and displayed circumferential cracking (see Figure 6 3 37)

Typically, the copper barrier in this failed rod was a delaminated layer consisting of a gray phase closest to the cladding and of copper on the side toward the fuel, as shown in Figure 6 3 44 The thickness of this layer was in the range from 0 2 to 0 4 mil with the gray phase generally accounting for more than 50% of the thickness This is some what thicker than the intermetallic phase observed in the unfailed Cu Barrier rod (Figures 6 3 45 and 6 3 46) and probably indicates oxidation of this layer by ingressing steam

Sections C156 and C157 had more of the copper layer bonded to the inside of the cladding but the layer had a "wrinkled" appearance both axially and circumferentially, and the gray portion was consistently present Areas of more bonding occasionally showed individual ruptures in the layer as in Figure 6 3 47 The copper in the region of the plenum (C158) showed more variation in character, but was extensively delaminated Delamination of the barrier was observed to universally occur at the cladding Zr, Cu intermetallic layer interface rather than at the copper intermetallic boundary

SRP-3/2 Extensive fuel center melting, a consequence of the rod bow problem, was also noted in this rod How ever the rod survived the ramp test and no incipient PCI cracks or significant cladding damage of any type were observed in the sections examined

The copper barrier layer was in excellent condition with only minor areas of separation from the cladding Two such areas are shown in Figure 6 3 45 The copper was generally separated from the intermetallic layer in these areas, in contrast to SRP 3/1 where the copper layer delaminated together with the intermetallic phase The total thickness of the copper intermetallic layer here was 0 0002 to 0 0003 inch Occasional areas of copper removal from the cladding were also observed (Figure 6 3 46), but it should be emphasized that the integrity and uniformity of the copper barrier in this unfailed rod was generally excellent Breaks in the copper layer amounted to less than 5% of the total circum ference of the sections examined

Table 6.3-14
ESTIMATED[a] HYDRIDE CONCENTRATIONS IN CLADDING

Rod	Section	H_2[a] (ppm)
SRP-3/1	C153	200–250
	C155	250–300
	C156	200–250
	C158	100
SRP-3/2	C161	<8
	C162	<8

[a] Estimated by visual comparison to reference photomicrographs Hydride case on cladding inner surface not included

As can be seen in Figure 6.3-47, there are actually two intermetallic phases between the copper and the cladding. W. T. Grubb at the GE Corporate Research and Development Center has done some work to characterize these layers. The intermetallic (gray) layer next to the copper has a composition of $ZrCu_{3.6}$. The second, thinner layer is too thin to analyze.

SRP-3/8. The PIE of this segment was of interest only insofar as it provided the insight which led to recognition of the rod bow problem and rapid implementation of corrective measures. Figure 6.3-41 shows the axially aligned corrosion pits on the fuel rod outer surface and their appearance in cross section.

Additional PIE. The PIE of the ramped segments listed in Table 6.3-13 is in progress. Results to date support the ramp test conclusions shown. A PCI crack at the peak power location in the failed reference rod SRP-3/12 is shown in Figure 6.3-48. The typical appearance of the non-bonded copper barrier and the zirconium liner in the sound remedy rods SRP-3/13 and SRP-3/17 respectively is depicted in Figure 6.3-49.

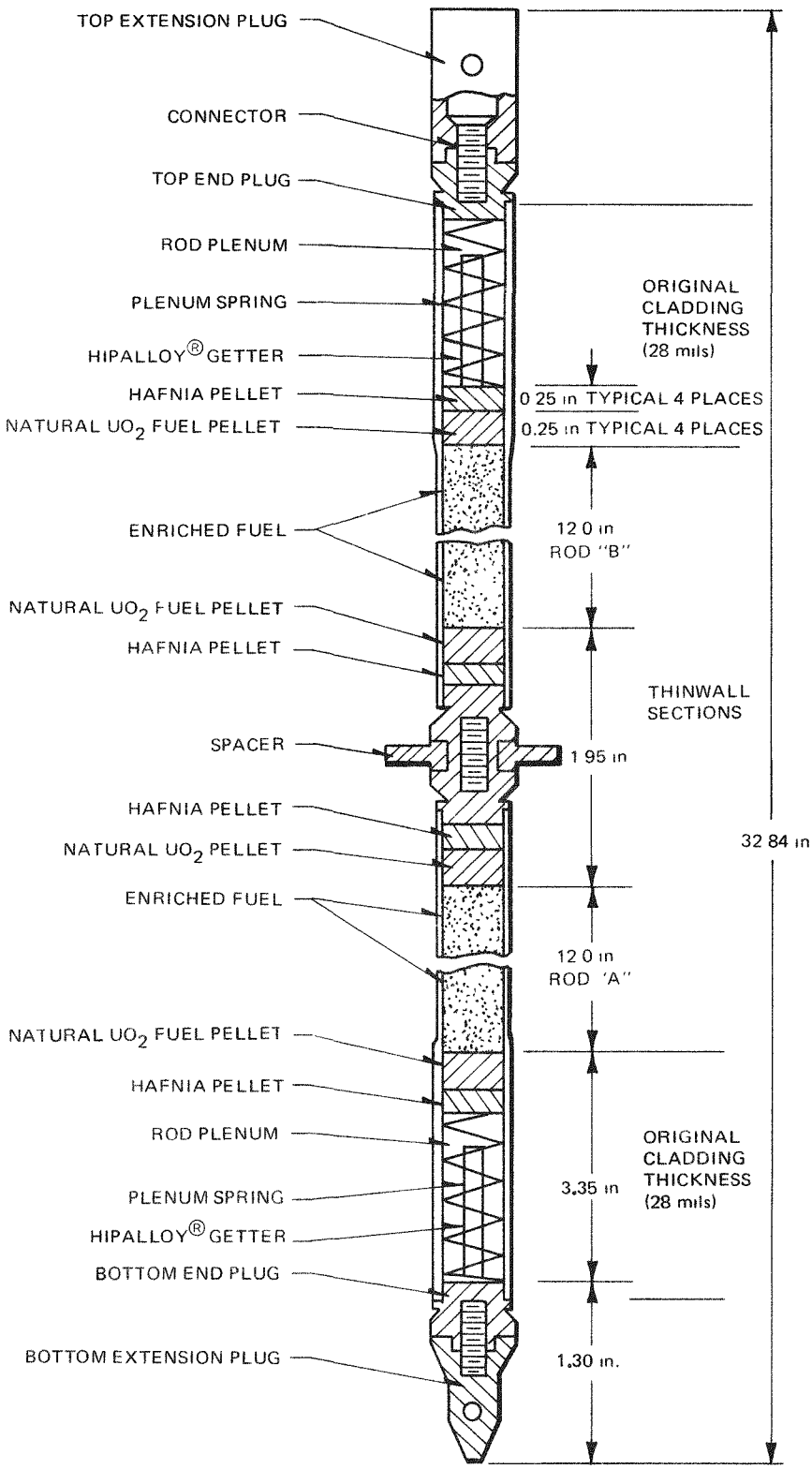

Figure 6.3-1. Sketch of Collapsed Cladding Fuel Rod Assembly

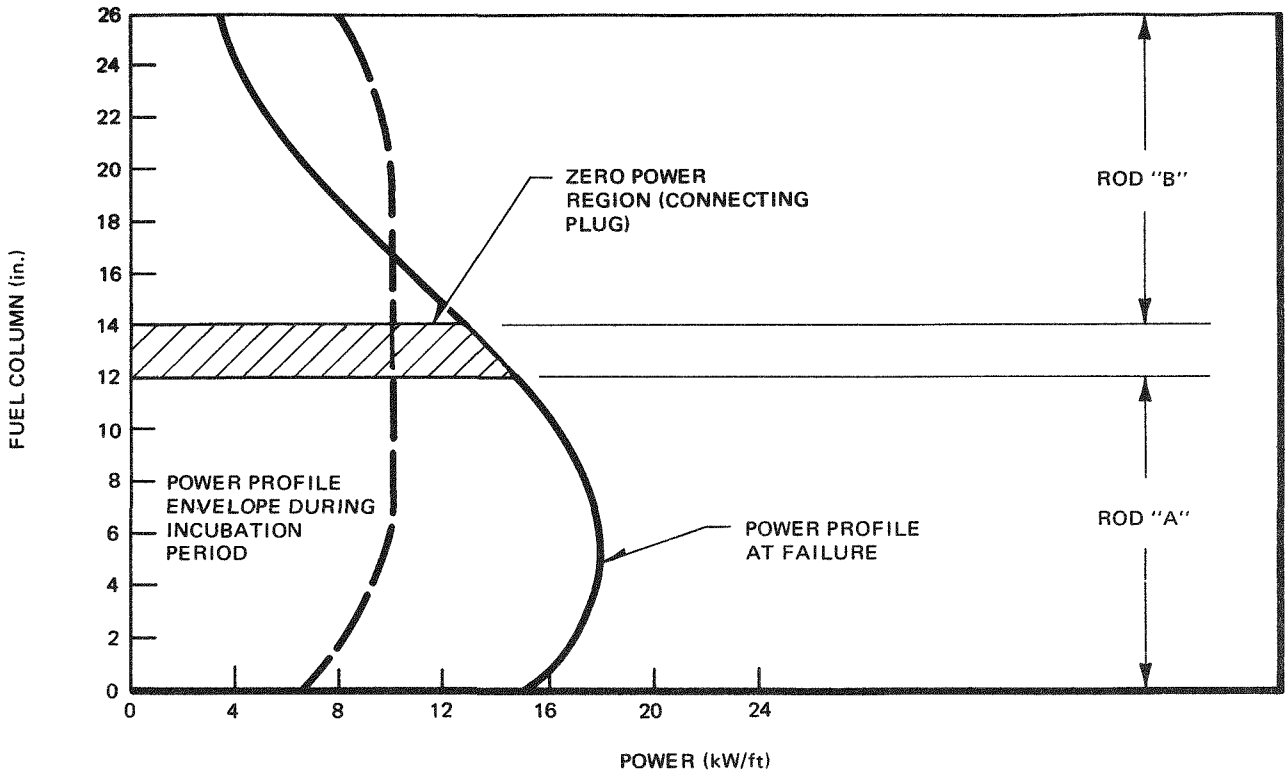

Figure 6.3-2. Typical Collapsed Cladding Fuel Rod Power Profiles

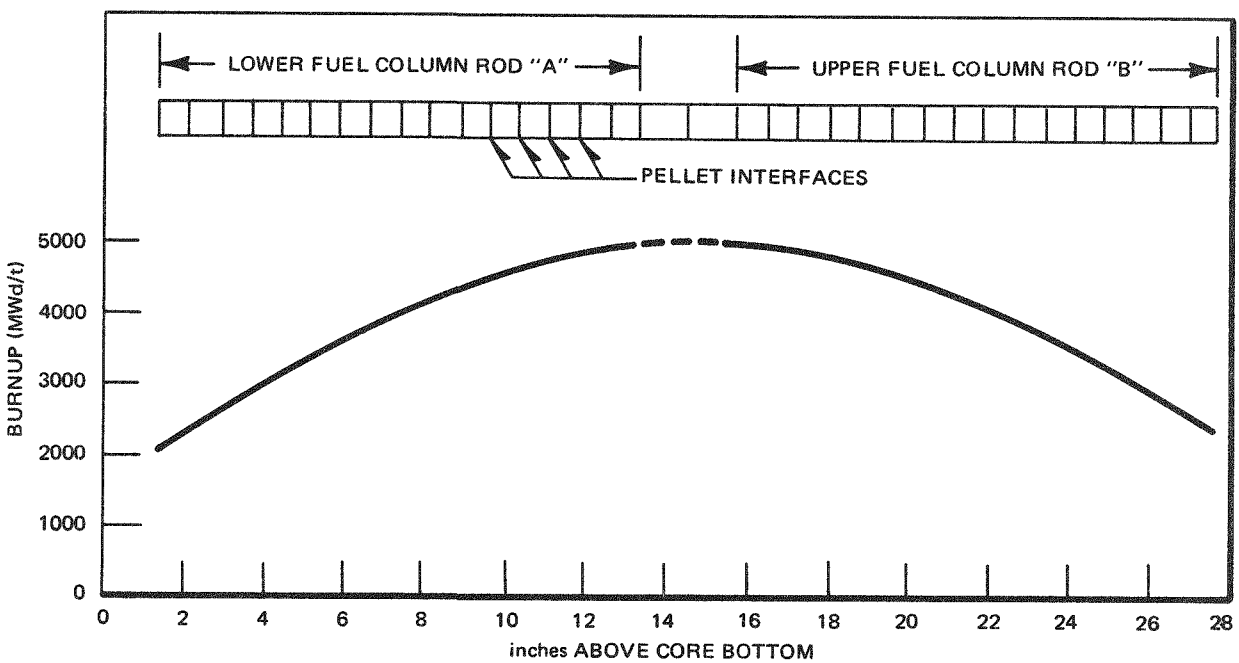

Figure 6.3-3. Calculated Burnup Profiles Along Rods Irradiated in the Incubating Mode

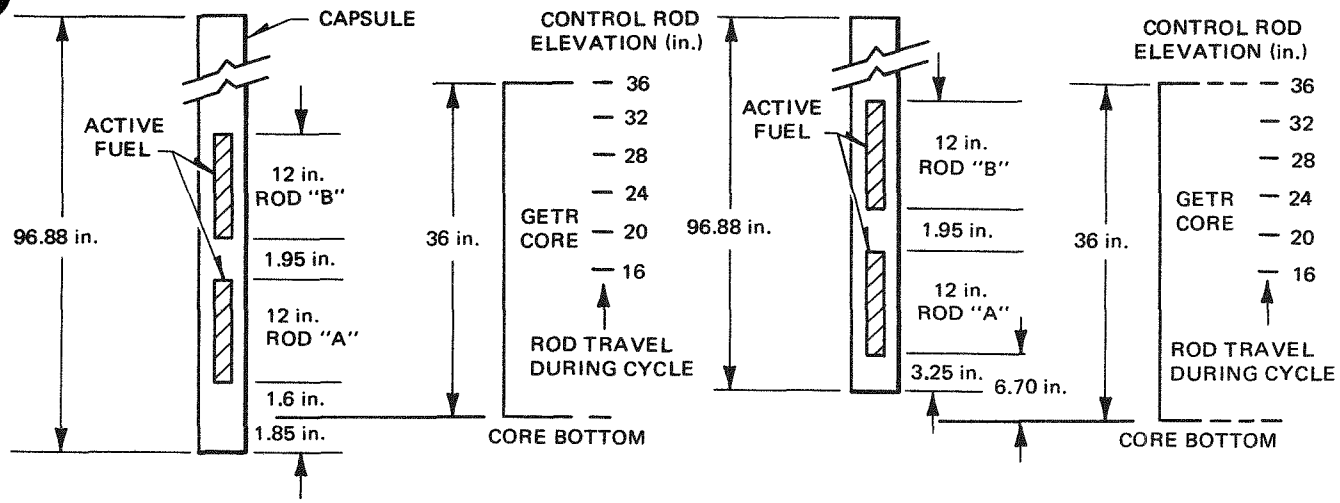

(a) INCUBATING MODE

POSITION FOR ACCUMULATING BURNUP
ROD BANK RANGE ~ 18 – ~ 30 in.

(b) MODE A - "RAISED"

ROD BANK TEST "WINDOW" 21.0-21.9 in.

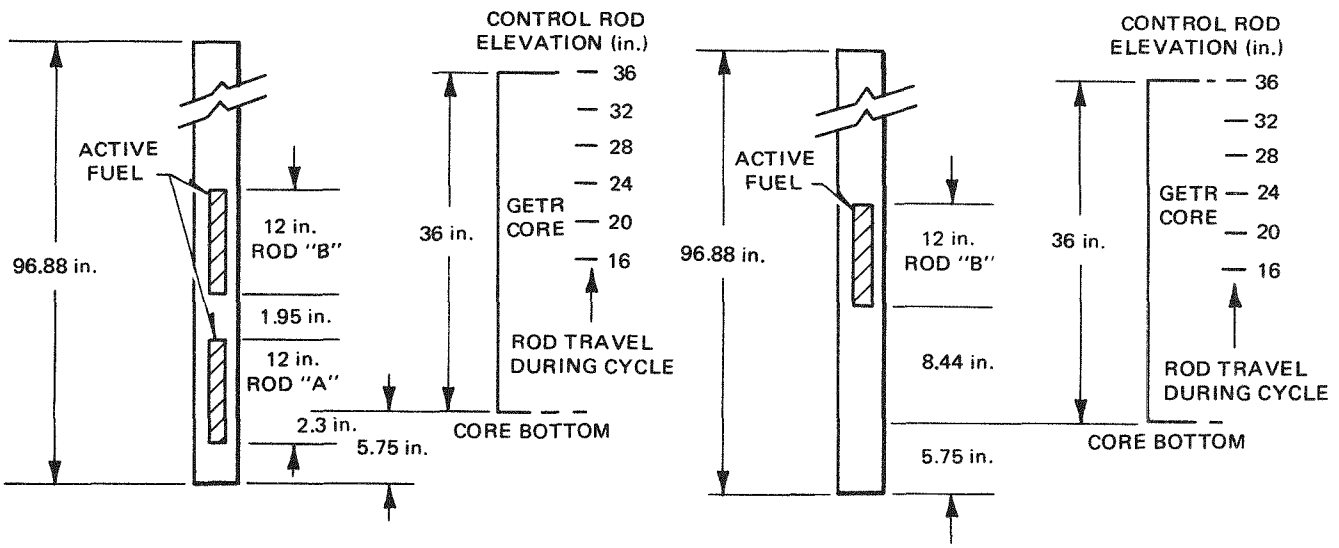

(c) MODE B "LOWERED"

ROD BANK TEST "WINDOW"
PREFERRED ⩾ 30.0 in.
ACCEPTABLE ⩾ 28.0 in.

(d) MODE C "RE-ENCAPSULATED"

INCUBATION AND TESTING
CC-6B, -8B, -16B, -18B
ROD BANK TEST "WINDOW" 24.0 - 24.9 in.

Figure 6.3-4. Test Modes

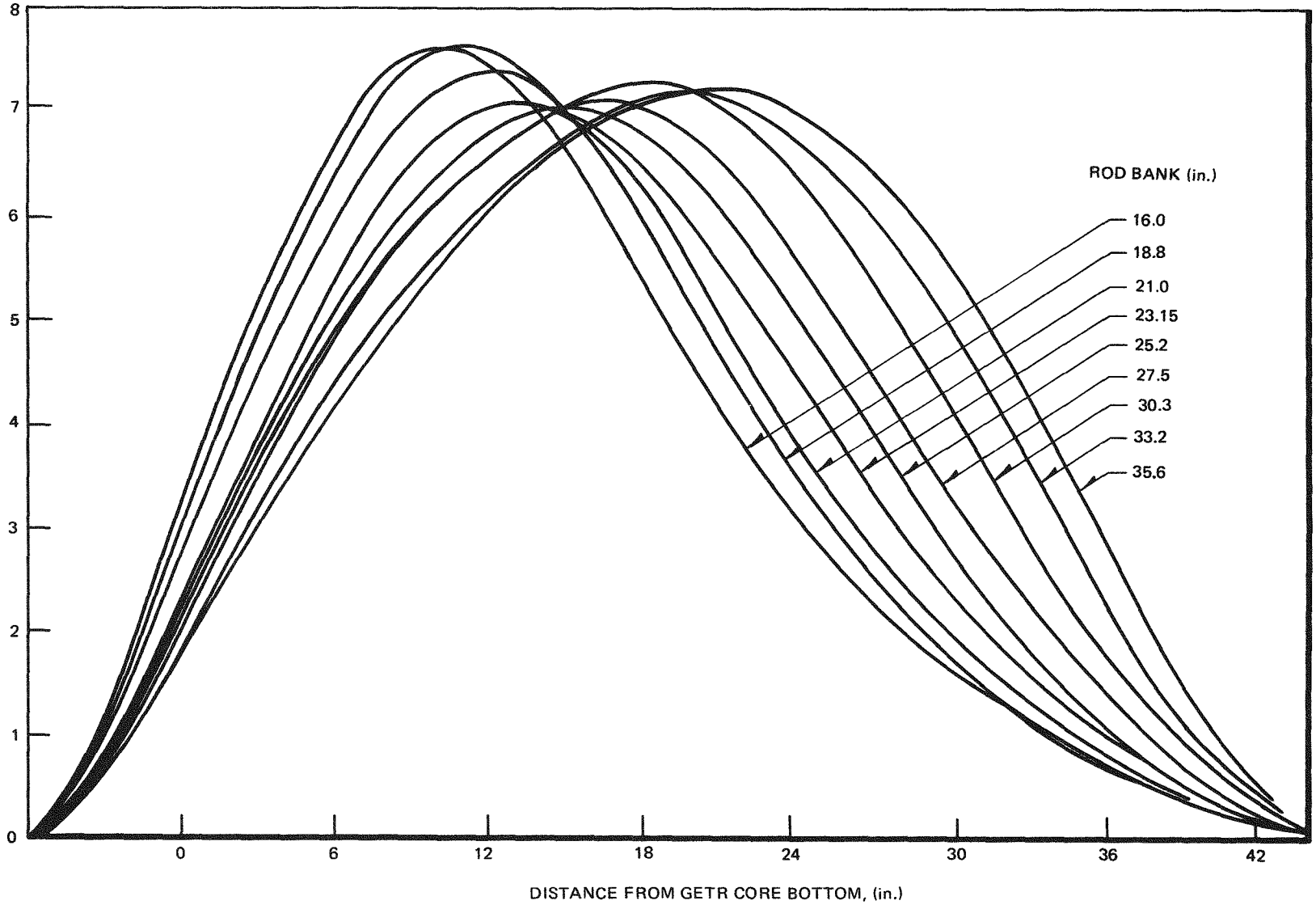

Figure 6.3-5. GETR Flux Profiles at Various Control Rod Bank Elevations

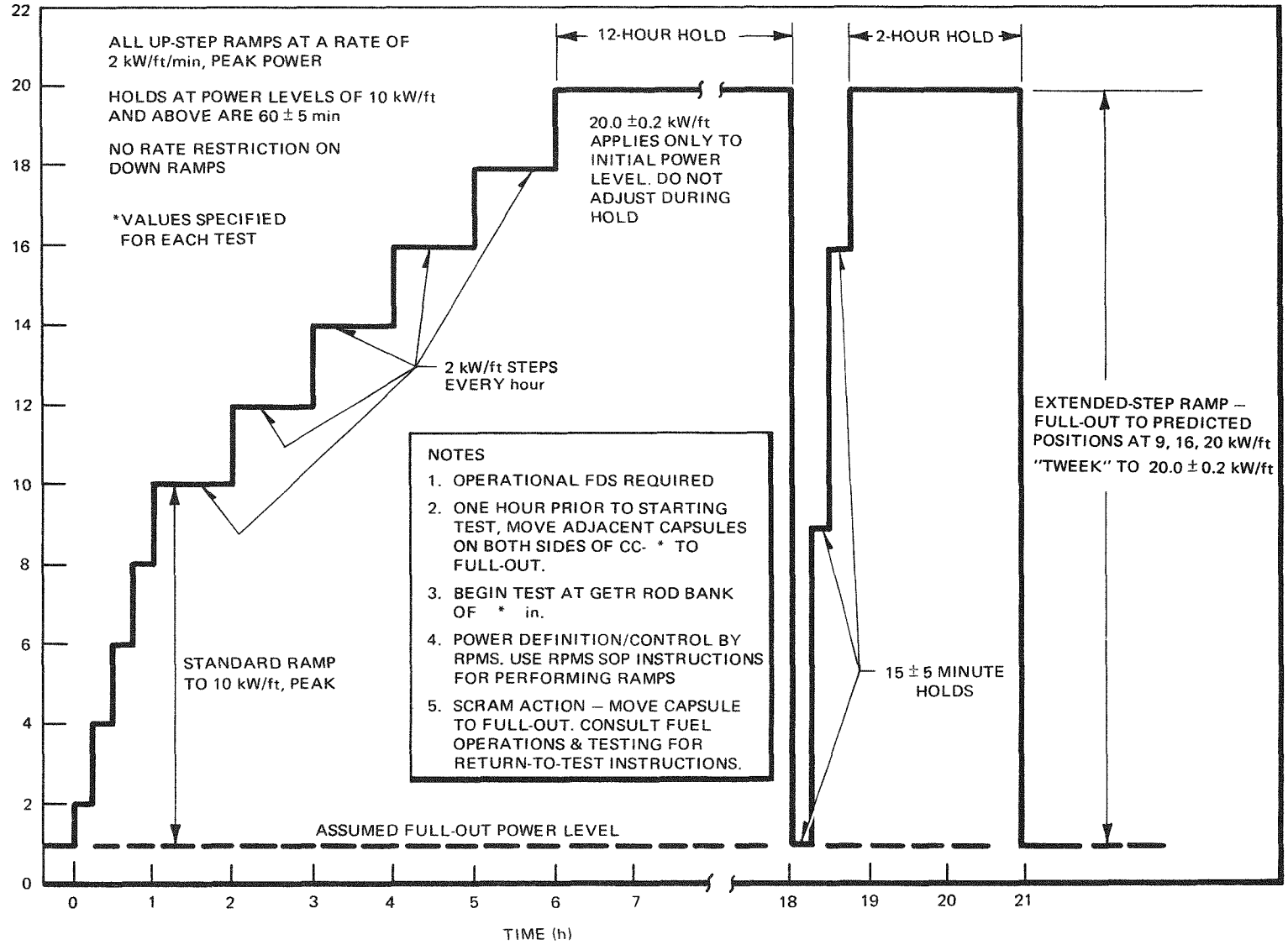

Figure 6.3-6. Collapsed Cladding Fuel Rod Basic Test Sequence

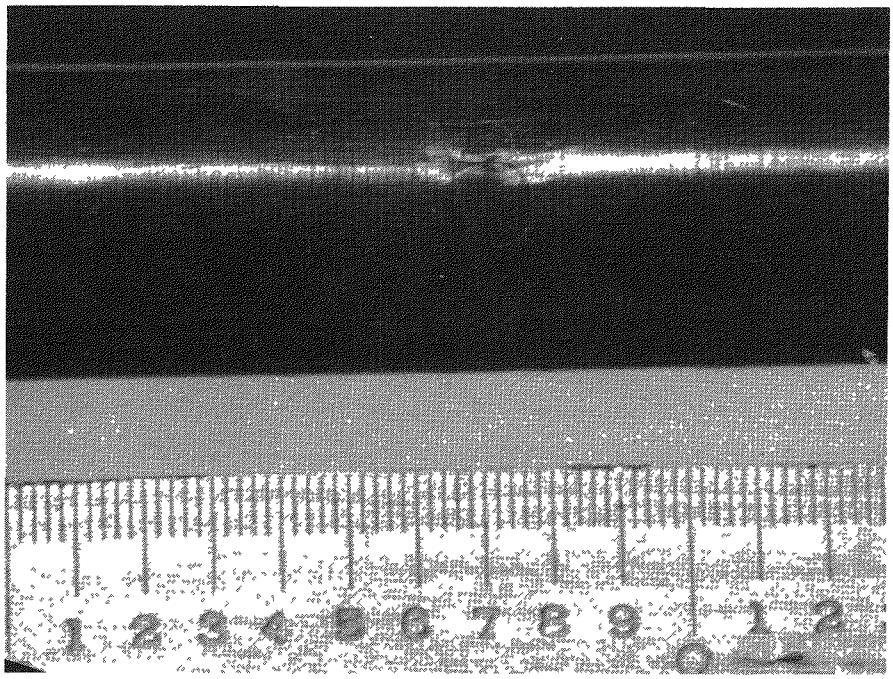

69929

Figure 6.3-7. Visible Defects in Failed Reference Rod CC-4A

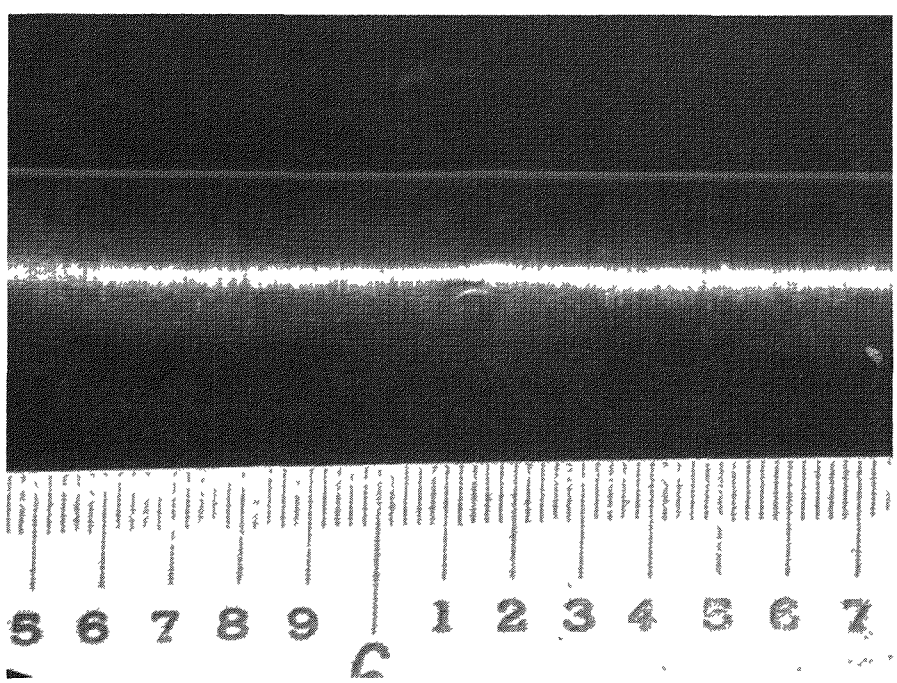

69935

Figure 6.3-8. Small Visible Defect in Failed Reference Rod CC-2B

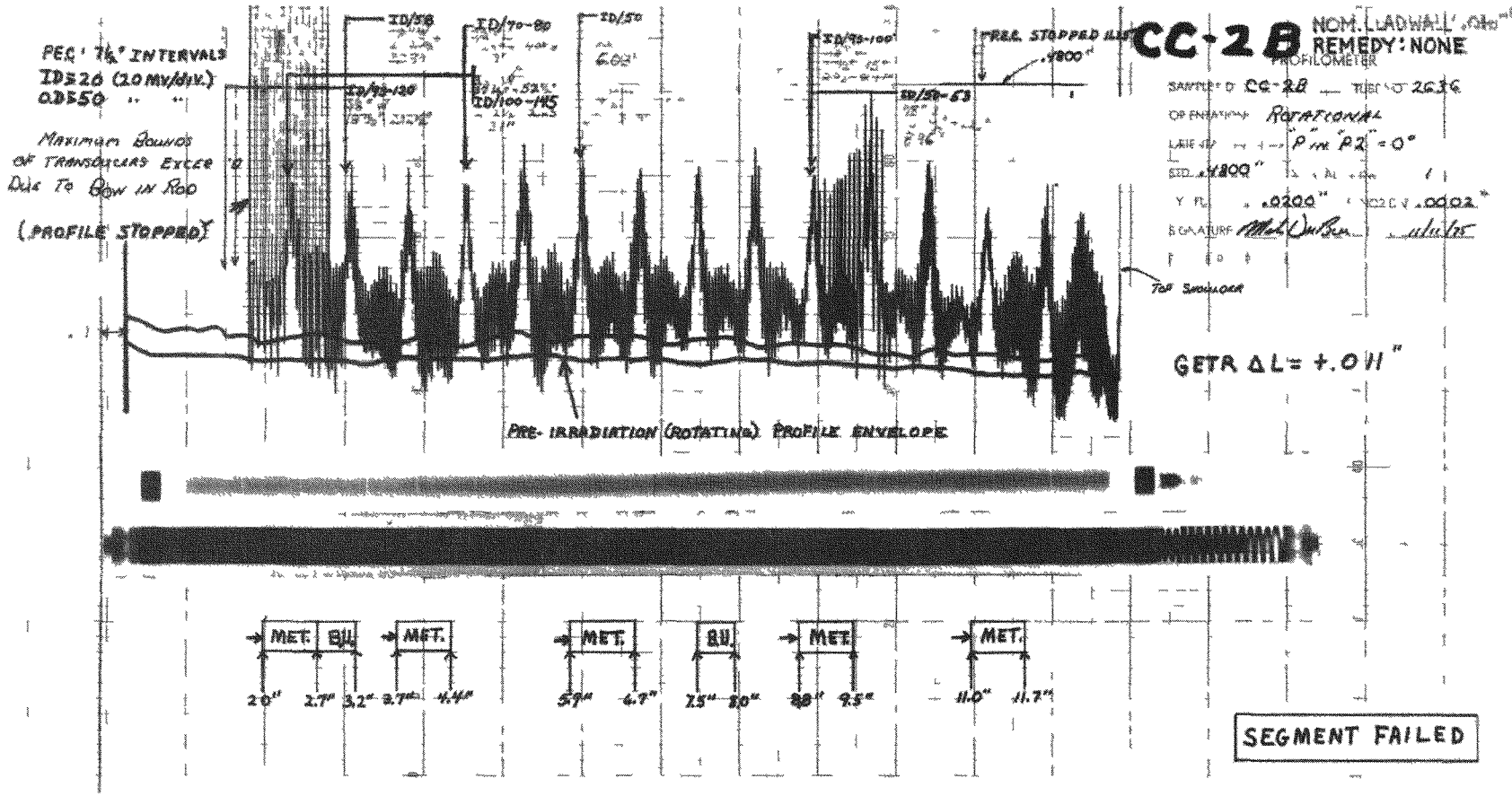

Figure 6.3-9. NDT Summary – Failed Reference Rod CC-2B

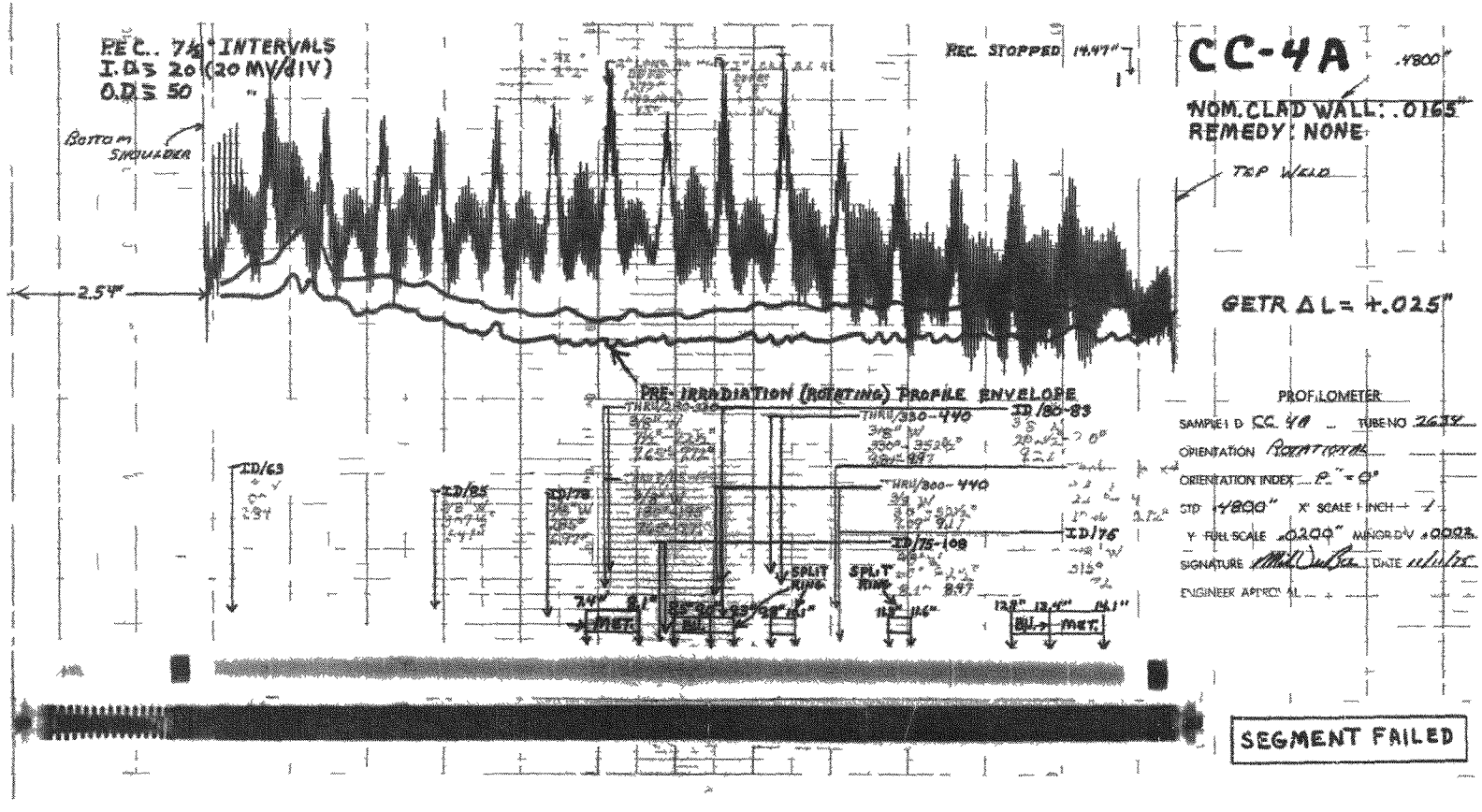

Figure 6.3-10. NDT Summary — Failed Reference Rod CC-4A

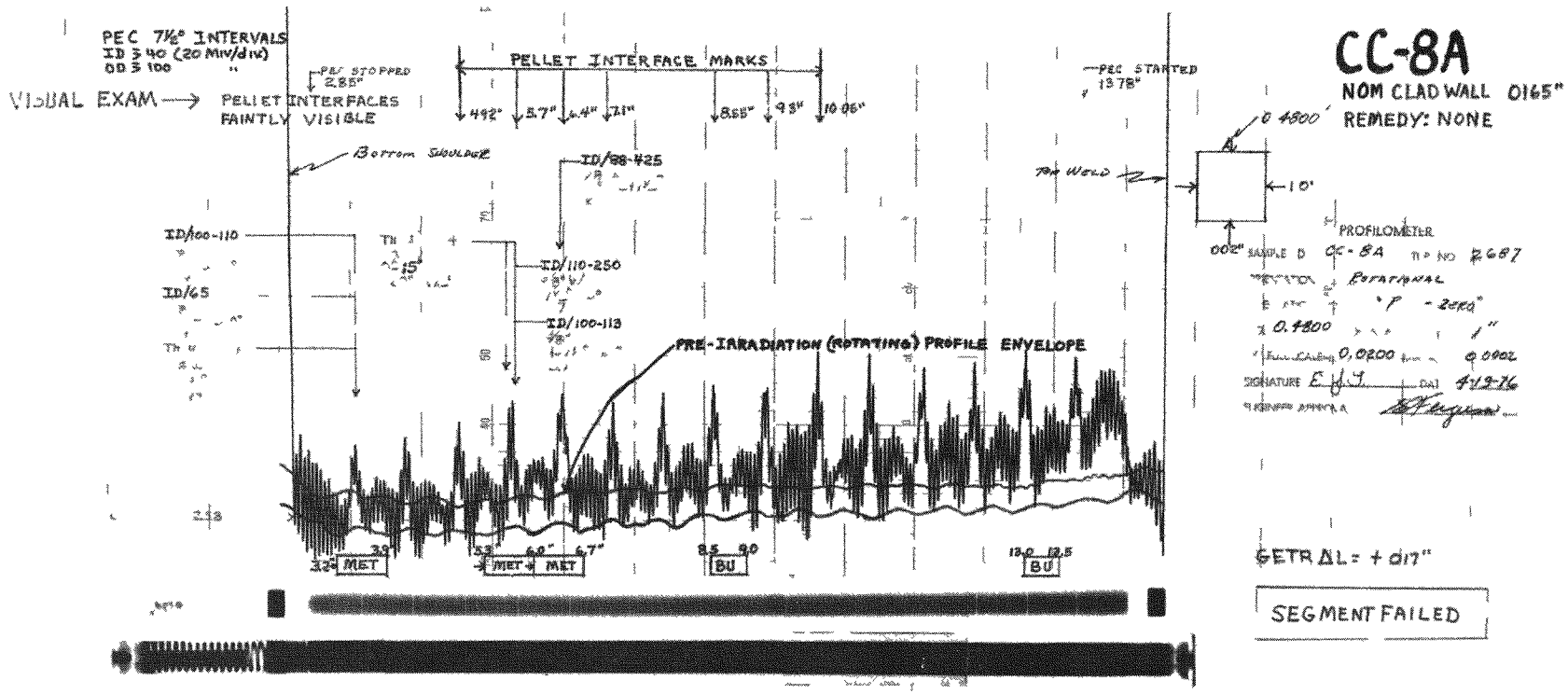

Figure 6.3-11. NDT Summary — Failed Reference Rod CC-8A

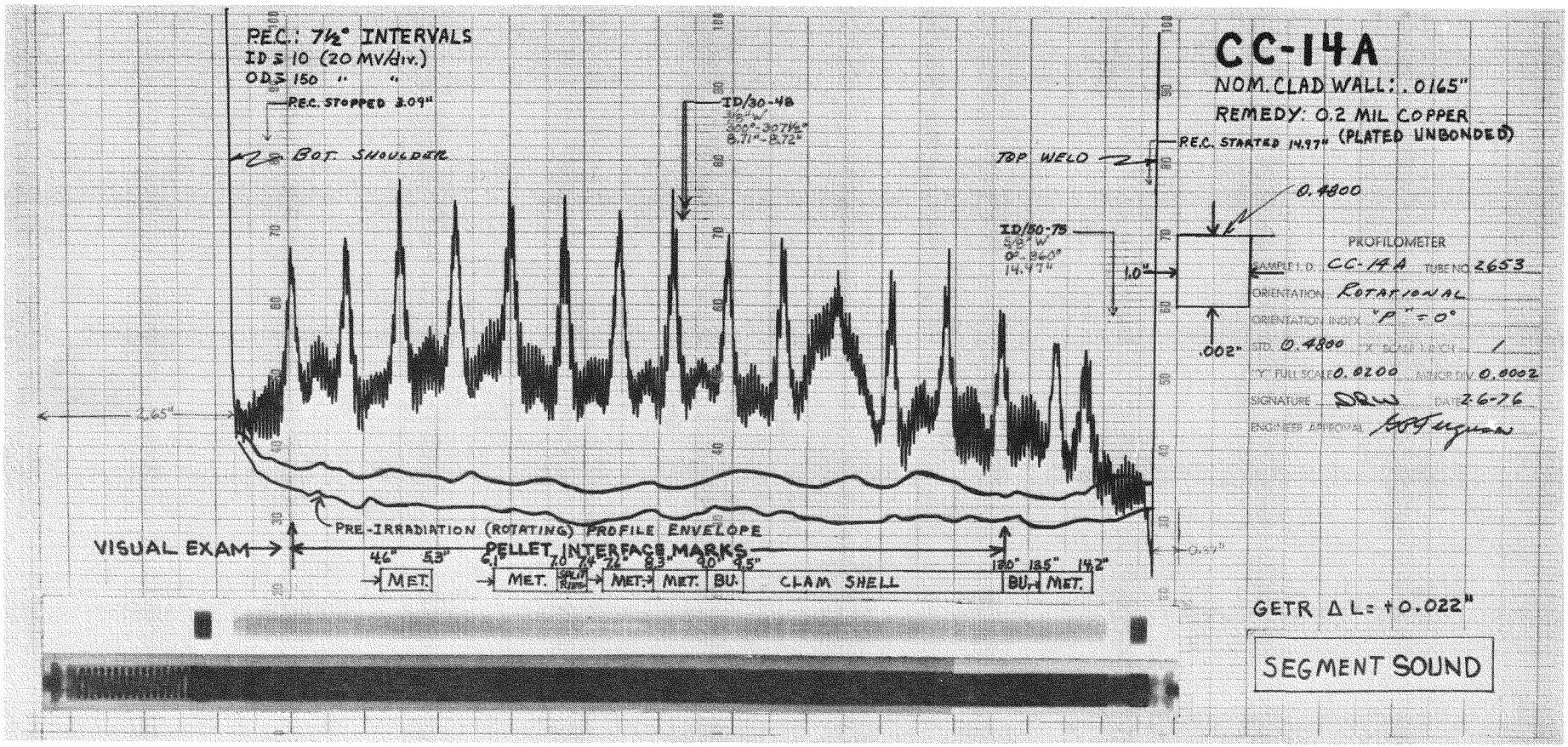

Figure 6.3-12. NDT Summary — Failed Reference Rod CC-14A

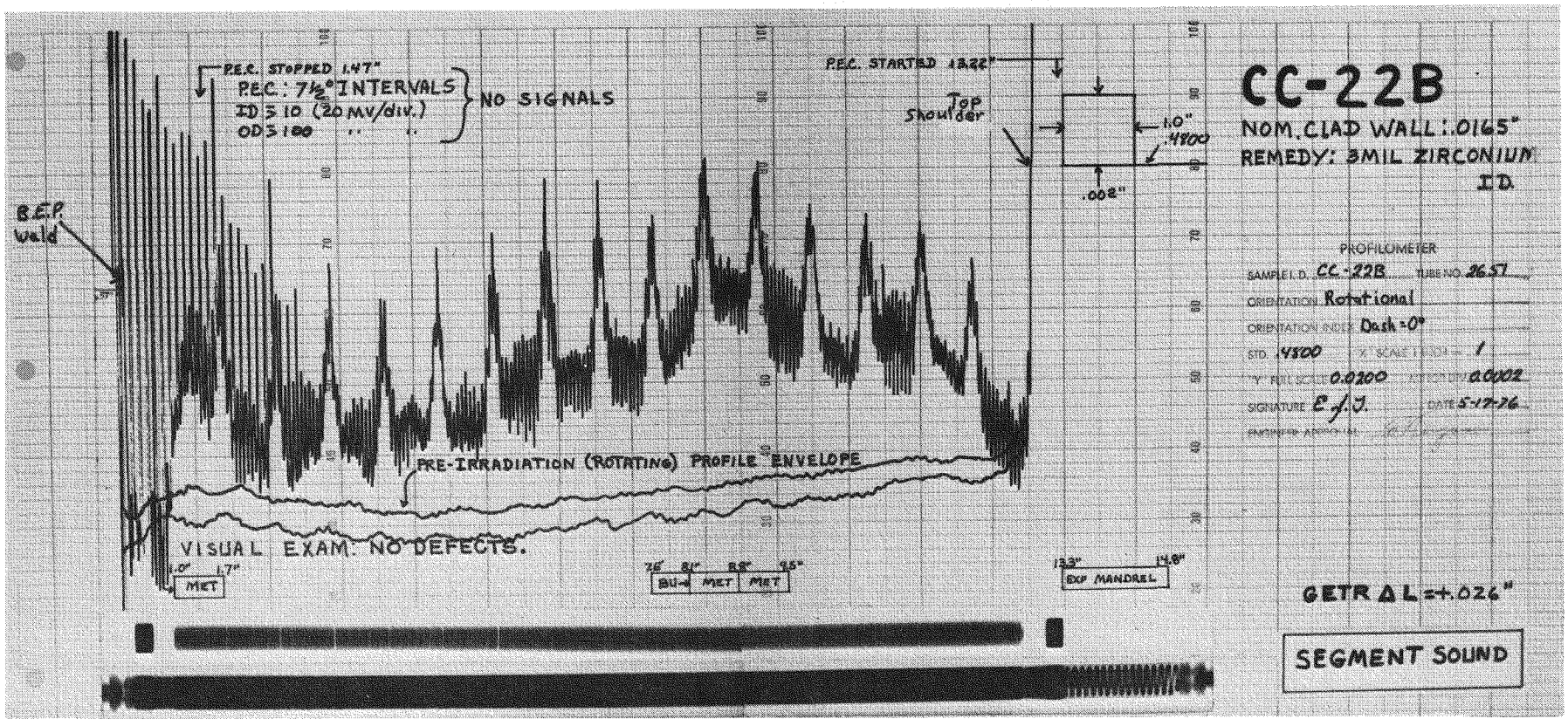

Figure 6.3-13. NDT Summary — Sound Zr-Liner Rod CC-22B

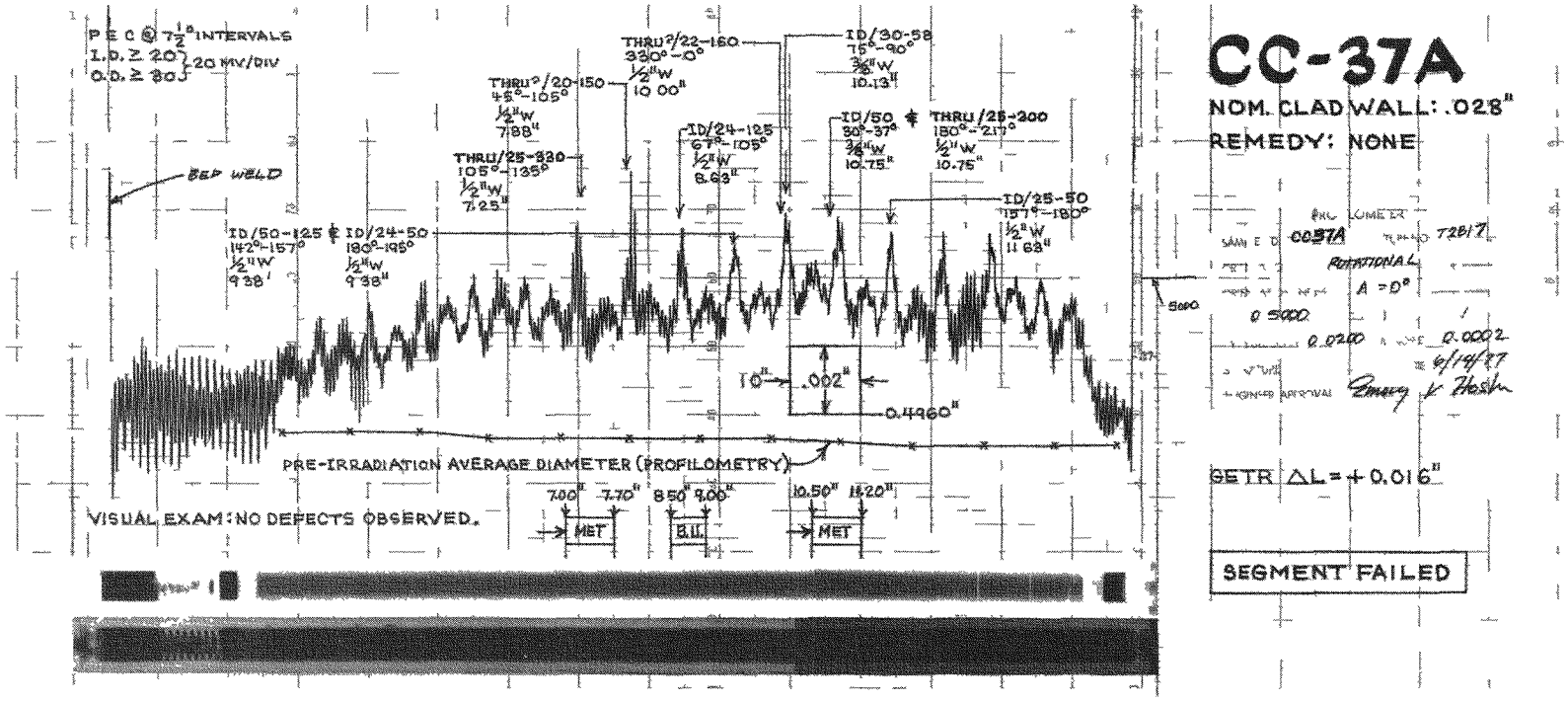

Figure 6.3-14. NDT Summary — Failed Reference Rod CC-37A

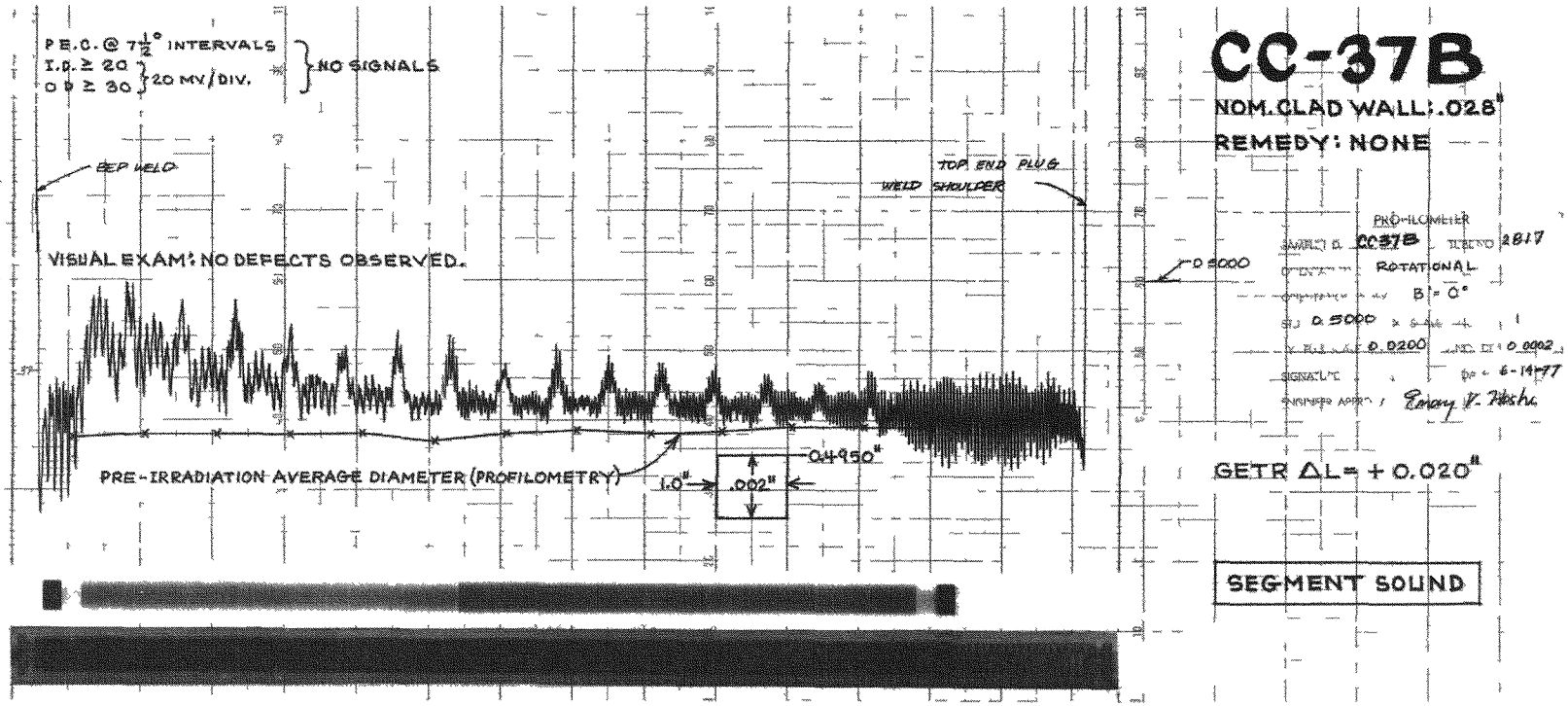

Figure 6.3-15. NDT Summary — Sound Reference Rod CC-37B

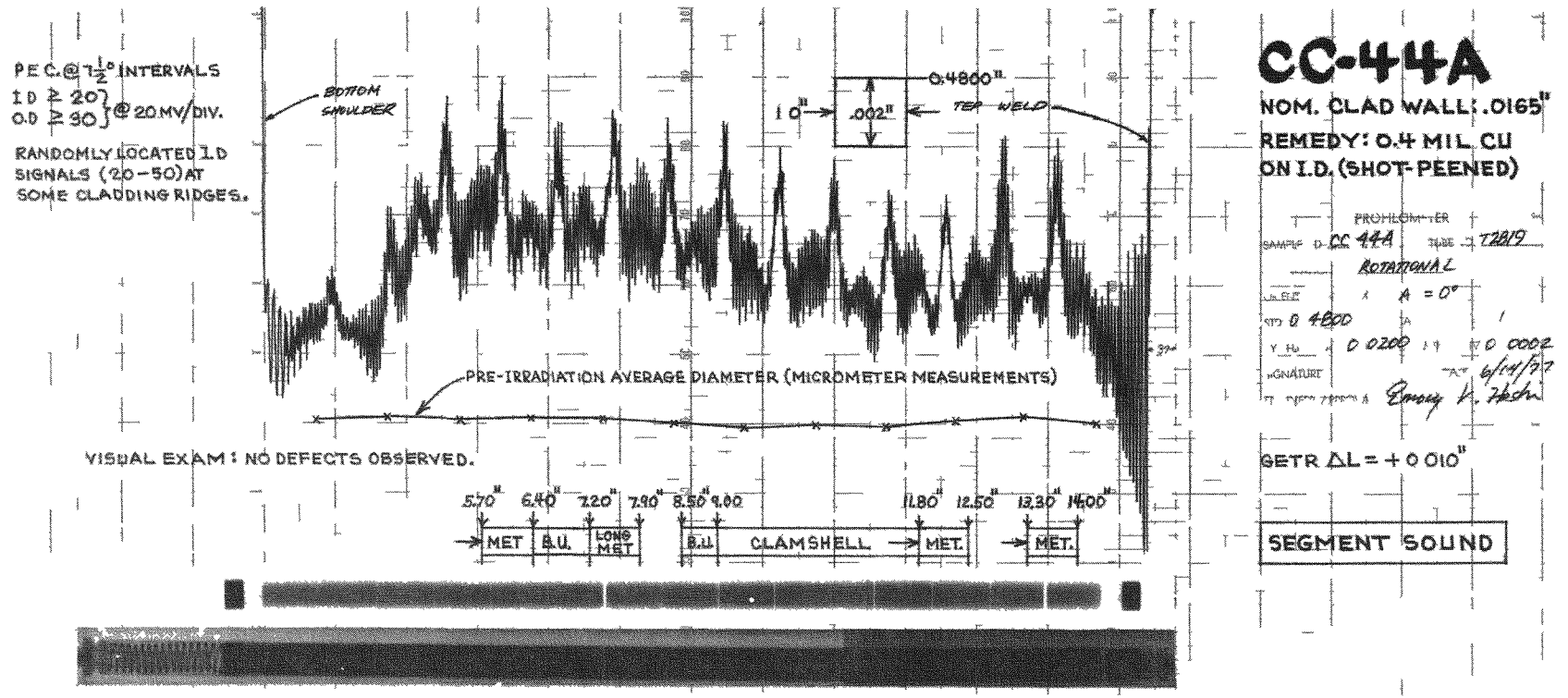

Figure 6.3-16 NDT Summary — Sound Cu-Barrier Rod CC-44A

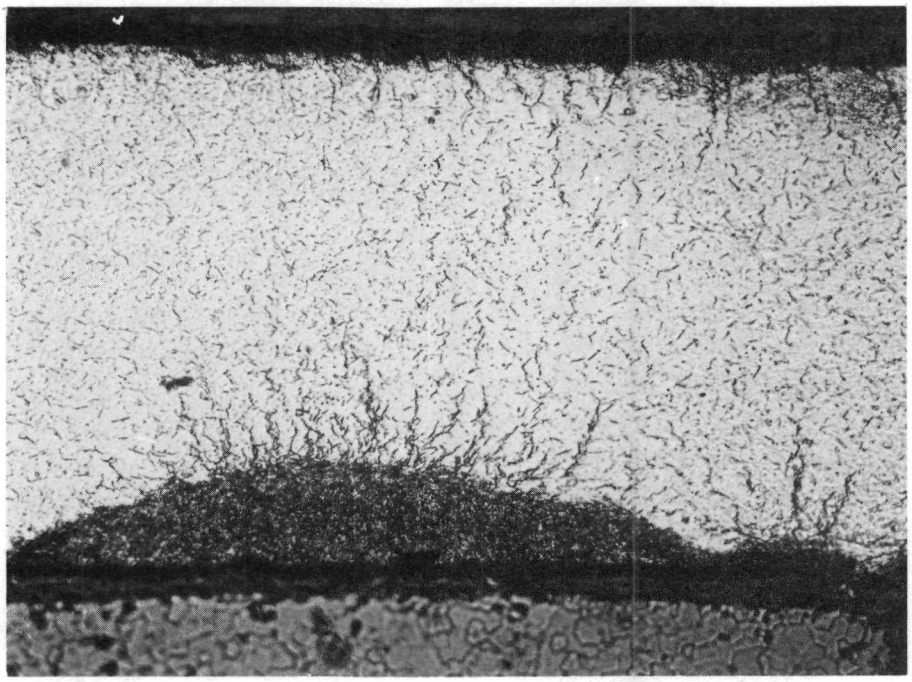

(a) B818-09, 250X, ETCHED

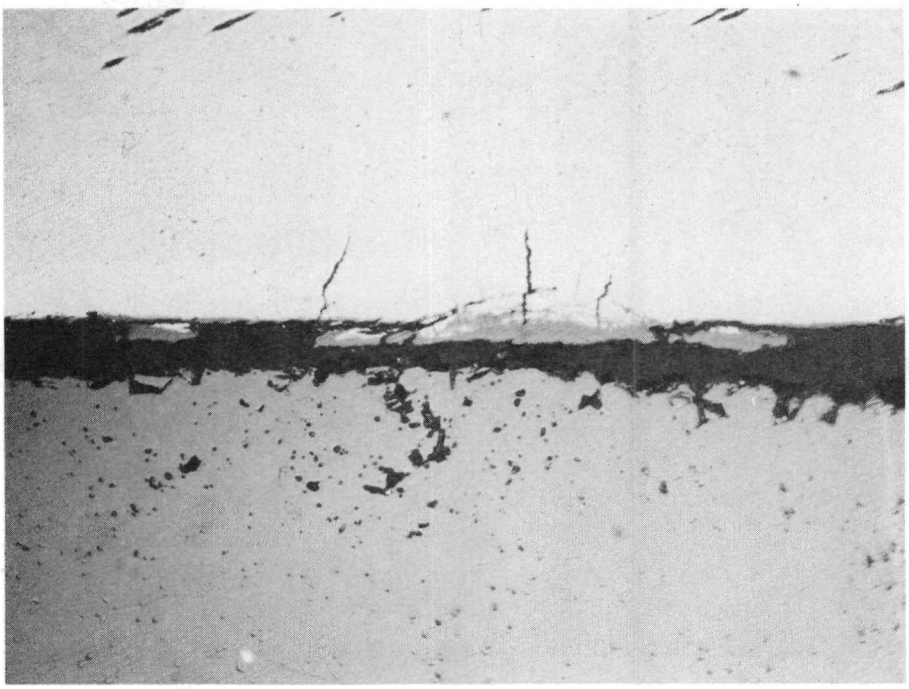

(b) B811-04, 500X, AS POLISHED

Figure 6.3-17. Post-Failure Hydriding Damage in Failed Reference Rods

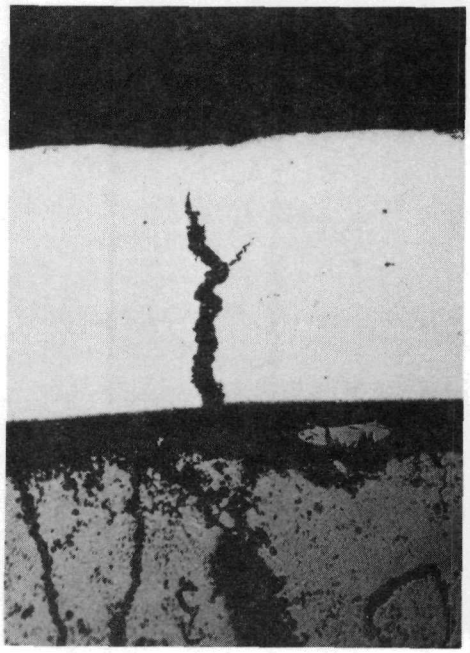

(a) PCI CRACK AND THINNING OF CLAD WALL
B897-07
100X

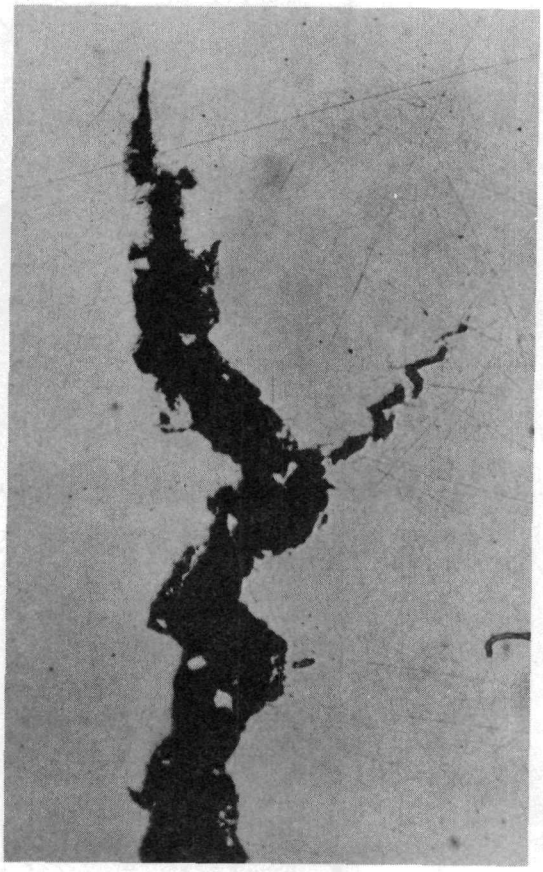

(b) OPENING OF CRACK AT TIP OF BRANCHING
B897-08

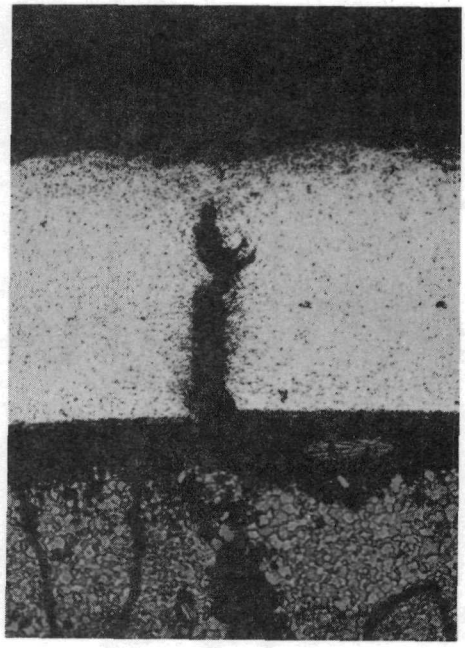

(c) SAME AREA AS (a) IN ETCHED CONDITION
B897-13
100X

Figure 6.3-18. PCI Crack in Failed Reference Rod CC-8A

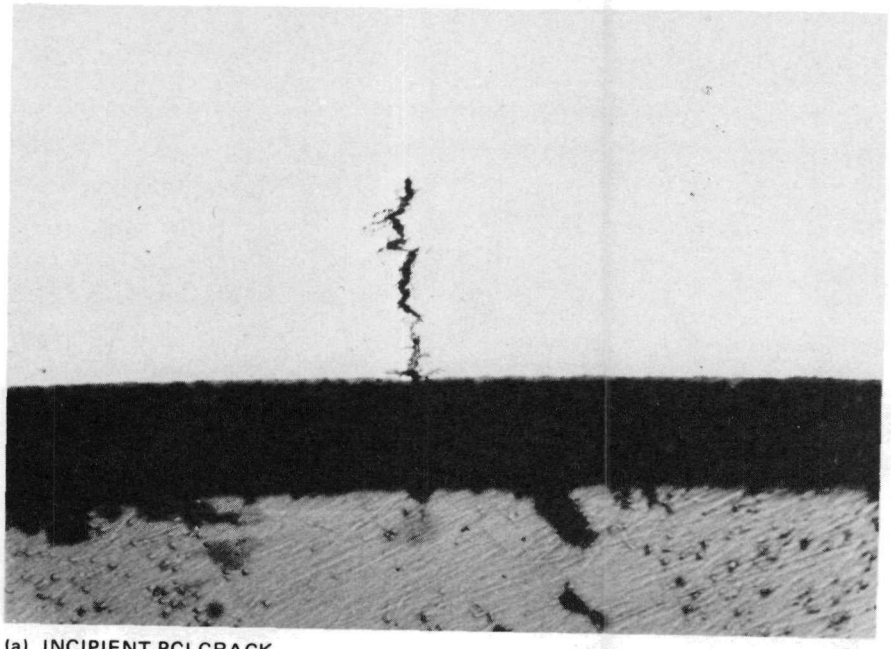

(a) INCIPIENT PCI CRACK

B897-02
500X

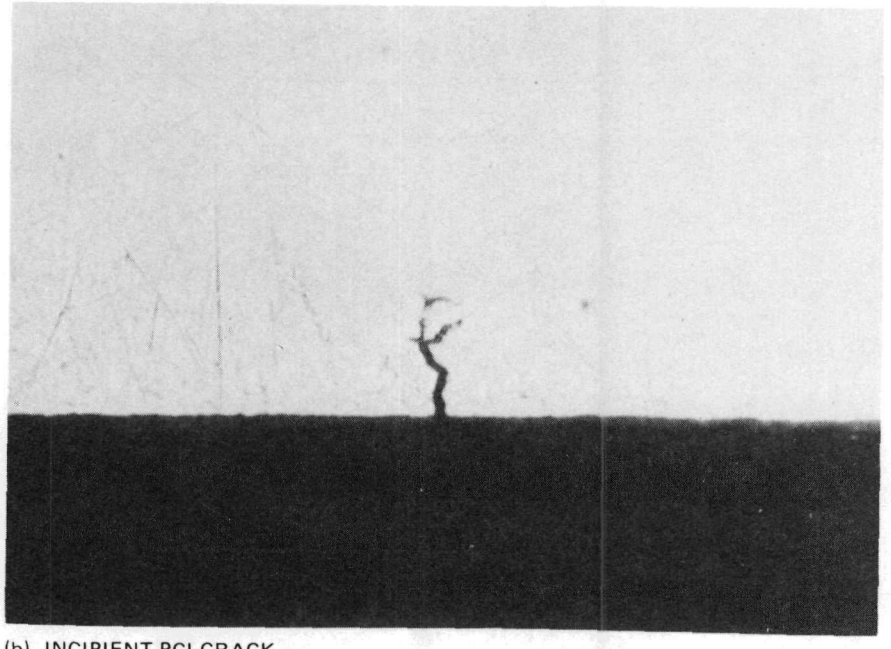

(b) INCIPIENT PCI CRACK

B897-06
1000X

Figure 6.3-19. Incipient PCI Cracks in Failed Reference Rod CC-8A

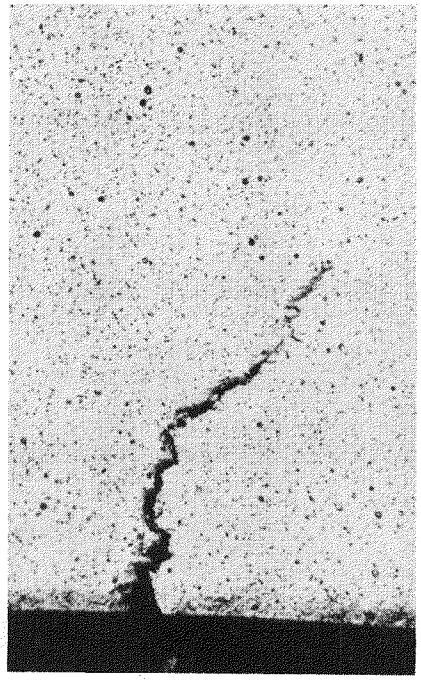

B828-03, ETCHED 250X

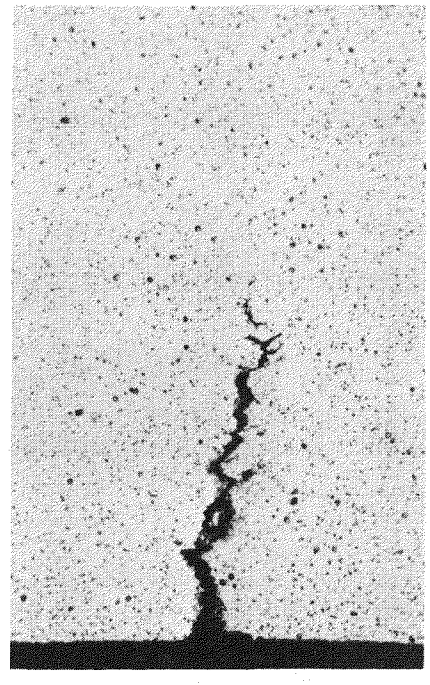

B828-04, ETCHED 250X

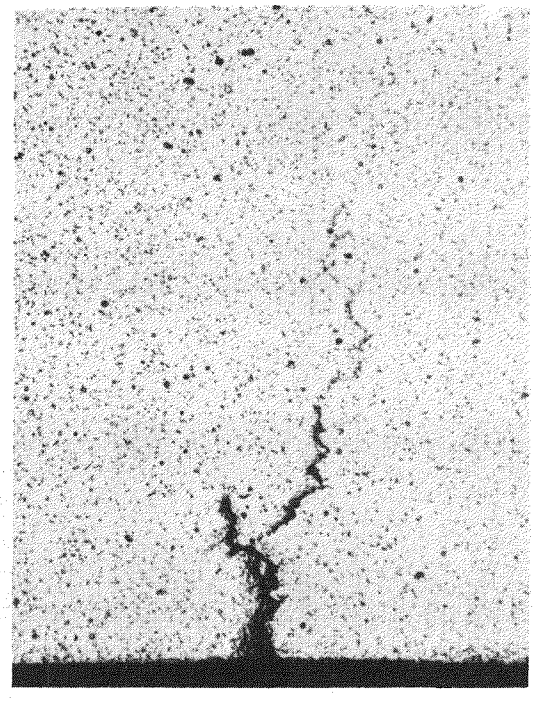

B827-04, ETCHED 250X

Figure 6.3-20. Incipient Cracks Located at Ridges in Sound Reference Rod CC-2A

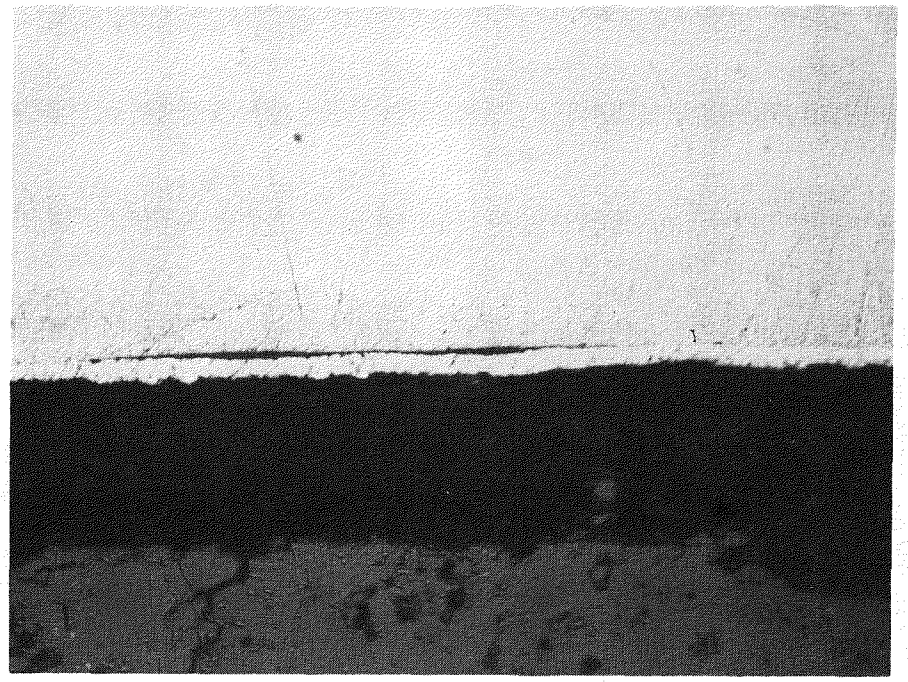

500X

B845-05, AS POLISHED

Figure 6.3-21. Copper Barrier, Showing Local Delamination, Rod CC-14B

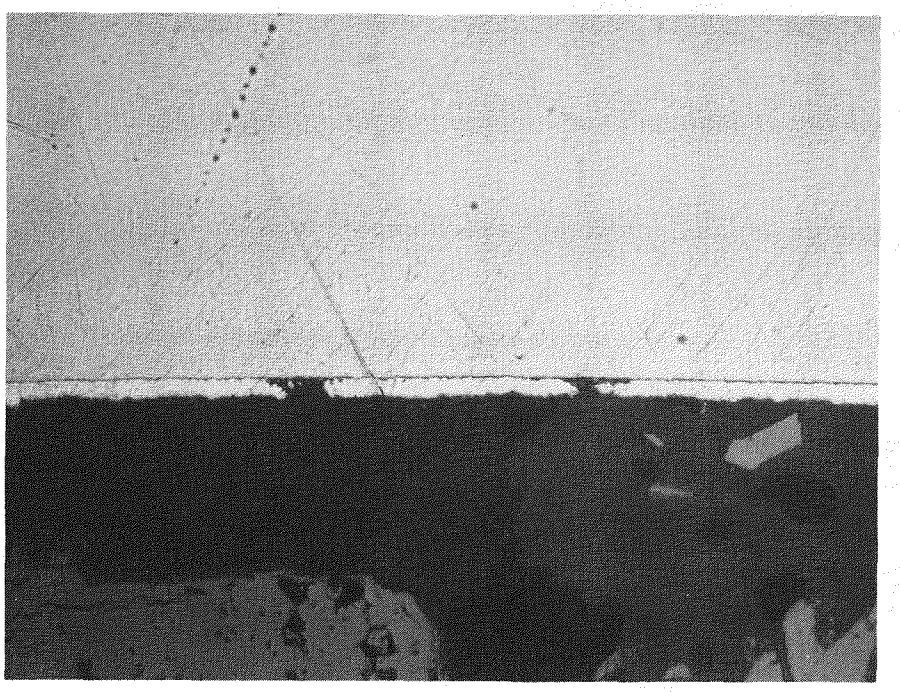

500X

B-845-08

Figure 6.3-22. Copper Barrier, Showing Gouging and Small Flaws, Rod CC-14B

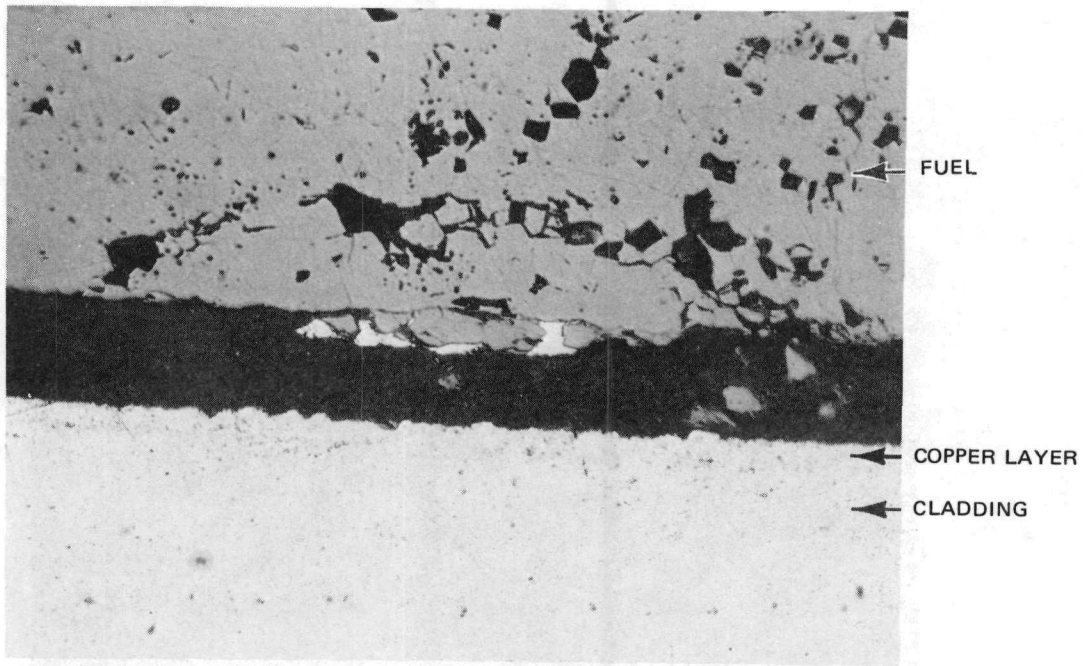

(a) B-846-03 500X

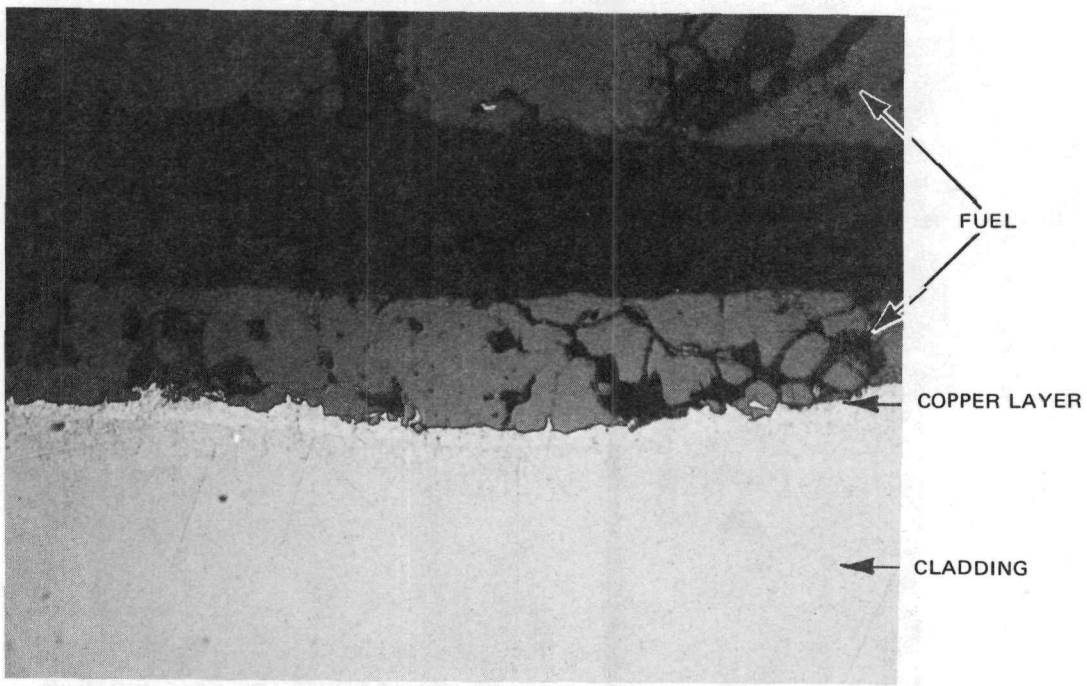

(b) B-846-04 500X

Figure 6.3-23. Fuel-Copper Bonding, Rod CC-14B

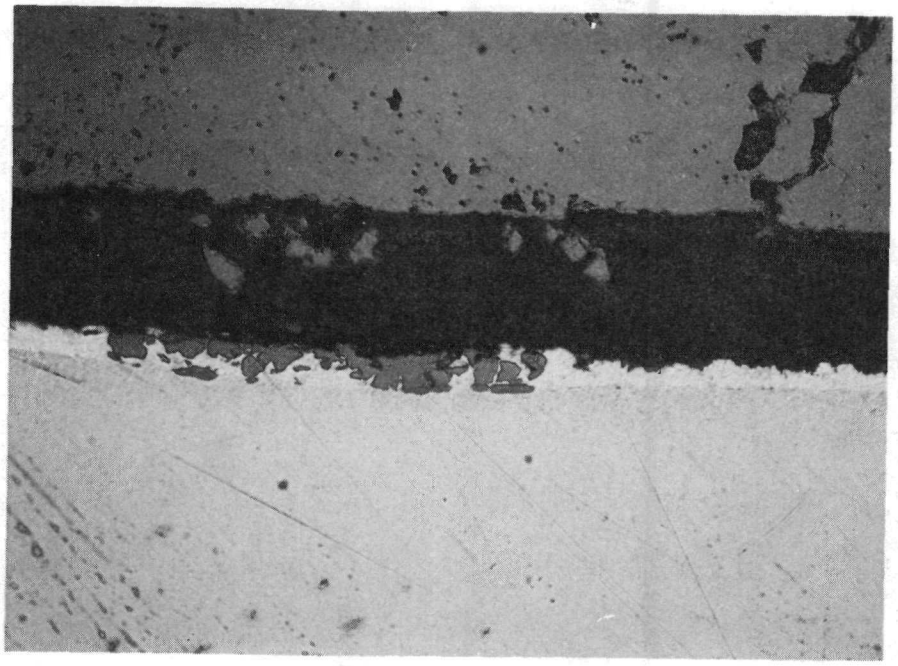

500X

(a) B-844-04, CC-14B

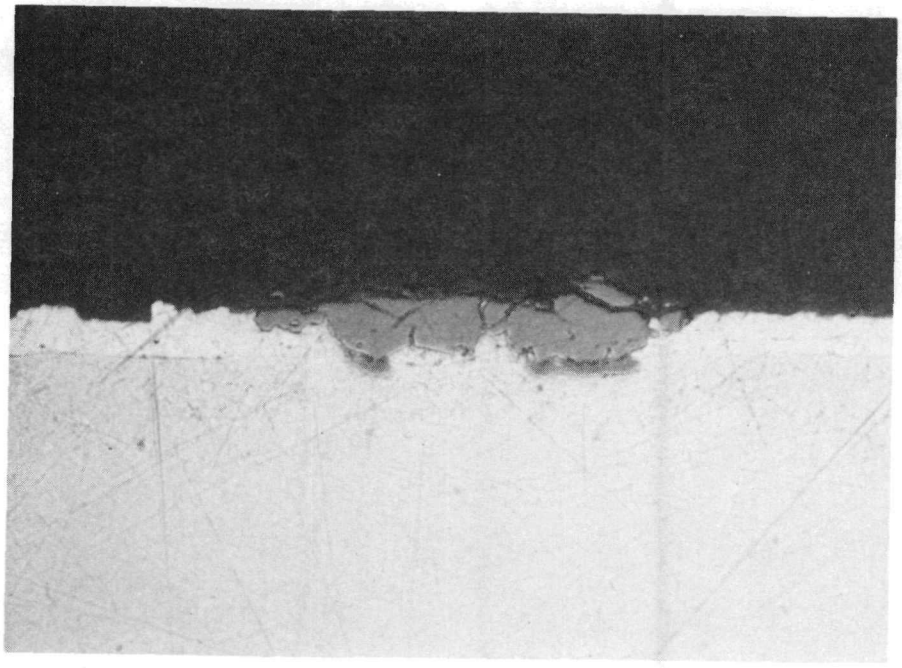

1000X

(b) B-851-04, CC-14A

Figure 6.3-24. Fuel-Copper Interaction, Rods CC-14A and CC-14B

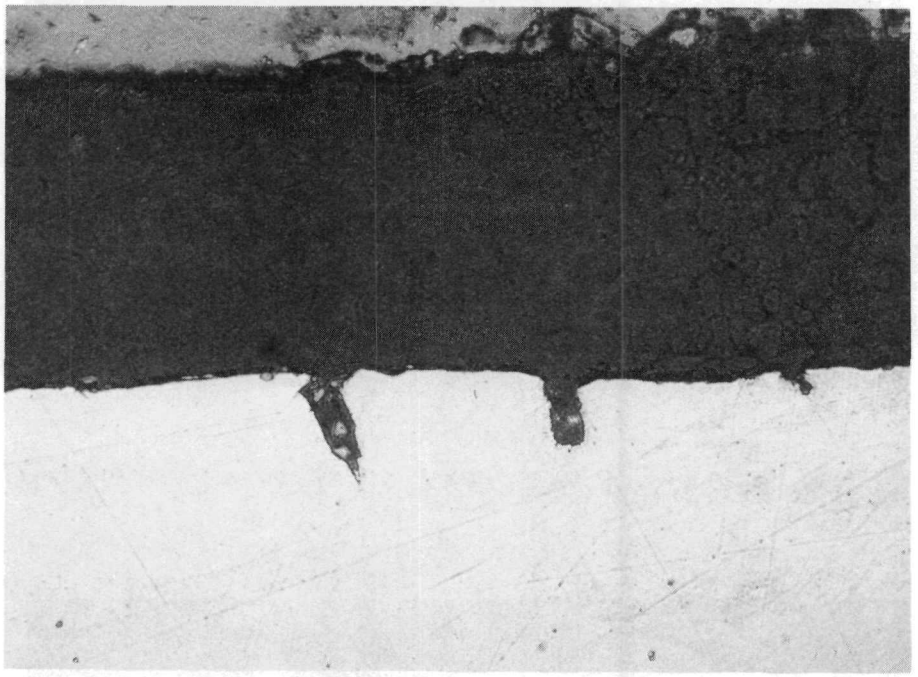

B-913-02 500X

Figure 6.3-25. Flaws in Zirconium Liner, Rod CC-22B

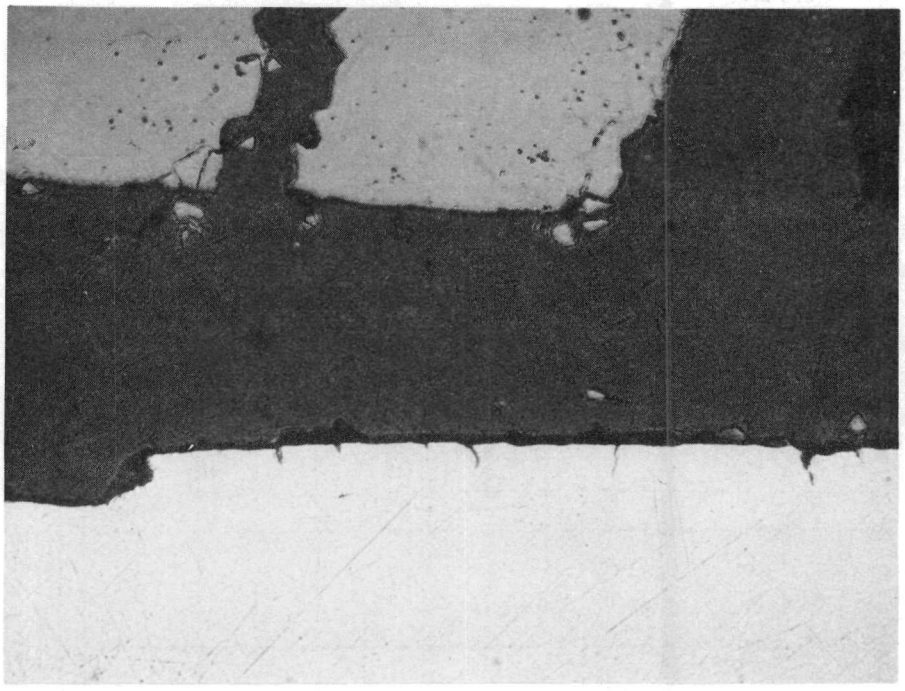

B-913-05 500X

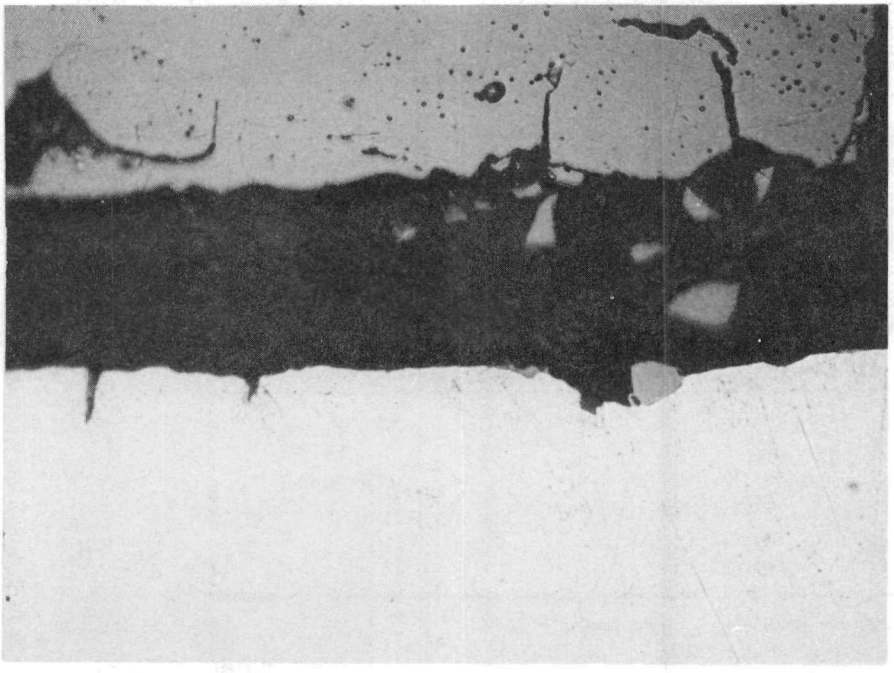

B-914-03 500X

Figure 6.3-26. Flaws in Zirconium Liner, Rod CC-22B

WIDE-WIDE GAP

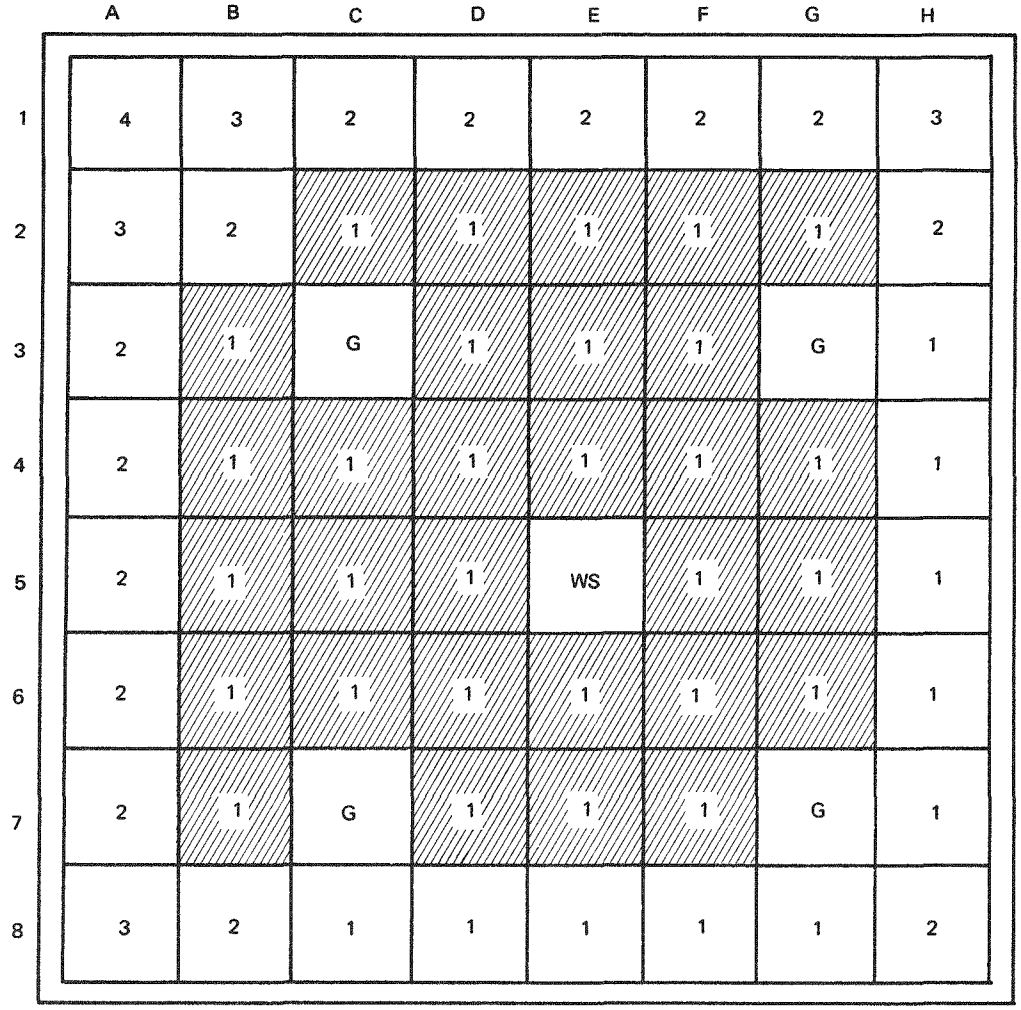

ROD TYPE	ENRICHMENT (wt % U-235)	NUMBER OF RODS
1	2.87	40
2	–	14
3	–	4
4	–	1
G	–	4
WS	–	1

WS – SPACER CAPTURE WATER ROD

G – GADOLINIA RODS (REPLACED BY SEGMENTED UO_2 RODS DURING FIRST RECONSTITUTION, SEE TABLE 7.3-7)

SEGMENTED RODS ARE CROSS HATCHED

Figure 6.3-27. Original Fuel Lattice — 8x8 STR Assembly

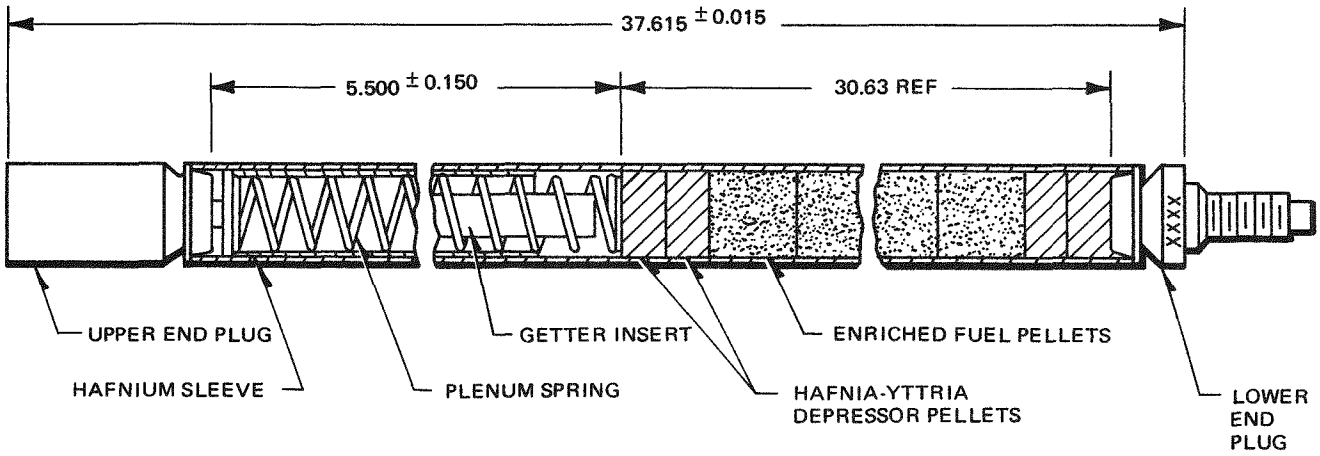

Figure 6.3-28. Sketch of Fuel Rod Segments

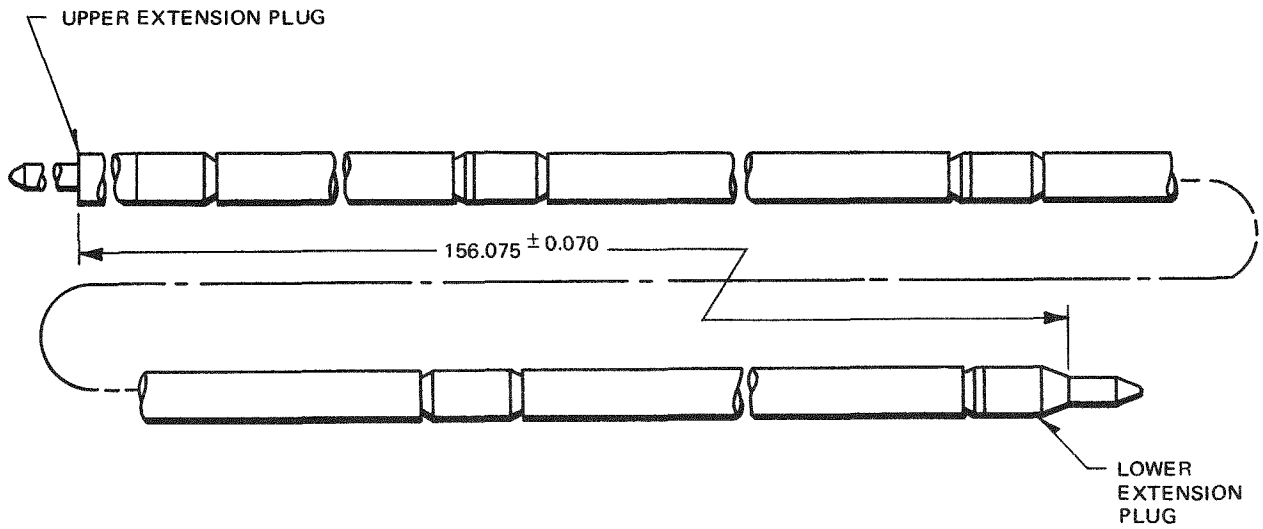

Figure 6.3.29. Sketch of Segmented Rod Assembly

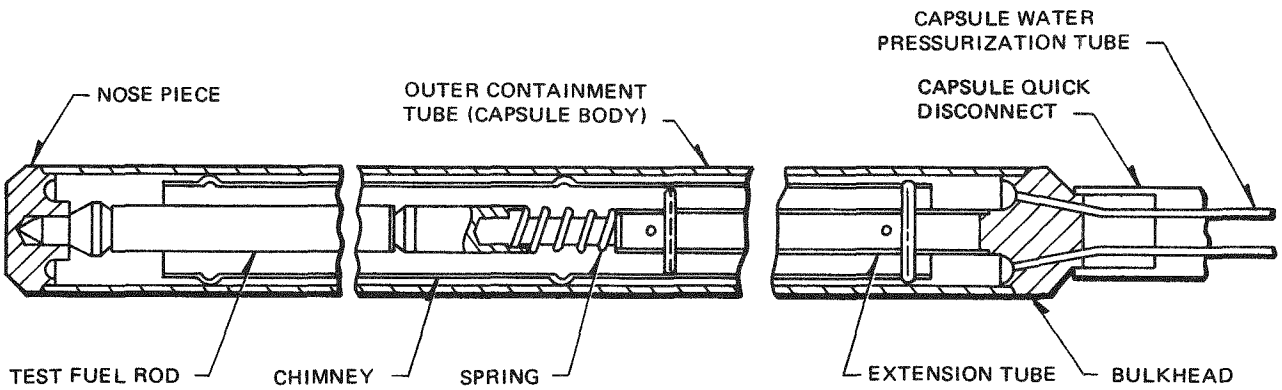

Figure 6.3-30. GETR Pool Fuel Test Capsule Assembly

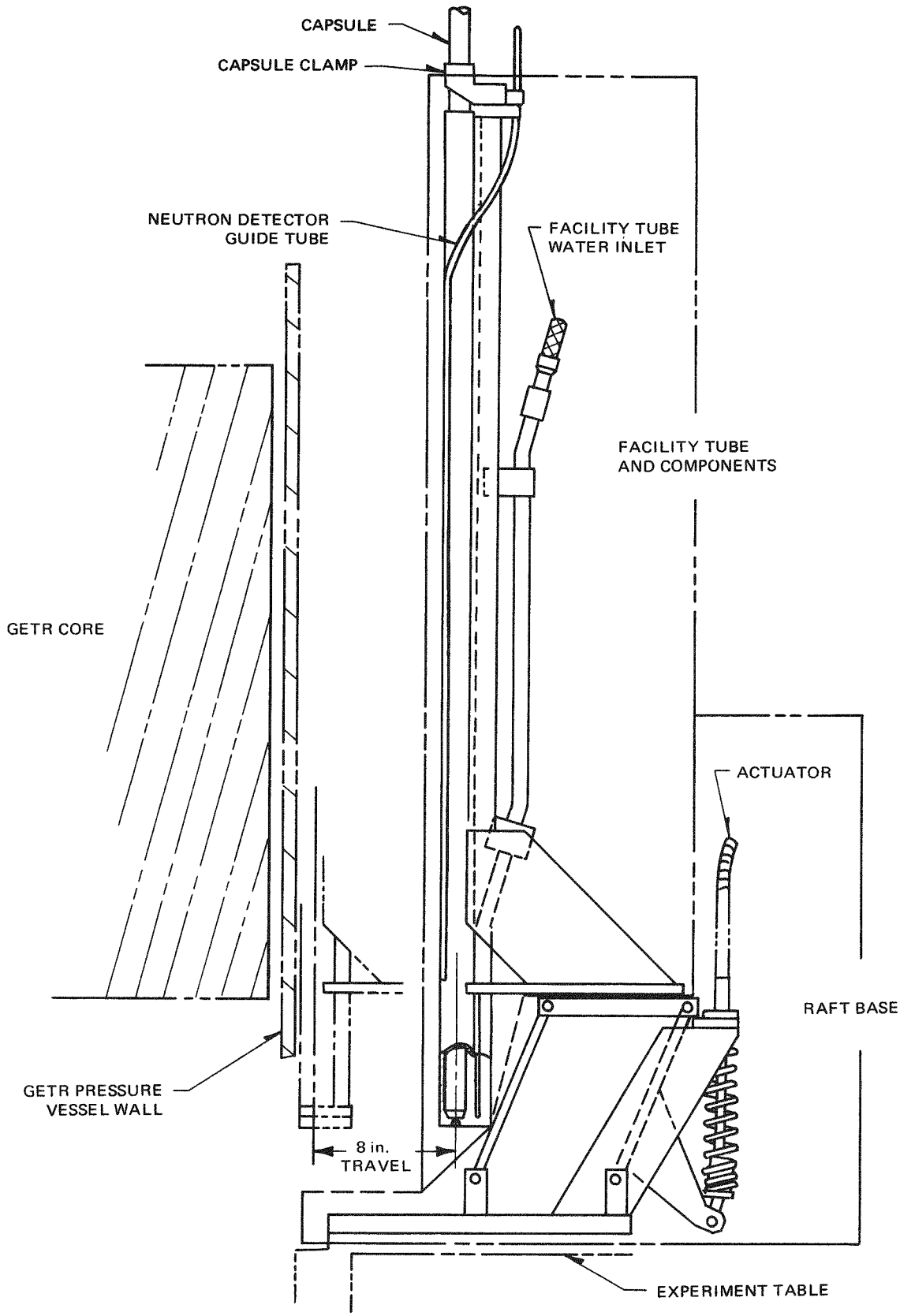

Figure 6.3-31. Radially Adjustable Facility Tube (RAFT) – Model Mark VII

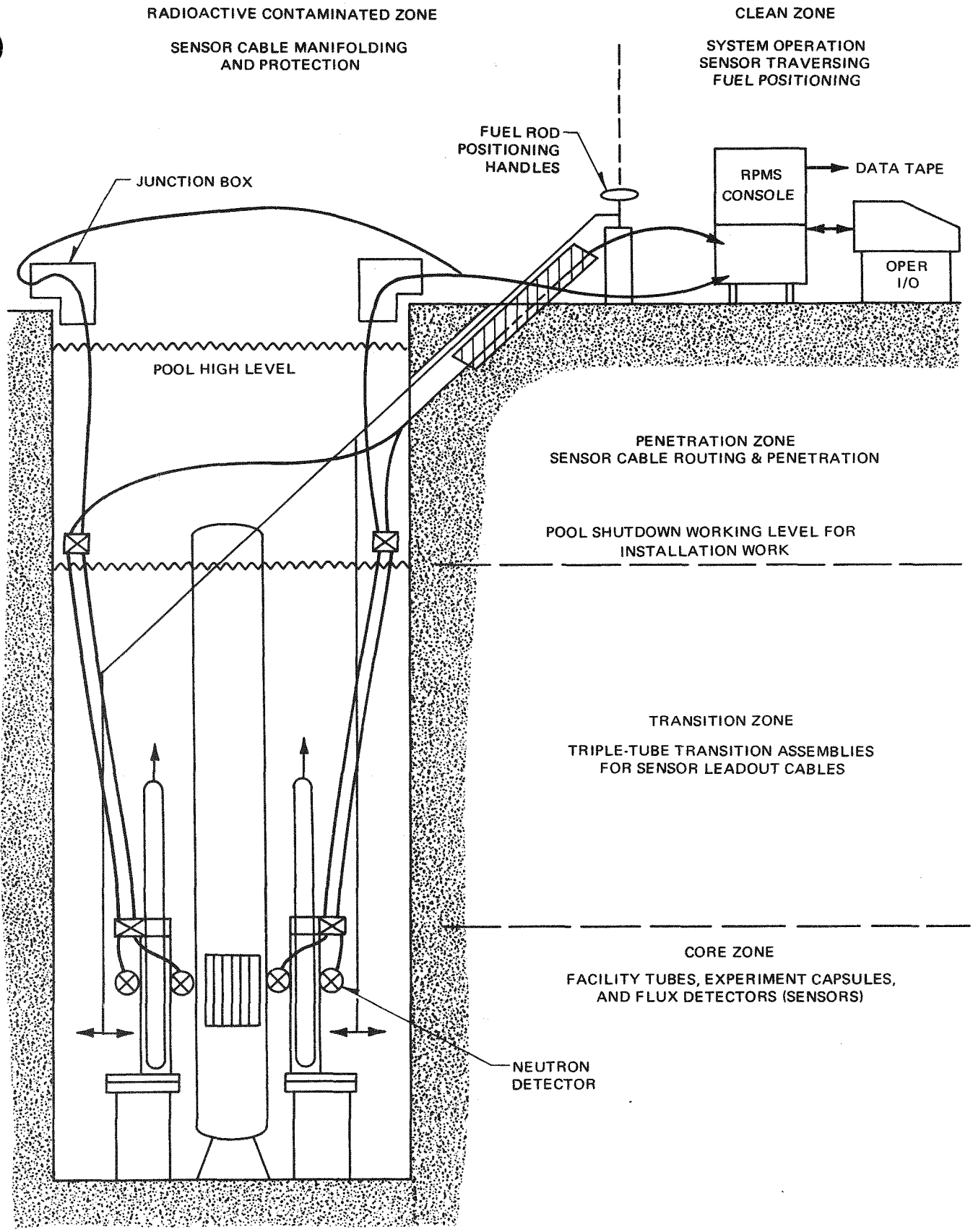

Figure 6.3-32. Schematic Diagram of GETR Ramp Test Facility

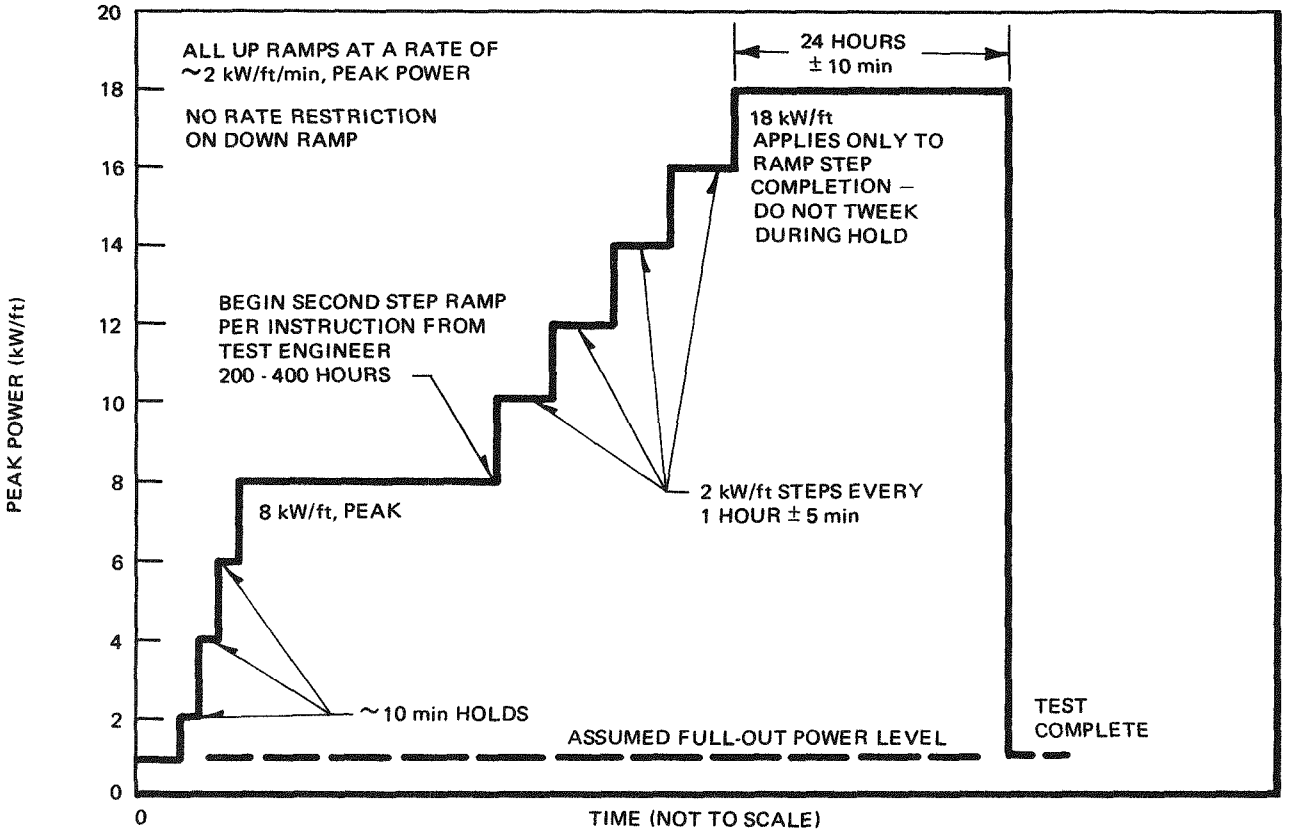

Figure 6.3-33. SRP Segment Test Sequence

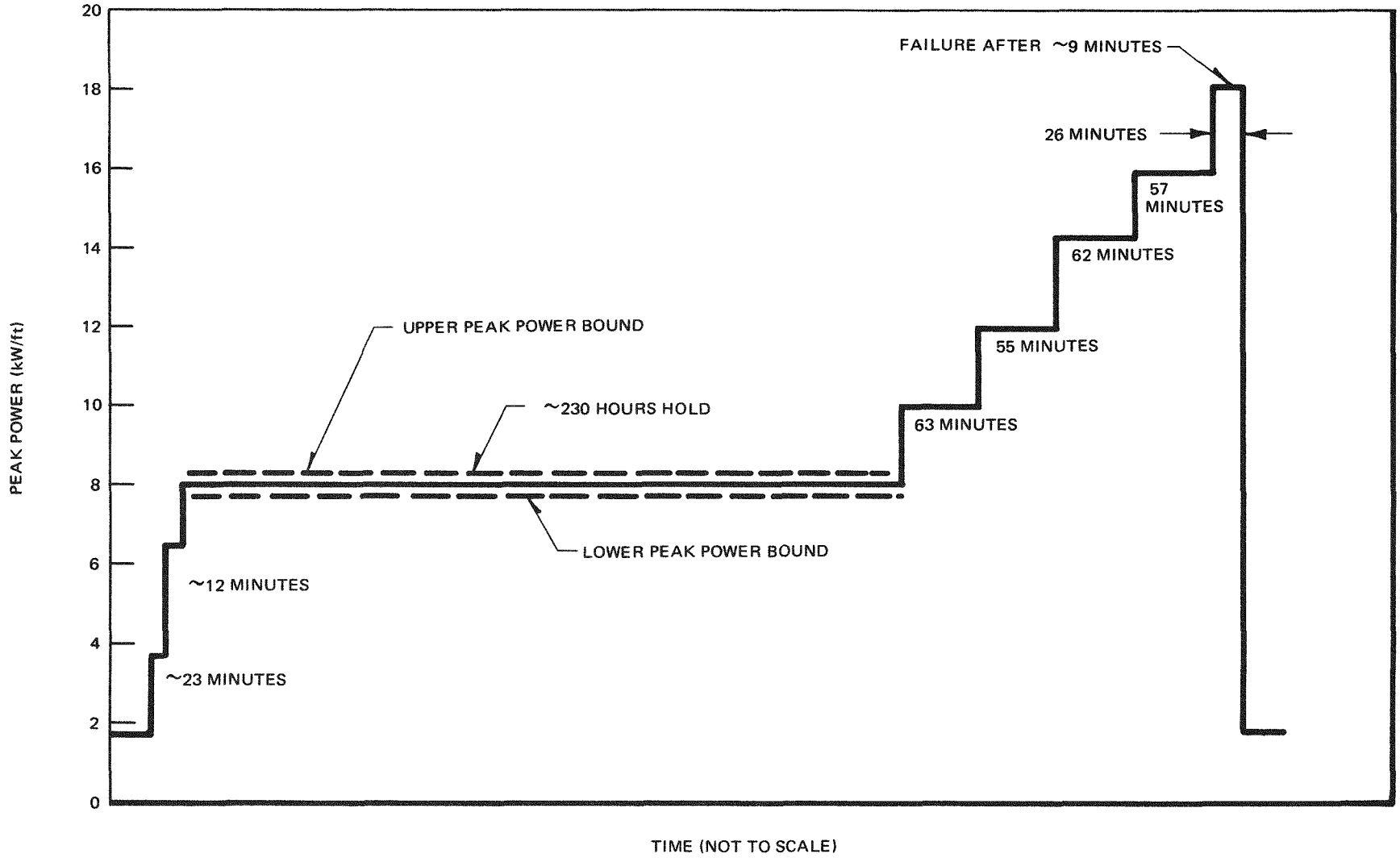

Figure 6.3-34. SRP 3/28 Ramp History

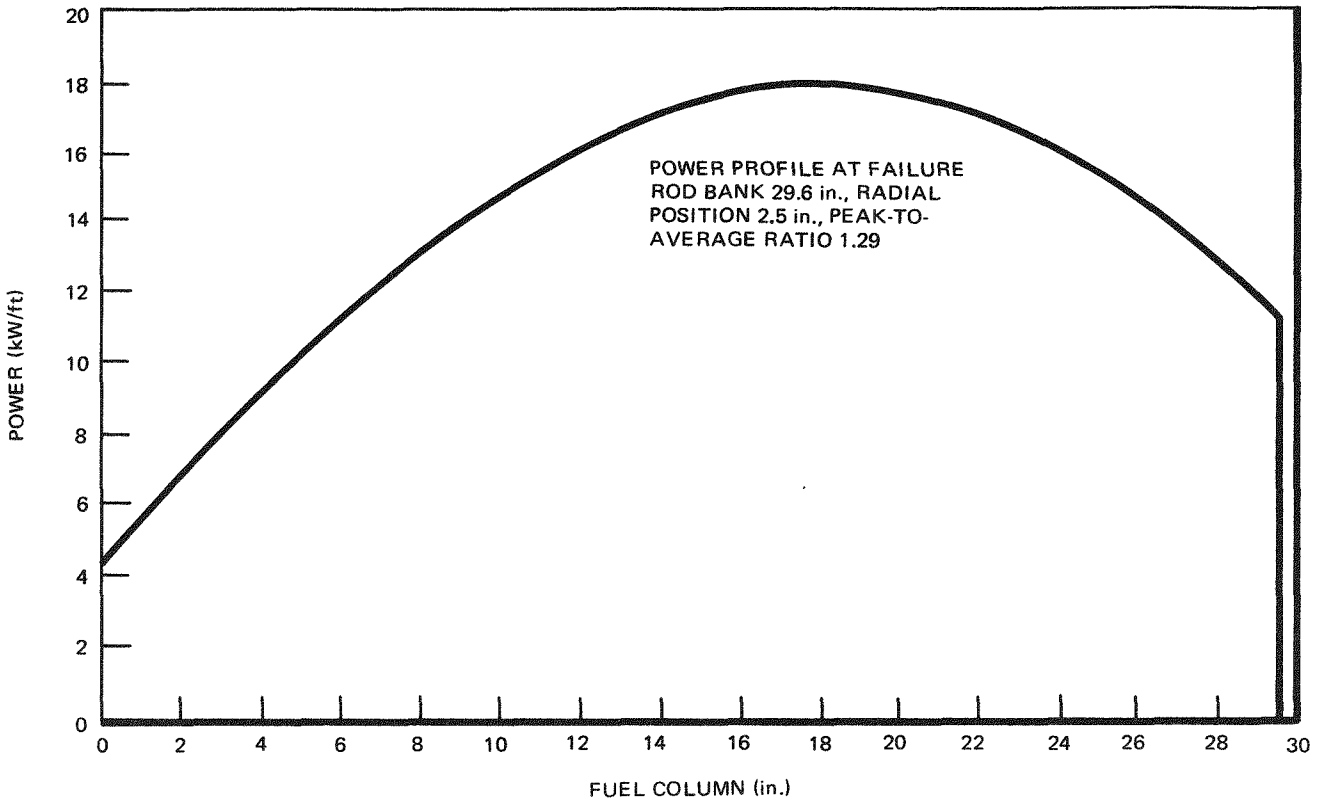

Figure 6.3-35. SRP-3/28 Power Profile (Approximate)

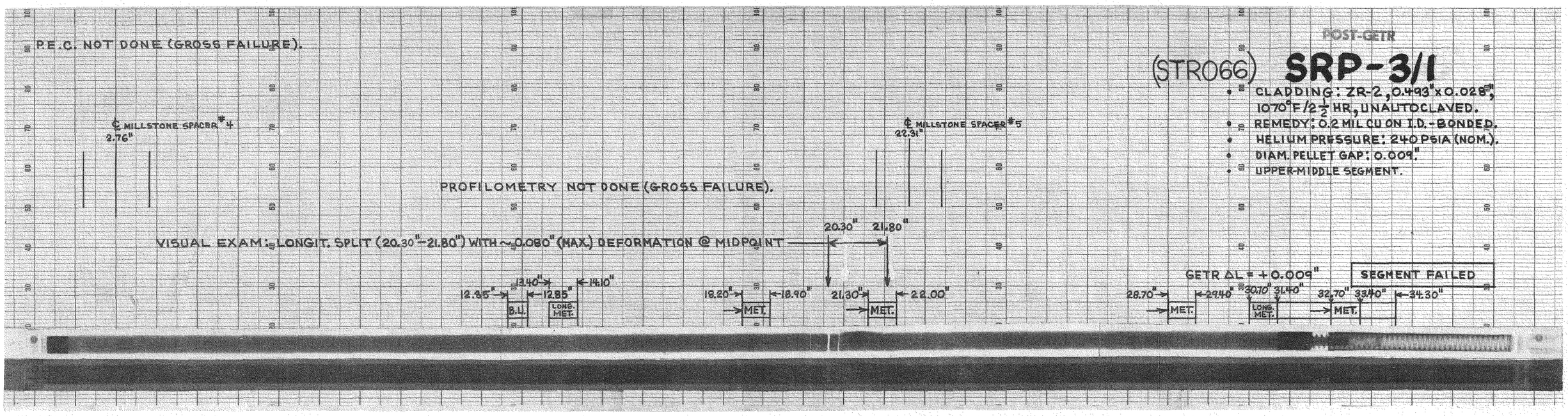

Figure 6.3-33. Post-Irradiation Examination Summary – SRP-3/1

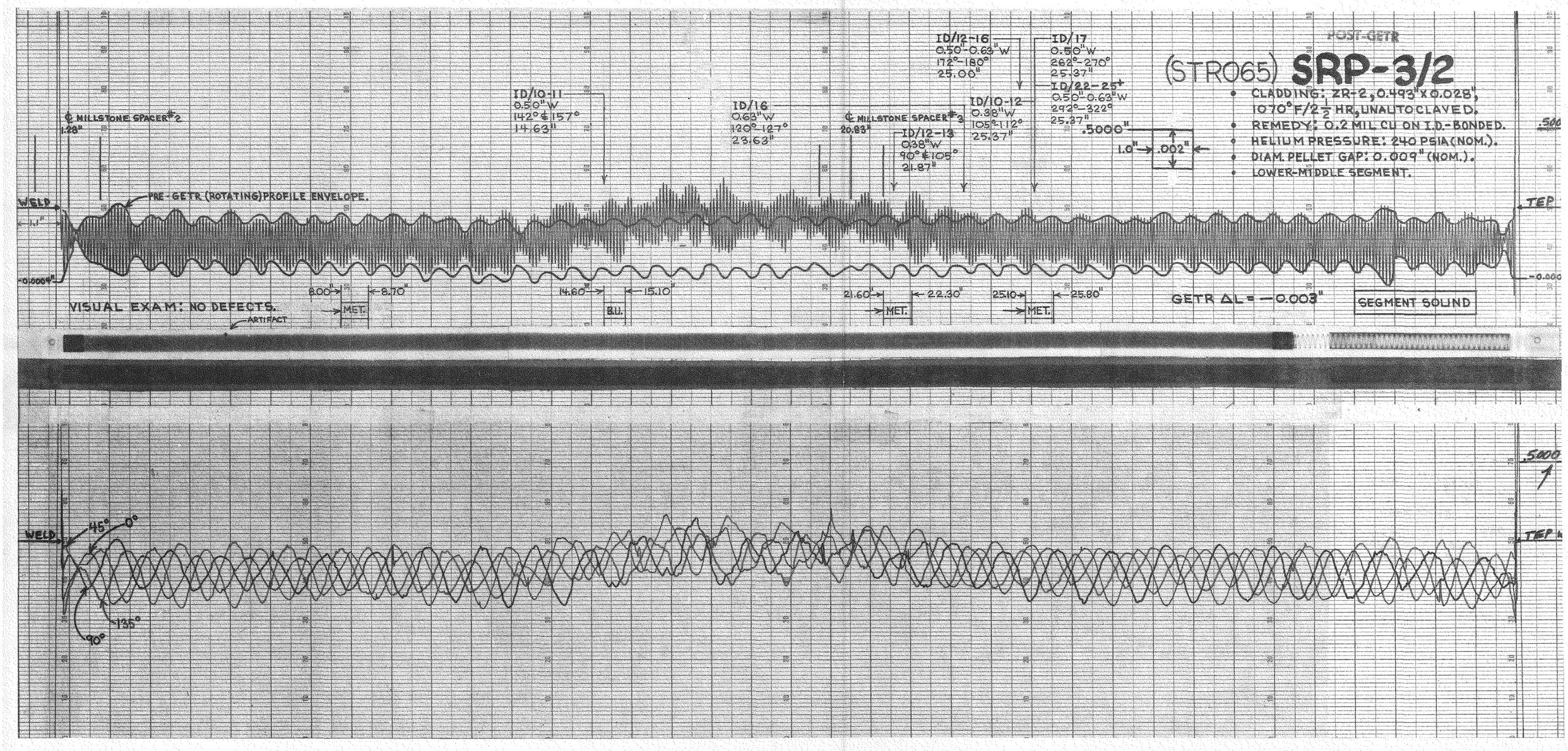

Figure 6.3-37. Post-Irradiation Examination Summary — SRP-3/2

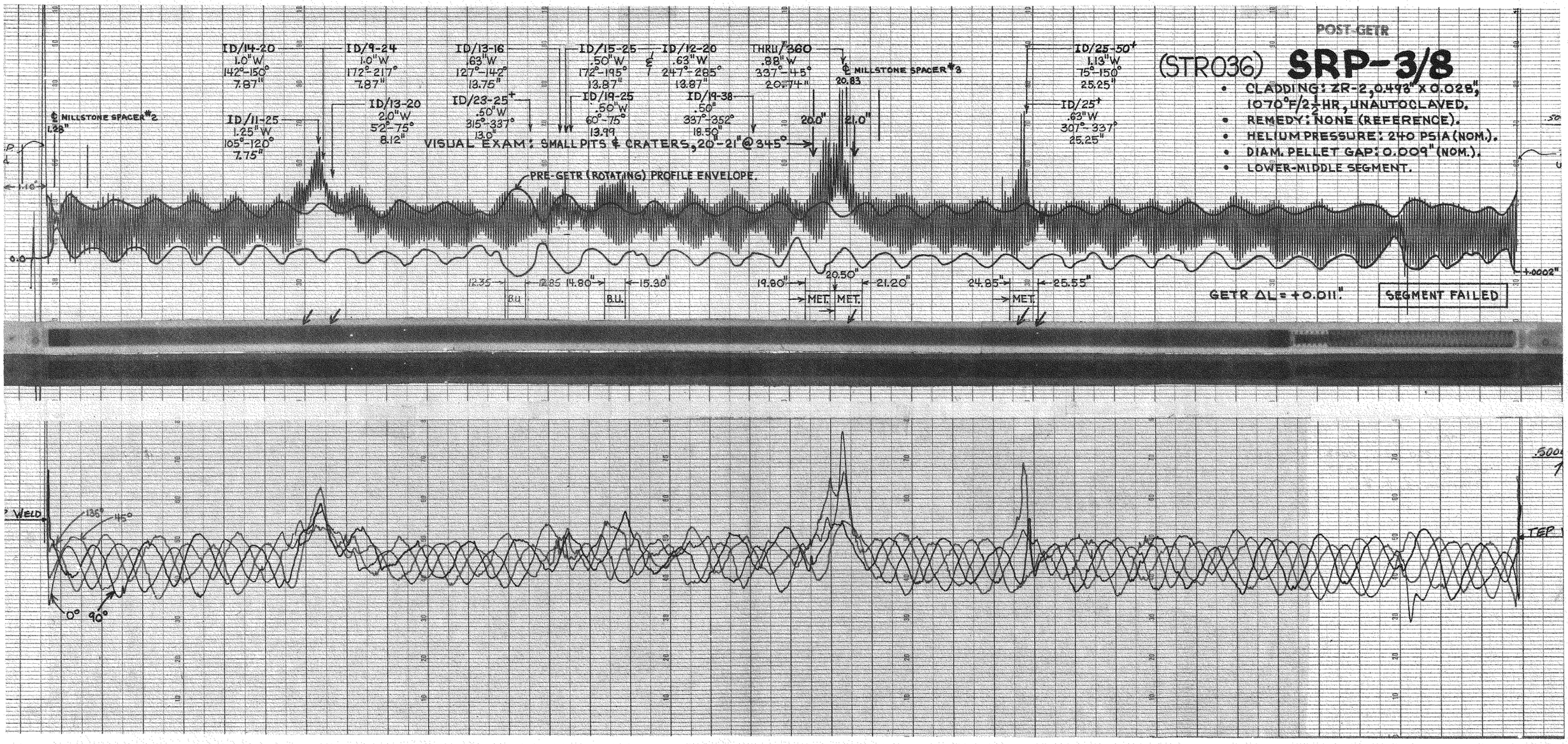

Figure 6.3-38. Post-Irradiation Examination Summary — SRP-3/8

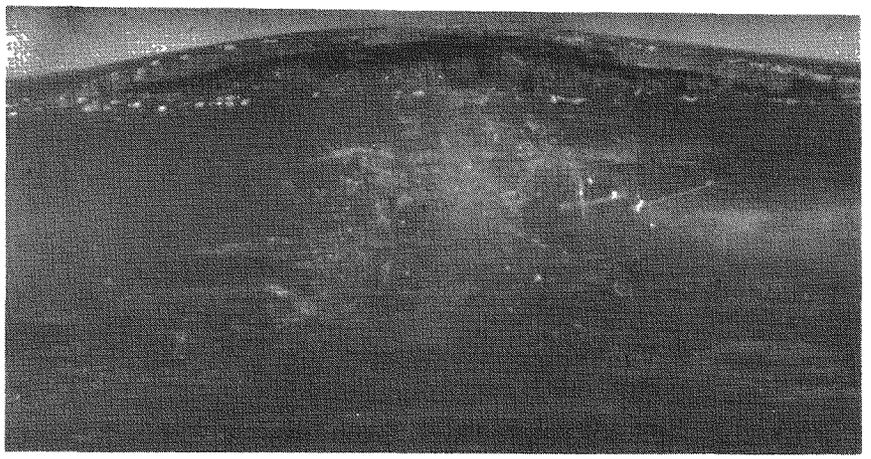

21

73639

(a) VISUAL EXAMINATION PHOTOGRAPH SHOWING HIGH-STRAIN FAILURE

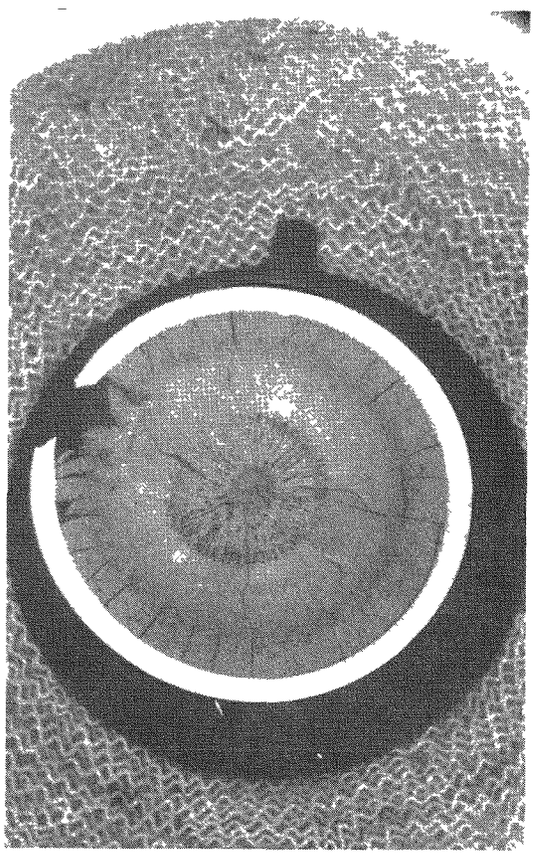

C155-01
~4X

(b) PHOTOMACROGRAPH OF SECTION THROUGH HIGH-STRAIN FAILURE REGION

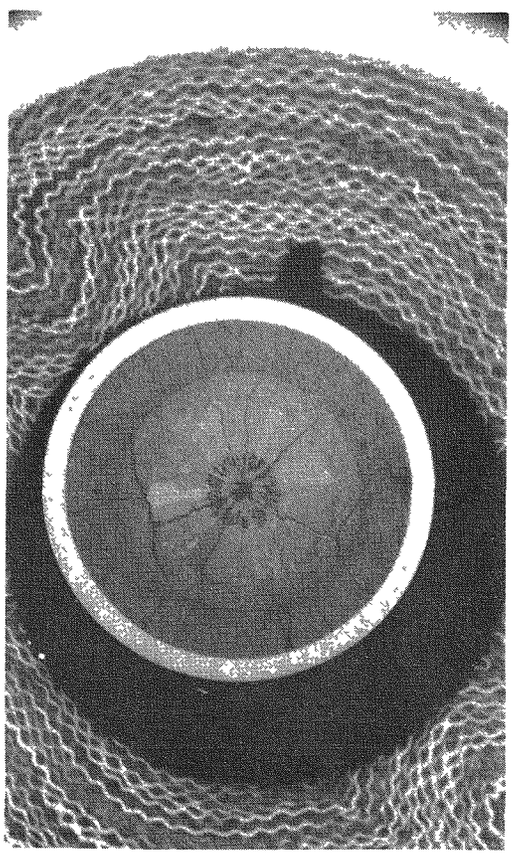

C154-01
~4X

(c) PHOTOMACROGRAPH OF SECTION THROUGH INTACT REGION.

Figure 6.3-39. Post-Irradiation Examination Photographs of SRP-3/1 (0.2-mil bonded copper barrier; experiment affected by rod bow)

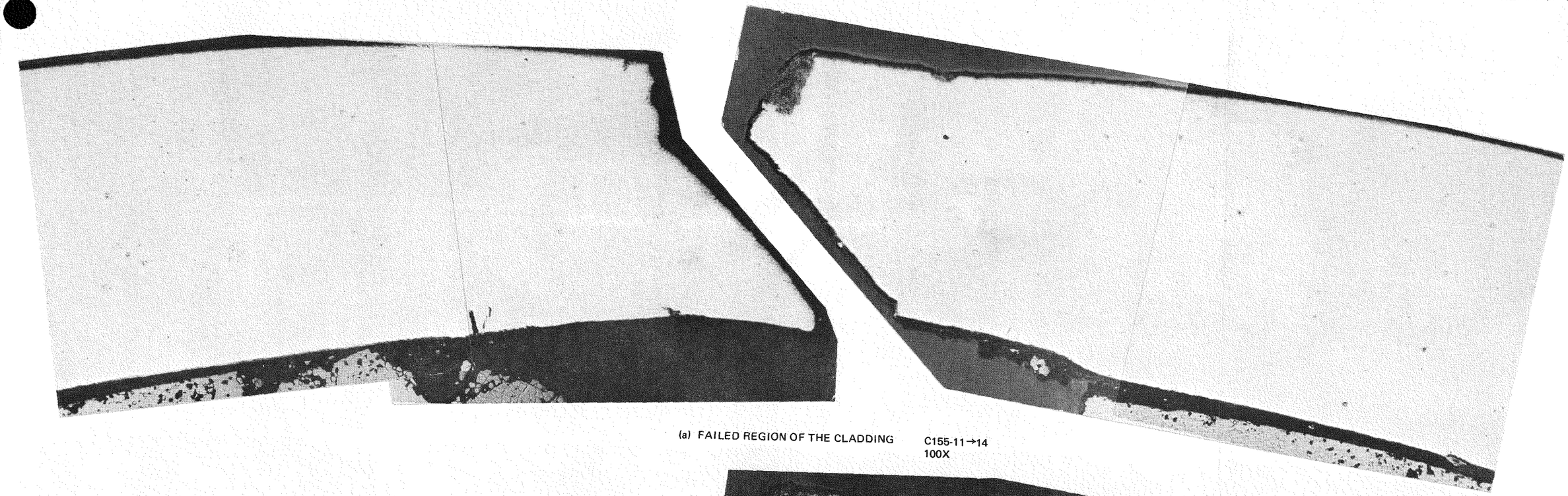

(a) FAILED REGION OF THE CLADDING C155-11→14 100X

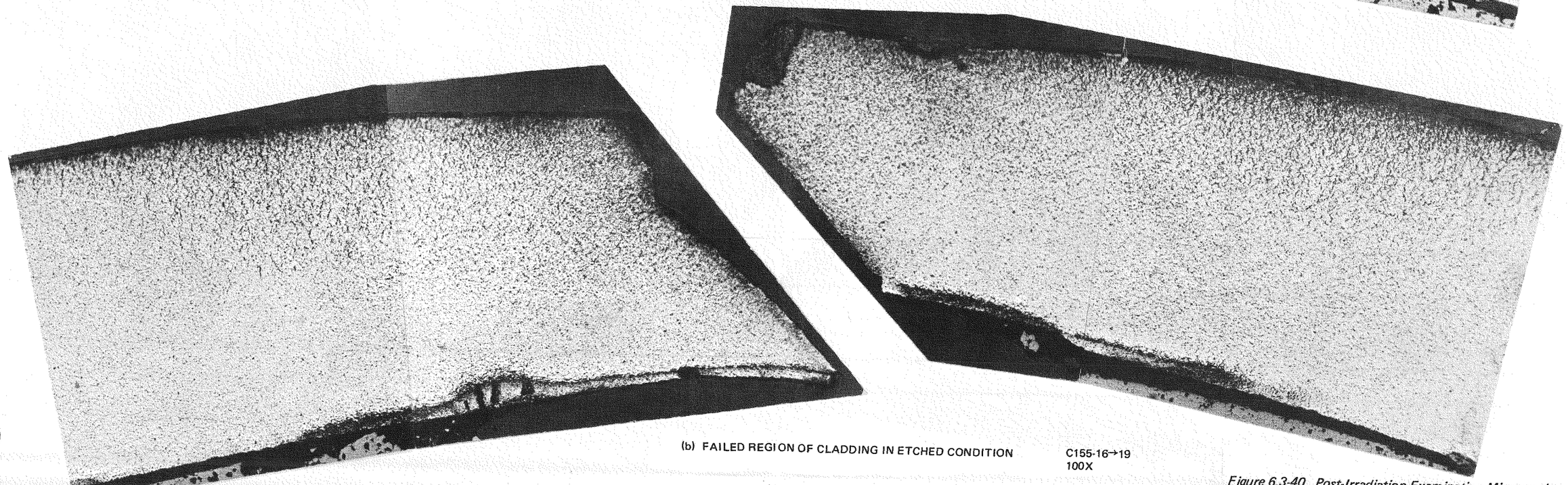

(b) FAILED REGION OF CLADDING IN ETCHED CONDITION C155-16→19 100X

Figure 6.3-40. Post-Irradiation Examination Micrographs of SRP-3/1 (0.2-mil bonded copper barrier; experiment affected by rod bow)

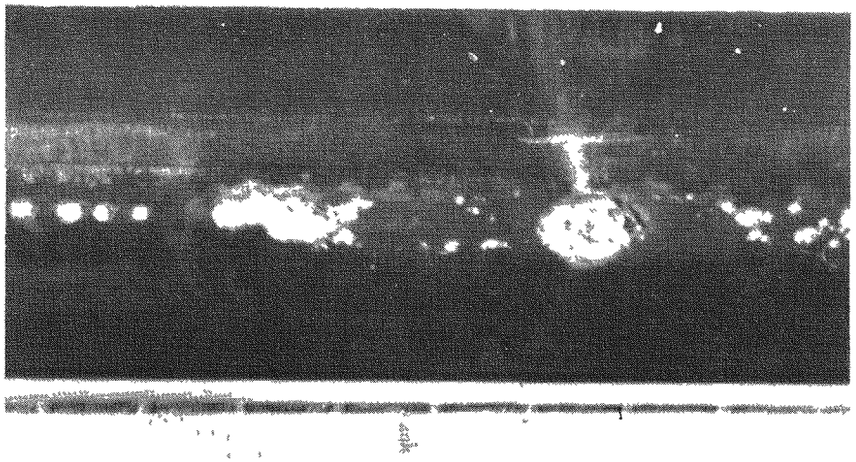

20 21

(a) VISUAL EXAMINATION PHOTOGRAPH SHOWING AXIALLY ALIGNED PITS/CRATERS 74755

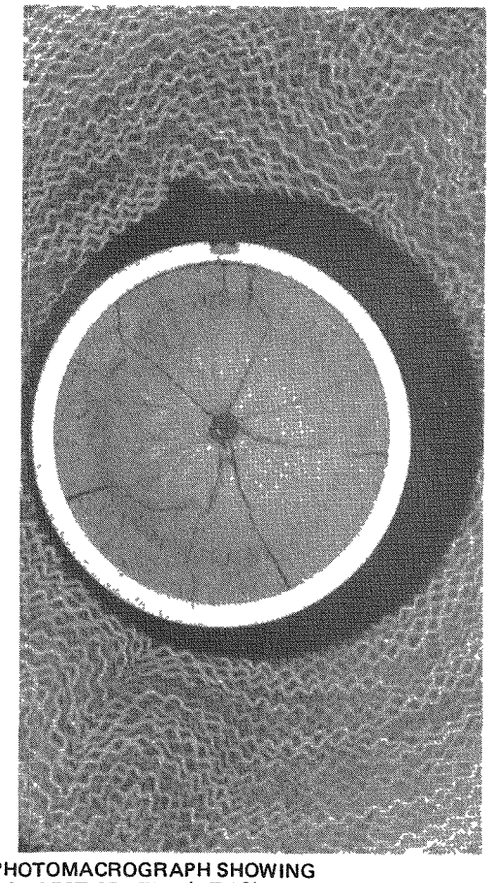

(b) PHOTOMACROGRAPH SHOWING LARGEST CRATER (AT 0°) C167-01 ~ 4X

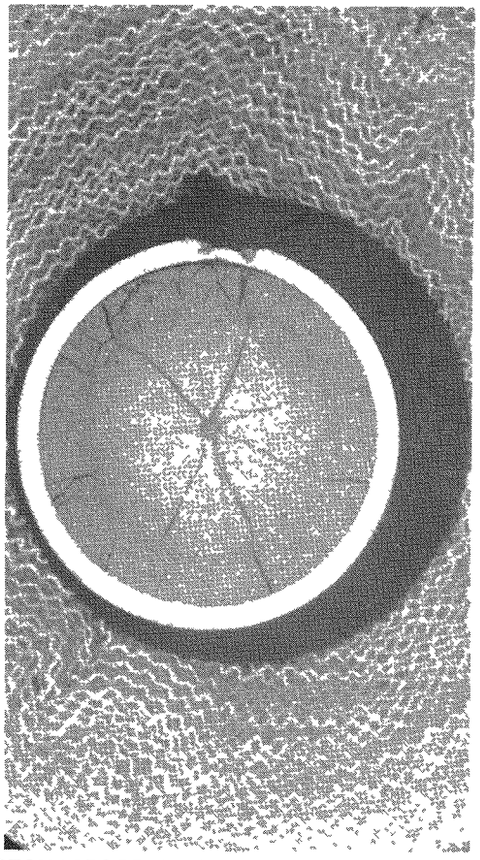

(c) PHOTOMACROGRAPH SHOWING LARGEST CRATER AFTER REMOVAL OF 0.074 INCH C167-11 ~4X

Figure 6.3-41. Post-Irradiation Examination Photographs of SRP-3/8 (reference, failed rod)

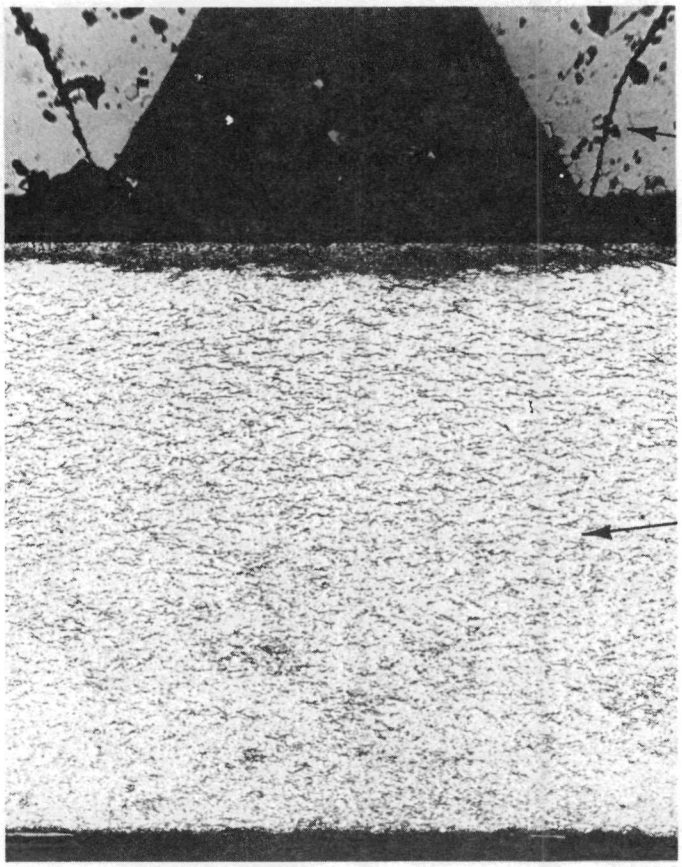

C153-09
100X

(a) HYDRIDE CASE ON INSIDE OF CLADDING

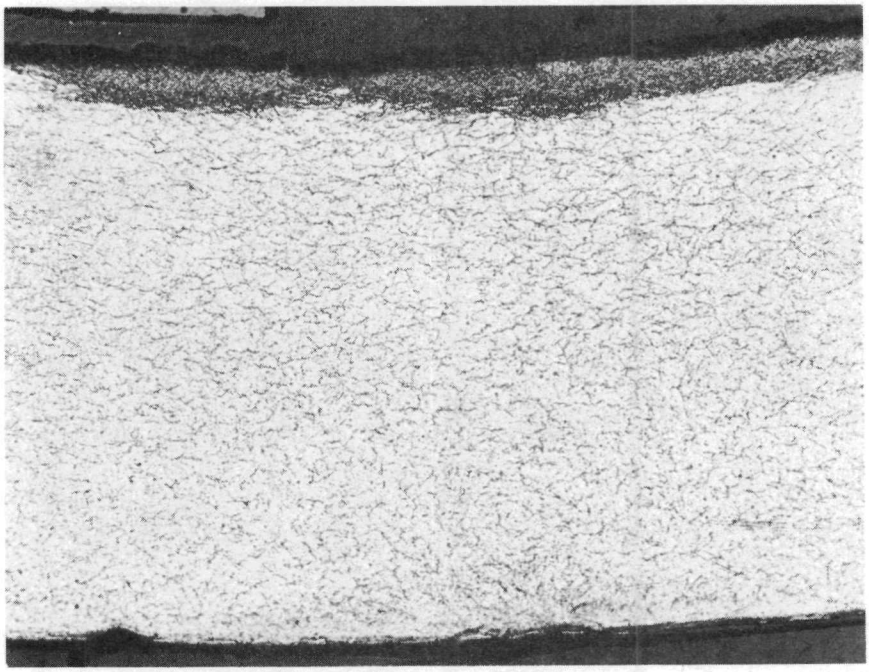

C156-08
100X

(b) HYDRIDE CASE ON INSIDE OF CLADDING

Figure 6.3-42. Post-Irradiation Examination Micrographs of SRP-3/1 (0.2-mil bonded copper barrier, failed rod)

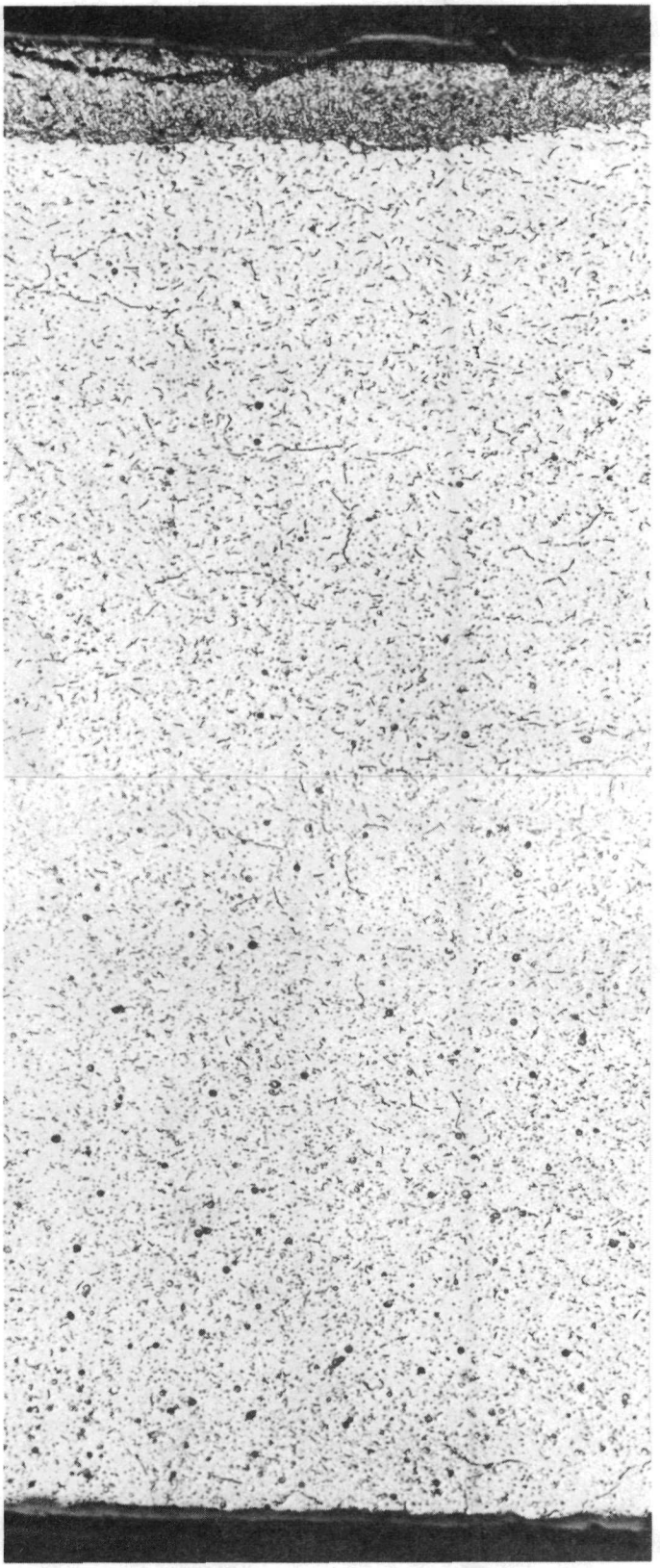

HYDRIDE CASE AND CIRCUMFERENTIAL CRACKING ALONG INSIDE OF CLADDING AND GENERAL HYDRIDING ACROSS THE CLADDING

C158-14, 15
250X

Figure 6.3-43. Post-Irradiation Examination Micrograph of SRP-3/1 (0.2-mil bonded copper barrier, failed rod)

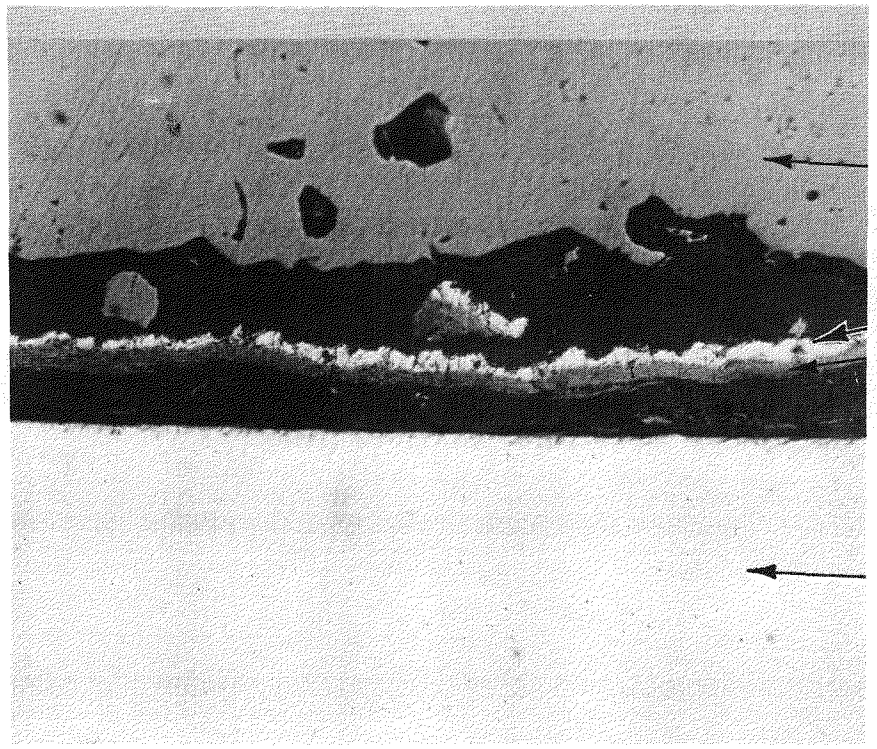

C155-04
500X

TYPICAL APPEARANCE OF DELAMINATED COPPER LAYER

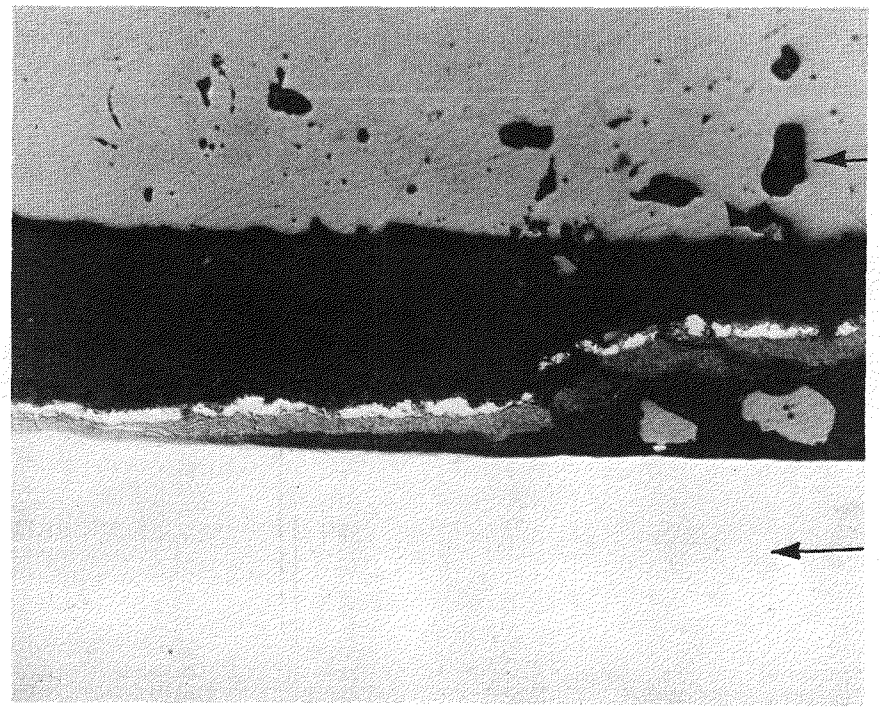

C155-05
500X

(b) TRANSITION OF COPPER LAYER FROM ADHERENT TO DELAMINATED

Figure 6.3-44. Post-Irradiation Examination Micrographs of SRP-3/1 (0.2-mil bonded copper barrier, failed rod)

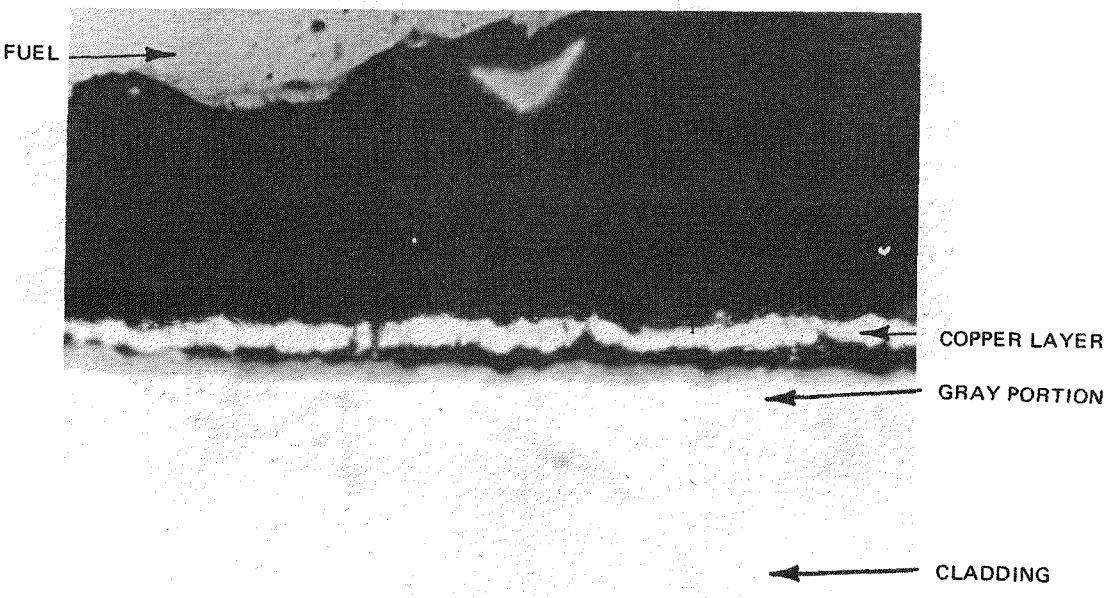

(a) MINOR DELAMINATION OF COPPER LAYER

C162-02
1000X

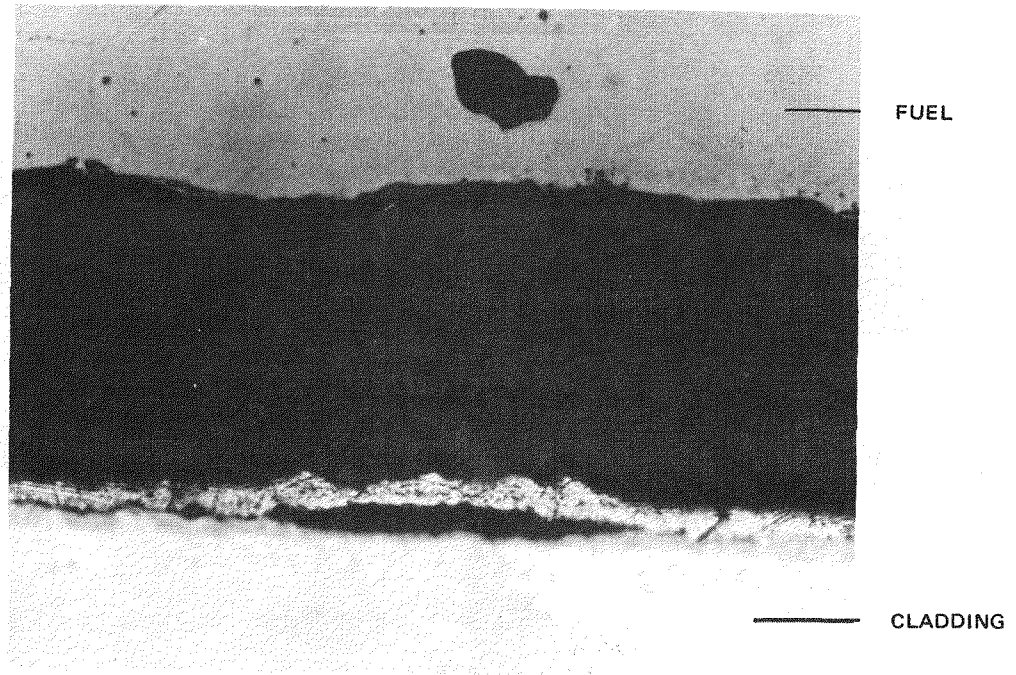

(b) MINOR DELAMINATION OF COPPER LAYER, APPEARING MORE BLISTER-LIKE

C162-03
1000X

Figure 6.3-45. Post-Irradiation Examination Micrographs of SRP-3/2 (0.2-mil bonded copper barrier, sound rod)

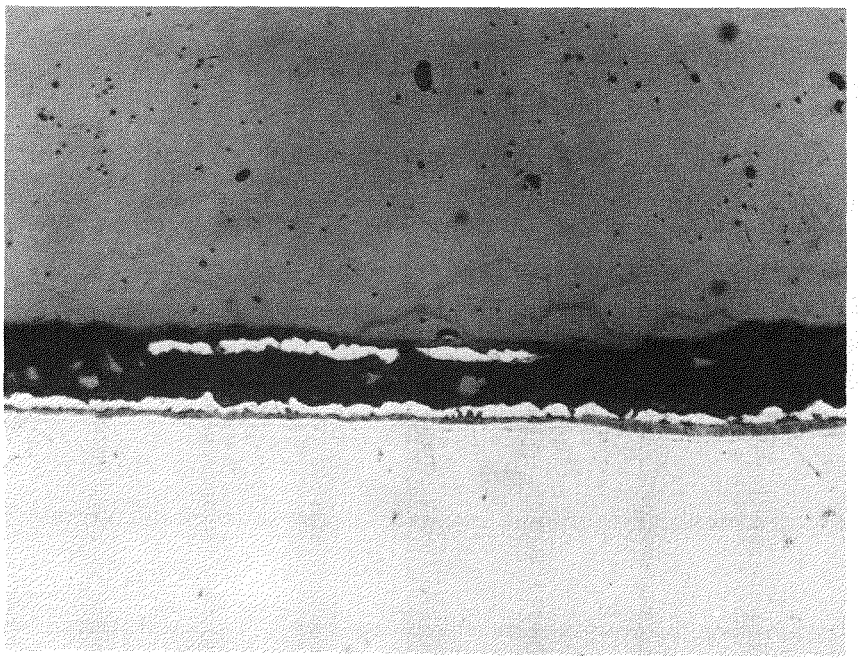

COPPER ON FUEL WHICH WAS REMOVED FROM INSIDE SURFACE OF CLADDING IN A DIFFERENT AXIAL LOCATION

C162-08
500X

Figure 6.3-46. Post-Irradiation Examination Micrographs of SRP-3/2 (0.2-mil bonded copper barrier, sound rod)

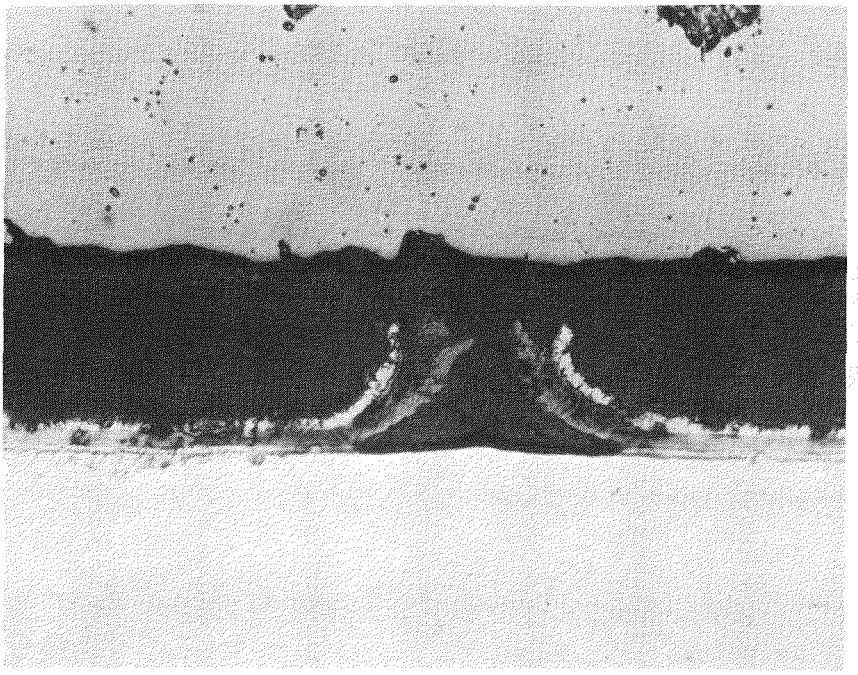

RUPTURE IN THE COPPER LAYER

C156-03
500X

Figure 6.3-47. Post-Irradiation Examination Micrograph of SRP-3/1 (0.2-mil bonded copper barrier, failed rod)

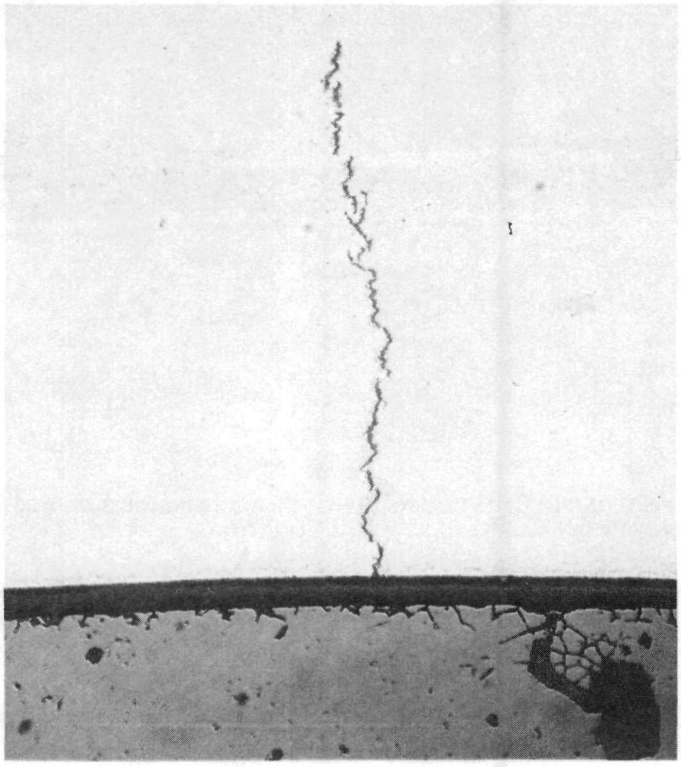

Figure 6.3-48. PCI Crack at Peak Power Location in Failed Reference Rod, SRP-3/12

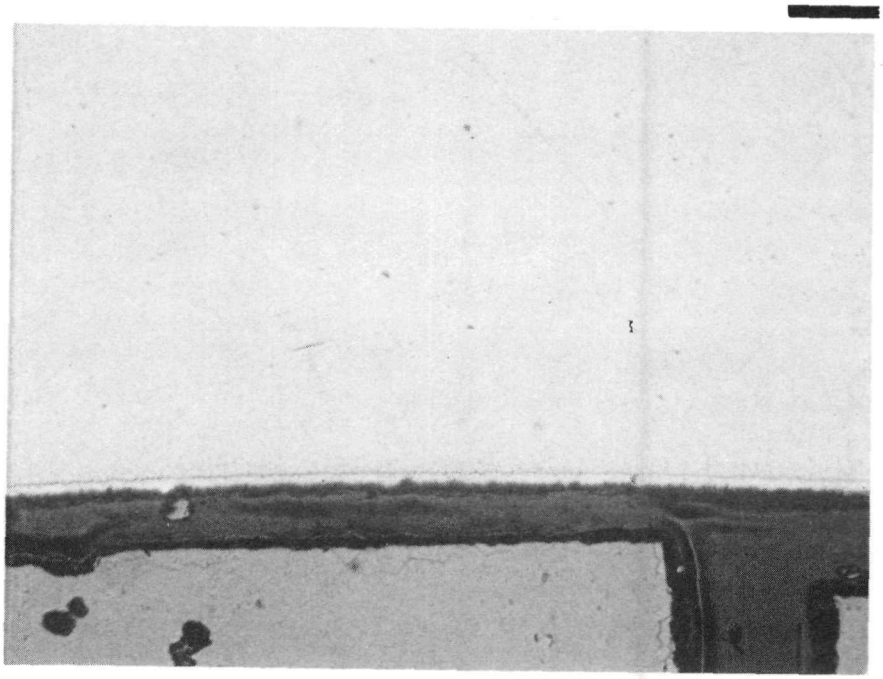

(a) 0.2 MIL UNBONDED Cu-BARRIER (SRP-3/13) C 230-21

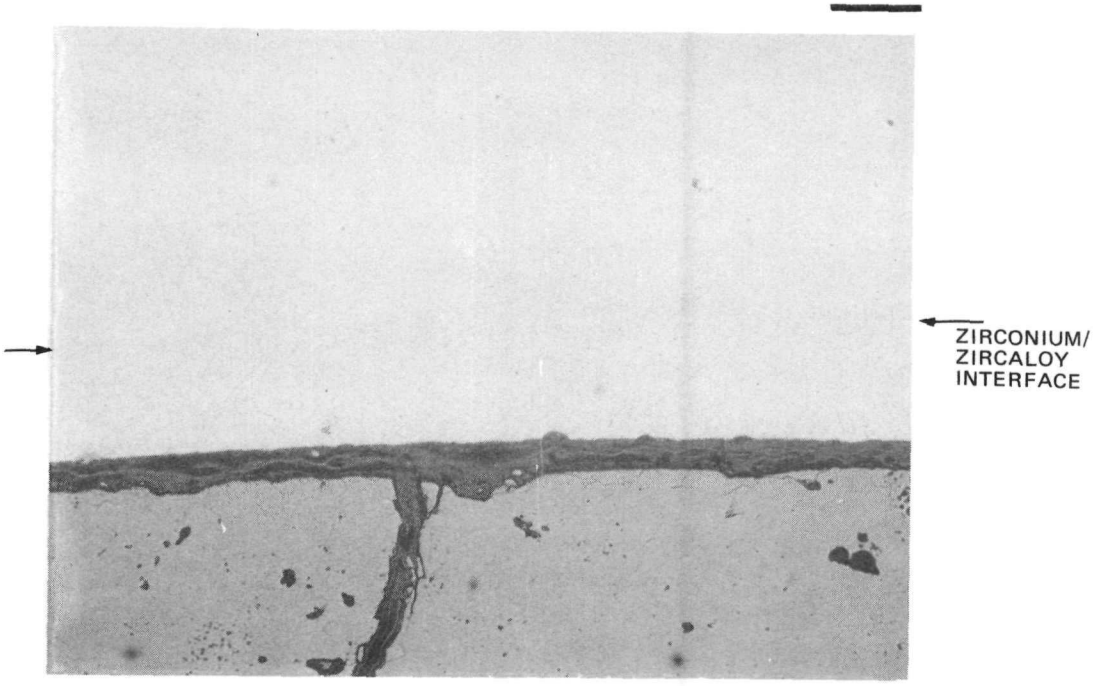

(b) Zr-LINER (SRP-3/17) C 245-13

Figure 6.3-49. Typical Appearance of Cu-Barrier and Zr-Liner at Peak Power Locations in Sound Remedy Rods 250X

7. PROGRESS IN CURRENT REPORT PERIOD – PART 3. LEAD TEST ASSEMBLIES

7.1 Task 1.0 DESIGN AND LICENSING (J. A. Baumgartner, BWRSED)

7.1.1 Design Approach

The Cu-barrier and Zr-liner LTA's are basically standard retrofit 8x8 bundles incorporating special cladding and two special segmented rods per bundle. The segmented rods are included to facilitate post-irradiation examination of barrier fuel rods. The short segments can be shipped more easily, ramp tested if desired, and readily accommodated in hot cells.

Nominal mechanical design characteristics of the barrier LTA's are listed in Table 7.1-1. The bundle lattice, showing the segmented rod locations and the distribution of fuel rod enrichments, is shown in Figure 7.1-1. The bundle average enrichment and individual rod enrichments are the same as the standard 2.82% enrichment reload bundles they will replace as part of the Quad Cities-1, Cycle 5 reload.

Standard bundle components used in the LTA design consist of:

1. Upper Tie Plate
2. Lower Tie Plate
3. Spacers
4. Water Rods
5. Expansion Springs, Finger Springs, Tie Rod Nuts, Lock Tab Washers
6. Fuel Rod: End Plugs, Retainer Assembly, Pellets

Special LTA design features are:

1. Fuel Rod Cladding – Cu-barrier or Zr-liner cladding is the prime characteristic of interest in the LTA's. Details of the materials and dimensions for each of the four LTA's are described in Figure 7.1-2. Overall dimensions of the LTA cladding are identical to standard fuel rod cladding.

2. Segmented Rods – Each LTA contains two segmented rods in the locations shown in Figure 7.l-1. The segmented rods consist of:

   a. Fuel Segments (four per rod) – See Figure 7.1-3.

   b. Upper extension plug.

   c. Lower extension plug.

   The segmented rods are assembled by screwing these components together (Figure 7.1-4). The extension plugs are designed to provide the same interface with the tie plates as the end plugs on full-length fuel rods.

Table 7.1-1
BARRIER LTA DESIGN CHARACTERISTICS

Number of Fuel Rods/LTA:	
Full Length	60
Segmented	2
Rod Pitch, in.	0.640
Fuel Rod Diameter, in.	0.483
Cladding Thickness (with Barrier), in.	0.032
Cu-Barrier Thickness, in.	0.0004
or	
Zr-Liner Thickness, in.	0.003
Pellet Diameter, in.	0.410
Active Fuel Length, in.	
Full-Length Rods	145.2[a]
Segments (Four/Rod)	29.63[b]
Fuel Rod Prepressurization, (helium) psig	30
Number of Water Rods	2
Water Rod Diameter, in.	0.591
Water Rod Wall Thickness, in.	0.030
Number of Spacers	7

[a] Includes 6 inches of natural uranium at each end

[b] Enriched uranium: segments also contain 0.5 inch of $HfO_2-Y_2O_3$ at each end of the fuel column

7.1.2 Design Analyses Results

Thermal and mechanical analyses, consistent with the generic analyses of standard fuel rods, were performed on both full-length and segmented Barrier LTA fuel rods. Results indicate that all applicable design limits are satisfied for the most-limiting LTA fuel rod geometry and expected operating history. No special operating restrictions will, therefore, be required from thermal or mechanical considerations.

Nuclear analyses were performed to assess the impact of the copper-barrier on nuclear performance of the Cu-barrier LTA's, and the effects of the segmented rods on local and radial peaking in all four LTA's. The zirconium liner will have no discernible effect on the bundle nuclear performance, while the copper barriers will cause up to a 0.6% increase in the maximum local peak-to-average (P/A) rod power at the Beginning-of-Life (BOL), and a decrease of 0.15% in the bundle neutron infinite multiplication factor, k_∞.

The analyses further demonstrate that the hafnia pellets in the segmented fuel rods will have an adverse effect on radial power distributions. At certain BOL in-channel void conditions, the presence of hafnia pellets could cause up to a 7.2% increase in maximum local P/A power. However, this effect will be countered by a decrease in the total bundle power of up to 6.8% in the same axial plane of the hafnia pellets. The conclusion from these analyses is that the barrier LTA's will perform in a manner very similar to the standard 2.82% enrichment reload bundles.

WIDE-WIDE CORNER GAP

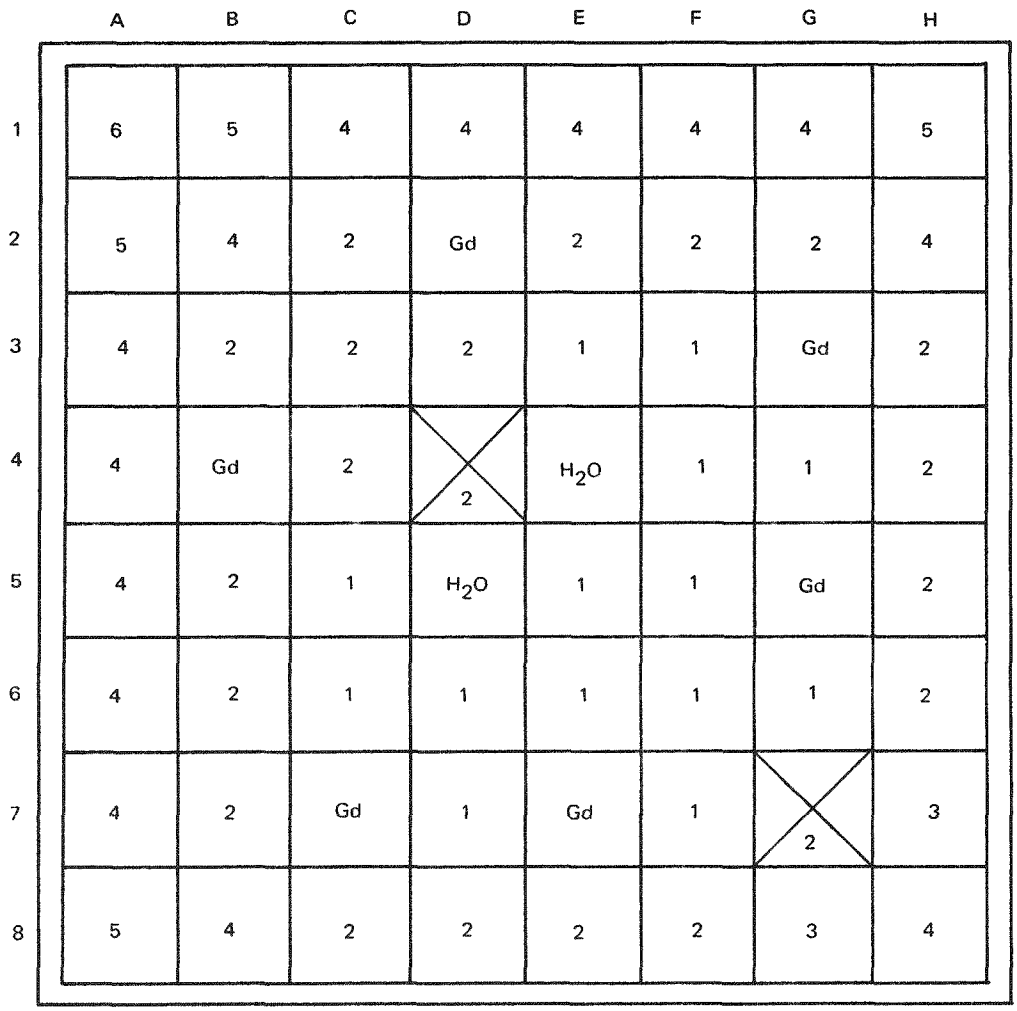

ROD TYPE	U-235 (wt%)	Gd_2O_3 (wt%)	NUMBER OF RODS
1	3.8	–	14
2	3.0	–	21
3	2.4	–	2
4	2.0	–	14
5	1.7	–	4
6	1.3	–	1
Gd	3.0	2.0	6
H_2O	WATER RODS	–	2

⊠ = SEGMENTED ROD POSITIONS

Figure 7.1-1. Cross Section of 2.82% Average Enrichment, 6 Gd_2O_3 Rod Bundle 8DRL282-6G2.0

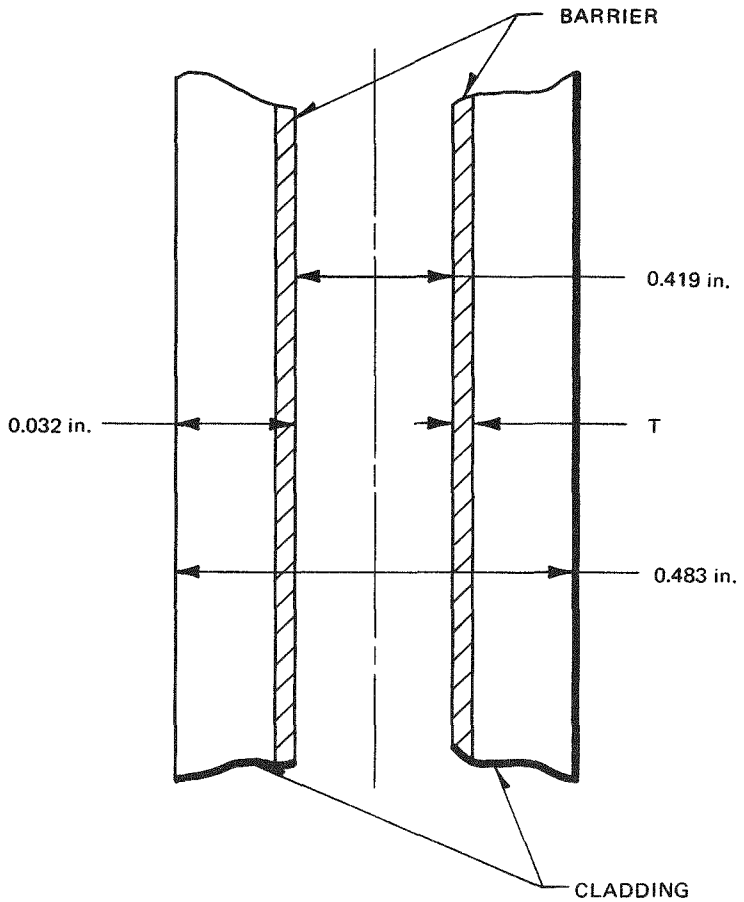

NUMBER	CLADDING	BARRIER	
		MATERIAL	THICKNESS, T (in.)
1	ZIRCALOY-2 (NON-AUTOCLAVED)	Cu	0.0004
2	ZIRCALOY-2 (AUTOCLAVED)	Cu	0.0004
3	ZIRCALOY-2	CRYSTAL BAR ZIRCONIUM	0.003
4	ZIRCALOY-2	LOW 0_2 SPONGE ZIRCONIUM	0.003

Figure 7.1-2. Lead Test Assembly Barrier Configuration

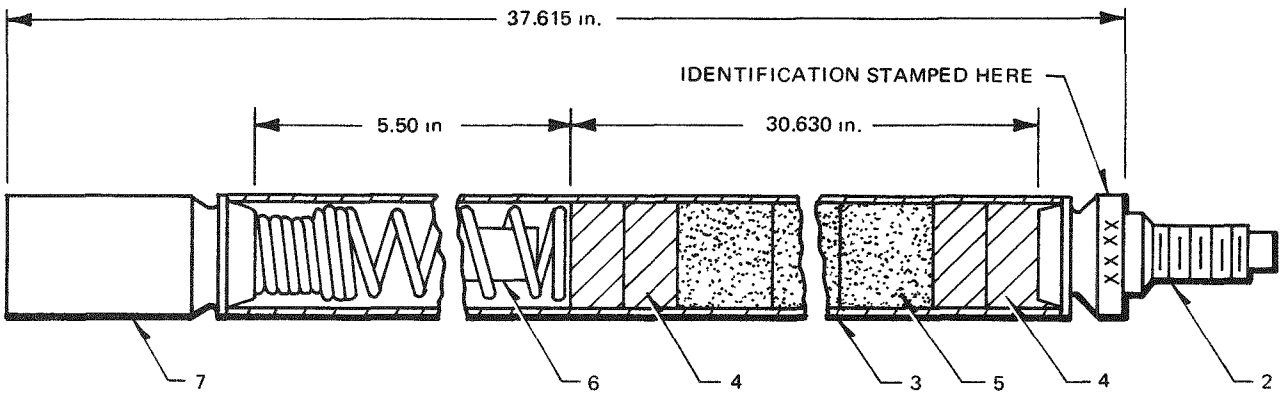

(1) SEGMENT ASSEMBLY

2	LOWER END PLUG	5	FUEL PELLETS
3	CLADDING	6	RETAINER ASSEMBLY
4	HfO_2-Y_2O_3 PELLETS	7	UPPER END PLUG

Figure 7.1-3. Fuel Segment

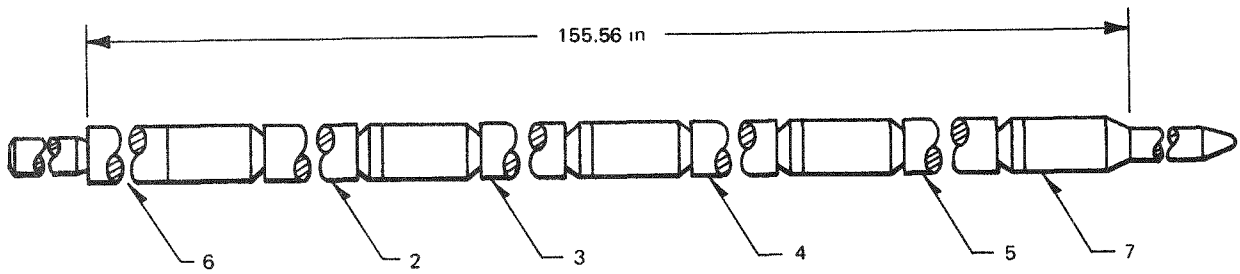

(1) SEGMENTED ROD ASSEMBLY

2)
3)
4) FUEL SEGMENTS
5)

6 UPPER EXTENSION PLUG
7 LOWER EXTENSION PLUG

Figure 7.1-4. Segmented Rod

7.2 TASKS 2.0 AND 3.0. FABRICATION/CHARACTERIZATION AND QUALITY ASSURANCE (R.E. Donaghy, R.S. Moore and C.D. Williams, WMD)

7.2.1 Cu-Barrier

Prior to the start of this program procedures for producing Cu-Barrier fuel using the electroless plating of copper had already been developed. Fuel rod segments for use in the Collapsed Clad and the Segmented Fuel Rod Irradiation Tests (see Subsections 6.2 and 6.3) had already been successfully fabricated. Such fuel segments, approximately 3 feet long, had been made in both basic configurations: (a) copper plated directly onto the Zircaloy, and (b) copper plated onto an oxidized Zircaloy surface. In both configurations, the copper was plated on the inner surface of Zircaloy-2 tubing. What remained to be done in preparation for fabrication of the Cu-barrier LTA's was to adjust the process to give uniform coverage of copper on the inner surfaces of full-length cladding tubes (approximately 14 feet long). In this report period this application of the plating procedures to full-length fuel cladding was accomplished and the resulting product is being evaluated for adherence, thickness and uniformity.

The plating procedure for the electroless plating of copper directly onto Zircaloy starts with product-line tubing after the final anneal and pickle (chemical polish) prior to the normal autoclave oxidation step. The as-pickled tubes are given the following treatments by flowing solutions through them:

a. Bifluoride etch (ammonium bifluoride, 15 g/l in a sulfuric acid aqueous solution)

b. Desmut (ultrasonic agitation or swabbing to remove loose reaction products produced by the bifluoride etch)

c. Electroless plate (MacDermid Solution 9038 at 60°C).

The procedure for plating onto oxidized Zircaloy is similar, but after the bifluoride etch and the desmut steps the tubing is oxidized in a steam autoclave (steam at 1 to 2 atm at 390°C for 14h).

The resulting oxidized surface has to be activated with a solution that promotes the nucleation of copper. The activator currently in use has the trade name Shipley 9F. This step allows continuation of the electroless plating procedure in a manner already described (similar to copper plated directly onto Zircaloy).

During the development program for copper-plating full-length Zircaloy fuel rods, a parallel effort was required to achieve a means of evaluating the plating process. Plate should have a smooth surface. Representative cross sections of the tubing are examined metallographically for determining the thickness of the plating. Four readings, 90 degrees apart, are measured and the averages of these readings are the reported values. On each tube a non-destructive thickness measurement is made using a calibrated electronic thickness tester. The tube is measured as it is moved uniformly through the coil on the tester. The electronic thickness tester is supplied with a strip chart recorder to obtain a thickness profile of the copper layer on each tube.

The electronic thickness tester is calibrated prior to use by using standards that have a thickness which has been verified by metallographic cross section. The standards consist of fuel cladding which has similar outside diameter and wall thickness as the cladding being measured. The copper thickness on the standards covers the range specified for the cladding being plated.

Adhesion is tested destructively by removing a short section (10 to 20 centimeters long) from a plated rod. This short section is cut longitudinally; a half section is clamped in a vise and bent back and fourth until fracture of the base metal occurs. The plating is examined at 1X along the fracture for signs of separation.

Copper purity must be at least 99%. One sample from each plating bath or a minimum of one sample from the beginning and end of the plating run is analyzed.

At present a workable process for plating the LTA fuel cladding has been developed. The process for plating on bare Zircaloy has been used to plate 10 full-length fuel rods of the correct dimensions for the LTA. These rods have been tested for thickness, adhesion, copper purity, and visual defects; based on this small sample, a 90% yield is expected. The process for plating on autoclaved Zircaloy has been used to plate 10 full-length fuel rods as above. These rods have been tested the same as above.

Difficulties have been encountered in plating on autoclaved Zircaloy. Blistering of the copper plate occurs when the thickness of the plate approaches 10 microns. This results in a reject rate of about 80%. Improved process techniques have enabled us to deposit 5-micron-thick copper that does not show any blistering initially. On 5 fuel rods plated with 5-micron copper, 1 rod showed blistering after 30 days and this could only be detected by microscopic (30X) examination. When the plating thickness was increased to 10 microns, no blistering was observed initially. After 30 days 4 of the 5 rods exhibited blistering, again detected by microscopic examination.

7.2.2 Zr-Liner (Coreduced) Tubing

Early exploratory work addressed material selection, billet design, extrusion techniques, and tube reduction considerations while producing small quantities of final tubing for various test purposes. Pursuit of this investigative program demonstrated the feasibility of coextrusion/coreduction as a fabrication route and achieved selection of a promising barrier material.

After earlier discussions with the vendor on a specification for coextruded tubeshells, a draft specification was issued by GE. Arrangements were made for production of six tubeshells lined with crystal bar zirconium first and six tubeshells lined with a low-oxygen sponge zirconium.

Using crystal bar zirconium on hand, the vendor melted an ingot, forged a billet, and extruded a tube hollow of crystal bar from which six "extrusion liners" were machined. Six "extrusion billets" of Zircaloy were machined to accept these liners as a close fitting sleeve inside the billet. Two of these billets were Zircaloy-4 and four were Zircaloy-2. (Zircaloy-4 was accepted as an expedient because Zircaloy-2 was then unavailable within the schedule requirements. The Zircaloy-4 will be used in process qualification but will not be used for the actual LTA.) Each assembly was then electron beam welded on each end to seal the gap between the mating components. Extrusion of these composite billets was performed in a normal manner. The coextruded tubeshells were honed on the inner surface, etched, and inspected prior to shipment to GE-WMD, Wilmington, N.C.

As a means of setting the process and parameters for fabrication of the crystal bar barrier bundle, it was decided to utilize the two Zircaloy-4 tubeshells in a documented shop run.

The starting tubeshells in this run were generally satisfactory. Minor out-of-specification dimensions were present on one; both had some inside and outside scratches and etched-over hone marks were discernible. Due to some extrusion marks on the inside, the vendor had performed significant honing and etching to improve the surface. Liner bonding appeared good. No problems were encountered with any of the cleaning or annealing operations. Tube reduction also was executed in a normal manner using standard lubricants and operating parameters.

Inspection for flaws revealed a reject rate of 14%. This is greater than that of standard Zircaloy tubing; however, for development experience the rate was quite satisfactory.

Zirconium liner bonding was good at all points of sampling and posed no problems during fabrication. Liner thickness, which started out in the tubeshell thinner than nominal, was found to fall generally around 0.003 inch on finished tubing. Uniformity of barrier thickness in tubeshells is a concern of the vendor and appears to be an area worthy of continued investigation.

Shop fabrication for these two tubeshells was completed in November 1977. While some laboratory work has yet to be finished, the performance of these tubeshells was compatible with that of previous developmental pieces to such degree that the four production tubeshells have been committed to the shop. The microstructure of the Zr-liner and the supporting Zircaloy is shown in Figure 7.2-1. Completion of tube-making activities, including inspection, is expected by late January 1978.

Shipment of six low-oxygen-sponge zirconium-lined tubeshells from the vendor is expected to be made in January 1978. Fabrication through the tubing mill is expected to start by late February and finish in late March.

7.2.3 Pre-Irradiation Characterization

The intended characterization of the LTA's prior to irradiation is shown in Table 7.2-1.

Table 7.2-1
BARRIER LEAD TEST ASSEMBLY PRE-IRRADIATION CHARACTERIZATION

Characteristic	Data	Sampling Plan
A. Fuel Pellets		
1. Vacuum H_2O Impregnation Density	Bulk density, open and closed porosity	10 pellets/enrichment
2. Microstructure	Microstructure type and average porosity size. Photographic records.	1 pellet/enrichment
3. Chemical Analysis	Normal commercial practice	Normal commercial practice
B. Tubing		
1. Ultrasonic Testing for Flaws	Strip chart records	All tubes
2. Dimensional Measurements	Inside diameter, wall thickness, ovality	All tubes
3. Plating Thickness (copper barrier)	Eddy current chart records	All tubes
4. Mechanical and Metallurgical Data	Tensile properties, elongation, liner purity (Cu), liner bonding, grain size, hydride orientation, chemical analysis, surface finish.	To be defined.
C. Fuel Rods		
1. Rod Diameter Profilometry	Helical traces recorded digitally	13 rods + 8 segments per bundle
2. Rod Length Measurements	Drawing requirement and tip-to-tip lengths	All rods and segments
3. X-ray	Plenum region	13 rods + 8 segments per bundle
4. Eddy Current and Ultrasonic Tests	Strip chart records	All rods (if schedule permits
D. Water Rods		
1. Tab Positions	Distance of each tab from bottom of rod	4 spacer-positioning water rods
2. Length	Drawing requirement and tip-to-tip lengths	8 water rods

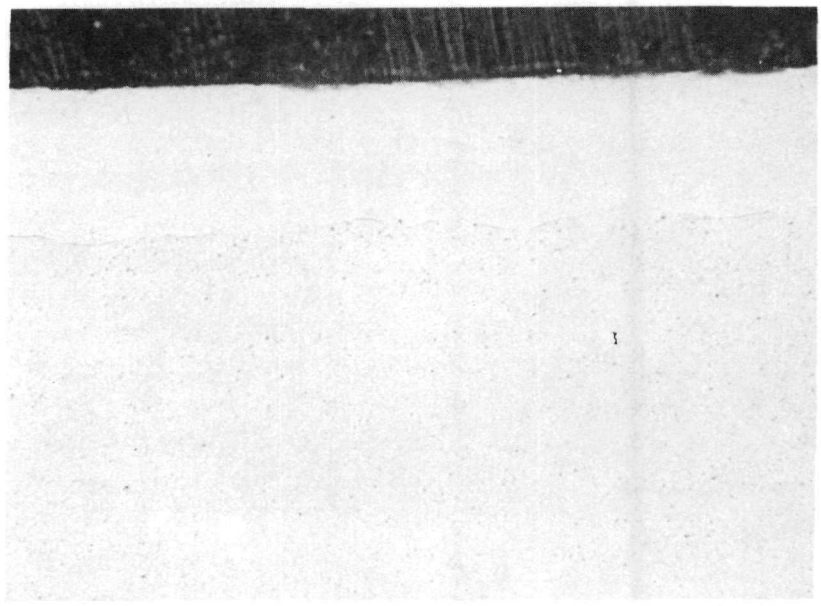

250X

a. AS-POLISHED, BRIGHT FIELD

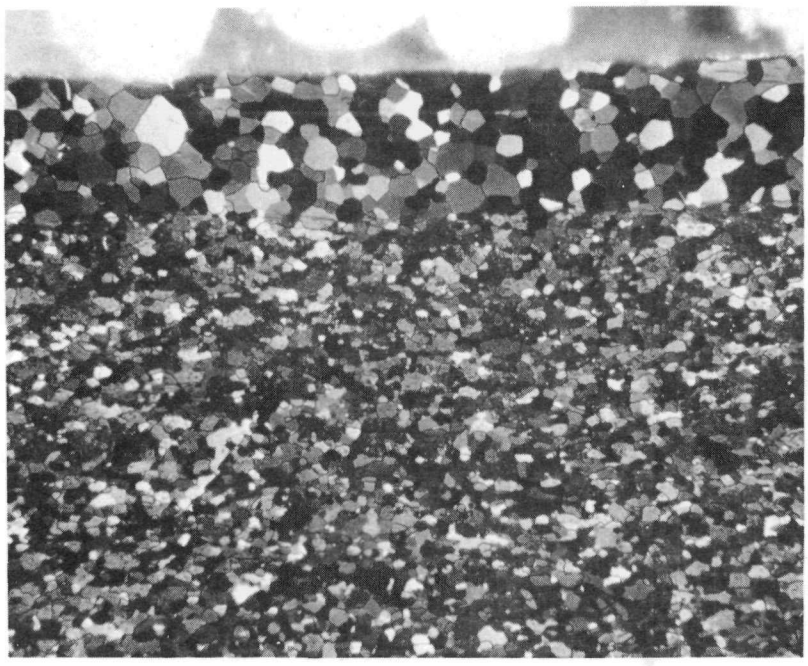

250X

b. ETCHED AND ANODIZED, POLARIZED LIGHT

Figure 7.2-1. Photomicrographs of Zr-Liner Tube Made by Coextrusion With Zircaloy-4 Test Billet, Longitudinal Section

8. REFERENCES

1. L. F. Coffin and R. P. Gangloff, *Integrated Laboratory Methods for Evaluating PCI in Zircaloy-2 Fuel Cladding,* General Electric Co. Report No. 77CRD148, July 1977.

2. D. S. Tomalin, *Zirconium in the Nuclear Industry,* ASTM-STP633, p. 557 (1977).

3. D. Lee and R. B. Adamson, *Zirconium in the Nuclear Industry,* ASTM STP633, p. 385 (1977).

4. C. E. Coleman, *Int. Conf Phys Metall of Reactor Fuel Elements,* Berkeley Nuclear Laboratory, London, 302 (1973).

5. D. S. Tomalin, R. B. Adamson, R. P. Gangloff, *Zirconium in the Nuclear Industry,* to be published, Stratford-on-Avon, England, June 1978.

6. D. W. Shannon, *Role of Oxidation Rate on the Hydriding of Zirconium Alloys in Gas Atmospheres Containing Hydrogen,* GE, HW-765670 Revised February 1963.

7. J. O. M. Bockris and A. K. N. Reddy, *Modern Electrochemistry,* 2, Plenum Press, New York (1970).

8. G. F. Rieger and D. Lee, "Strength and Ductility of Neutron Irradiated and Textured Zircaloy-2", *Zirconium in Nuclear Applications,* ASTM STP 551, p. 355 (1977).

9. A. S. Bain, J. C. Wood, and C. E. Coleman, "Fuel Designs to Eliminate Defects on Power Increases", Paper 56, Conf. British Nuclear Engineering Soc., October 1973.

10. J. C. Wood (AECL), Presented in Discussion on Pellet Cladding Interaction at the ANS-CNA Topical Meeting, Toronto, April 1975.

11. J. H. Davies, H. S. Rosenbaum, J. S. Armijo, R. A. Proebstle, T. C. Roland, J. R. Thompson, E. L. Esch, G. Romeo, and D. R. Rutkin, *Irradiation Tests to Characterize the PCI Failure Mechanism,* General Electric Nuclear Energy Division Report NEDO-21551 (1977).

12. M. F. Lyons, T. C. Rowland, and D. T. Weiss, "BWR Fuel Testing at General Electric – An Overview," paper presented at International Conference on Nuclear Fuel Performance, BNES, London, October 1973.

DISTRIBUTION

Director, Division of Nuclear Power Development
Mail Stop B-107
U S Department of Energy
Washington, DC 20545

Assistant Director for Light Water Reactor Development
Division of Nuclear Power Development
Mail Stop B-107
U S Department of Energy
Washington, DC 20545

Director, Reactor Programs Office
Chicago Operations Office
U S Department of Energy
9800 South Cass Avenue
Argonne, IL 60439

P R Clark
Associate Director for Reactors
Division of Naval Reactors
Mail Stop H-404
U S Department of Energy
Washington, DC 20545

Victor Stello, Director
Division of Operating Reactors
Mail Stop 542
U S Nuclear Regulatory Commission
Washington, DC 20555

L S Tong
Division of Reactor Safety Research
Mail Stop 1130SS
U S Nuclear Regulatory Commission
Washington, DC 20555

Robert H Steele, Chief
Reactor Materials Branch
Division of Naval Reactors
Mail Stop H-404
U S Department of Energy
Washington, DC 20545

Joseph Prestele
Water Reactors Assistant Department Director
Electric Power Research Institute
3412 Hillview Avenue
P O Box 10412
Palo Alto, CA 94304

M Levenson, Director
Nuclear Power Division
Electric Power Research Institute
3412 Hillview Avenue
P O Box 10412
Palo Alto, CA 94304

E Zebroski, Director
Systems and Materials Department
Electric Power Research Institute
3412 Hillview Avenue
P O Box 10412
Palo Alto, CA 94304

W D Crawford, President
Edison Electric Institute
90 Park Avenue
New York, NY 10016

Harvey F Brush
Bechtel Power Corporation
50 Beale Street
San Francisco, CA 94119

A E Swanson
Director of Nuclear Activities
Black & Veatch Consulting Engineers
1500 Meadow Lake Parkway
Kansas City, MO 64114

G L Morris, Vice President Engineering
Power Plant Department
Brown & Root, Inc
P O Box 3
Houston, TX 77001

Seymour Baron
Vice President, Engineering
Burns and Roe, Inc
700 Kinderkamack Road
Oradell, NJ 07649

B E Wells
Vice President of Operations, Power Group
Daniel Construction Company
Daniel Building
Greenville, SC 29602

Earl Borque
Vice President, Construction
Ebasco Services, Inc
2 Rector Street
New York, NY 10006

Wade Larkin
Vice President, Engineering
Fluor-Pioneer
200 West Monroe Street
Chicago, IL 60606

Robert Gordon
Vice President, Power Projects
Gibbs and Hill, Inc.
393 Seventh Avenue
New York, NY 10001

Hans Lorenz
Vice President & General Manager
Power Engineering Division
Gilbert Commonwealth
525 Lancaster Avenue
Reading, PA 19603

W. H. Chittenden
Director of Engineering
Sargent & Lundy Engineers
55 East Monroe Street
Chicago, IL 60603

William Kennedy
Stone & Webster Engineering Corp.
P.O. Box 2325
Boston, MA 02107

John Crowley
United Engineers and Constructors
1401 Arch Street
Philadelphia, PA 19105

Lamar Bupp
Exxon Nuclear Company, Inc.
777 106th Avenue, NE
Bellevue, WA 98009

Sherman Naymark
Nuclear Services Corporation
1700 Dell Avenue
Campbell, CA 95008

E. A. Saltarell
Senior Vice President
Engineering and Operating Services
NUS Corporation
4 Research Place
Rockville, MD 20850

Edward Chipman
Contract Research Division
Babcock and Wilcox Company
P.O. Box 1260
Lynchburg, VA 24505

George E. Kulynych
Manager, Research and Development
Nuclear Power Generation Division
Babcock and Wilcox Company
P.O. Box 1260
Lynchburg, VA 24505

William Jacobi
Manager, System Engineering
Westinghouse Electric Corporation
Nuclear Energy Systems
P.O. Box 355
Pittsburgh, PA 15230

Thomas Hursen
Manager, Equipment Engineering
Westinghouse Electric Corporation
Nuclear Energy Systems
P.O. Box 355
Pittsburgh, PA 15230

Warren Chernock, Vice President
Development Nuclear Power Systems
Combustion Engineering, Inc.
1000 Prospect Hill Road
P.O. Box 500
Windsor, CT 06095

A. Strasser
The S. M. Stoller Corp.
1250 Broadway
New York, NY 10001

Frank Bevilacqua
Vice President of Engineering
Combustion Engineering, Inc.
1000 Prospect Hill Road
Windsor, CT 06095

Philip Bray
Vice President & General Manager
Nuclear Energy Projects Division
General Electric Company
175 Curtner Avenue
San Jose, CA 95125

H E Stone
Vice President & General Manager
Nuclear Energy Engineering Division
General Electric Company
175 Curtner Avenue
San Jose, CA 95125

A R Barton
Senior Vice President
Alabama Power Company
P O Box 2641
600 North 18th Street
Birmingham, AL 35202

Robert S Hunter
Vice President for Nuclear Engineering
American Electric Power Corporation
2 Broadway
New York, NY 10004

E E Van Brunt, Jr
Vice President for Nuclear Services
Arizona Public Service Company
411 North Central Avenue
Phoenix, AZ 85004

J D Phillips, Senior Vice President
Production, Transmission and Engineering
Arkansas Power and Light Company
9th and Louisiana
Little Rock AR 72203

John W Gore, Jr , Vice President
Engineering and Construction
Baltimore Gas and Electric Company
Gas and Electric Building
Baltimore, MD 21203

J E Howard
Vice President, Nuclear
Boston Edison Company
800 Boyston Street
Boston MA 02199

J A Jones, Executive Vice President
Engineering, Construction & Operations
Carolina Power and Light Company
336 Fayetteville Street
Raleigh, NC 27602

W H Dickhoner
President and Chief Executive Officer
Cincinnati Gas and Electric Company
139 East Fourth Street
Cincinnati, OH 45201

D R Davidson
Vice President for Engineering
Cleveland Electric Illuminating Company
55 Public Square
Cleveland, OH 44101

Wallace B Behnke, Jr
Executive Vice President
Commonwealth Edison Company
One First National Plaza
P O Box 767
Chicago, IL 60690

Richard E Jortberg, General Manager
Commonwealth Research Corporation
One First National Plaza
P O Box 428
Chicago, IL 60690

D Switzer, President
Connecticut Yankee Atomic Power Company
P O Box 270
Hartford, CT

William Cahill, Vice President
Consolidated Edison Company of New York, Inc
4 Irving Place
New York, NY 10003

Russell B DeWitt, Manager
Production — Nuclear
Consumers Power Company
212 West Michigan Avenue
Jackson, MI 49201

Walter McCarthy
Executive Vice President of Division
Detroit Edison Company
2000 Second Avenue
Detroit, MI 48226

W O Parker, Jr
Vice President for Generation
Duke Power Company
422 South Church Street
Charlotte, NC 28242

E J Woolever, Vice President
Engineering and Construction
Duquesne Light Company
435 Sixth Avenue
Pittsburgh, PA 15219

R. E. Uhrig
Vice President for Nuclear Engineering
Florida Power and Light Company
9250 West Flagler Street
Miami, FL 33174

Maurice F. Hebb, Jr.
Vice President for Nuclear Engineering
Florida Power Corporation
3201 South 34th Street
P.O. Box 14042
St. Petersburg, FL 33733

Ronald L. Williams
Manager of Engineering
GPU Service Corporation
260 Cherry Hill Road
Parsippany, NJ 07054

J. H. Miller, Jr.
Executive Vice President
Georgia Power Company
270 Peachtree Street, NW
Atlanta, GA 30303

S. L. Adams, Senior Vice President
Production-Construction
Gulf States Utilities
285 Liberty Avenue
Beaumont, TX 77701

G. W. Oprea, Jr.
Executive Vice President
Houston Light and Power Company
P.O. Box 1700
Houston, TX 77001

L. J. Koch
Manager, Nuclear Project
Illinois Power Company
500 South 27th Street
Decatur, IL 62525

John Dolan
Vice President & Chief Engineer
Indiana & Michigan Power Company
AEP Corporation
2 Broadway
New York, NY 10004

L. Liu
Vice President for Engineering
Iowa Electric Light & Power Co.
200 First Street, SE
Cedar Rapids, IA 52401

I. R. Finfrock, Jr.
Vice President, Generation
Jersey Central Power and Light Co.
260 Cherry Hill Road
Parsippany, NJ 07054

Donald T. McPhee, Vice President
Kansas City Power and Light Company
1330 Baltimore Avenue
Kansas City, MO 64141

Elmer Hall, Vice President
Kansas Gas and Electric Company
201 North Market Street
Wichita, KS 67201

Andrew Wofford
Vice President for Project Management
Long Island Lighting Company
Central Operations Headquarters
175 East Old Country Road
Hicksville, NY 11801

D. L. Aswell
Manager for Power Productionn
Louisiana Power and Light Company
142 Delaronde Street
New Orleans, LA 70174

D. W. Edwards
Assistant to Vice President
Maine Yankee Atomic Power Company
20 Turnpike Road
Westboro, MA 01581

Richard M. Klingaman, Manager
Generation Engineering
Metropolitan Edison Company
2800 Pottsville Pike
Reading, PA 19605

J. F. Vogt, Jr., Vice President
Engineering and Operations
Middle South Utilities
225 Baronne Street
P.O. Box 61000
New Orleans, LA 70161

Norris L. Stampley
Vice President for Production
Mississippi Power and Light Company
P.O. Box 1640
Jackson, MS 39205

L. C. Kuncl, Director
General Engineering and Construction
Nebraska Public Power District
P.O. Box 499
Columbus, NE 68601

Larry E. Bailey
New England Power Service Company
20 Turnpike Road
Westboro, MA 01581

George L. Houston
New York State Electric and Gas Corp.
4500 Vestal Parkway East
Binghamton, NY 19302

Rudolph R. Schneider
Vice President — Electric Operations
Niagara Mohawk Power Corporation
300 Erie Boulevard West
Syracuse, NY 13202

Robert A. Evans, Assistant Vice President
Generation and Engineering and
Construction Division
Northeast Utilities Service Corporation
Selden Street
Berlin, CT 06037

H. P. Lyle, Vice President
Electrical Production and Engineering
Northern Indiana Public Service Co.
5265 Hohman Avenue
Hammond, IN 46320

Arthur V. Dienhart, Vice President
Engineering and Construction
Northern States Power Company
414 Nicollet Mall
Minneapolis, MN 55401

Nicholas A. Petrick
Executive Director, SNUPPS
Nuclear Projects, Inc.
5 Choke Cherry Road
Rockville, MD 20850

J. W. Junttila, General Superintendent
Nuclear Operations
Ohio Edison Company
76 South Main Street
Akron, OH 44308

L. C. Shalla
Group Manager for Operations
Omaha Public Power District
1623 Harney Street
Omaha, NE 68102

D. V. Kelley, Chief,
Mechanical & Nuclear Engineering
Pacific Gas and Electric Company
77 Beale Street
San Francisco, CA 94106

N. W. Curtis, Vice President
Engineering and Construction
Pennsylvania Power and Light Company
Two North Ninth Street
Allentown, PA 18101

V. S. Boyer, Vice President
Engineering and Research
Philadelphia Electric Company
2301 Market Street
Philadelphia, PA 19101

J. L. Williams
Vice President for Engineering
Portland General Electric Company
621 SW Alder Street
Portland, OR 97205

P. Lyon, Manager of Nuclear Operations
Power Authority of the State of New York
10 Columbus Circle
New York, NY 10019

John E. Martin
Manager, Engineering Division
Public Service Company of Colorado
P.O. Box 840
Denver, CO 80201

W. C. Tallman, President
Public Service Company of New Hampshire
1000 Elm Street
Manchester, NH 03105

G. W. Muench
Public Service Company of Oklahoma
P.O. Box 201
Tulsa, OK 74102

R. M. Eckert, Vice President
Engineering and Construction
Public Service Electric and Gas
80 Park Place
Newark, NJ 07101

Larry Minnick, President
Yankee Atomic Electric Company
20 Turnpike Road, Route 9
Westboro, MA 05181

R J Gray
Executive Vice President & General Manager
Texas Utilities Generating Company
2001 Bryan Tower Building
Dallas, TX 75201

Lowell Roe
Vice President for Facility Development
Toledo Edison Company
Edison Plaza
300 Madison Avenue
Toledo, OH 43632

John K Bryan, Vice President
Engineering and Construction
Union Electric Company
1 Memorial Drive
St Louis, MO 63166

C M Stallings, Vice President
Power Supply and Production Operations
Virginia Electric and Power Company
700 East Franklin Street
Richmond, VA 23261

D L Renberger
Assistant Director for Operation and Tech
Washington Public Power Supply System
3000 George Washington Way
P O Box 968
Richland, WA 99352

Glenn A Reed
Superintendent, Nuclear Power
Wisconsin Electric Power Company
231 West Michigan Avenue
Milwaukee, WI 53201

Evan W James, Senior Vice President
Power Supply and Engineering
Wisconsin Public Service Corporation
600 North Adams
Green Bay, WI 54301

F W Buckman
Consumers Power Company
1945 Parnall Road
Jackson, MI 49201

Remi C Pattyn, Vice President
Administrative Services
Public Service Indiana
1000 East Main Street
Plainfield, IN 46168

Robert Kroprowski, Vice President
Rochester Gas and Electric Corporation
89 East Avenue
Rochester, NY 14649

J J Mattimoe
Assistant General Manager and Chief Engineer
Sacramento Municipal Utility District
6201 S Street
P O Box 15830
Sacramento, CA 95813

Louis Bernath, Assistant Project Manager
Sun Desert Nuclear Plant
San Diego Gas and Electric Company
P O Box 1831
San Diego, CA 92112

E H Crews, Jr , Vice President
Engineering and Construction
South Carolina Electric and Gas Company
328 Main Street
P O Box 764
Columbia, SC 29218

J B Moore, Vice President
Advanced Engineering
Southern California Edison Co
P O Box 800
Rosemead, CA 91770

Rubel A Thomas
Vice President, Nuclear
Southern Services, Inc
800 Shades Creek Parkway
P O Box 2625
Birmingham, AL 35202

Jack R Calhoun
Assistant Director of Power Production
Tennessee Valley Authority
716 Edney Building
Chattanooga, TN 37401

G H Kimmons, Manager
Engineering, Design and Construction
Tennessee Valley Authority
New Sprankle Building
Knoxville, TN 37902

M S Freshley
Battelle-Northwest Laboratory
Richland, WA 99352

C R Hann
Battelle-Northwest Laboratory
Richland, WA 99352

K Woods
Exxon Nuclear Company, Inc
Richland, WA 99352

C E Crouthamel
Exxon Nuclear Company, Inc
Richland, WA 99352

G Sofer
Exxon Nuclear Company, Inc
Richland, WA 99352

T Snead
Duke Power Company
P O Box 2178
Charlotte, NC 28342

J Korthever
Duke Power Company
P O Box 2178
Charlotte, NC 28342

J T A Roberts
Electric Power Research Institute
P O Box 10412
Palo Alto, CA 94303

F E Gelhaus
Electric Power Research Institute
P O Box 10412
Palo Alto, CA 94303

J R Tomonto
Florida Power and Light Company
P O Box 013100
Miami, FL 33101

J S Armijo
General Electric Company
Nuclear Energy Group
175 Curtner Avenue
San Jose, CA 95125

Gordon Bond
GPU Service Corporation
260 Cherry Hill Road
Parsippany, NJ 07054

W. J Tunney
Long Island Lighting Company
175 East Old Country Road
Hicksville, NY 11801

Howard Sobel
American Electric Power Service Corp
Nuclear Materials and Fuel Management Section
2 Broadway
New York, NY 10004

Orville Cypret
Arkansas Power & Light
P O Box 551
Little Rock, AK 72203

J Tulenko
Babcock & Wilcox Company
Nuclear Power Generation Division
P O Box 1260
Lynchburg, VA 24505

R N Duncan
Combustion Engineering, Inc
1000 Prospect Hill Road
Windsor, CT 06095

W M Kiefer (6)
Commonwealth Edison Company
P O Box 767
Chicago, IL 06090

M L Lee
Consolidated Edison Company of New York
4 Irving Place
New York, NY 10003

D B Wehmeyer
Detroit Edison Company
2000 Second Avenue
Detroit, MI 48226

S W Wilczek, Jr
Niagara Mohawk Power Corporation
300 Erie Boulevard West
Syracuse, NY 13202

J P Cagnetta
Northeast Utilities Service Company
P O Box 270
Hartford, CT 06101

John Hallam
Nuclear Services Corporation
1700 Dell Avenue
Campbell, CA 95008

G F Daebeler
Philadelphia Electric Company
2301 Market Street
P O Box 8699
Philadelphia, PA 19101

Kashmiri Mahna
Public Service Electric and Gas Company
80 Park Place
Newark, NJ 07101

R R O Laughlin
Public Service Indiana
1000 East Main Street
Plainfield, NH 46168

R J Mullin
Tennessee Valley Authority
1410 Commerce Union Bank Building
Chattanooga, TN 37402

D L Larkin
Washington Public Power Supply System
P O Box 968
Richland, WA 99352

R S Miller
Westinghouse Electric Corporation
Nuclear Fuel Division
P O Box 355
Pittsburgh, PA 15230

R M Grube
Yankee Atomic Electric Company
20 Turnpike Road
Westboro MA 01581

E Straker
Science Applications, Inc
8400 Westpark Drive
McLean, VA 22101

R Omberg
Hanford Engineering Development Laboratory
P O Box 1970
Richland, WA 99352

W Lipinski
Argonne National Laboratory
9700 South Cass Avenue
Argonne, IL 60439

W R Harris
Rand Corporation
1700 Main Street
Santa Monica, CA 90406

T Row
Oak Ridge National Laboratory
P O Box X
Oak Ridge, TN 37830

U S Department of Energy
NASAP Control Office
Room F-409 (Mail Stop B-107)
Germantown, MD 20767

I I Spiewak
Oak Ridge National Laboratory
P O Box X
Oak Ridge, TN 37830

B A Pasternak
Booz-Allen Applied Research
4330 East-West Highway
Bethesda, MD 20014

D R O Boyle
Commonwealth Edison Company
P O Box 767
Chicago, IL 60690

L A Niemark
Argonne National Laboratory
9700 South Cass Avenue
Argonne, IL 60439

R W Weeks
Argonne National Laboratory
9700 South Cass Avenue
Argonne, IL 60439

Carl Johnson
Argonne National Laboratory
9700 South Cass Avenue
Argonne, IL 60439